



MDOT RC-1563



High Skew Link Slab Bridge System with Deck Sliding over Backwall or Backwall Sliding over Abutments

FINAL REPORT – SEPTEMBER 2011

Part I



Western Michigan University
Department of Civil & Construction Engineering
College of Engineering and Applied Sciences

RESEARCH

Intentionally left blank

Technical Report Documentation Page

1. Report No. Research Report RC-1563	2. Government Accession No.	3. MDOT Project Manager Steve Kahl, P.E.	
4. Title and Subtitle High skew link slab bridge system with deck sliding over backwall or backwall sliding over abutments		5. Report Date September 30, 2011	
7. Author(s) Dr. Haluk Aktan, P.E., and Dr. Upul Attanayake, P.E.		6. Performing Organization Code WMU	
9. Performing Organization Name and Address Department of Civil and Construction Engineering College of Engineering and Applied Sciences Western Michigan University 1903 W. Michigan Ave, Kalamazoo, MI 49008		8. Performing Org Report No.	
12. Sponsoring Agency Name and Address Michigan Department of Transportation Construction and Technology Division PO Box 30049, Lansing MI 48909		Work Unit No.	
		11. Contract Number : 2006-0415	
		11(a). Authorization Number: 3	
15. Supplementary Notes		13. Type of Report and Period Covered Final Report, 2008-2011	
		14. Sponsoring Agency Code	
16. Abstract <p>A new bridge design and construction trend to help improve durability and rideability is to remove expansion joints over piers and abutments. One approach to achieve this is to make the deck continuous over the piers by means of a link slab while the girders remain simply supported. The need to implement link slabs is indicated by AASHTO LRFD section 2.5.2.4 which requires using a minimum number of expansion joints to improve rideability. Further, due to durability concerns associated with bridge deck joints, it is preferred to have a least number of joints or develop jointless decks. The expansion joints over the abutments can be removed by one of three methods: deck sliding over back wall, semi-integral abutments, and integral abutments. This results in expansion joints at either or both ends of the approaches. The design concerns other than link slab include backwall and wing-wall design and bearing movement. The behavior of a jointless bridge brings about many challenges to bridge designers. The complexity is augmented when skew is involved.</p> <p>This report complements an earlier report based on previous research on <i>Combining Link Slab, Deck Sliding Over Backwall and Revising Bearings</i> (Aktan et al., 2008) where the behavior of straight and moderately skew (skew < 20⁰) link slab bridges were investigated and design recommendations were developed. This report describes the behavior and performance of high skew (skew > 20⁰) jointless bridges with link slabs and two abutment configurations. These abutment configurations are deck sliding over backwall and backwall sliding over abutments (i.e. semi-integral abutments).</p> <p>Four tasks were performed in this project. The first task was to review and synthesize information related to the behavior, performance, design, and analysis of skew bridges. The second task was field assessment of skew bridge behavior under static truck loads and thermal loads. The third task was analytical and numerical analysis of skew link slabs. The final task was analytical and numerical analysis of skew sliding deck over backwall systems and semi-integral abutments.</p> <p>Design recommendations are developed based on literature, field assessment data analysis, finite element modeling, and subsequent simulations of the numerous models developed in this project. One recommendation deals with the skew link slab design and the remaining recommendations are for bearing selection and selection and design of a transverse restraint system at abutments of skew link slab bridges.</p>			
17. Key Words: Abutment, Concrete, Finite Element, Jointless Bridge, Link Slab, and skew.		18. Distribution Statement No restrictions. This document is available to the public through the Michigan Department of Transportation.	
19. Security Classification (report) Unclassified	20. Security Classification (Page) Unclassified	21. No of Pages 249	22. Price

Intentionally left blank

High Skew Link Slab Bridge System with Deck Sliding over Backwall or Backwall Sliding over Abutments

Project Manager: Mr. Steve Kahl, P.E.

Submitted to:



Submitted by

Dr. Haluk Aktan, P.E.
Professor & Chair
(269) – 276 – 3206
haluk.aktan@wmich.edu

Dr. Upul Attanayake, P.E.
Assistant Professor
(269) – 276 – 3217
upul.attanayake@wmich.edu



Western Michigan University
Department of Civil & Construction Engineering
College of Engineering and Applied Sciences
Kalamazoo, MI 49008
Fax: (269) – 276 – 3211

Intentionally left blank

DISCLAIMER

The content of this report reflects the views of the authors, who are responsible for the facts and accuracy of the information presented herein. This document is disseminated under the sponsorship of the Michigan Department of Transportation in the interest of information exchange. The Michigan Department of Transportation assumes no liability for the content of this report or its use thereof.

Intentionally left blank

ACKNOWLEDGEMENTS

This project is funded by the Michigan Department of Transportation. The authors would like to acknowledge the support and effort of Mr. Steve Kahl for initiating this research. The authors also wish to acknowledge the continuing assistance of the Research Advisory Panel (RAP) members in contributing to the advancement of this study. Contribution of graduate students Abdul Mohammed, Alp Servi, Duy Nguyen, Michael Romkema, and Mohamed Rusthi for the successful completion of this study is highly appreciated.

Intentionally left blank

EXECUTIVE SUMMARY

INTRODUCTION

The new bridge design trend is to avoid having expansion joints over piers and abutments to prevent premature deterioration of bridges due to faulty joints. For this purpose joints over the piers are eliminated using link slabs where the deck is continuous and the underlying girders are simply supported. The expansion joints over the abutments are also eliminated by allowing the deck to slide over the backwall or by allowing the deck-backwall combined system to slide over the abutment (semi-integral abutments). As a result, the movement of the superstructure is transferred to the ends of the approach slab that sits on a sleeper slab.

This research was designed to respond to the concerns of the designers in terms of the design of specific components of high skew jointless link slab bridges with deck sliding over backwall or semi-integral abutment configurations.

The objectives of this study were identified as follows:

1. Study the behavior of high skew bridge structural system by load testing and analytical modeling and analysis.
2. Develop finite element models of selected components, or combinations of several components, of the link slab bridge deck system with deck sliding over backwall and semi-integral abutment to understand the behavior and interaction between components under various load conditions, including volume change load.
3. Develop recommendations for changes or modifications to the design of the link slab, and bearings, abutment types, and lateral restraint systems of bridges with link slabs.

To satisfy the objectives, this project was organized into four main tasks: literature review, field assessment of skew bridge behavior under static truck loads and thermal loads, analytical and numerical analysis of skew link slabs, and analytical and numerical analysis of skew sliding deck over backwall systems and semi-integral abutments.

LITERATURE REVIEW

Literature on the following topics was reviewed: skewed bridge behavior under gravity loading, skewed bridge behavior under volume change loads, design challenges of skewed/jointless bridges, and performance of skew/ jointless bridges. A summary of key points identified through literature review is given below:

1. Skewed bridges with semi-integral abutments would tend to rotate about an axis normal to their horizontal plane. The rotation is due to the passive pressure developed behind the backwall under thermal expansion. Deck extensions also have a tendency to develop in-plane rotations but not as critical as semi-integral systems. In both deck extension and semi-integral systems, the rotation may be affected by the approach slab-base interface friction, the shearing resistance of the elastomers in the bearings, and by the compressive resistance of fillers used in the movable joints between the superstructure and wingwalls.
2. The current MDOT deck sliding over backwall system uses Expanded polystyrene (EPS) in between deck and backwall to introduce the sliding surface. The EPS elastic strain limit is very small and can deform beyond the elastic limit under deck self-weight and live loads. Further, peak and residual friction coefficients between EPS and concrete are 2.3 and 1.0, respectively. Because of these reasons, neoprene pads over backwall may be used. In addition, the polyethylene sheet used under approach should be extended to the backwall face on the span side to minimize friction at the interface.
3. A current semi-integral configuration used by Ontario and several State Highway Agencies has the advantages of allowing the backwall to move independently from the abutment, providing access space for bearing inspection, maintenance, and replacement; and preventing backfill infiltration through the backwall.
4. Isolation of the backwall from its abutment requires developing specific design details to constrain transverse movement of skew bridges. In that regard, placing the backwall over the abutment and restraining transverse movement by placing the

- wingwall against the backwall and deck, similar to the current MDOT semi-integral details, provides many benefits if adequate measures are taken to minimize interface friction and infiltration of backfill material through the joints. Use of EPS form behind the backwall helps reduce passive earth pressure and prevent infiltration of backfill material.
5. In order to allow the translation and rotation of skew bridges and provide sufficient load capacity, plain elastomeric pad (PEP), fiberglass-reinforced pad (FRP), and steel-reinforced elastomeric bearings or pads (SREB or SREP) are suitable for support bearings for semi-integral and deck sliding over backwall bridges. Also, polytetrafluorethylene (PTFE) sliding bearings can be combined with the support bearing types stated above to accommodate large superstructure movements.
 6. Rub plates, girder stops, or any other mechanism designed to resist large forces is needed to control lateral movement of skew bridges.
 7. With increasing backfill stiffness, forces at the wingwalls of high skew bridges increase dramatically. EPS can be specified as a suitable backfill material for semi-integral bridges to reduce passive pressure. However, an approach slab should not be directly supported on EPS because of potential creep. EPS should also be protected using geotextiles and gasoline containment geomembranes.

FIELD ASSESSMENT OF SKEW BRIDGE BEHAVIOR UNDER STATIC TRUCK LOADS AND THERMAL EXPANSION

Bridge deflections and bearing translations were measured under static truck as well as thermal loads. Measured girder deflections showed that girder end movements were controlled by bearing friction. It is worth mentioning here that the bearing movements under static truck loads were very small compared to allowance made at the design for thermal expansion and contraction. The measured bearing movement under thermal expansion loads from May to July indicates that the bearings are frozen and an in-plane twist of the deck occurs due to bearing movement that is not expected at the design stage. Though there was no damage to the superstructure and substructure of this 120 ft long single span bridge, this

behavior is critical when link slabs are implemented and the deck over the abutments is made continuous. The observations highlight the importance of using durable bearings that are capable of accommodating large deformation and a certain degree of rotation demands.

LINK SLAB ANALYSIS FOR DEVELOPING DESIGN GUIDELINES

Finite element analysis was utilized to understand the behavior of the jointless skew bridge structural system with link slabs to verify the design assumptions and propose fine-tuning to the current link slab design procedures to accommodate changing load demands due to bridge skew. This task was accomplished by developing and analyzing refined finite element models representing a two span bridge with a skew link slab. The major interest is how skew affects the link slab moments. Skew reduction factors were calculated using moment ratios and presented in Chapter 4. Skew reduction factors vary significantly with the live load configurations, support configurations under the link slab, and with the direction of moment (i.e., negative or positive). Skew reduction factors show that load demand decreases with increasing skew.

A detailed link slab design example is given in Appendix C. The 45⁰ skew bridge, in this case, has a RHHR (Roller-Hinge-Hinge-Roller) support configuration, which develops the largest link slab moments and forces under applied loads. Yet, the amount of required link slab reinforcement is governed by the minimum reinforcement amount requirements of AASHTO LRFD (2010).

Following are further key summary observations on analysis results:

1. The RHHR boundary condition develops significantly larger link-slab moments compared to other support conditions.
2. NTG can be excluded from design load combination with HRRR and RRHR support conditions.
3. NTG load case moments that develop in the link slab of bridges with zero skew and RHHR support configuration, should be directly used in design without any reduction for skew.
4. The negative moment design of a link slab with the RHHR support configuration is governed by the combined effect of live and NTG loads.

5. Positive moment design of a link slab with the RHHR support configuration is governed by a PTG load.
6. Moment developed in a link slab under thermal gradient loads (PTG and NTG) remains constant irrespective of span.
7. Providing the minimum reinforcement amount required in AASHTO LRFD Section 5.7.3.3.2 is adequate for the majority of skew link slabs with HRRR or RRHR support configuration for spans up to 110 feet. However, additional reinforcement at the bottom layer is needed to resist large tensile stresses developed near the boundaries of the debonded region. A top layer of #6 bars at 4 in. spacing and bottom layer of #6 bars at 4 in. spacing are adequate for high skew link slabs. Proposed detail in standard MDOT Bridge Design Guide format is presented in Appendix E.
8. Simplified analysis models are not able to represent three dimensional effects such as positive moments under live load or negative moments under PTG. New analysis models and procedures are required.

SKEW ABUTMENT ANALYSIS AND DESIGN GUIDELINES

This report provides a detailed analysis of two skew abutment configurations namely deck sliding over backwall and semi-integral systems for a range of skew angles from 0° to 45° under loads and configurations specified in AASHTO (2010) and Michigan Bridge Design Manual (MDOT 2005). Deck sliding over backwall and semi-integral abutment details presented in Aktan et al. (2008) represented the basis of the FE models. These models were modified to incorporate various bearing configurations and wingwalls. The following is a summary of conclusions that are derived based on analysis results and information presented in related literature and design specifications /guidelines

1. A bridge span with deck sliding over backwall or semi-integral abutments can be analyzed as simply supported spans to calculate girder end rotations and translation (expansion/contraction) demands.
2. Skew bridges expand and contract along the diagonal between acute corners. The movement results in transverse forces at the bearings and other restraint systems. The restraint force magnitudes become considerably larger if adequate tolerances are not

provided to accommodate the movements due to thermal loads. The situation requires special consideration when link slabs are implemented over the piers, which in turn increase the effective length of thermal expansion and contraction. Further, the direction of bridge movement under expansion and contraction loads needs to be restricted to the bridge axis. In plane twisting results in large stresses along the edge of link slab (see Chapter 4). Link slab is also flexible under torsion compared to the deck-girder integrated system. Hence, controlling bridge alignment is critical when link slabs are implemented.

3. It is recommended that deck sliding over backwall abutments, is restrain the transverse movement of the center girder end (for odd number of girders) or two centermost girder ends (for even number of girders) using concrete keys with rub plates (shown on Figure 5-8.). Also, larger tolerance is required for the slot in the sole plate and bearings in order to accommodate the transverse movement of unrestrained girder ends. Proposed detail in standard MDOT Bridge Design Guide format is presented in Appendix F. The required formulations and variables for movement calculations are presented with the drawings. The rub plate design procedure is based on the VDOT Bridge Design Manual section 20.04 (2010) with modifications and presented in Appendix G.
4. Transverse movement of bearings over the semi-integral abutment is facilitated by increasing the tolerance of the slot at the bearing plate. Transverse restraint for expansion thermal load is provided by a wingwall at the acute corner. Alignment of semi-integral abutment bridge deck with backwall offset from the abutment is managed under contraction thermal loads by placing a concrete key at the center girder. Calculation of the transverse force on the wingwall is adopted from the procedure described in VDOT (2010). Proposed detail in standard MDOT Bridge Design Guide format is presented in Appendix H.
5. It is recommended that an EPS layer is placed behind the backwall of semi-integral bridges. This will minimize the passive pressure and results in lower transverse forces at the wingwall. Although the passive pressure coefficient of EPS is in reality

much lower than four (4), a coefficient of four (4) is recommended for conservative design until additional supporting data is developed (VDOT (2010)). Further, the equation given in VDOT (2010) section 20-06-6 can be used to calculate EPS layer thickness (i.e., Eq. 2-2 in Chapter 2 section 2.4.4).

6. It is recommended that the maximum bearing tolerance in transverse direction is limited to 0.25 in. Further investigations can be carried out analyzing the impact of the increased fit tolerances of the girder position dowels on the bridge components.
7. Following link slabs are implemented, controlling friction at the approach slab interfaces is very critical. Increased friction hinders bridge movement restricting expansion bearing movement over the abutment. This results in stresses greater than the concrete modulus of rupture under negative thermal loads. Hence, it is vital to reduce friction at all the contract surfaces at the abutment and approach to facilitate movement of the bridge under expansion and contraction thermal loads. To reduce friction a 0.025 in. thick polyethylene sheet can be placed during construction over the fill supporting the approach slab.
8. Bridge expansion length, which is the distance along the longitudinal axis measured from abutment to the nearest fixed bearing, is a function of bridge length, width, and skew. Expansion joint effective movement rating and allowable movement at bearings are the limiting factors of bridge expansion length when link slabs are implemented. Hence, the bridge expansion length should be calculated following the procedure given in chapter 5 and be enforced when link slabs are implemented. As an example, based on maximum strip seal joint width of 3 in. and expansion and contraction thermal load of 115 °F, the following maximum expansion length are recommended:

Straight concrete bridge \leq 300 ft.

45° skew concrete bridge of 100 ft wide \leq 200 ft.

Straight steel bridge \leq 275 ft.

45° skew steel bridge of 100 ft wide \leq 175 ft.

CONCLUSIONS

A literature review was performed, along with a field assessment of a skew bridge behavior under static truck loads and thermal loads, an analytical and numerical analysis of skew link slabs, and an analytical and numerical analysis of skew sliding deck over backwall systems and semi-integral abutments tasks.

Current link slab design procedures do not incorporate skew effects. A design procedure was developed following a detailed analysis of skew link slabs and the moment and force envelopes for various boundary and load configurations. Two major findings are (1) moment developed in a link slab under temperature gradient loads remains constant irrespective of span and (2) moment developed in a link slab under live load decreases with increased span. Analysis results verified that the minimum reinforcement amount required in AASHTO LRFD Section 5.7.3.3.2 is adequate for the majority of skew link slabs with HRRR or RRHR support configuration. However, additional reinforcement at the bottom layer is needed to resist large tensile stresses that develop near the boundaries of the debonded region. A detailed design example is presented in Appendix C. Proposed link-slab detail in standard MDOT Bridge Design Guide format is presented in Appendix E. Three saw cuts are recommended: one at each end of the link slab and one directly over the pier centerline.

The implementation of link slabs on deck sliding over backwall and semi-integral systems presents specific challenges. This report provides a detailed analysis of two skew abutment configurations namely deck sliding over backwall and semi-integral systems for a range of skew angles from 0^0 to 45^0 under loads and configurations specified in AASHTO (2010) and Michigan Bridge Design Manual (MDOT 2005). Bearing details, wingwall and concrete key configurations, and abutment configurations were developed. Proposed detail in standard MDOT Bridge Design Guide format is presented in Appendix F and H. All the required mathematical relationships and variables are presented with the drawings. The rub plate design procedure was adopted from VDOT Bridge Design Manual section 20.04 (2010) with some modifications and presented in Appendix G.

TABLE OF CONTENTS

ACKNOWLEDGEMENTS	ix
EXECUTIVE SUMMARY	xi
LIST OF TABLES	xxiii
LIST OF FIGURES	xxv
1 INTRODUCTION	1
1.1 Overview	1
1.2 Project Objectives and Tasks	2
1.3 Report Organization	2
2 STATE-OF-THE-ART LITERATURE REVIEW	5
2.1 Overview	5
2.2 Skewed Bridge Behavior under Gravity Loading	7
2.2.1 Finite Element (FE) Simulation of Skew Bridge Behavior under Gravity Loading	9
2.3 Skewed Bridge Behavior under Volume Change Loads	16
2.3.1 Skew Bridge Behavior under Thermal Loads	21
2.4 Design Challenges of Skewed/Jointless Bridges	34
2.4.1 Length, Skew and Curvature Limits	34
2.4.2 Volume Change Loads and Behavior of Jointless Bridges	35
2.4.3 Semi-Integral Abutment Details	39
2.4.4 EPS Backfill	45
2.4.5 EPS-Concrete Interface Friction	49
2.4.6 Support Bearing Selection and Design	49
2.4.7 Deck Reinforcement Details with Skew	54
2.5 Field Performance of Skewed/Jointless Bridges	56
2.6 Summary	60
3 MODELING AND FIELD TESTING OF A HIGH SKEW BRIDGE ..	63
3.1 Objective and Approach	63
3.2 Bridge Description	63

3.3	Abutment, Bearing, and Deck Condition.....	69
3.3.1	Abutment Condition.....	69
3.3.2	Bearing Condition.....	69
3.3.3	Deck Condition	72
3.4	FE Modeling and Preliminary Analysis for Load Testing.....	73
3.4.1	Bridge FE Modeling	73
3.4.2	Truck Placement and Loading Configurations	74
3.4.3	Calculated Bridge Deflections and Translations.....	75
3.5	Measured Bridge Deflections and Translations.....	78
3.5.1	Field Measurement Equipment and Procedures	78
3.5.2	Bridge Deflection.....	86
3.5.3	Bearing Translation.....	90
3.6	Summary	98
4	LINK SLAB ANALYSIS AND DESIGN GUIDELINES	99
4.1	Overview and Objectives.....	99
4.2	Contact Simulation.....	99
4.3	Modeling and Analysis of a Link Slab Bridge.....	101
4.3.1	Overview and Objectives.....	101
4.3.2	Prototype Bridge	101
4.3.3	Material Properties.....	102
4.3.4	Bridge Model Geometry	102
4.3.5	Bridge Model Orientation	104
4.3.6	Link Slab Length.....	105
4.3.7	FE Discretization of the Bridge Model.....	105
4.3.8	Skew Mesh.....	106
4.3.9	Contact Surfaces in the FE Model	109
4.3.10	Boundary Conditions	110
4.3.11	Loads.....	110
4.4	Sign Convention, Model Verification, and Results	114
4.4.1	Overview.....	114
4.4.2	Sign Convention.....	114

4.4.3	FE Model Verification	115
4.4.4	Results.....	116
4.4.5	Skew Link Slab Design Procedure	163
5	SKEW ABUTMENT ANALYSIS AND DESIGN GUIDELINES	169
5.1	Overview and Objectives.....	169
5.2	Abutment Configurations and Analysis Models.....	169
5.3	Lateral Restraint Systems in Skew bridges.....	173
5.3.1	Restraint Systems at the Abutment	175
5.3.2	Restraint System over the Pier	175
5.4	Analysis of High Skew Bridge with Deck Sliding over Backwall and Semi-Integral Abutments	175
5.4.1	Material Properties.....	176
5.4.2	Loads.....	176
5.4.3	Load Combinations.....	182
5.4.4	Boundary Conditions	183
5.4.5	Deck Sliding over Backwall Abutment	184
5.4.6	Semi-Integral Abutment.....	199
5.5	Analysis and Design Procedures and Details for Abutments and Bearings	205
6	SUMMARY, CONCLUSIONS, DESIGN RECOMMENDATIONS, AND IMPLEMENTATION PLAN	209
6.1	Summary and Conclusions	209
6.2	Recommendations.....	210
6.2.1	Link Slab Design.....	210
6.2.2	Deck Sliding over Backwall	211
6.2.3	Semi-Integral Abutment.....	211
6.3	Implementation Plan	212
7	REFERENCES	213
APPENDIX A: Acronyms and Abbreviations		
APPENDIX B: Holland Bridge Data		
APPENDIX C: High Skew Link Slab Design - Example		
APPENDIX D: Link Slab Moment due to Thermal Gradient (MathCAD)		

APPENDIX E: Proposed Details for Skew Link Slab

APPENDIX F: Proposed Details for Deck Sliding over Backwall System

APPENDIX G: Rub Plate Design Procedure

APPENDIX H: Proposed Details for Semi-Integral Abutments

LIST OF TABLES

Table 2-1. Range of Design Criteria Used for Selection of Jointless Bridges.....	34
Table 2-2. Bearing Suitability (Source: AASHTO LRFD 2010)	50
Table 2-3. Summary of Bearing Capabilities (Source: Roeder and Stanton 1996).....	50
Table 3-1. Bridge Components, Dimensions, and Element Types used in the Model	73
Table 3-2. Ambient Conditions at 2:30pm on December 16 2010.....	85
Table 3-3. Target Position Coordinates – Baseline Measurements (Dec. 16, 2010).....	86
Table 3-4. Girder-End Translations over South Abutment under Uniform Temperature Loading	97
Table 4-1. ABAQUS Syntax for Various Contact Options	100
Table 4-2. Bearing Configurations and Corresponding Support Conditions.....	110
Table 4-3. Total Sectional Moment and Force Variation Trend with Increased Skew under Various Load and Support Configurations	131
Table 4-4. Skew Reduction Factors for HRRR	159
Table 4-5. Skew Reduction Factors for RRHR	160
Table 4-6. Skew Reduction Factors for RHHR	161
Table 4-7. Girder-End Rotations and Skew Reduction Factors - Lane1 Load Case	162
Table 4-8. Girder-End Rotations and Skew Reduction Factors - Lane2 Load Case	162
Table 4-9. Girder-End Rotations and Skew Reduction Factors – LaneAlt1 Load Case.....	162
Table 4-10. Girder-End Rotations and Skew Reduction Factors – LaneAlt2 Load Case....	162
Table 4-11. Girder-End Rotations and Skew Reduction Factors - NTG Load Case	162
Table 4-12. Girder-End Rotations and Skew Reduction Factors - PTG Load Case.....	163
Table 4-13. Material and Geometric Properties used in Link Slab Design Example	164
Table 4-14. Analytical Rotation and Analytical Design Moment Magnitudes	165
Table 4-15. Ratios of 3D FE to Analytical Design Moment for a Straight Bridge	165
Table 4-16. Analytical Rotation and Analytical Design Moment Magnitudes for Different Spans	166
Table 4-17. Ratio of 3D FE to Analytical Bending Moment for Straight Bridge with Different Spans	167
Table 5-1. Girder End Rotations against Different Truck Positions on Skew Bridge.....	181

Table 5-2. Thermal Load for Bridge Expansion and Contraction 182
Table 5-3. Expansion and Contraction of Girder 1 End over Semi-Integral Abutment 201

LIST OF FIGURES

Figure 2-1. Geometric relation of skew angle and angle of crossing	6
Figure 2-2. Percentages of skew bridges in Michigan.....	6
Figure 2-3. Percentage of skewed bridges in Michigan (a) concrete and (b) steel.....	7
Figure 2-4. Load distribution pattern in skewed stringer and slab bridges.....	8
Figure 2-5. Characteristics of skewed slab deck (Hambly 1991).	8
Figure 2-6. (a) Cross section and (b) isometric views of the stringer models	10
Figure 2-7. Plan view of FE models	10
Figure 2-8. Transverse bending stress distribution of deck for (a) stringer bridge deck and (b) solid slab for 40° skew under self-weight	12
Figure 2-9. Longitudinal bending stress distribution (a) stringer (b) solid slab bridge of 40° skew under self-weight (negative moment regions only)	12
Figure 2-10. Longitudinal bending moment variation against skew for full-width stringer bridge under self-weight	13
Figure 2-11. Longitudinal bending moment variation against skew for full-width stringer bridge under a concentrated load	13
Figure 2-12. Mid-span moment variation vs. skew angle under self-weight and concentrated load for stringer bridge.....	14
Figure 2-13. Torsion for full-width of stringer bridge under self-weight.....	14
Figure 2-14. Torsion for full-width of stringer bridge under concentrated load	15
Figure 2-15. Support reaction vs. skew angle for stringer bridge under self-weight.....	15
Figure 2-16. Direction of skew simply supported bridge movement under uniform thermal load.....	16
Figure 2-17. Bearing orientation for constraint cases (a) traditional, (b) radial from corner, (c) radial from center (Tindal and Yoo 2003).....	17
Figure 2-18. Longitudinal displacement profile of deck for right and 45° skew bridge.....	19
Figure 2-19. Transverse displacement profile of deck for right and 45° skew bridge.....	20
Figure 2-20. Maximum normalized longitudinal and transverse displacement vs. skew angle	20
Figure 2-21. Forces on deck due to resistance encountered in expansion joints	21

Figure 2-22. Positive and negative temperature gradient loads used in the analyses	22
Figure 2-23. Displacement contours under the traditional bearing condition for skew angles	23
Figure 2-24. Displacement contours under radial from corner bearing condition for skew angles	24
Figure 2-25. Displacement contours under the radial from center bearing condition for skew angles	25
Figure 2-26. Deformed shape under the traditional bearing condition for skew angles.....	26
Figure 2-27. Deformed shape under radial from corner bearing condition for skew angles .	27
Figure 2-28. Deformed shape under radial from center bearing condition for skew angles .	28
Figure 2-29. Transverse (left) and longitudinal (right) displacement contours under the traditional bearing condition for skew angles (a) 0° (b) 15° (c) 30° (d) 45° (e) 60°	30
Figure 2-30. Transverse (left) and longitudinal (right) displacement under the radial from corner bearing condition for skew angles (a) 0° (b) 15° (c) 30° (d) 45° (e) 60°	31
Figure 2-31. Transverse (left) and longitudinal (right) displacement under the radial from center bearing condition for skew angles (a) 0° (b) 15° (c) 30° (d) 45° (e) 60°	32
Figure 2-32. Longitudinal bending moment for full-width of simply supported stringer bridge under negative temperature gradient	33
Figure 2-33. Torsion for full-width of simply supported stringer bridge under negative temperature gradient	33
Figure 2-34. Percent of states that account for different forces in the design of jointless bridges.....	35
Figure 2-35. Resultant force components that develop at the abutment under thermal expansion (Oesterle et al. 1999).....	36
Figure 2-36. Forces on the bridge (Steinberg et al. 2004)	37
Figure 2-37. Deformed shape of the deck of a two-span continuous skew stringer bridge under uniform expansion	38
Figure 2-38. Rub plate detail (VDOT).....	39

Figure 2-39. VDOT deck extension detail with buried approach slab	40
Figure 2-40. Semi-integral abutment detail with end diaphragm moving over a fixed abutment.....	41
Figure 2-41. Semi-integral abutment details of concrete girder bridge with overall span < 328 ft	42
Figure 2-42. Semi-integral abutment details of concrete girder bridge with overall span > 328 ft	43
Figure 2-43. Semi-integral abutment details of steel girder bridge with overall span < 328 ft	44
Figure 2-44. Semi-integral abutment details of steel girder bridge with overall span > 328 ft	44
Figure 2-45. VDOT semi-integral system with EPS (Hoppe 2005)	46
Figure 2-46. Typical details of EPS abutment (Stark et al. 2004)	48
Figure 2-47. Deck sliding over backwall: (a) NYDOT and (b) MDOT	49
Figure 2-48. Preliminary bearing selection diagram for minimal design rotation (rotation \leq 0.005 radians) (source: Roeder and Stanton 1996).....	51
Figure 2-49. Preliminary bearing selection diagram for moderate design rotation (rotation \leq 0.015 radians) (source: Roeder and Stanton 1996).....	51
Figure 2-50. Preliminary bearing selection diagram for large design rotation (rotation > 0.015 radians) (source: Roeder and Stanton 1996).....	52
Figure 2-51. Preliminary bearing selection diagram (Badie, et al. 2001).....	52
Figure 2-52. MDOT semi-integral abutment configuration	53
Figure 2-53. Backwall and abutment configuration of a bridge with different girder depths	54
Figure 2-54. Reinforcement layout (AASHTO LRFD 2007).....	54
Figure 2-55. End zone reinforcement details (MDOT Bridge Design Guide 6.41.02)	56
Figure 2-56. Link slab cracking on S08 of 63101 (Gilani and Jansson 2004).....	57
Figure 2-57. Link slab design detail and an inspection photo (Gilani and Jansson 2004)	58
Figure 2-58. Abutment wall cracking near an acute corner of the superstructure	59
Figure 2-59. Semi-integral abutment configuration used by the Ontario MOT before most recent details	60
Figure 3-1. Bridge location (Source: Google map)	64

Figure 3-2. Arial view of the bridge (Source: Google map).....	64
Figure 3-3. Isometric and elevation views of the bridge	65
Figure 3-4. Schematic view of bridge cross section	65
Figure 3-5. Schematic view of diaphragms and girders with labels	66
Figure 3-6. Schematic view of end and intermediate diaphragms (cross frames)	66
Figure 3-7. Schematic view of abutment section with backwall, girder and foundation.....	67
Figure 3-8. Schematic view of girder plan and elevation	68
Figure 3-9. Schematic view of respective bearing details	69
Figure 3-10. Interior and exterior bearing condition at north abutment	70
Figure 3-11. Expansion bearing and joint condition at south abutment	70
Figure 3-12. Expansion bearing condition at south abutment	71
Figure 3-13. Expansion joint and deck condition	72
Figure 3-14. FE model configuration.....	73
Figure 3-15. Truck configuration and wheel loads	74
Figure 3-16. Truck positions and bridge configuration	75
Figure 3-17. Mutually exclusive bridge loading configurations.....	75
Figure 3-18. Girder labels and 16 displacement measurement points	76
Figure 3-19. Girder bottom flange out of plane deformation, girder end translations, and vertical deflection contours under loading configuration-I	76
Figure 3-20. Girder bottom flange out of plane deformation, girder end translations, and vertical deflection contours under loading configuration-II	77
Figure 3-21. Girder bottom flange out of plane deformation, girder end translations, and vertical deflection contours under loading configuration-III.....	77
Figure 3-22. Girder bottom flange out of plane deformation, girder end translations, and vertical deflection contours under loading configuration-IV.....	78
Figure 3-23. Laser Tracker	79
Figure 3-24. Reflectors (targets) used with the Laser Tracker	80
Figure 3-25. AT MeteoStation.....	80
Figure 3-26. Graphical user interface (GUI) window.....	80
Figure 3-27. Accessories used for mounting girder end and abutment targets.....	82
Figure 3-28. Laser Tracker, server, and computer.....	83

Figure 3-29. South abutment of the westbound bridge (targets on abutment and girder ends)	84
Figure 3-30. North abutment of the westbound bridge (targets on abutment and girder ends)	84
Figure 3-31. Target positions on girders	85
Figure 3-32. Coordinate system for Tracker measurements and target positions on north abutment and girder ends	85
Figure 3-33. Truck configurations and wheel loads	87
Figure 3-34. Truck positions and bridge configuration	87
Figure 3-35. Mutually exclusive bridge loading configurations	88
Figure 3-36. Girder A deflection under loading configuration II	89
Figure 3-37. Girder G deflection under loading configuration IV	89
Figure 3-38. Bearing movement under truck loads (FE analysis)	90
Figure 3-39. 3-D view of bearing movement (towards south abutment) under loading configuration IV	91
Figure 3-40. Bearing movement under truck loads (Tracker measurements)	92
Figure 3-41. Bearing positions after loading and unloading following load configuration II and IV	92
Figure 3-42. Bearing translation under uniform thermal loads (FE analysis)	94
Figure 3-43. Maximum and minimum daily temperature variation at the site	95
Figure 3-44. Average temperature variation at the site	96
Figure 3-45. Bearing translation from Dec. 2010 to May 2011 and July 2011 (Tracker measurements)	97
Figure 4-1. Cross section of Bridge S12-7 of 25042	101
Figure 4-2. Current MDOT requirements for two-lane highway bridges	102
Figure 4-3. MDOT New Jersey Type 4 barriers	103
Figure 4-4. Cross section of bridge	103
Figure 4-5. Elevation view of FE bridge	104
Figure 4-6. Bridge model orientation and labeling system	104
Figure 4-7. Cross section view of single girder and deck	106
Figure 4-8. Elevation view of mesh at link slab region	106

Figure 4-9. Isometric view of bridge models.....	107
Figure 4-10. Skew link slab mesh.....	108
Figure 4-11. Contact surfaces in the FE models.....	109
Figure 4-12. Abaqus syntax used in FE bridge model.....	109
Figure 4-13. Bearing configuration layout.....	110
Figure 4-14. Live load cases.....	111
Figure 4-15. Truck and lane load locations.....	112
Figure 4-16. Temperature gradient.....	113
Figure 4-17. Sign convention.....	115
Figure 4-18. Total sectional moment - Lane1 load case.....	118
Figure 4-19. Total sectional moment - Lane2 load case.....	119
Figure 4-20. Total sectional moment – LaneAlt1 load case.....	120
Figure 4-21. Total sectional moment – LaneAlt2 load case.....	121
Figure 4-22. Total sectional moment - NTG load case.....	122
Figure 4-23. Total sectional moment - PTG load case.....	123
Figure 4-24. Total sectional force - Lane1 load case.....	124
Figure 4-25. Total sectional force - Lane2 load case.....	125
Figure 4-26. Total sectional force – LaneAlt1 load case.....	126
Figure 4-27. Total sectional force – LaneAlt2 load case.....	127
Figure 4-28. Total sectional force - NTG load case.....	128
Figure 4-29. Total sectional force - PTG load case.....	129
Figure 4-30. Effective width segments.....	132
Figure 4-31. Effective moment - Lane1 load case.....	133
Figure 4-32. Effective moment - Lane2 load case.....	134
Figure 4-33. Effective moment – LaneAlt1 load case.....	135
Figure 4-34. Effective moment – LaneAlt2 load case.....	136
Figure 4-35. Effective moment - NTG load case.....	137
Figure 4-36. Effective moment - PTG load case.....	138
Figure 4-37. Effective force - Lane1 load case.....	139
Figure 4-38. Effective force - Lane2 load case.....	140
Figure 4-39. Effective Force – LaneAlt1 load case.....	141

Figure 4-40. Effective Force – LaneAlt2 load case	142
Figure 4-41. Effective force - NTG load case.....	143
Figure 4-42. Effective force - PTG load case	144
Figure 4-43. Edge stresses of link slab with HRRR support conditions under live loads ...	147
Figure 4-44. Edge stresses of link slab with RRHR support conditions under live loads ...	148
Figure 4-45. Edge stresses of a 45 ⁰ skew link slab under PTG	149
Figure 4-46. Stresses developed in 45 ⁰ skew link slab with HRRR support conditions under LaneAlt1 load case.....	151
Figure 4-47. Gross section moment with and without soft material – LaneAlt1 load case.	152
Figure 4-48. Edge stresses developed under PTG - 45 ⁰ skew link slab with soft material over girder ends.....	154
Figure 4-49. Link slab bottom fiber stresses under PTG load	155
Figure 4-50. Longitudinal stress distribution across north end of the 45 ⁰ skew link slab bottom fiber under PTG with HRRR support configuration	156
Figure 4-51. Longitudinal stress distribution across south end of the 45 ⁰ skew link slab bottom fiber under PTG with RRHR support configuration	156
Figure 4-52. Stresses in link slab with HRRR under PTG	157
Figure 4-53. AASHTO Type III girder and composite section geometric properties	164
Figure 5-1. Deck sliding over backwall details	170
Figure 5-2. Semi-integral abutment details.....	171
Figure 5-3. Semi-integral abutment detail used in Ontario and several other states	172
Figure 5-4. Rub plates at backwall - wingwall interface (Source: VDOT 2010)	173
Figure 5-5. Rub plates at deck-wingwall interface (Source: VDOT 2010)	173
Figure 5-6. Bearing retainer detail (Source: Steinberg and Sargand 2010; Roeder and Stanton 1996)	174
Figure 5-7. Dowel bar details for resisting lateral loads on shallow bearing (Source: Roeder and Stanton 1996).	174
Figure 5-8. Concrete key system for resisting lateral forces (Source: Roeder and Stanton 1996).	174
Figure 5-9. Live load configuration for <i>CASE IV Contraction</i>	177
Figure 5-10. Live load configuration for <i>CASE IV Expansion</i>	178

Figure 5-11. Location of girder 1 and 8 where girder end rotation was calculated.....	179
Figure 5-12. Truck position 1 for girder end rotation calculation	180
Figure 5-13. Truck position 2 for girder end rotation calculation	180
Figure 5-14. Truck position 3 for girder end rotation calculation	181
Figure 5-15. Deck sliding over backwall model description	184
Figure 5-16. Abutment and girder end distress.....	186
Figure 5-17. Girder 1 and 8 end rotation over abutment	187
Figure 5-18. Thermal expansion of a skew bridge	190
Figure 5-19. Maximum longitudinal bridge contraction and expansion.....	190
Figure 5-20. Variation of concrete bridge expansion length against width and skew when strip seal joint width of 3 in. available for thermal movement	191
Figure 5-21. Variation of steel girder bridge expansion against width and skew when strip seal joint width of 3 in. available for thermal movement	191
Figure 5-22. Girder 1 and 8 reaction variation over the abutment and pier.....	193
Figure 5-23. Transverse bearing force over abutment under thermal contraction strength load combination.....	196
Figure 5-24. Transverse bearing force over abutment under thermal expansion strength load combination.....	197
Figure 5-25. Typical bearing details	198
Figure 5-26. Semi-integral bridge model with wingwalls (not drawn to scale)	199
Figure 5-27. Girder 1 reaction of semi-integral bridge	200
Figure 5-28. Transverse bearing force over abutment under thermal contraction strength load combination.....	203
Figure 5-29. Transverse bearing force over abutment under thermal expansion strength load combination.....	204
Figure 5-30. Wingwall force due to thermal expansion without transverse restraint over the abutment under strength load combination.....	204

1 INTRODUCTION

1.1 OVERVIEW

High skew link slab design and design details are described in this report. Abutment and bearing redesign is also described for implementing link slabs on existing high skew bridges during repair activities.

A new bridge design and construction trend to help improve durability and rideability is to remove expansion joints over piers and abutments. One approach to achieve this is to make the deck continuous over the piers by means of a link slab while the girders remain simply supported. The need to implement link slabs is indicated by AASHTO LRFD (2010) section 2.5.2.4 that stipulates the use of minimum number of expansion joints to improve rideability. Further, due to durability concerns associated with bridge deck joints, as stated in Aktan et al. (2002), it is preferred to have as few joints as possible or to develop jointless decks.

In most unremarkable bridges, expansion joints over the abutments can be removed during repair activities. The deck and approach slab can be made continuous based on one of three designs: deck sliding over backwall, semi-integral abutments, and integral abutments. These designs will develop expansion joints at either or both ends of the approaches. Link slabs can be incorporated in repair activities such as partial deck replacement and shallow or deep overlay projects. In the case of full deck replacement, bearings can also be redesigned to allow for the desired movement. The design concerns, other than link slab, include backwall, wing-wall, and bearings. The behavior of jointless bridges brings about many challenges to bridge designers. The complexity is augmented when skew is involved.

The skew policy described in section 7.01.14 of the MDOT Bridge Design Manual (2005), requires special design by refined analysis methods for bridges with skew greater than 30° but less than or equal to 45° . Further, for skew greater than 45° , special approval through bridge design is required. These requirements reflect the complexity of the structure when the skew is involved.

This report complements an earlier report on *Combining Link Slab, Deck Sliding Over Backwall and Revising Bearings* (Aktan et al. 2008) where the behavior of straight and moderately skew ($\text{skew} \leq 20^\circ$) link slab bridges were investigated, and design recommendations were developed. This report will describe the behavior and performance of high skew ($\text{skew} > 20^\circ$) jointless bridges with link slabs and two abutment configurations. These abutment configurations are deck sliding over backwall and backwall sliding over abutments (semi-integral abutments). This report is intended to be a tool to the designers in the design of specific components and design detail recommendations that are intended to improve the durability performance of high skew bridges constructed with the link slabs and deck sliding over backwall or backwall sliding over the abutments.

1.2 PROJECT OBJECTIVES AND TASKS

The objective of this project was to assess the performance and behavior of a high skew bridge structural system with link slabs and sliding deck over backwall or backwall sliding over abutment (semi-integral). The high skew bridge assessment was based on literature review, load testing, and analytical modeling and analysis. The project goal was to propose fine-tuning of the design assumptions and design details for the link slab and the abutment region.

The project tasks were as follows: (1) literature review, (2) assessment of skew bridge behavior under static truck loads and thermal expansion, (3) analytical and numerical analysis of skew link slabs, and (4) analytical and numerical analysis of skew sliding deck over backwall systems and semi-integral abutments.

1.3 REPORT ORGANIZATION

The report is organized with 7 chapters.

- The Literature Review is presented in chapter 2 describing skew/jointless bridge behavior, modeling and analysis of skew bridge structural system/components, design and detailing of deck sliding over backwall and semi-integral abutments, and performance of jointless bridges.

- High skew bridge assessment under truck loads and thermal loads is presented in chapter 3.
- Chapter 4 describes skew link slab analysis and design.
- Chapter 5 describes skew abutment analysis and design.
- Chapter 6 presents the comprehensive results, recommendations, the need for further work, and
- Chapter 7 lists the references.

Intentionally left blank

2 STATE-OF-THE-ART LITERATURE REVIEW

The objective of the literature review was to identify, review, and synthesize information related to skewed/jointless bridges. Finite element modeling of simply supported skewed bridges is also incorporated in various sections of the chapter to compare with and/or to benchmark the pertinent information available in literature. Concentration areas for the review are established for the project, and the following aspects will be discussed:

- Skewed bridge behavior under gravity loading,
- Skewed bridge behavior under volume change loads,
- Design challenges of skewed/jointless bridges, and
- Performance of skew/ jointless bridges.

2.1 OVERVIEW

A skewed bridge is one in which the major axis of the substructure is not perpendicular to the longitudinal axis of the superstructure. The skew angle (most commonly in degrees) is defined as the angle between the axis normal to the bridge centerline and the axis along the abutment or pier cap centerline. Some highway agencies use a different convention. As an example, Michigan uses the angle of crossing which is the acute (small) angle formed between the longitudinal bridge axis and the abutment or pier cap centerline axis (Figure 2-1).

The majority of bridge decks built today have some form of skew, taper or curve. Because of the increasing restriction on available space for traffic schemes, the alignment of a transportation system can seldom be adjusted to reduce the skew. A skew angle greater than 20° alters the bending moment and shear developed in a bridge compared to those of a straight bridge. Skew bridge decks are prone to develop deck corner cracking (Fu et al. 2007).

About two-thirds of bridges nationwide are skewed (AASHTO LRFD 2010). According to the Pontis database, as of 2006, there are about 2,800 bridges in Michigan with a skew angle greater than 20° (Figure 2-2). This is in excess of 20 percent of the total bridge population of

12,691 bridges. Twenty percent of the concrete bridges and 30 percent of the steel bridges in Michigan's bridge inventory have a skew angle greater than 20° (Figure 2-3).

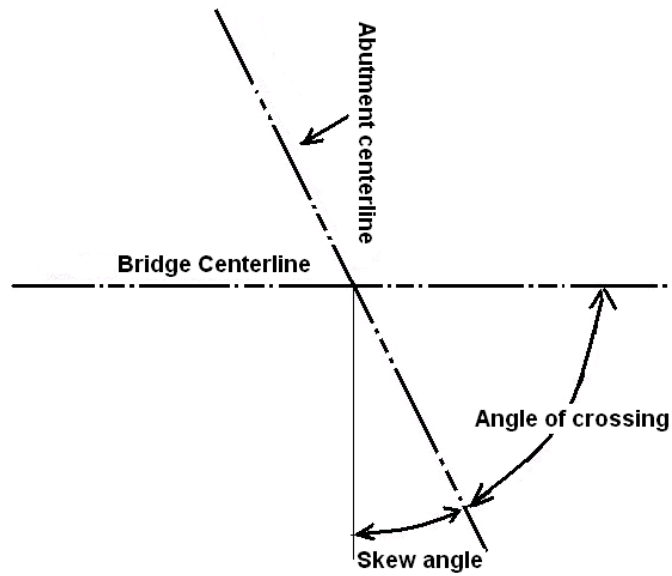


Figure 2-1. Geometric relation of skew angle and angle of crossing

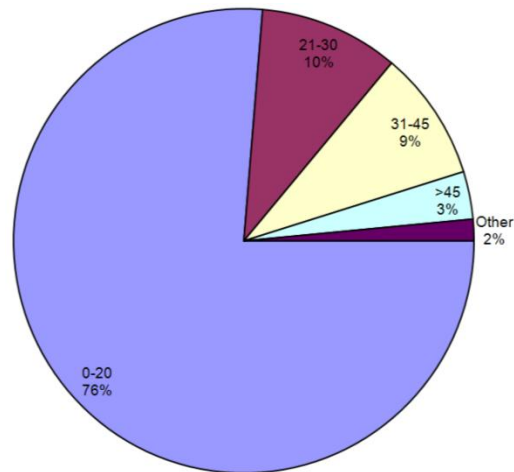


Figure 2-2. Percentages of skew bridges in Michigan

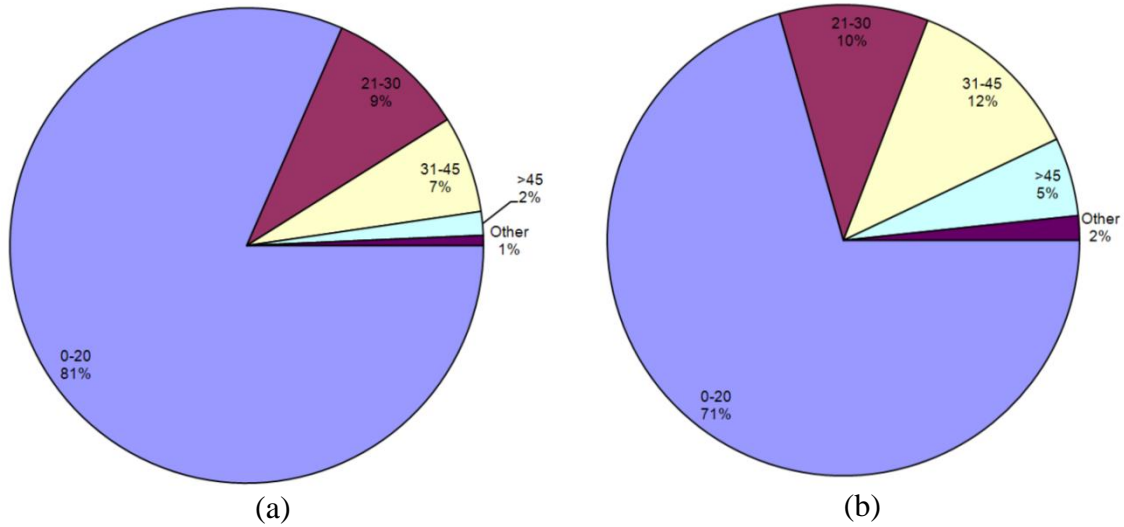


Figure 2-3. Percentage of skewed bridges in Michigan (a) concrete and (b) steel

2.2 SKEWED BRIDGE BEHAVIOR UNDER GRAVITY LOADING

In slab bridges and other bridges with high torsional rigidity, the load path develops between the obtuse ($>90^\circ$) corners of the span (Figure 2-4). Longitudinal bending moments are reduced, but shear forces are increased in the obtuse corners (Figure 2-5). The special characteristics of the load response characteristics of a skewed solid slab bridge are summarized in Hambly (1991) as follows:

1. Variation in direction of calculated maximum bending moment across bridge width (Figure 2-5),
2. Hogging (negative) moments near obtuse ($>90^\circ$) corner,
3. Torsion developing on the deck,
4. Larger reactions and shear forces near obtuse corner, and
5. Lower reactions and possible uplift in acute ($<90^\circ$) corner.

The effects described above may also occur in stringer bridges, but they are much less pronounced. In stringer bridges, such as I- Tee- or bulb-tee beam bridges, the load tends to flow along the length of the supporting beams, and the effect of skew on the bending moments is reduced (Figure 2-4).

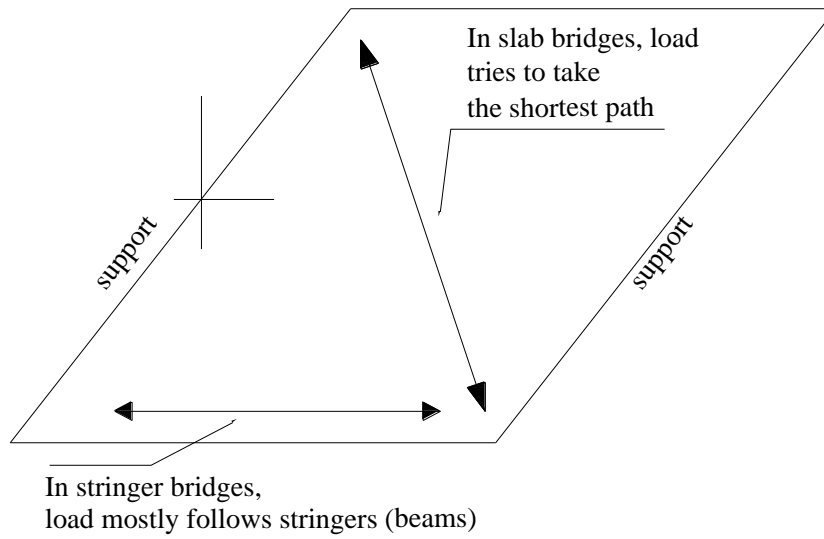


Figure 2-4. Load distribution pattern in skewed stringer and slab bridges.

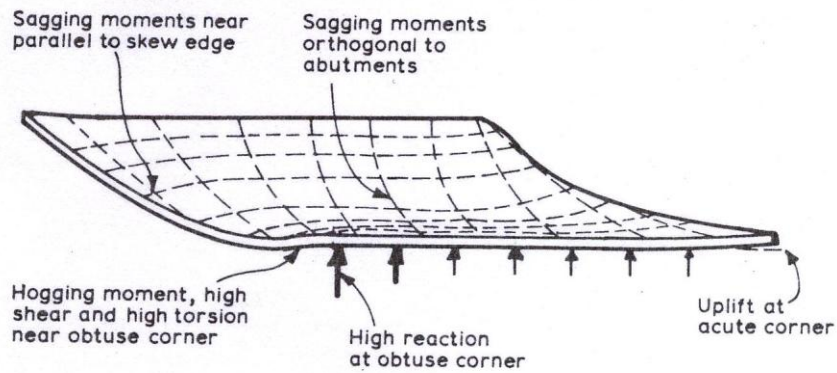


Figure 2-5. Characteristics of skewed slab deck (Hambly 1991).

Non-uniform girder end rotations of skew bridges under uniformly distributed load are observed across the bridge. If the torsional stiffness of the slab and girders is low, this distortion of deck may occur without creating large reaction forces. Under a concentrated load, beams behave similar to those of orthogonal bridges, and the load distribution still takes place by transverse bending of the slab. However, the increase in shear force and reaction at the obtuse corner may be significant and should be considered in girder and bearing design. Continuous decks may also exhibit large shear forces and reactions, particularly in the region of intermediate supports (Hambly 1991). The size of these effects depends on the skew angle, width to span ratio, and primarily on the type of deck construction and the supports.

2.2.1 Finite Element (FE) Simulation of Skew Bridge Behavior under Gravity Loading

Finite element (FE) models are developed to evaluate the effects of various types and levels of loads on the behavior of simply supported skewed bridges. The primary aim in FE analyses is to develop a clear representation of the behavior of skewed bridges as presented in literature. Three-dimensional FE models are developed representing two major design categories: a solid slab bridge and a stringer bridge. A three-dimensional solid continuum brick element, which has three translational degrees of freedom at each node, is used to model bridge components (girders and deck). The analyses are particularly concentrated on stringer type bridges due to their significant presence.

The models developed for the analysis of skewed bridges are for a fictitious bridge with a span to width ratio of two (2). The span length is 63-ft 4-in. (760 in.) and the bridge width is 31-ft 8-in. (380 in.). The stringer bridge has five PCI Type III interior girders with a nine inches thick concrete deck (Figure 2-6). The span and width of the solid slab bridge are identical to the stringer bridge. A solid slab bridge with the current dimensions would neither meet the strength nor service requirements. However, the primary aim in these analyses is to demonstrate the skew effects. The bridges are constrained so that one end would be free for longitudinal movement. The other end would be restrained in the longitudinal and vertical directions with only the center node pinned in all three translational directions as shown in Figure 2-7. Skew angle is varied between zero and 60°. Resulting moment outputs are obtained at multiple points along the lines parallel to the skewed edge (Figure 2-7). Moment resultants are obtained for the full-width of the structure. In the case of stringer bridges, individual girder moments are not obtained since the primary aim is not set towards live load distribution.

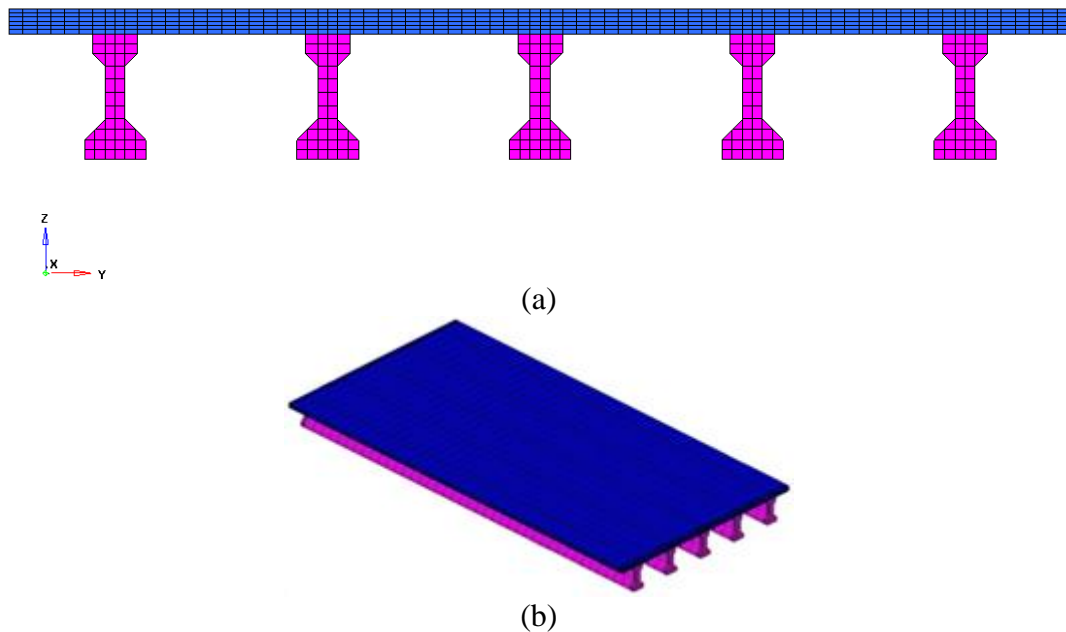


Figure 2-6. (a) Cross section and (b) isometric views of the stringer models

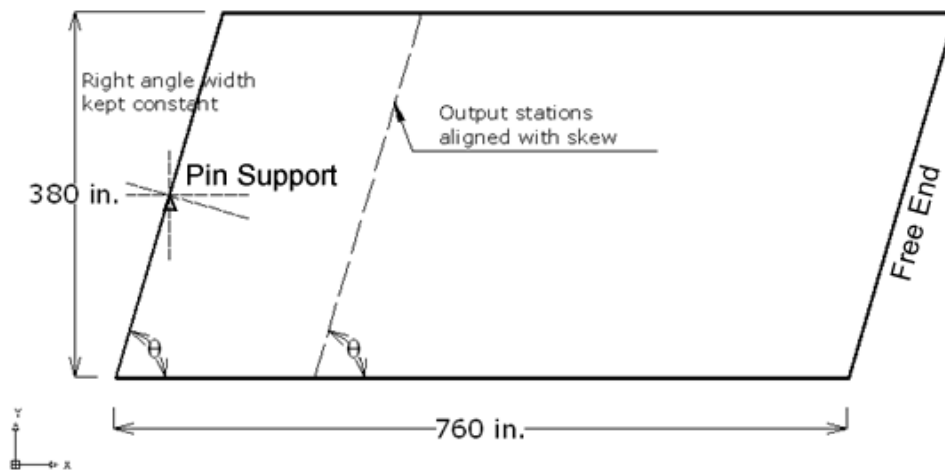


Figure 2-7. Plan view of FE models

Deck and girder design strengths are different in various states throughout the U.S. The Michigan Department of Transportation (MDOT) requires a minimum compressive strength of the girder and deck concrete of 4500 psi. This is the value used to calculate the concrete modulus as per AASHTO LFRD (2010) Section 5.4.2.4 for the FE models. Poisson's ratio of 0.2 is used for both deck and girder concrete. Unit weight of concrete is taken as 150 lb/ft³. Two independent load cases are considered: self-weight and a concentrated load of 50 kips that is placed at the center of mid-span.

2.2.1.1 Analysis Requirements of Simple Span Skew Bridges

Menassa et al. (2007) investigated the effects of different skew angles on reinforced concrete slab bridges. Ninety-six bridge configurations were developed and analyzed considering various geometric bridge characteristics including the span length and slab width with six different skew angles. FE analyses results of skewed bridges were compared to the reference straight bridges as well as the AASHTO Standard Specifications and LRFD procedures. Under live load, maximum longitudinal moment decreased, whereas, maximum transverse moment increased with increasing skew angles. The variation in moment was significant for skew angles greater than 20° . The research concluded that skew angles less than or equal to 20° can be designed as a straight bridge. This conclusion complies with the AASHTO Standard and LRFD (2002 and 2010). Menassa et al. (2007) recommended using three-dimensional finite element analysis for bridges with a skew angle greater than 20° .

The skew policy described in the MDOT Bridge Design Manual (MDOT 2005) section 7.01.14 requires special design by refined analysis methods for bridges with skew greater than 30° but equal or less than 45° . Further, if the skew is greater than 45° , refined analysis as well as special approval through bridge design is required.

2.2.1.2 FE Simulation of Simple Span Skew Bridges under Gravity Loads

Finite element analyses results are utilized to make a comparison with the available literature on skewed bridges. First, a brief comparison between the stringer and solid slab type bridges is presented, and then detailed results are provided only for the stringer type bridges.

The transverse bending stress (stress Y-Y) distribution of stringer and solid slab type bridges under self-weight are shown in Figure 2-8 which agrees with the representation of the load path depicted in Figure 2-4. Figure 2-9 shows only the negative (hogging) longitudinal bending stress regions under self-weight for the two different bridge types. Hogging (negative) moment regions are displayed near obtuse corners. The general effects of gravity loading, i.e., decreased longitudinal moments, high shear and reactions in obtuse corners, can be seen under both dead and concentrated load.

Longitudinal bending moment plots for stringer type bridges are given in Figure 2-10 and Figure 2-11 under self-weight and concentrated loads, respectively. The longitudinal bending moment decreases nonlinearly with an increasing skew angle, irrespective of the load type (Figure 2-12). The bending moments decrease by about 13 and 19 percent with an increased skew from 0° to 60° under self-weight and concentrated loads, respectively. Straight simply supported bridges do not develop any torsion under symmetrical gravity loading. However, with skew, significant torsion of the deck is generated. Torsion distribution along the length of the stringer bridge for different skew angles is shown in Figure 2-13 and Figure 2-14 under self-weight and concentrated loads, respectively. Torsion is constant apart from the supports and increases with increasing skew angle. Support Reaction variations for obtuse and acute corners are presented in Figure 2-15 under self-weight. The reaction force in the obtuse corner increases by up to 30 percent, whereas a 10 percent decrease is observed in the acute corner when skew angle is increased from 0° to 60° .

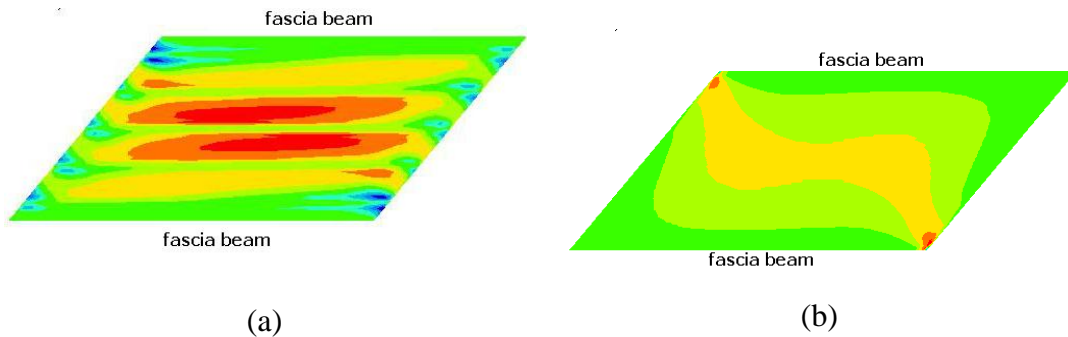


Figure 2-8. Transverse bending stress distribution of deck for (a) stringer bridge deck and (b) solid slab for 40° skew under self-weight

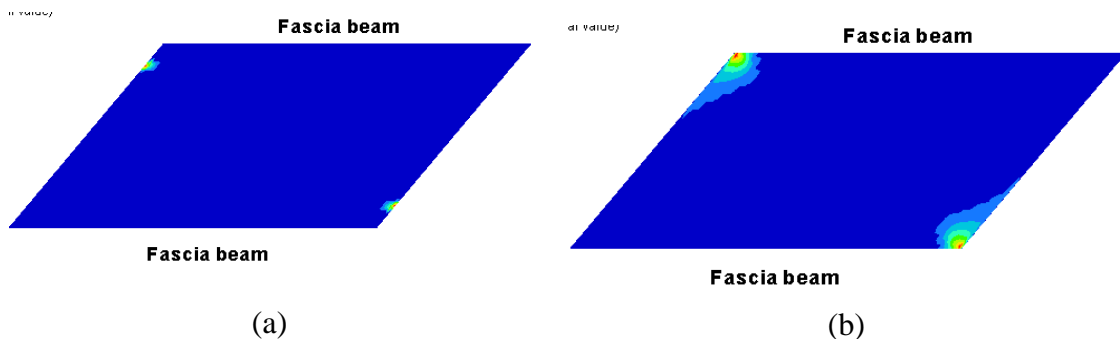


Figure 2-9. Longitudinal bending stress distribution (a) stringer (b) solid slab bridge of 40° skew under self-weight (negative moment regions only)

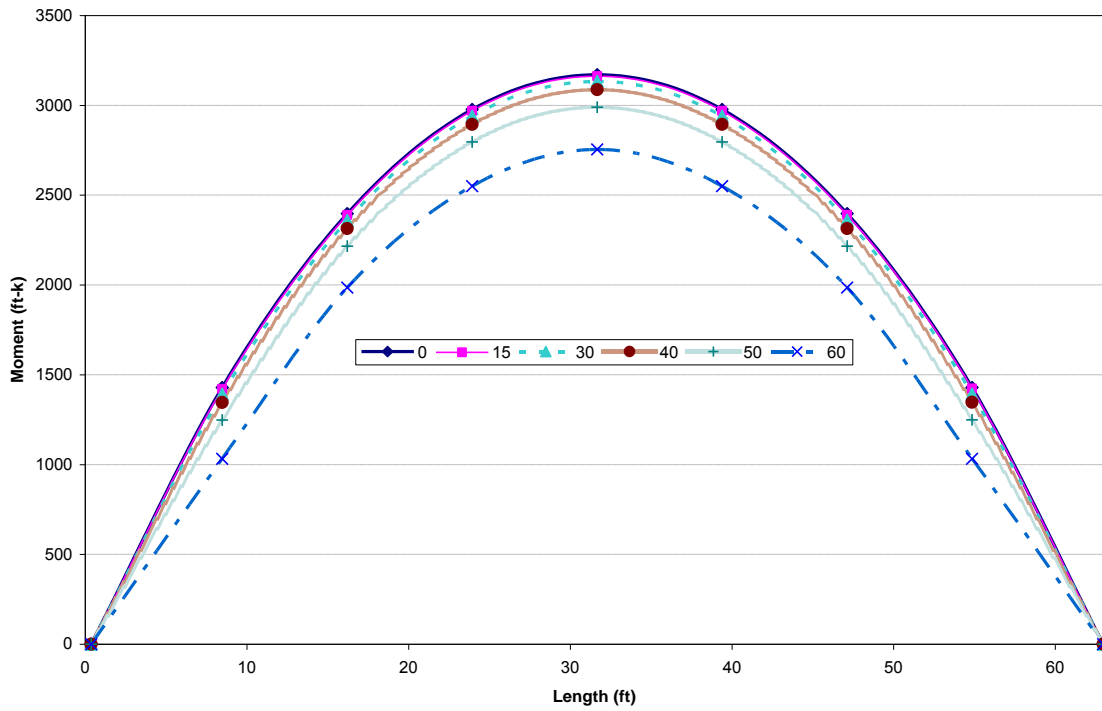


Figure 2-10. Longitudinal bending moment variation against skew for full-width stringer bridge under self-weight

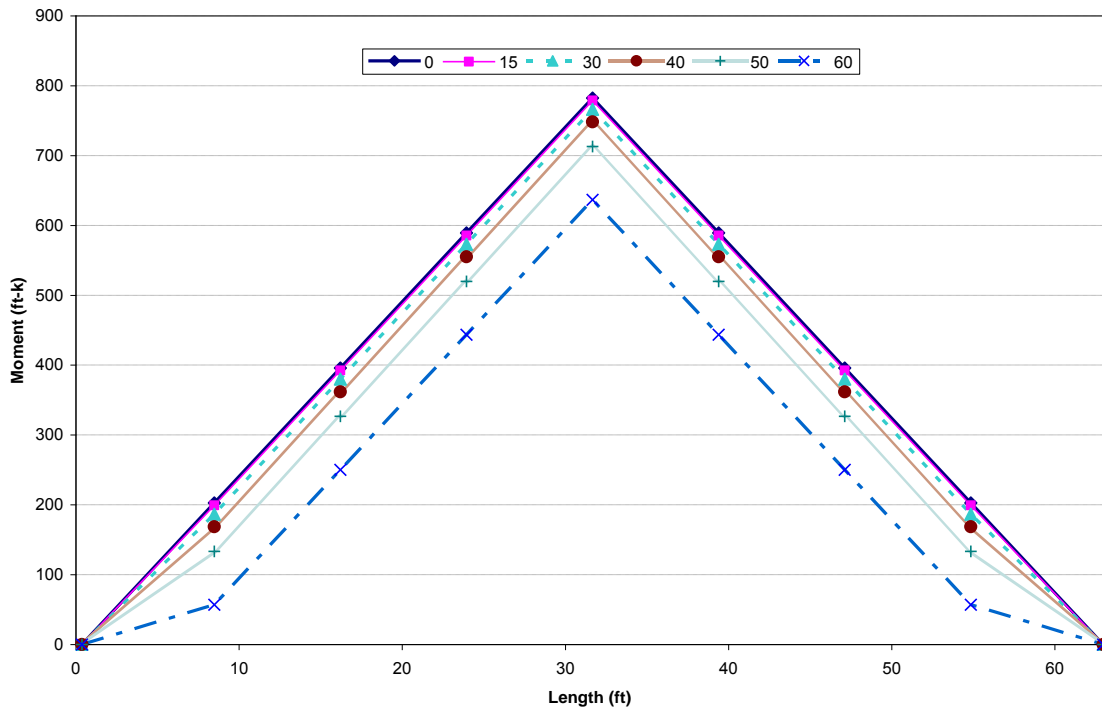


Figure 2-11. Longitudinal bending moment variation against skew for full-width stringer bridge under a concentrated load

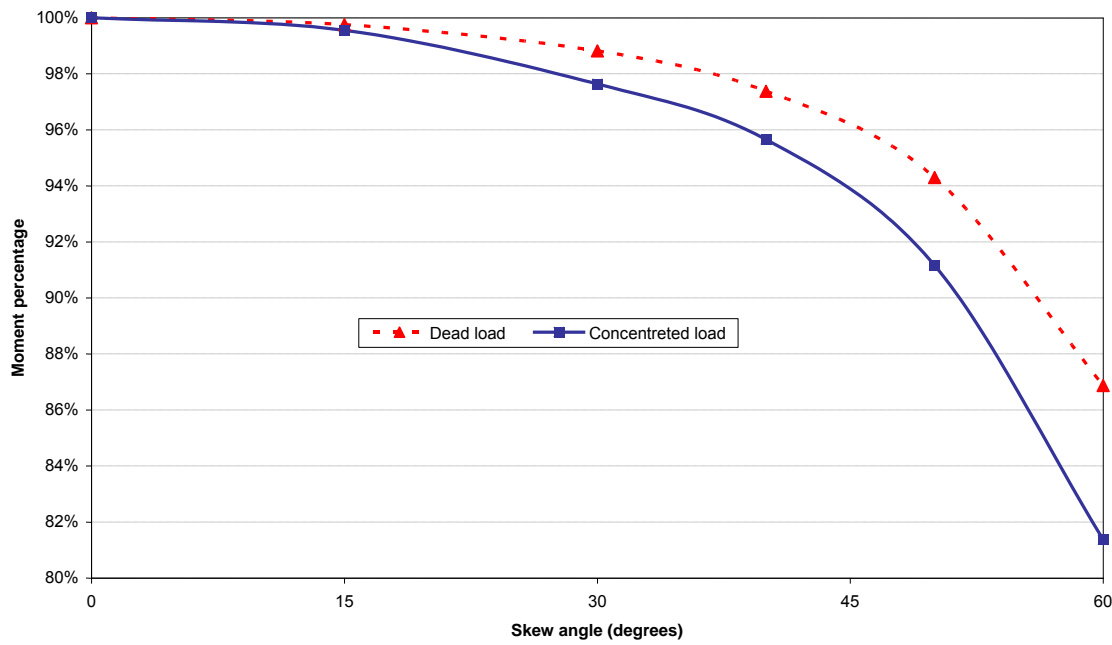


Figure 2-12. Mid-span moment variation vs. skew angle under self-weight and concentrated load for stringer bridge

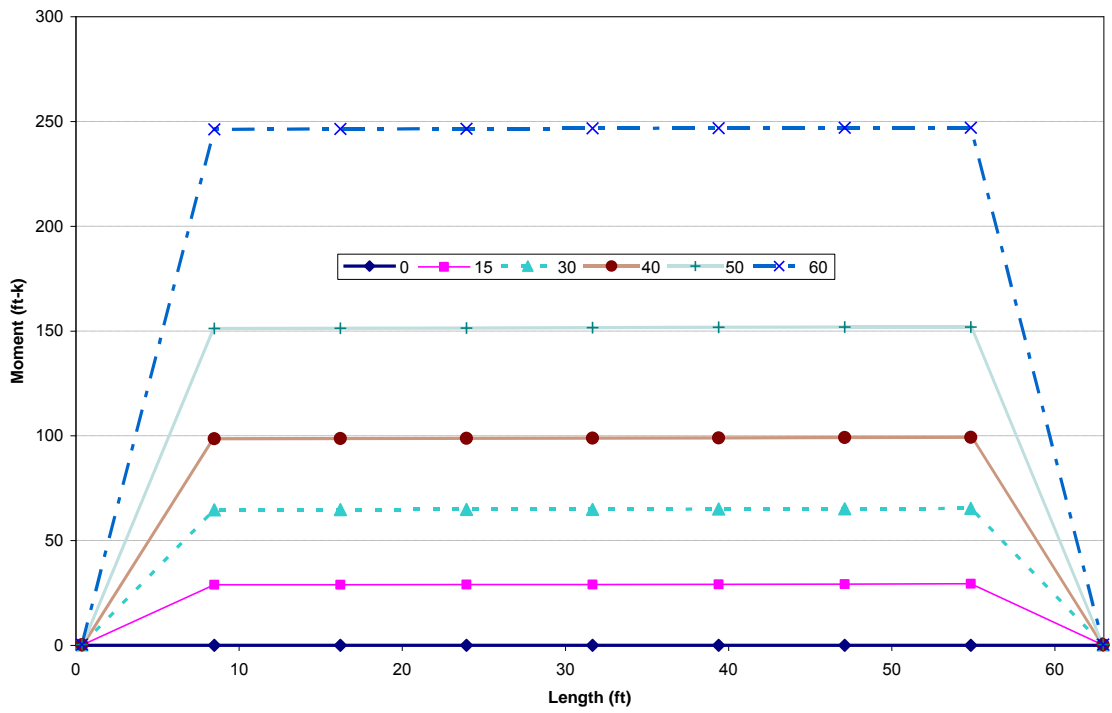


Figure 2-13. Torsion for full-width of stringer bridge under self-weight

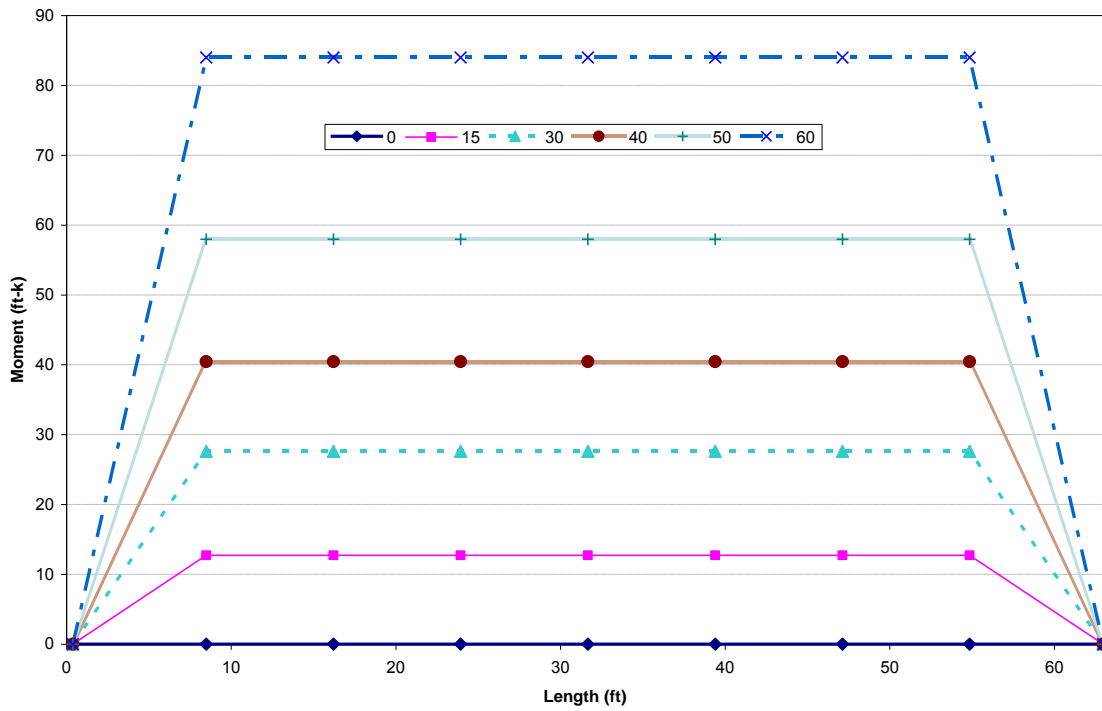


Figure 2-14. Torsion for full-width of stringer bridge under concentrated load

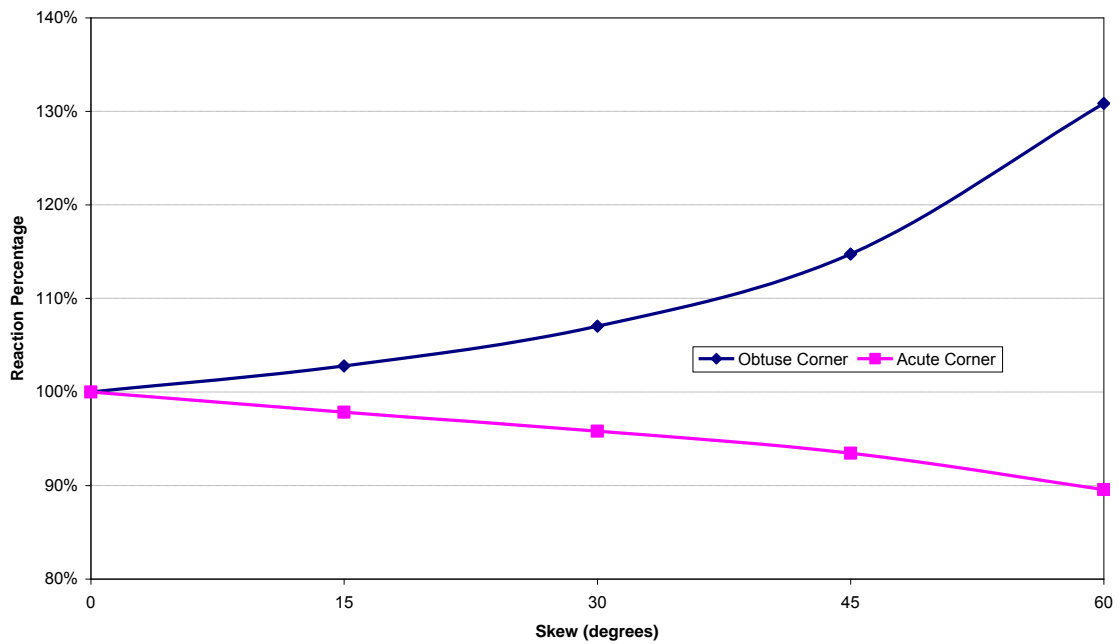


Figure 2-15. Support reaction vs. skew angle for stringer bridge under self-weight

2.3 SKEWED BRIDGE BEHAVIOR UNDER VOLUME CHANGE LOADS

Skewed bridges exhibit a complex response pattern under volume change loads with regard to both bearing deformations and restraint forces. Transverse movement is generated in wider bridges that tend to rotate with respect to the vertical axis. Restraint forces vary considerably with skew and show nonlinear behavior (Tindal and Yoo 2003). The direction of movement and rotation of bearings for curved and high skew bridges depends on many factors and is not easily determined. However, the major axis of thermal movement on a high skew bridge is most generally along the diagonal between the acute corners (Figure 2-16). The alignments of the bearings and layout of the keeper blocks parallel to the axis relieve all the stresses; yet implementation is not very practical (AASHTO LRFD 2010).

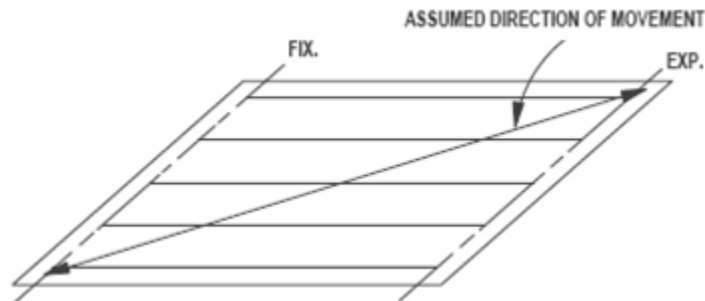


Figure 2-16. Direction of skew simply supported bridge movement under uniform thermal load

Round bearings are recommended for curved and high skew bridges since they can accommodate movement and rotations in multiple directions. Round bearings also require a narrower bridge seat on skew bridges (Najm et al. 2007).

According to a survey conducted by Najm et al. (2007), eight out of 39 state DOTs (21%) have used round bearings. Eighteen states (46%) were willing to consider using them. Agencies have used round bearings on curved and high skew bridges, and on pier caps with limited space. According to the survey results, 29% of the round bearing applications were for mild skew bridges, 50% for high skew, and 21% for curved bridges. As for bridge length and type, most of the bridges with round bearings have spans less than 115 ft long, and two-thirds of these bridges were precast concrete girder bridges while the remaining were steel stringer .

An FHWA study conducted by Yazdani and Green (2000) showed that the effect of increasing bearing stiffness is both beneficial and detrimental to the skew bridge system depending on boundary conditions. Bearing pads with a higher shear modulus will reduce midspan deflection in high skew bridges. Intermediate diaphragms also reduce overall midspan deflection and maximum stresses; yet the reductions were smaller for high skew bridges. Deflections would decrease by about 17% for straight bridges, but only about 5% for 60° skew bridges when intermediate diaphragms are used.

There are various bearing orientations discussed in literature (Tindal and Yoo 2003) that allow transverse movement as shown in Figure 2-17. In the traditional case, bearings are fixed both longitudinally and transversely at one end allowing expansion at the opposite end, only in the longitudinal direction (Figure 2-17a). In other alternatives, a single bearing at the corner (Figure 2-17b) or at the center (Figure 2-17c) of one end is restrained allowing rest of the bearings to expand or contract freely in both longitudinal and transverse directions. It should be noted that for cases where only single bearing is restrained (radial from corner or radial from center), longitudinal or transverse bearing forces will not develop under uniform strain (i.e., under uniform thermal loading). However, under thermal gradient load, transverse bearing forces will develop.

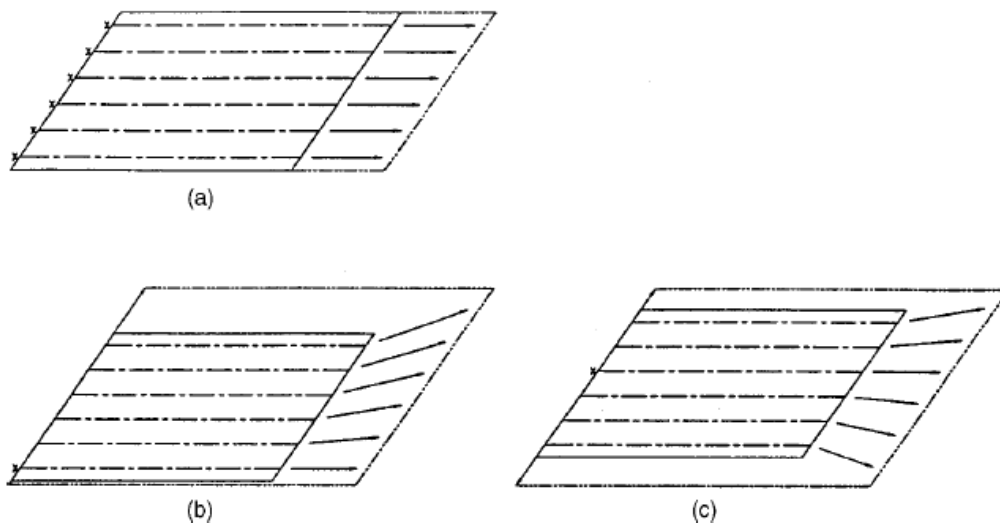


Figure 2-17. Bearing orientation for constraint cases (a) traditional, (b) radial from corner, (c) radial from center (Tindal and Yoo 2003)

Tindal and Yoo (2003) performed a parametric study investigating all three constraint configurations shown in Figure 2-17 for simply supported skew bridges under both winter and summer thermal loads. It should be noted that, although not explicitly stated in the study, in order to achieve the expansion profiles shown in Figure 2-17, expansion bearings should have guided plates to facilitate deformations in the direction of reference line. If the expansion bearings were only vertically restrained, the expansion profile would also change and follow a more random pattern. This behavior is further investigated and will be discussed later in this chapter.

Tindal and Yoo (2003) also investigated the effect of thermal gradient loading. A uniform temperature profile was imposed through the girder depth and linearly increasing profile along the deck thickness. Restraint forces at bearings varied considerably with skew angle. Restraint force trends for all cases were nonlinear and showed substantial differences. In both radial from corner and radial from center cases, bearing forces substantially reduced for all skew angles. Bearing orientation, shown in Figure 2-17b, performed best for skew angles less than 20° and greater than 55° , whereas the orientation shown in Figure 2-17c performed better for intermediate skew angles. Skewed bridges developed large bearing forces under the traditional bearing configuration (Figure 2-17a), which would explain the tendency of the bridges to rotate about their supports (i.e., about the vertical axis of a bridge). Under the traditional and the radial from corner bearing orientations, maximum reaction was always at the acute angle of the fixed end. This was not always the case for radial from center bearing orientation.

Moorthy and Roeder (1992) performed a parametric study considering skew angle, width and length, and the expansion joint and bearing pad characteristics of a bridge. A three-span, composite, continuous steel-girder bridge was used as the primary structural system. Girder translations were fixed with pin bearings on one abutment, whereas beams were supported on rocker bearings on all other supports that restrained transverse translations. The bridge included expansion joints at both abutments. A thermal gradient load was applied with a nearly uniform profile along the height of the girder while varying nonlinearly about 20°F through the concrete deck. The resulting longitudinal displacements of the straight bridge were uniform across the width. With increasing skew, maximum longitudinal displacements

were calculated along the diagonal between acute corners (Figure 2-18). The transverse displacements of the straight bridge were symmetrical about the longitudinal axis. With increasing skew, maximum transverse displacements were obtained along the diagonal between acute corners (Figure 2-19). A comparison of normalized longitudinal and transverse displacements with respect to skew angle is also shown in Figure 2-20. Longitudinal and transverse displacements increased with increasing skew. The increase in transverse displacements of the deck generated girder torsional rotations along the longitudinal axis. This was because the girder bottom flanges were restrained for transverse movement while the girders and the deck were rigidly connected. Transverse movements are particularly damaging since the bridge is restrained in that direction. This is especially critical to relatively short and wide bridges because of their higher rotational stiffness.

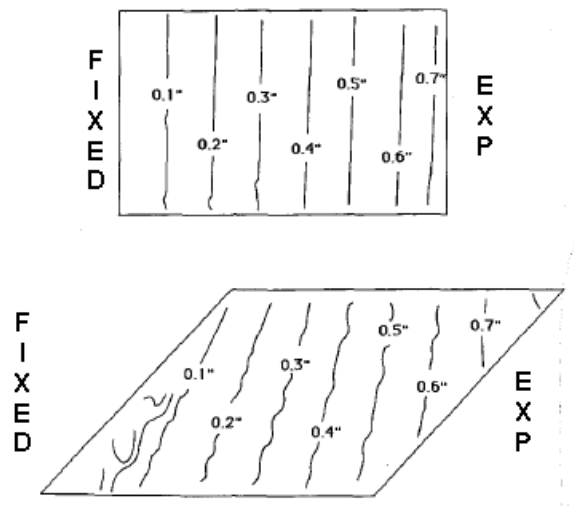


Figure 2-18. Longitudinal displacement profile of deck for right and 45° skew bridge (Moorthy and Roeder 1992).

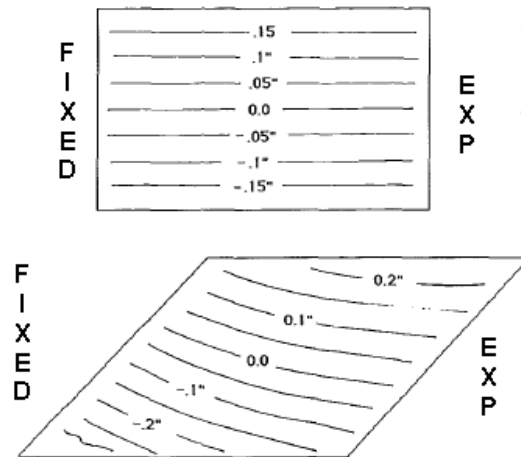


Figure 2-19. Transverse displacement profile of deck for right and 45° skew bridge (Moorthy and Roeder 1992).

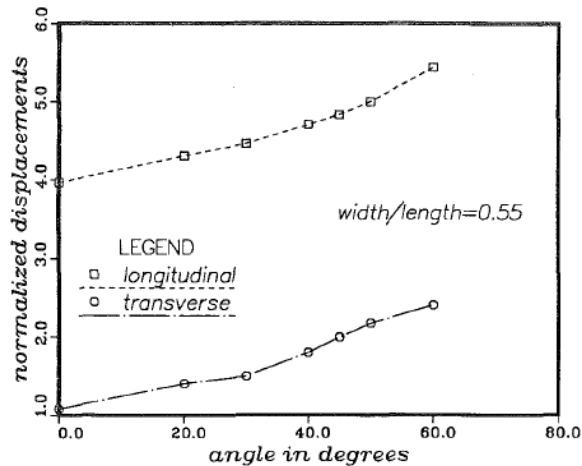


Figure 2-20. Maximum normalized longitudinal and transverse displacement vs. skew angle (Moorthy and Roeder 1992).

Moorthy and Roeder (1992) investigated the effects of bearing resistance to the longitudinal movement. According to the study, the rocker bearings did not move until a threshold slip force was reached and moved freely afterwards. The effect of resistance to longitudinal movement, provided by the bearings and expansion joints, was examined by changing the slip force between 0 and 80% of the self-weight reaction force acting on the bearing. As the bearing slip force was increased, there was an increase in transverse movement along the diagonal between acute corners. Also, the forces in the girders and bearings increased considerably. The resistance of expansion joints to the longitudinal movement increased

transverse movement as well as the deck and bearing stresses while reducing the longitudinal movement. The study recommended use of elastomeric bearings or those with unguided sliding surfaces for high skew, short, and wide bridges since the potential transverse movement was permitted.

Moorthy and Roeder (1992) stated that resistance encountered in expansion joints or support locations can considerably increase the transverse movement in skew bridges. Compressive reaction force, F , is developed across the skew angle as shown in Figure 2-21. Compressive force, F_n is developed in the normal direction due to limited shear strength between pavement and the granular base. The transverse component F_t , will push the bridge transversely which may generate larger transverse movements in the absence of bearing guides or other transverse restraints.

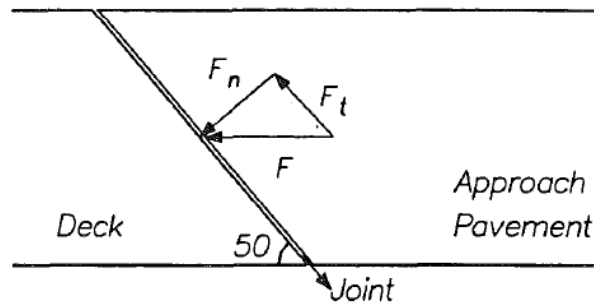


Figure 2-21. Forces on deck due to resistance encountered in expansion joints (Moorthy and Roeder 1992).

Moorthy and Roeder (1992) investigated the effects of pier stiffness. The pier stiffness did not have a great impact on the movements noted for relatively short skew bridges that experience large transverse movements but had a notable impact on longer bridges.

2.3.1 Skew Bridge Behavior under Thermal Loads

The skew bridge behavior is analyzed under uniform thermal as well as positive and negative thermal gradient loads. Thermal gradient loads from AASHTO LRFD (2010) Section 3.12.3 for Zone-3 are used. A negative temperature gradient (NTG) is obtained by multiplying the positive temperature values by -0.30. The height (h) in Figure 2-22 is the depth of full composite section (45 in. = 36 in. girder + 9 in. deck). A thermal expansion coefficient of $6.0 \times 10^{-6}/^{\circ}\text{F}$ is used for both deck and girder concrete. Uniform expansion and contraction

temperature differentials of +42.3 °F and -72.7 °F are used as uniform thermal loads as per AASHTO LRFD Procedure B. Temperature gradient and uniform thermal loads are applied only to stringer bridge models.

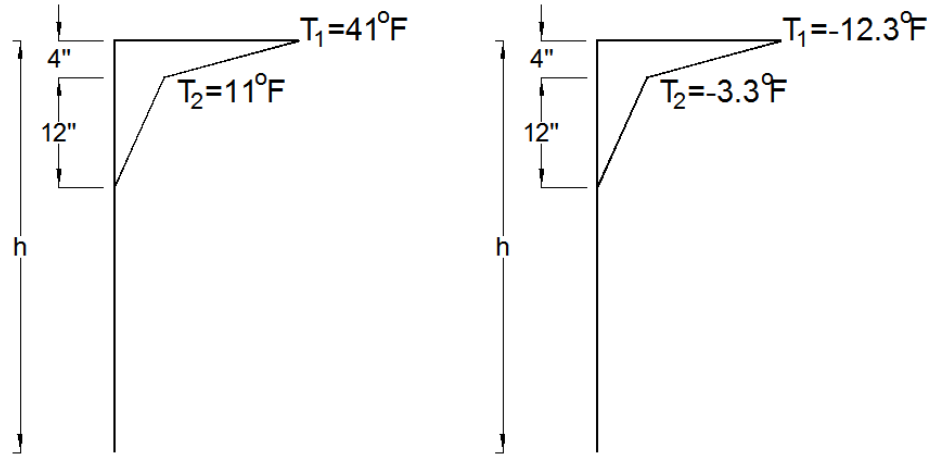


Figure 2-22. Positive and negative temperature gradient loads used in the analyses

2.3.1.1 FE Simulation of Simple Span Skew Bridge Behavior under Uniform Thermal Loads

To verify the findings documented in the literature, FE models of a simply supported stringer bridge are developed for skew angles of 0, 15, 30, 45 and 60 degrees. The models were analyzed under a uniform contraction thermal load for three different bearing orientations shown in Tindal and Yoo (2003). Traditional bearing systems limit the supports to move only along the longitudinal axis of the bridge. Radial from corner and radial from center bearing systems allow a movement pattern along the diagonal between acute corners as shown in Figure 2-23, Figure 2-24, and Figure 2-25. In these analyses gravity loads are not applied; that is, the displacement contours represented show the translations in longitudinal and transverse directions. Findings shown in Figure 2-24, Figure 2-25, and Figure 2-26 are in agreement with what is described in AASHTO Steel Bridge Bearing Design and Detailing Guidelines (AASHTO 2004, Figure 2-16). Radial from single bearing orientations (radial from corner and radial from center) are determinate systems and do not develop any reaction forces or stresses under uniform thermal load. However, the traditional bearing system experiences high reactions as well as stresses at the fixed end. The girder ends at the fixed end may also rotate developing girder torsion (Figure 2-26, Figure 2-27, and Figure 2-28).

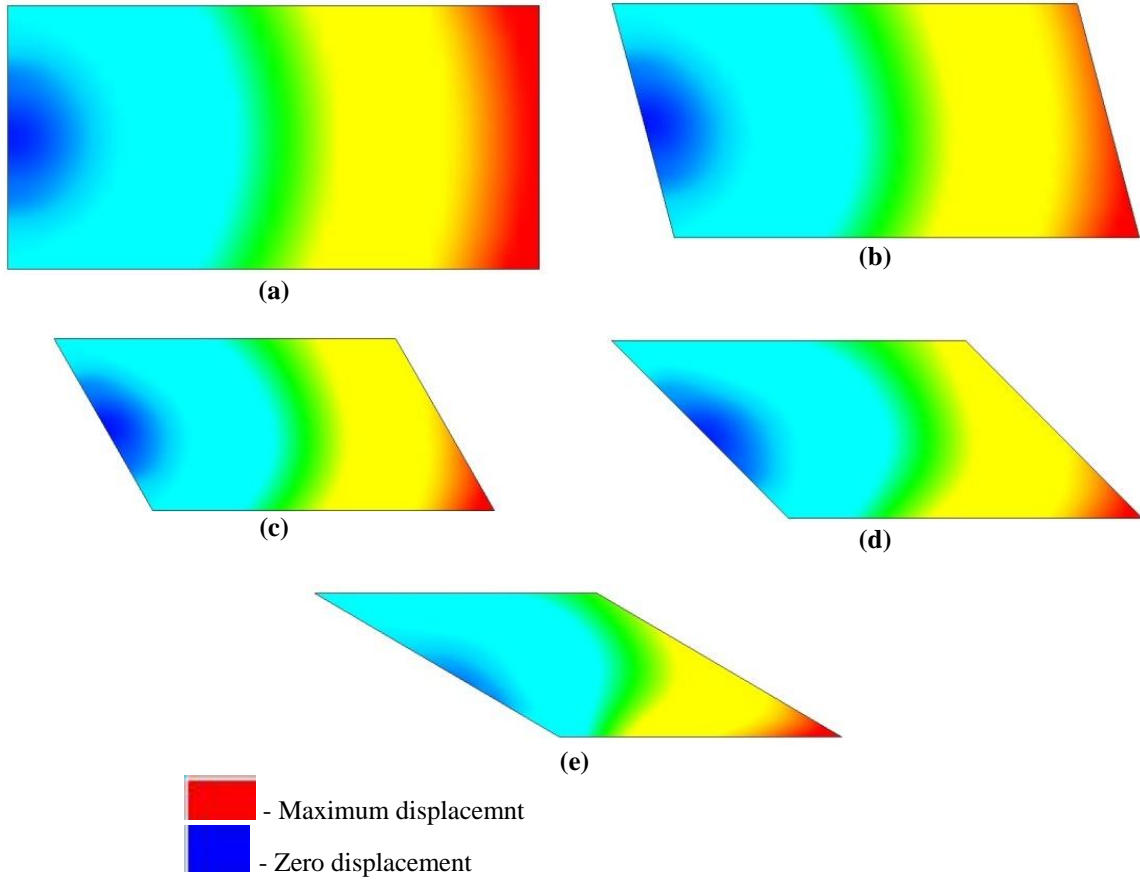


Figure 2-23. Displacement contours under the traditional bearing condition for skew angles
 (a) 0° (b) 15° (c) 30° (d) 45° (e) 60°

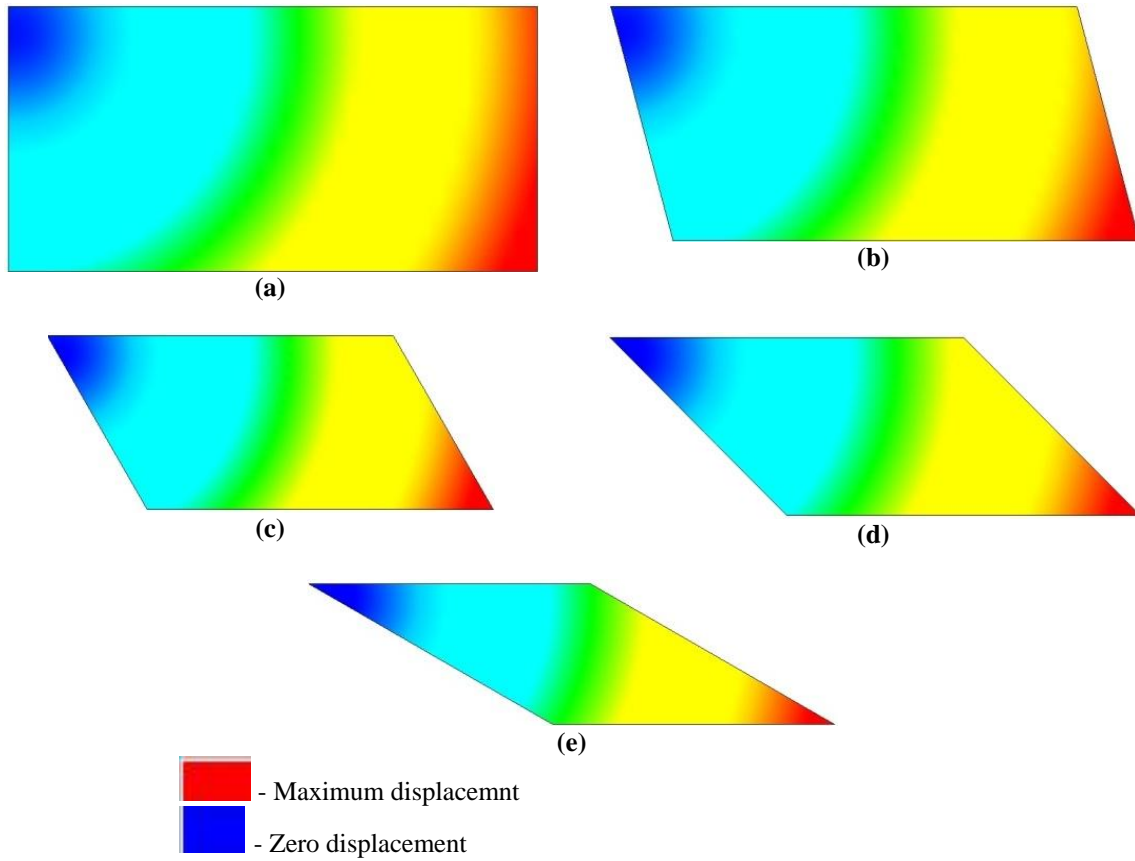


Figure 2-24. Displacement contours under radial from corner bearing condition for skew angles
 (a) 0° (b) 15° (c) 30° (d) 45° (e) 60°

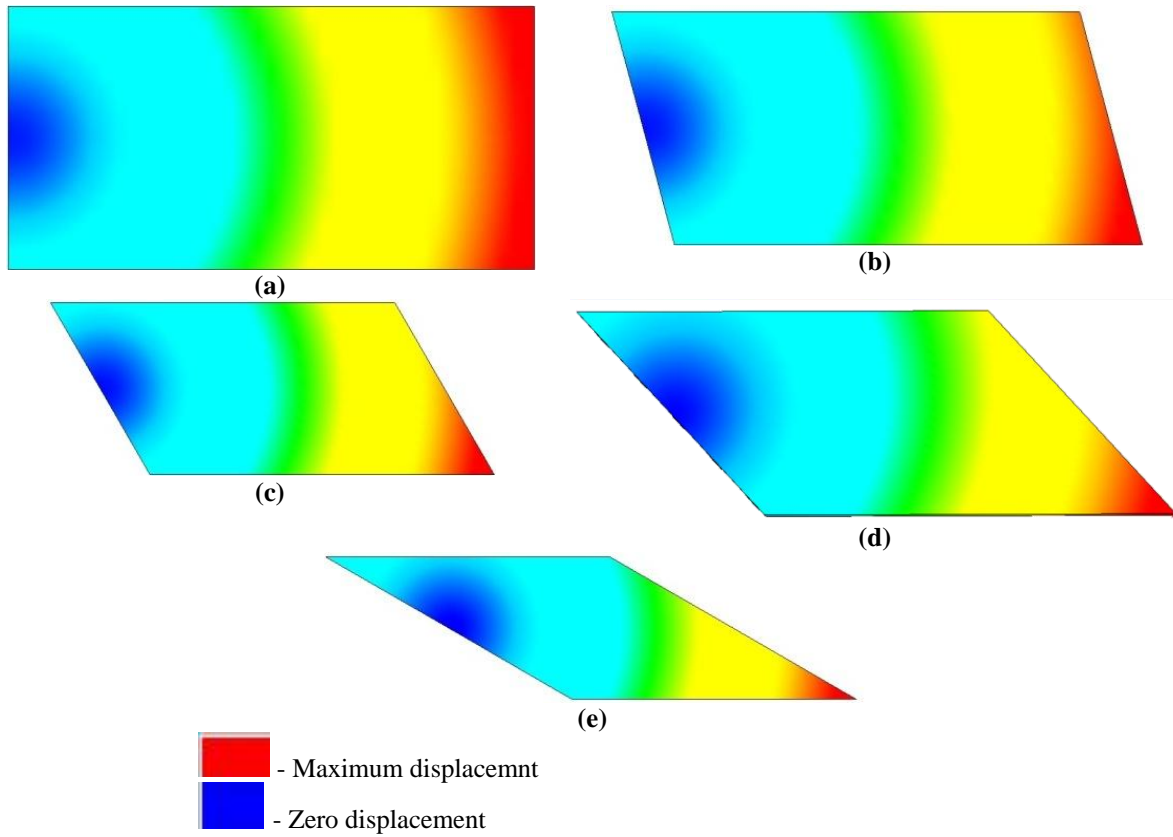
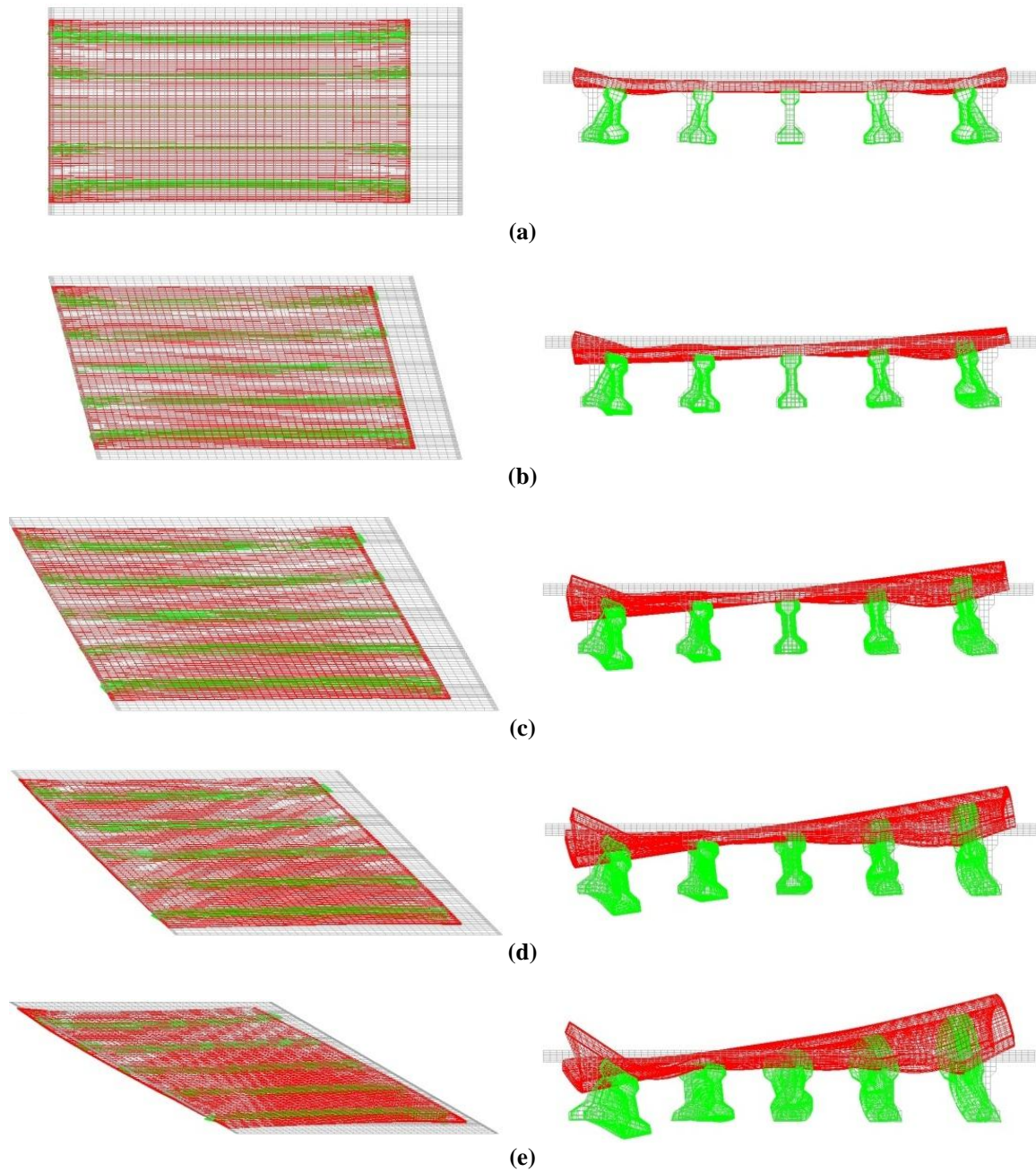


Figure 2-25. Displacement contours under the radial from center bearing condition for skew angles
 (a) 0° (b) 15° (c) 30° (d) 45° (e) 60°



**Figure 2-26. Deformed shape under the traditional bearing condition for skew angles
 (a) 0° (b) 15° (c) 30° (d) 45° (e) 60°**

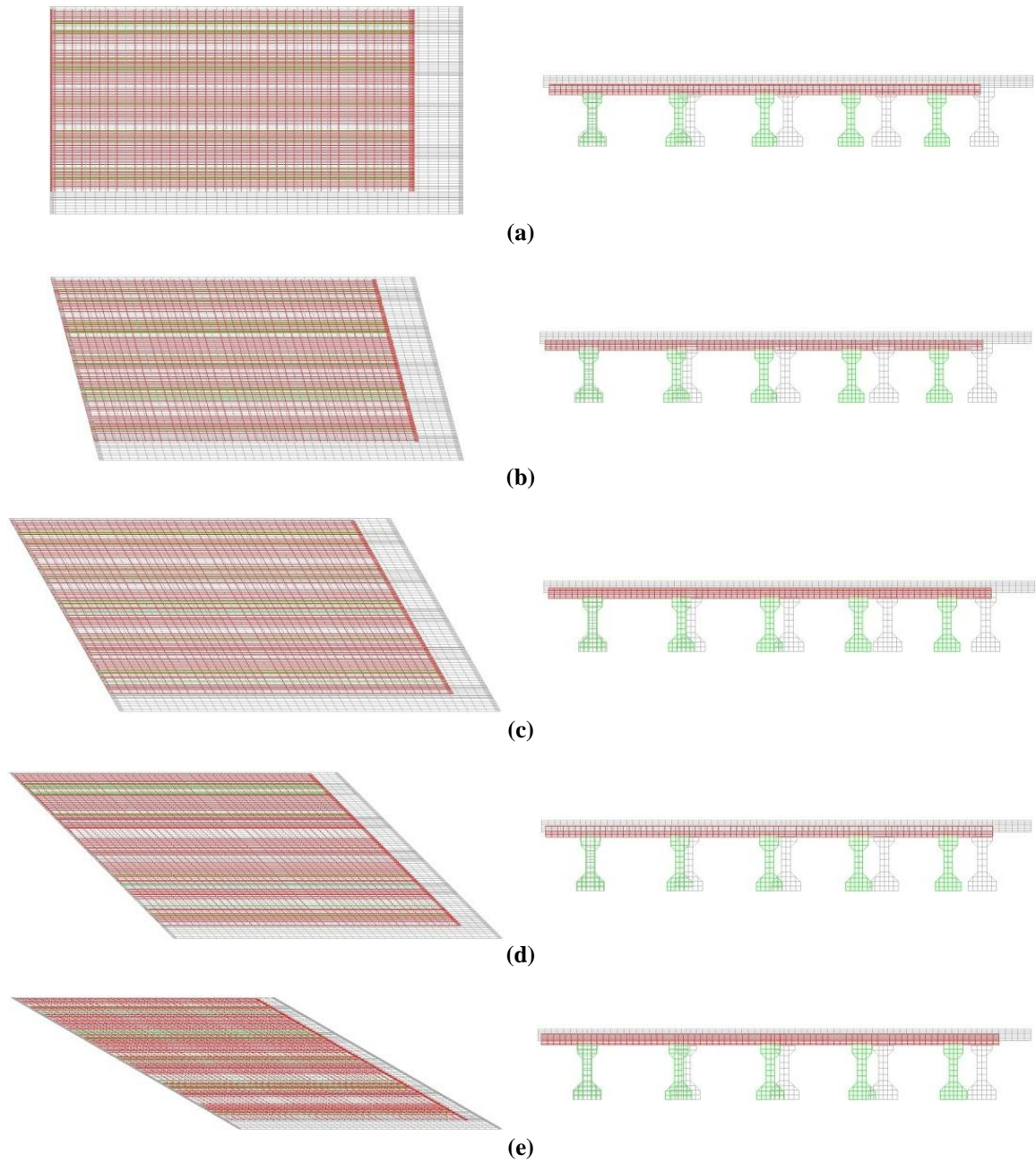


Figure 2-27. Deformed shape under radial from corner bearing condition for skew angles

(a) 0° (b) 15° (c) 30° (d) 45° (e) 60°

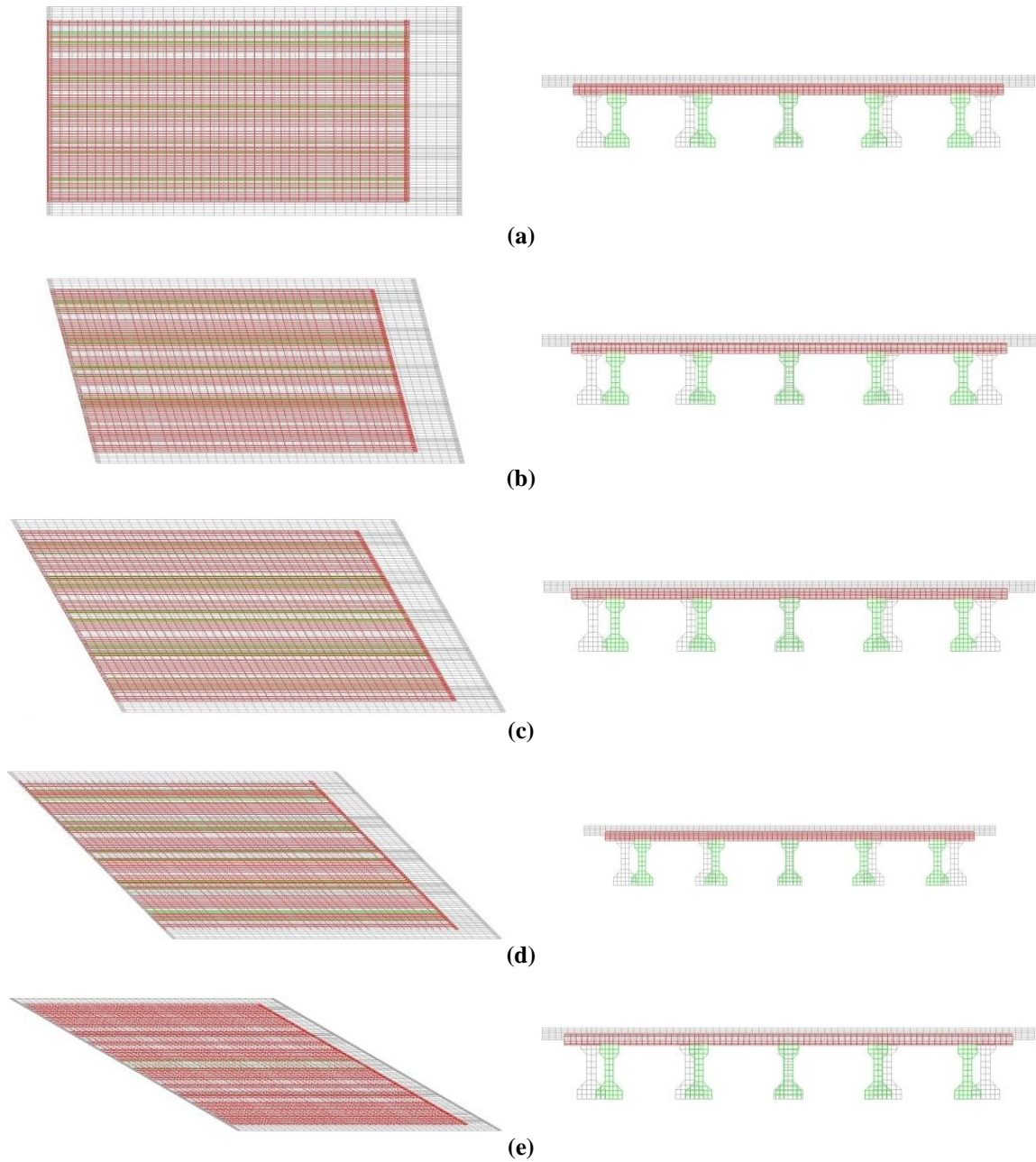


Figure 2-28. Deformed shape under radial from center bearing condition for skew angles

(a) 0° (b) 15° (c) 30° (d) 45° (e) 60°

Displacement contours in transverse and longitudinal directions are shown separately so that they can be compared with those of Moorthy and Roeder (1992). Figure 2-29, Figure 2-30, and Figure 2-31 show the displacement contours in transverse and longitudinal directions under three different bearing configurations. Irrespective of support configurations, maximum longitudinal bearing movement is at the acute corner. In traditional bearing configuration, longitudinal movement of the bridge is almost parallel to the angle of crossing (i.e., maximum movement at the acute corner and the minimum at the obtuse corner). In the radial cases, the longitudinal displacement contours are almost perpendicular to the diagonal between acute corners. As bridge skew increases, the direction of transverse displacement contours of bridge with traditional bearings changes from parallel to longitudinal axis to parallel to the diagonal between obtuse corners. In the case of radial bearing configuration, transverse displacement contours are parallel to the longitudinal axis of the bridge. The contraction (or expansion) profiles of the three different constraint cases do not follow the reference lines, and the deformed shapes do not resemble the ones previously shown in Figure 2-17. Thus, guided bearings that would allow movement along the reference line are necessary to achieve the expansion profiles shown in Figure 2-17. The same behavior is also discussed in Nakai and Yoo (1988), but no design details are provided.

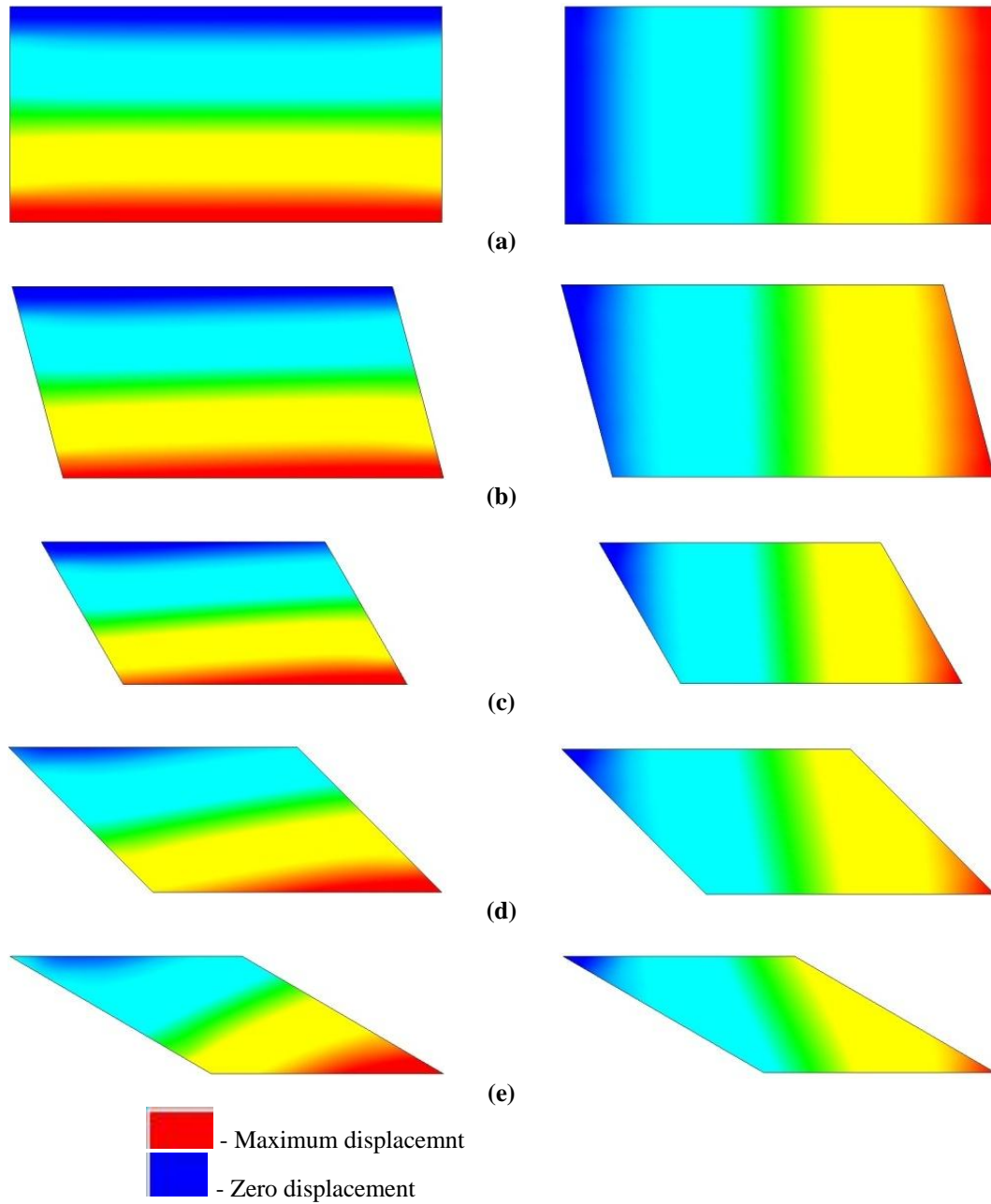


Figure 2-29. Transverse (left) and longitudinal (right) displacement contours under the traditional bearing condition for skew angles (a) 0° (b) 15° (c) 30° (d) 45° (e) 60°

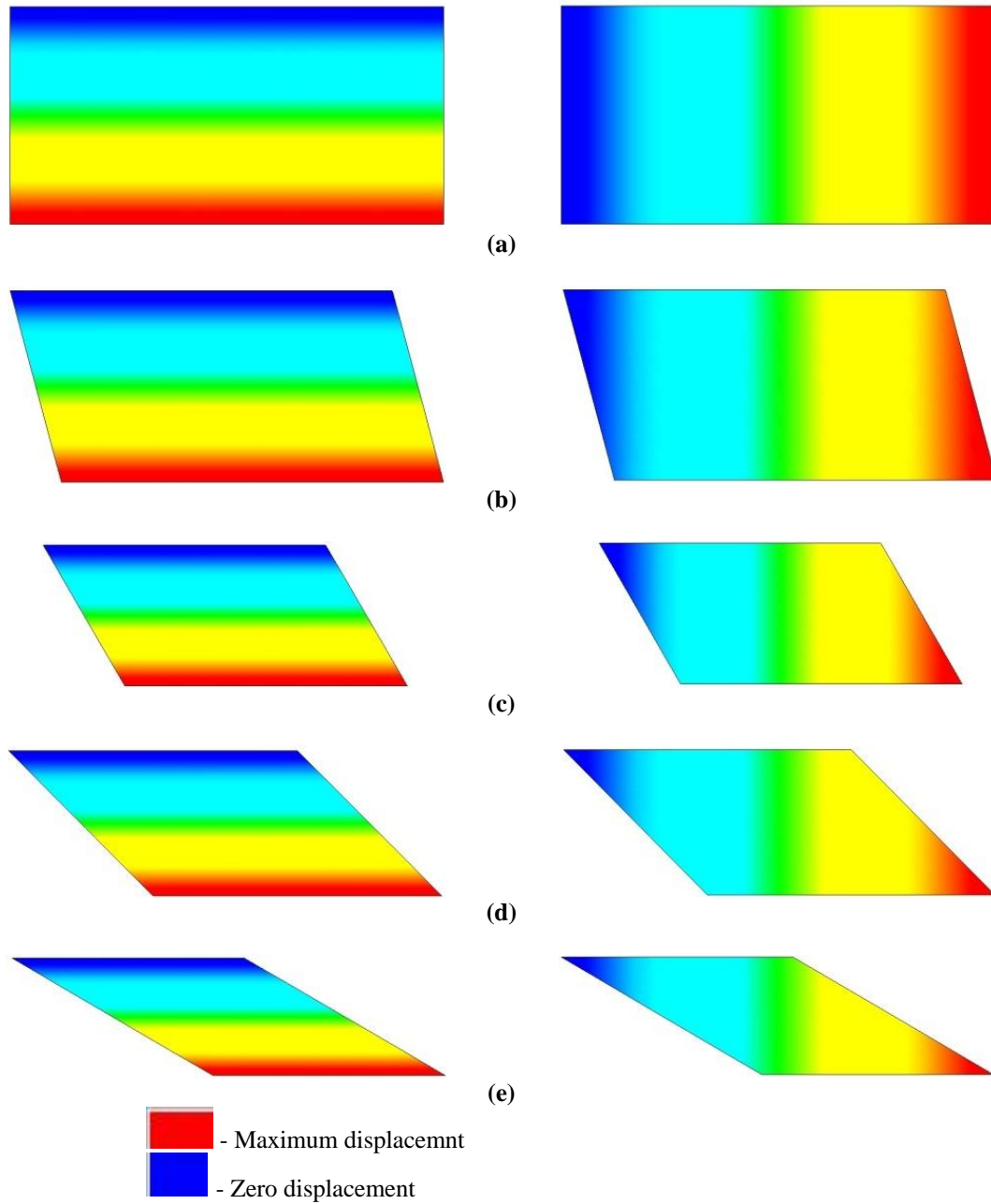


Figure 2-30. Transverse (left) and longitudinal (right) displacement under the radial from corner bearing condition for skew angles (a) 0° (b) 15° (c) 30° (d) 45° (e) 60°

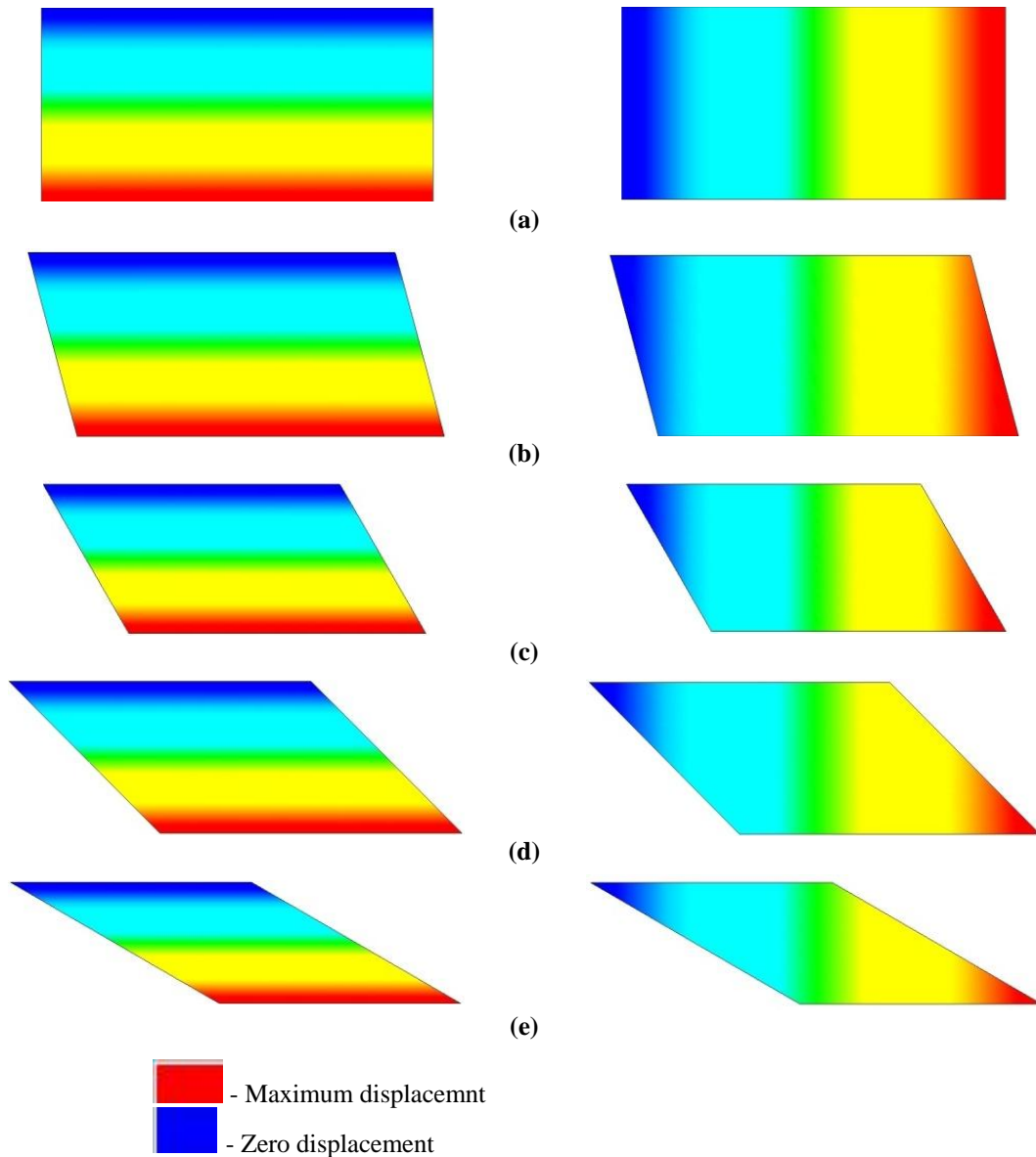


Figure 2-31. Transverse (left) and longitudinal (right) displacement under the radial from center bearing condition for skew angles (a) 0° (b) 15° (c) 30° (d) 45° (e) 60°

The simply supported straight bridge is not expected to develop any bending or torsion under thermal gradient loading. With increasing skew, combined bending and torsion develops under thermal gradient load. The longitudinal bending moment and torsion plots of simply supported bridges under negative temperature gradient are given in Figure 2-32 and Figure 2-33, respectively. Both bending and torsion is zero at both abutments and constant through the length of span. The bending moment increases with increasing skew angle. However, torsion increases with increasing skew up to 50°, but there is a sharp drop at the skew of 60°

(Figure 2-33). The reasons for this behavior need to be separately investigated with further refinement in skew angles and different span-to-width ratios.

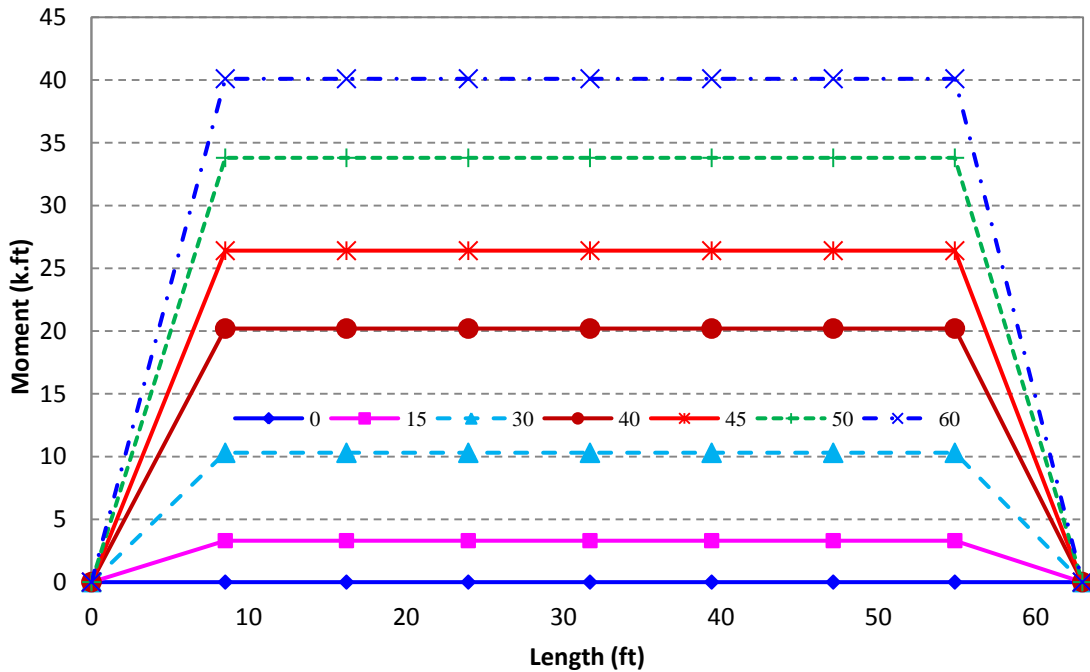


Figure 2-32. Longitudinal bending moment for full-width of simply supported stringer bridge under negative temperature gradient

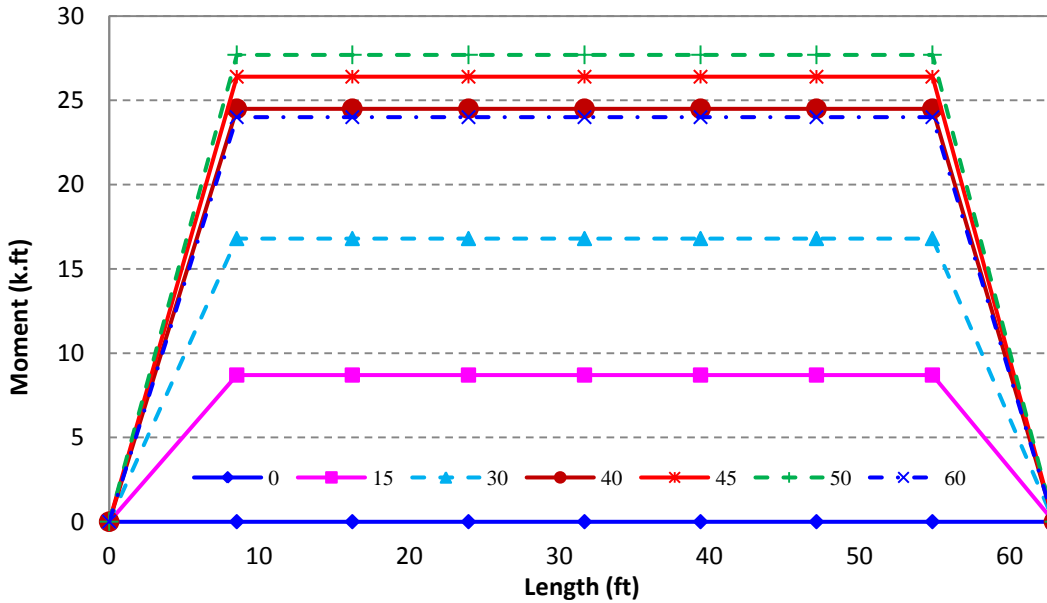


Figure 2-33. Torsion for full-width of simply supported stringer bridge under negative temperature gradient

2.4 DESIGN CHALLENGES OF SKEWED/JOINTLESS BRIDGES

2.4.1 Length, Skew and Curvature Limits

A typical maximum skew angle limit for jointless bridges specified by many states' highway agencies (SHAs) is 30° (Oesterle et al. 1999). However, maximum limit angle varies from 0° to no limit (Chandra et al. 1995). A 2004 survey (Maruri and Petro 2005) revealed that a majority of SHAs do not have restrictions on the maximum span length within the bridge, but they do limit the total length and the skew angle.

Table 2-1 summarizes the span length, total bridge length, skew, and curvature limits for prestressed concrete and steel girder bridges specified by the state highway agencies. The table was developed from the responses of 39 SHAs. For the purposes of this survey, Maruri and Petro (2005) specified bridge configurations as full integral abutment, semi-integral abutment, deck extension, and integral pier configurations.

**Table 2-1. Range of Design Criteria Used for Selection of Jointless Bridges
(Maruri and Petro 2005)**

Girder Type	PC	Steel
Maximum Span (ft)		
Full Integral	60-200	65-300
Semi-integral	90-200	65-200
Deck extensions	90-200	80-200
Integral piers	120-200	100-300
Maximum Total Bridge Length (ft)		
Full Integral	150-1175	150-650
Semi-integral	90-3280	90-500
Deck extensions	200-750	200-450
Integral piers	300-400	150-1000
Maximum Skew (Degrees)		
Full Integral	15-70	15-70
Semi-integral	20-45	30-40
Deck extensions	20-45	20-45
Integral piers	15-80	15-No Limit
Maximum Curvature (Degrees)		
Full Integral	0-10	0-10
Semi-integral	0-10	0-10
Deck extensions	0-10	0-10
Integral piers	3-No Limit	0- No Limit

An additional point of reference outside the US is from the Ontario Ministry of Transportation. They limit the overall length of semi-integral bridges to 492 ft (150m) based on seasonal temperature variation considerations because of the capacity and efficiency of movement systems (Husain and Bagnariol 1999).

2.4.2 Volume Change Loads and Behavior of Jointless Bridges

Maruri and Petro (2005) used the survey data to identify the type of forces that states account for in the design of integral abutments such as earth pressure, temperature, creep, shrinkage, settlement, and additional forces due to skew or curvature (Figure 2-34).

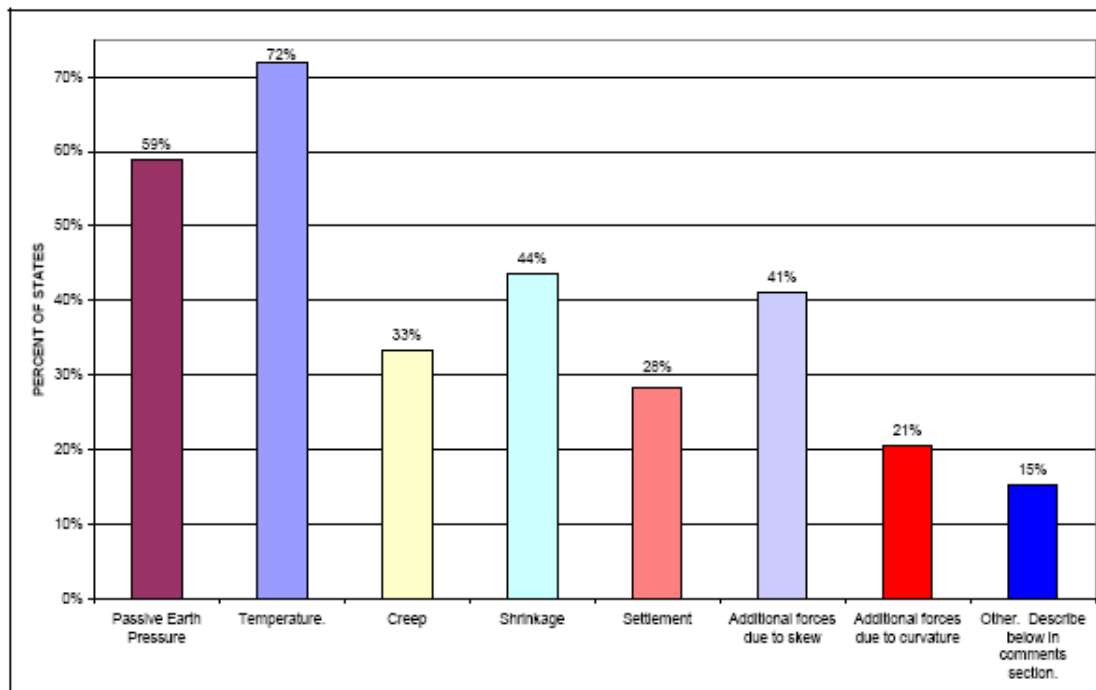


Figure 2-34. Percent of states that account for different forces in the design of jointless bridges (Maruri and Petro 2005).

Skew bridges respond to thermal loads with both longitudinal and transverse movements. Transverse movement magnitude depends on bridge geometry, level of restraints at the piers and abutments, skew or angle of crossing with respect to the abutments and/or piers, and magnitude of the thermal loads (Oesterle et al. 1999). Forces developed at the abutments due to thermal expansion are presented in Figure 2-35. According to Oesterle et al. (1999), transverse forces developed in the system are high enough to cause abutment and wing-wall

distress. For relatively short bridges, which undergo small expansions due to slight changes in effective temperature, the abutment needs to be designed to resist loads from batter piles and/or lateral passive soil resistance anticipating limited transverse deformations (Oesterle et al. 1999). Batter piles are inclined members that develop axial and shear forces due to abutment movement.

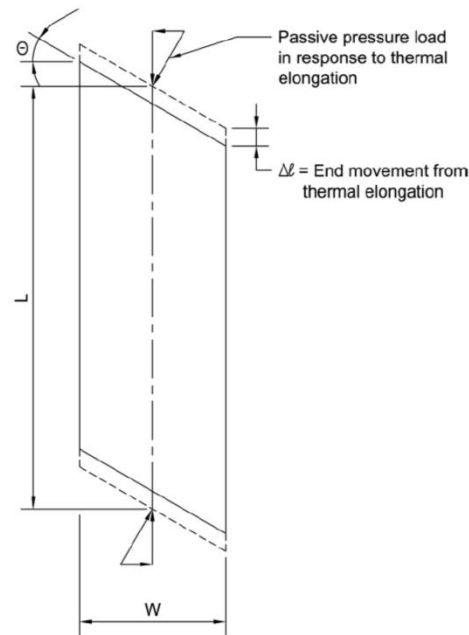


Figure 2-35. Resultant force components that develop at the abutment under thermal expansion (Oesterle et al. 1999)

According to Burke (1994a), skew in semi-integral bridges forces deck rotation about an axis normal to the plane of the deck. To resist the rotation, guide bearings and/or backwall guides are necessary. Guide bearings and/or backwall guides and a supporting structure need to be designed for the forces required to resist transverse movement.

The passive soil pressure forces behind the backwall due to superstructure elongation will not be collinear with the bridge axis and force deck to rotate (Burke 1994a, Figure 2-36). The rotation of semi-integral bridges and its effects have also been documented in the field (Sanford and Elgaaly 1993; Burke 1999; Van Lund and Brecto 1999). To prevent the deck rotation thus, to keep the superstructure of a skewed bridge stable, the force couple resisting rotation ($P_p \tan \delta \times L \cos \theta$) must be equal or greater than the force couple causing rotation ($P_p L \sin \theta$).

$$P_p \times L \sin \theta \leq (P_p \times \tan \delta \times L \cos \theta) (FS) \quad (2-1)$$

Where

- P_p : total passive pressure
- θ : skew angle
- δ : backfill-abutment interface friction angle
- L : bridge deck length
- FS: factor of safety

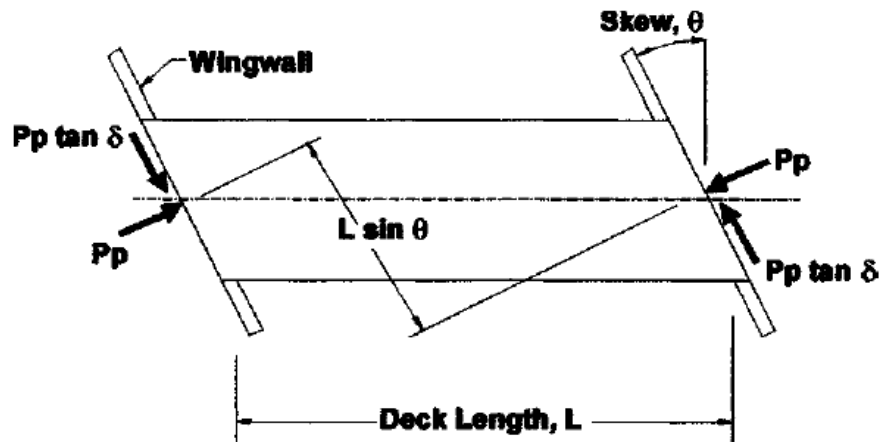


Figure 2-36. Forces on the bridge (Steinberg et al. 2004)

Providing a factor of safety of 1.5 and assuming an angle of friction of 22° at the structural backfill interface (δ), Burke (1994a) concluded that the bridge to remain stable, skew angle must be equal to or less than 15° . For greater skews, guide bearings and/or backwall guides can be provided to resist the forces generated by the restrained transverse movement. Based on this relationship, the required design strength of the guides needs to be equal to $0.5 P_p$ for 30° skew, and $0.7 P_p$ for 45° skew bridges.

Burke (1994a) also noted that the deck rotation motion may be reduced as a result of the approach slab-subbase friction, the shearing stiffness of the elastomeric bearings, and by the compressive stiffness of fillers in the movable joints between the superstructure and wingwalls.

Eq. 2-1 holds valid for single span bridges and multi-span bridges if the piers do not provide rotational resistance through the connection between the girders and piers. For bridges with integral piers or piers with fixed bearings, the unrestrained rotation of superstructures about a

vertical axis can induce torsion on the pier (Burke 1999). For example, consider the case of a 40° skewed two-span bridge with expansion bearings at both ends and fixed bearings at the pier. Under uniform thermal expansion, longitudinal reactions developing at the intermediate supports due to the nature of skew would tend to rotate the superstructure about its vertical axis. Since bearings at the abutment are not restrained for horizontal movement, the resisting twisting moment obtained can only develop at the piers. Thus, piers would experience significant twisting (Figure 2-37).

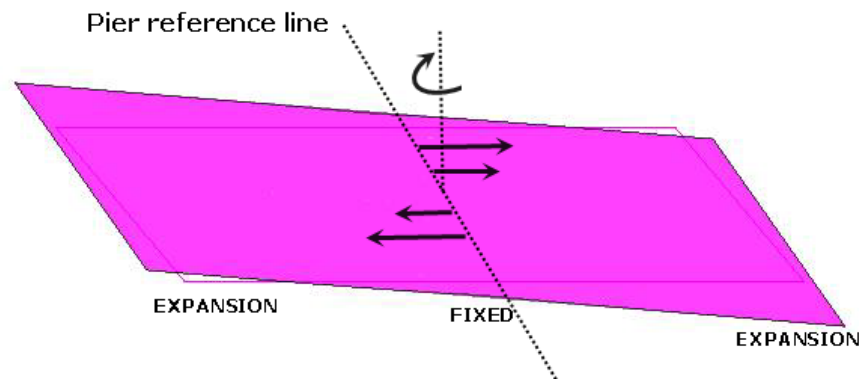


Figure 2-37. Deformed shape of the deck of a two-span continuous skew stringer bridge under uniform expansion

Steinberg et al. (2004) monitored the wingwall/diaphragm joint of two semi-integral bridges in Ohio. The first bridge had a single span of 87 ft, a roadway width of 32 ft and skew of 65° . The second bridge had four spans with a total length of 314 ft and a width of 40 ft at a skew of 25° . The maximum forces measured on the wingwalls were 35.7 and 30.1 kips, respectively. The finite element simulations revealed that lower skews would result in lower wingwall forces at lower backfill stiffness values. As the backfill stiffness increased, the wingwall reaction increased more rapidly at higher skews compared to lower skews.

Oesterle et al. (1999) stated that for bridges with skew greater than 20° , wingwalls should be designed for the forces that develop in the transverse direction. Further, U-shaped wingwalls are recommended for skewed bridges since they would help resisting transverse movement of the abutments.

2.4.3 Semi-Integral Abutment Details

Aktan et al. (2008) recommended changes to current MDOT semi-integral abutment details for straight and moderately skewed (up to 20° skew) bridges. MDOT current and proposed details are not presented here for brevity. Readers are encouraged to refer to Aktan et al. (2008) for details. Current effort is to document the best practices of a few selected SHAs to identify key details/configurations to improve the durability performance of high skew ($20^\circ < \text{skew} \leq 45^\circ$) semi-integral and deck sliding over backwall bridge systems.

For skewed semi-integral and deck extension bridges, VDOT uses rub plates that act as a bearing between the superstructure and the wing haunch in the acute corners (Figure 2-38). The rub plates transfer horizontal force from the superstructure to the abutment, while allowing longitudinal sliding. Typically, rub plates are made of stainless steel with shear studs cast into concrete. This practice started after the rotation of integral bridges under passive pressure became evident during monitoring of a 5° skew, 323 ft long, and 85 ft wide bridge built in 1993. Rub plates have continuously been used since then regardless of size, skew and span configuration (Weakley 2005). This detail is amenable to the use of deck extensions with Massachusetts-type approach slab (Figure 2-39). Since the approach is buried below the plane of deck extension, there is no conflict with the superstructure longitudinal movement. There is potential for pavement damage due to deck expansion, if proper measures are not taken. However, there is no information related to the joint performance between the pavement and the extended deck.

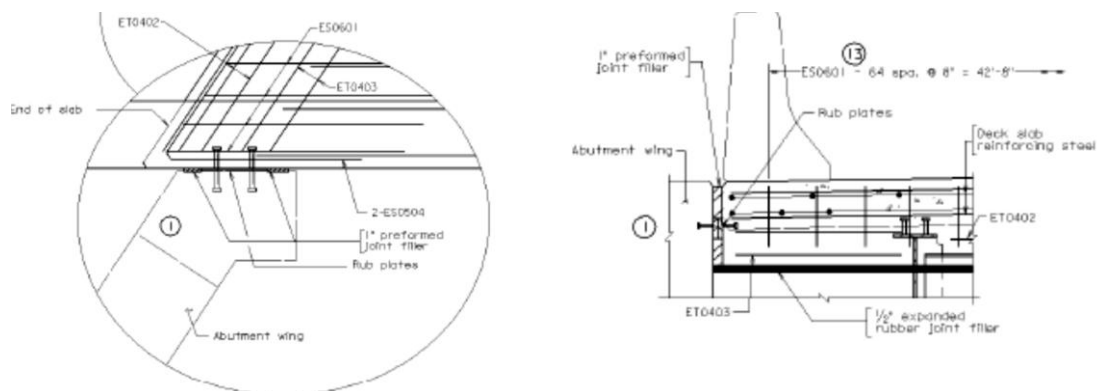


Figure 2-38. Rub plate detail (VDOT)

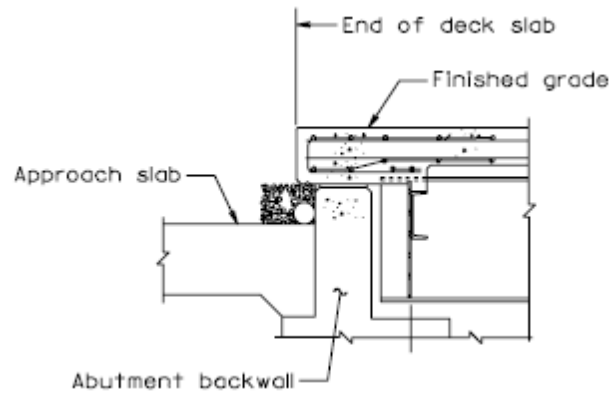
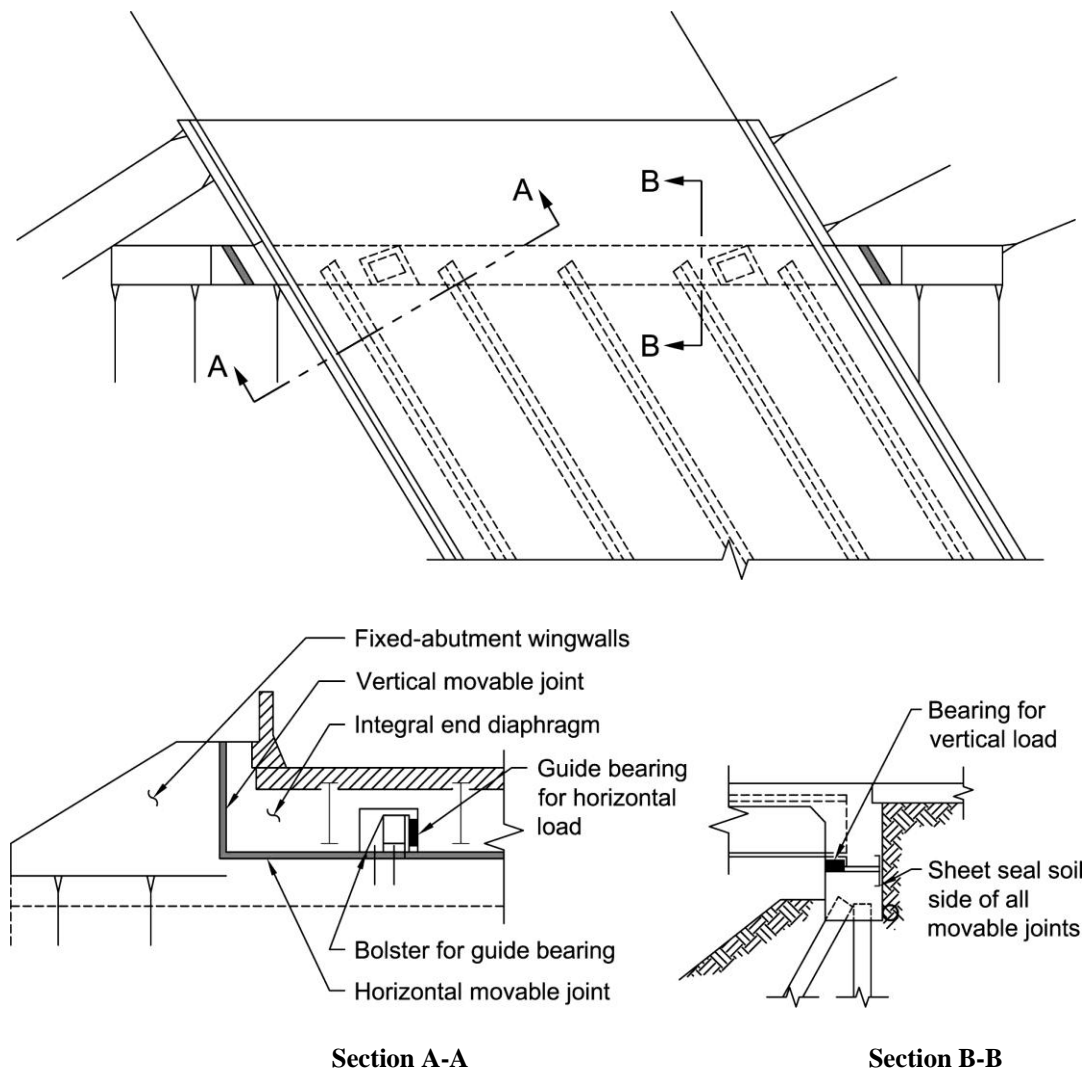


Figure 2-39. VDOT deck extension detail with buried approach slab

Burke (1994b) proposed a semi-integral abutment detail with an end diaphragm (a backwall) sliding with respect to a fixed abutment. With this concept, the restraint on the superstructure is reduced to passive pressure behind the backwall and resistance coming from bearings. This concept has some similarities to current MDOT (2006) practice but uses filler material for the vertical joints between the bridge deck and wingwalls. This detail requires end movement guides for both horizontal and vertical supports. The bearing for horizontal supports and the backwall need to be designed for passive pressure behind the backwall (Figure 2-40).



**Figure 2-40. Semi-integral abutment detail with end diaphragm moving over a fixed abutment
(Burke 1994a and Oesterle et al. 1999)**

Ontario Ministry of Transportation does not impose skew limitations on semi-integral abutment bridges. However, skew bridges must comply with the following provisions (Husain and Bagnariol 1999):

1. *Lateral restraint should be provided to prevent superstructure rotation due to passive earth pressure.*
2. *The movement system at the end of the approach must be able to accommodate the deformations associated with the skew, and*
3. *The length of the wingwalls cantilevered from the abutment should be minimized.*

Figure 2-41 and Figure 2-42 show semi-integral abutment configurations for concrete girder bridges with overall span less than and greater than 328 ft (100 m), respectively. The major difference between these two configurations is the gap provided at the abutment-backwall interface (i.e., backwall configuration).

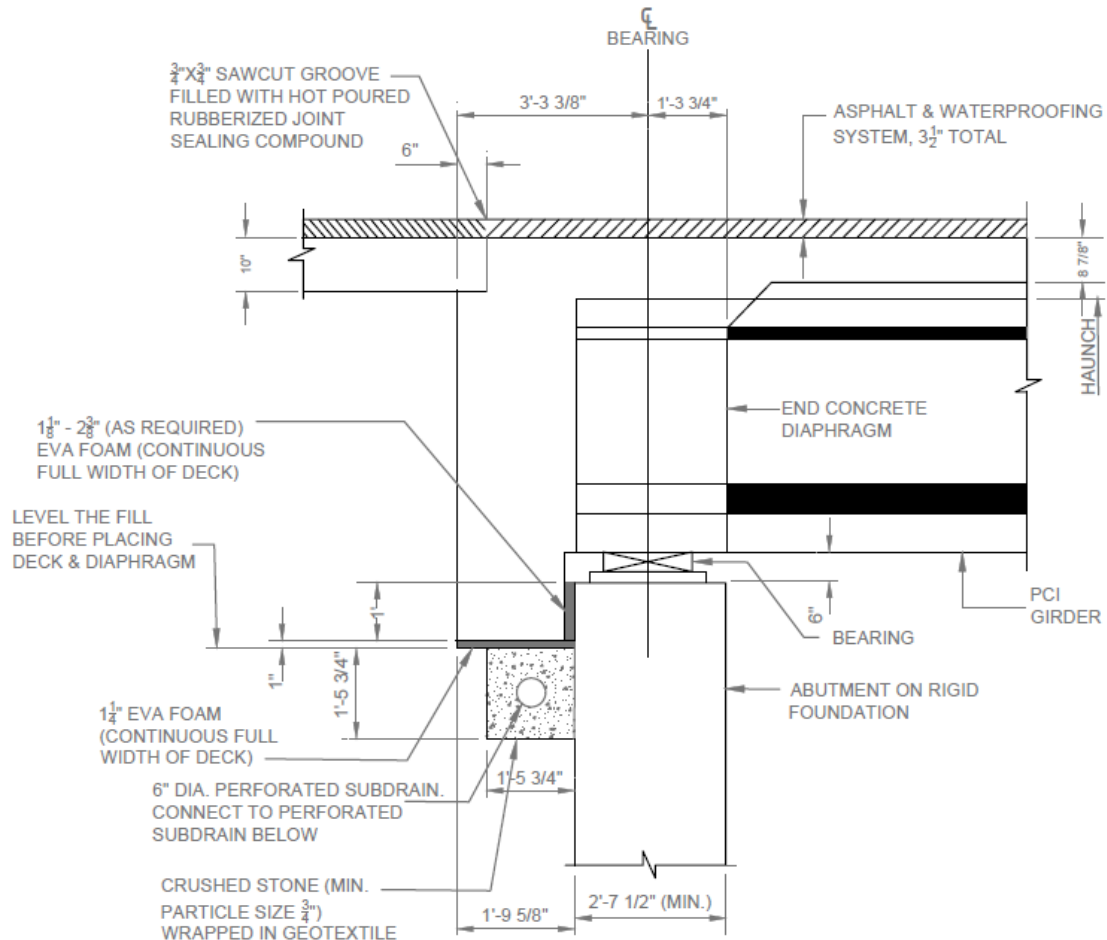


Figure 2-41. Semi-integral abutment details of concrete girder bridge with overall span < 328 ft

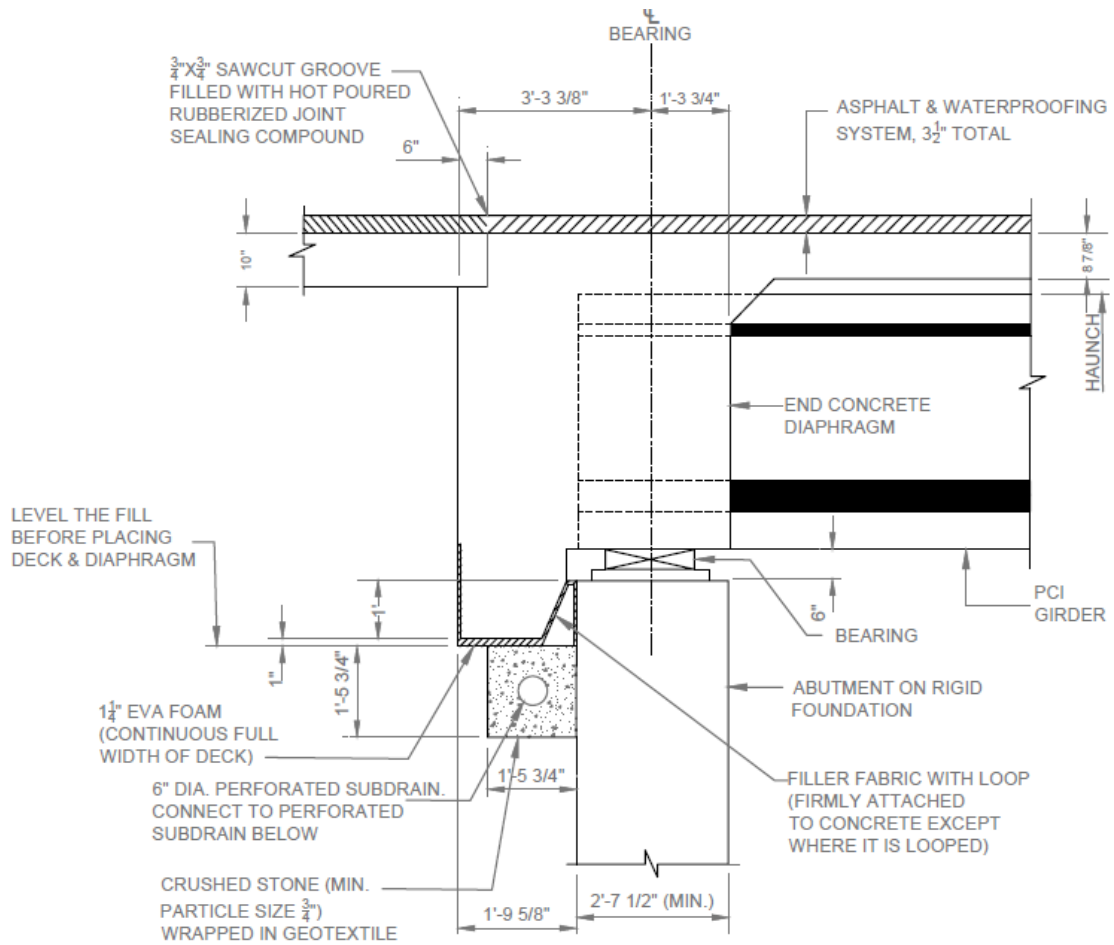


Figure 2-42. Semi-integral abutment details of concrete girder bridge with overall span > 328 ft

Figure 2-43 and Figure 2-44 show semi-integral abutment configurations for steel girder bridges with overall span less than and greater than 246 ft (75 m), respectively. The major difference between these two configurations is the gap provided at the abutment-backwall interface (i.e., backwall configuration).

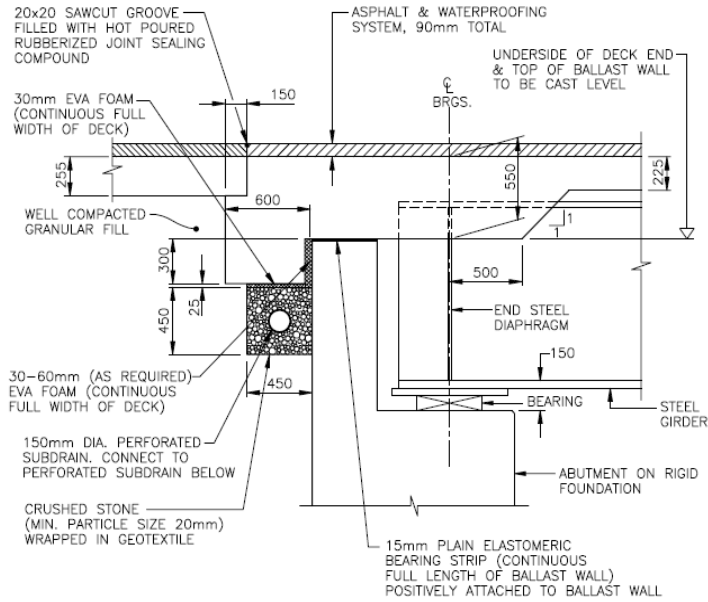


Figure 2-43. Semi-integral abutment details of steel girder bridge with overall span < 328 ft

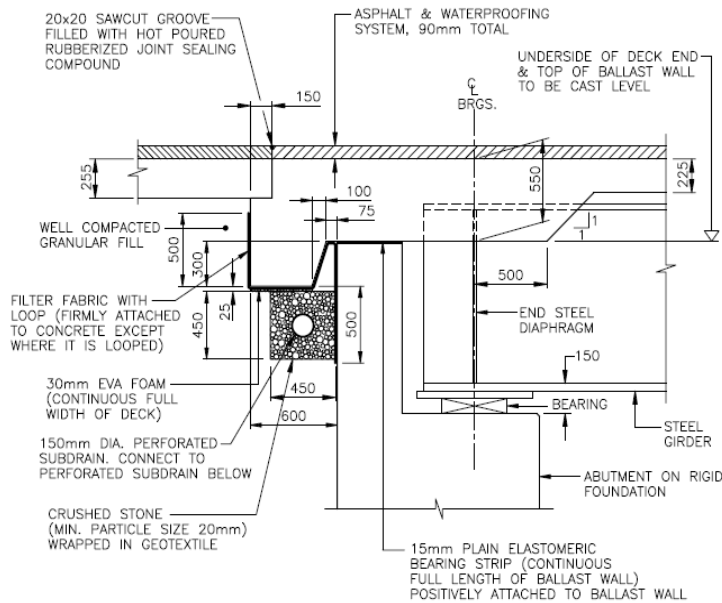


Figure 2-44. Semi-integral abutment details of steel girder bridge with overall span > 328 ft

Major aspects of Ontario details are: (1) allowing the deck to slide over the backwall when steel girders are used and (2) use of elastomeric bearing strips to provide a sliding surface between the backwall and the deck.

2.4.4 EPS Backfill

As discussed in the previous section, passive pressure developed by backfill generates a reactive force perpendicular to the backwall. In skew bridges, this force is not parallel to the longitudinal axis and, in the absence of adequate restraints, the force rotates the superstructure about an axis normal to the plane of the deck during bridge expansion. Providing restrains to prevent the rotation can induce large forces at the abutments or wingwalls. The high forces can cause cracking and other forms of distress if not properly accounted for in the design. In order to minimize the reactive force development due to backfill effects, expanded polystyrene (EPS) is being used by several states.

The Federal Highway Administration (FHWA) promotes the use of EPS geofoam as a backfill material for accelerated bridge construction projects. Several advantages of using EPS are rapid construction, reduced lateral load behind retaining structures, minimum differential settlement, etc (FHWA 2011).

The advantage of using EPS behind the backwall of integral or semi-integral systems is the attenuation of the effect of bridge movement on backfill during thermal expansion. Also, use of EPS behind the backwall is an effective means of reducing properly compacted backfill material settlement (Hoppe 2005). Figure 2-45 shows the abutment cross-section of experimental implementation of EPS by Virginia DOT (VDOT) in a semi-integral bridge.

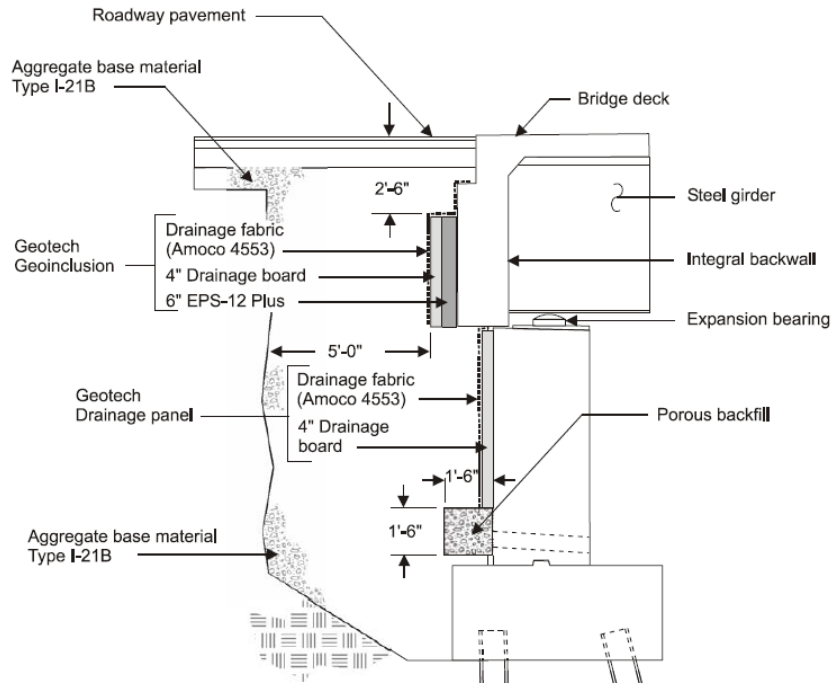


Figure 2-45. VDOT semi-integral system with EPS (Hoppe 2005)

The Structure and Bridge Manual of VDOT (2010) provides details on EPS implementation shown in Figure 2-45. Eq. 2-2 is recommended by VDOT for calculating the EPS thickness.

$$\text{EPS thickness (EPSt)} = 10 [0.01 h + 0.67 \Delta L] \geq 10 \text{ in.} \quad (2-2)$$

where, h is the height of the backwall in inches and ΔL is the total bridge movement under the full temperature range. VDOT (2010) recommends using the passive earth pressure coefficient (K_p) of 4 when EPS is used behind the backwall and analysis of the backwall considering a continuous beam supported by the girders. However, using field monitoring data of a 45° skew integral abutment bridge, Hoppe and Bagnall (2008) demonstrated that the K_p can be as low as 1.2 when the angle of backfill-abutment wall friction is 20° or 0.6 when the angle of friction is zero. Field observations have shown that the skew bridge superstructure rotation is as low as 5° ; hence, the interface angle of friction can be assumed to be zero (Hoppe and Bagnall 2008).

EPS properties such as compressive stress, elastic limit strain, modulus, Poisson's ratio, creep, durability, etc are discussed in the literature (Lutenegger and Ciufetti. 2009; Stark et al. 2004). EPS material properties are controlled by its density. For EPS with 1.25 lb/ft^3

density, the elastic property limit is at a compression strain of less than 1%. The special provisions presented in Hoppe and Bagnall (2008) require providing EPS with linear-elastic stress-strain behavior up to 10 percent strain. In addition to density, EPS compressive strength is a nonlinear function of temperature. Strength remains constant for a temperature less than 32 °F. When the temperature increases beyond 32 °F and up to 73 °F, strength decreases at a rate of 7% per 18 °F. Conversely, temperature increase from 73 °F to 140 °F increases EPS strength at a rate of 7% per 18 °F.

For calculating the Poisson's ratio (ν) of EPS Lutenegeger and Ciufetti (2009) proposed the following equation:

$$\nu = 0.091\gamma + 0.0024 \quad (2-3)$$

where γ is the density of EPS in lb/ft³.

According to Lutenegeger and Ciufetti (2009), the coefficient of passive EPS pressure (K_p) can be expressed in terms of Poisson's ratio as follows:

$$K_p = \nu / (1 + \nu) \quad (2-4)$$

For commonly available EPS, the passive earth pressure coefficient (K_p) ranges from 0.1 to 0.2, negligible for design. Lutenegeger and Ciufetti (2009) state that the horizontal pressure, when a uniformly distributed load is applied over EPS, is about 1/10th of the vertical load. This shows that the magnitude of overburden pressure should be considered in analysis rather than using a constant value as recommended by VDOT. Creep of EPS is highly dependent on temperature. For example, at 140 °F exposure compared to 73 °F, uniaxial strains increased by 88% for 1.25 lb/ft³ density EPS under a sustained stress of 626 lb/ft² for approximately 3 months. However, when the sustained stress is increased to 835 lb/ft², with all other conditions remaining the same, creep strain increased to 195% (Lutenegeger and Ciufetti 2009).

Norway has a long history of using EPS, and significant data has been collected on EPS performance. According to Frydenlund and Aabøe (2001), EPS can be a very durable

material that can be used for a life cycle of 100 years provided that the buoyancy forces are properly accounted, EPS is well protected from dissolving agents like gasoline, and the stress level to which EPS is subjected is kept below 30-50% of its compressive strength.

Stark et al. (2004) illustrated some typical details of EPS abutment (Figure 2-46) where the approach is directly supported by a sand subgrade placed over the EPS. This detail is not preferable since the approach slab and the subgrade becomes a surcharge load over the EPS fill, which will promote EPS creep. This surcharge load can be eliminated by including a sleeper slab, to support the approach. From the design procedure presented by Stark et al. (2004), only active soil pressure will be the load acting on the abutment when the approach slab is supported by a sleeper slab. Passive earth pressure can be neglected as it can only form under large deformation within the EPS. Considering all the benefits, EPS is a practical solution to reduce the backfill effect on the backwall or abutment wall of skew bridges. When the use of EPS is specified, a sleeper slab should be provided to support the approach slab, buoyancy forces on the EPS should be accounted for in the design, and adequate protection should be provided using geotextile and gasoline containment geomembranes.

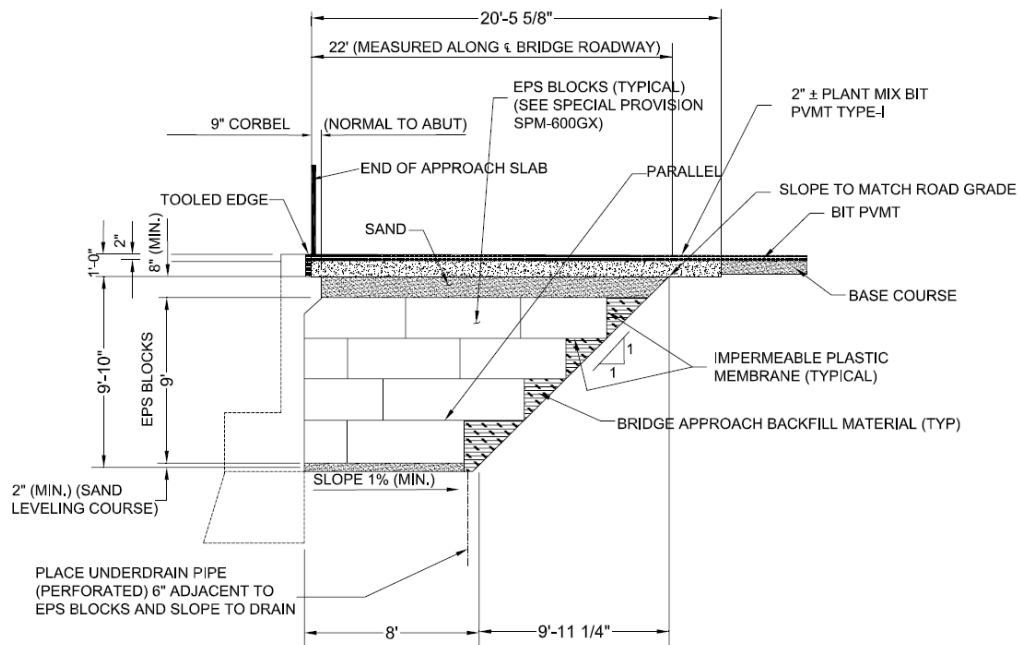


Figure 2-46. Typical details of EPS abutment (Stark et al. 2004)

2.4.5 EPS-Concrete Interface Friction

Several jointless abutment configurations are being used. One such configuration shown in Figure 2-47 is the deck sliding over backwall where a bond breaker is placed between the deck and the backwall. The function of the bond breaker is to provide a sliding surface between the deck and the abutment. When EPS is utilized as the bond breaker, there is a possibility to develop significant friction force on the sliding surface. According to Elragi (2011), the peak and residual friction coefficients between EPS and concrete are 2.3 and 1, respectively.

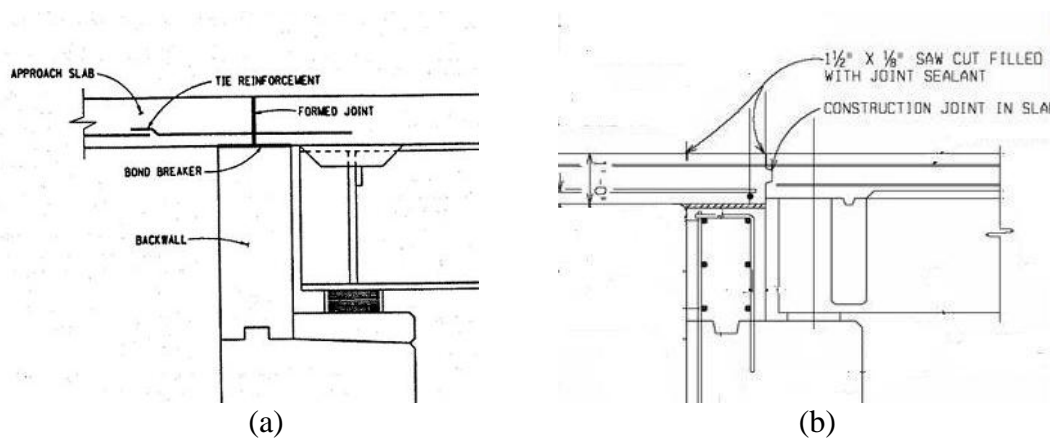


Figure 2-47. Deck sliding over backwall: (a) NYDOT and (b) MDOT

2.4.6 Support Bearing Selection and Design

Section 2.3 detailed literature recommendations on support bearing configurations to minimize stresses developed in the structure. As acknowledged in AASHTO LRFD (2010), a majority of these recommendations are not practical and cannot be implemented. Further, only a limited number of bearing types can be effectively used in semi-integral bridges (Table 2-2). Skew, semi-integral, or deck sliding over backwall bridges require bearings to allow longitudinal movement and rotation about all three axes and to provide resistance for transverse and vertical loads. Considering deformation and load demands on skew bridge support bearings, plain elastomeric pad (PEP), fiberglass-reinforced pad (FRP), and steel-reinforced elastomeric bearings or pads (SREB or SREP) are suitable for skew, semi-integral, or deck sliding over backwall bridges. Table 2-3 summarizes capabilities, limitations, and cost of bearings. Following load and translation magnitudes calculations, limitations given in the table can be used for preliminary selection (Roeder and Stanton 1996). Also, sliding

bearings can be combined with other types listed in Table 2-2 to accommodate large movements (Roeder and Stanton 1996; Parke and Hewson 2008).

Table 2-2. Bearing Suitability (Source: AASHTO LRFD 2010)

Type of Bearing	Movement		Rotation about Bridge Axis Indicated			Resistance to Loads		
	Long.	Trans.	Long.	Trans.	Vert.	Long.	Trans.	Vert.
Plain Elastomeric Pad	S	S	S	S	L	L	L	L
Fiberglass-Reinforced Pad	S	S	S	S	L	L	L	L
Steel-Reinforced Pad	S	S	S	S	L	L	L	S
Plane Sliding Bearing	S	S	U	U	S	R	R	S

L: Suitable for limited applications; S: Suitable; R: May be suitable, but requires special considerations or additional elements such as sliders or guideways; U: Unsuitable.

Table 2-3. Summary of Bearing Capabilities (Source: Roeder and Stanton 1996)

Type of Bearing	Load (kip)		Translation (in.)		Rotation (Rad.)	Cost	
	Min.	Max.	Min.	Max.	Limit	Initial	Maintenance
Plain Elastomeric Pads (PEP)	0	100	0	0.6	0.01	Low	Low
Fiberglass-Reinforced Pad (FRP)	0	135	0	1	0.015	Low	Low
Steel-Reinforced Elastomeric Bearing	50	785	0	4	0.04	Low	Low
Flat PTFE (Polytetrafluorethylene) Slider	0	> 2250	1	> 4	0	Low	Moderate

Roeder and Stanton (1996) and Badie, et al. (2001) developed charts for use in preliminary selection of bearings (Figure 2-48, Figure 2-49, Figure 2-50, and Figure 2-51). These charts were developed for steel girder bridges. But, they are equally valid for PC girder bridges. Other bearing types covered in the charts are pot bearing, cotton duck pads (CDP), and random oriented fiber pads (ROFP).

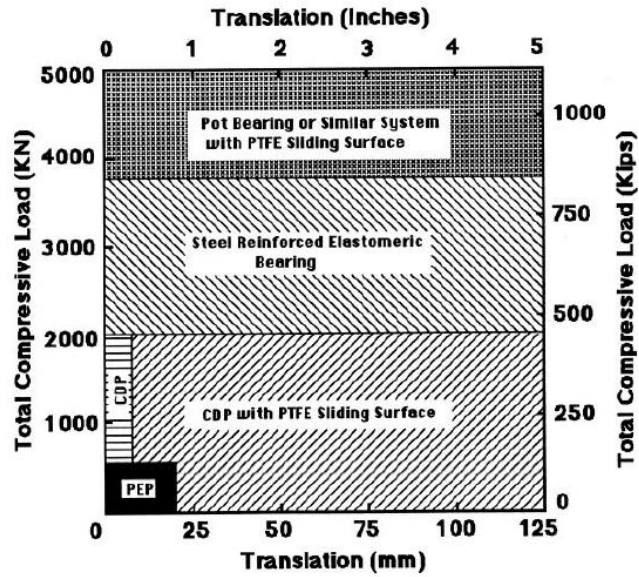


Figure 2-48. Preliminary bearing selection diagram for minimal design rotation (rotation ≤ 0.005 radians) (source: Roeder and Stanton 1996)

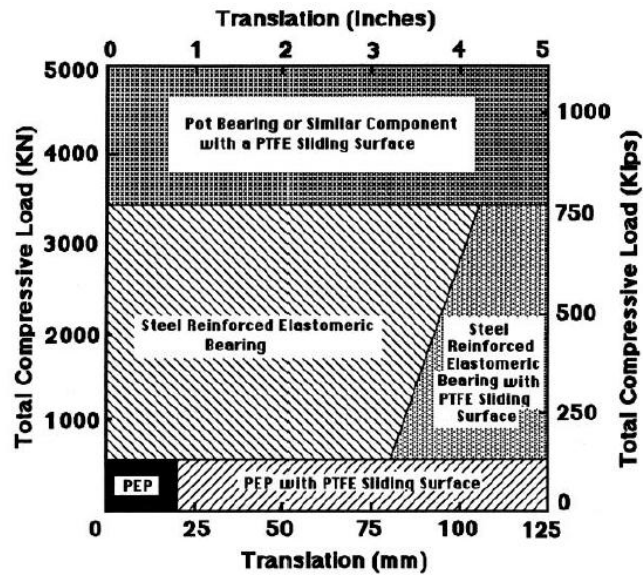


Figure 2-49. Preliminary bearing selection diagram for moderate design rotation (rotation ≤ 0.015 radians) (source: Roeder and Stanton 1996)

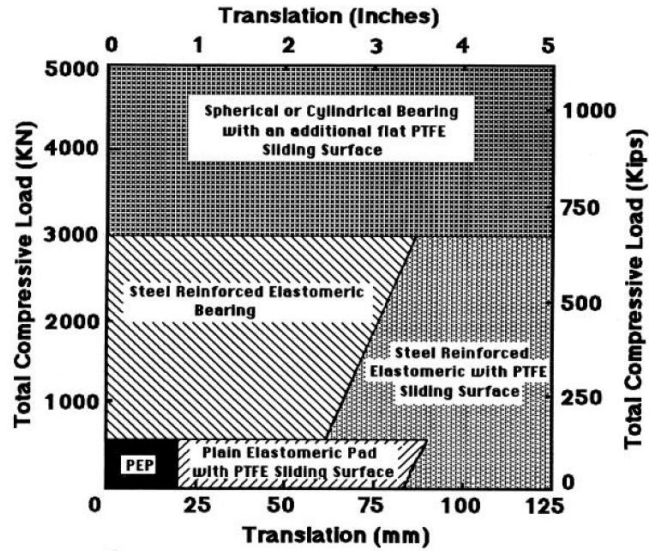


Figure 2-50. Preliminary bearing selection diagram for large design rotation (rotation > 0.015 radians) (source: Roeder and Stanton 1996)

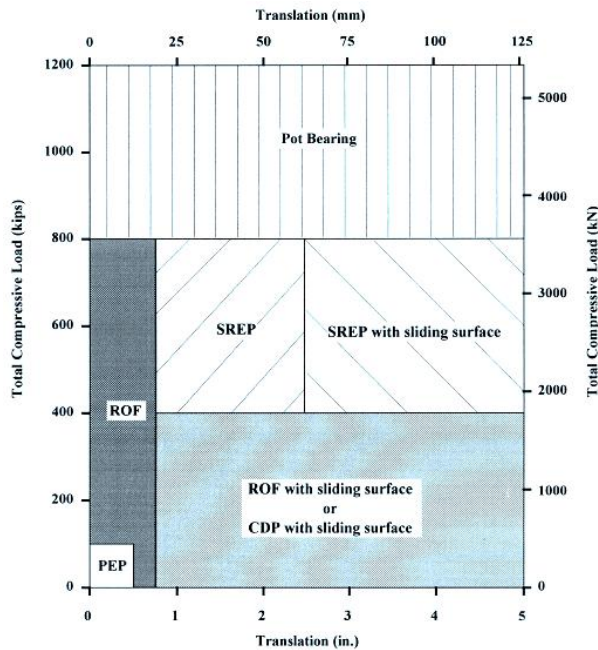


Figure 2-51. Preliminary bearing selection diagram (Badie, et al. 2001)

Inspection and maintenance are critical tasks in bridge management. Adequate access should be provided around the bearings for inspection, maintenance, and replacement (Parke and Hewson 2008; Roeder and Stanton 1996). In that regard, Ontario details (Figure 2-41, Figure 2-42, Figure 2-43, and Figure 2-44) are preferred over the current MDOT semi-integral details. In MDOT details, support bearings under the girders are encased by the backwall.

The joint filler between the backwall and the abutment establishes the sliding surface (Figure 2-52). In addition to concealing the support bearing, joint filler between the backwall and abutment used in this detail may generate large friction forces. High friction forces between the backwall and abutment may be the source of D-cracking documented on abutments of semi-integral bridges (Figure 2-52). The current design trend is to isolate the backwall from the abutment using configurations similar to Ontario and several other SHA. Implementation of these configurations allows the use of elastomeric bearings, sliding plate bearings or a combination thereof and minimizing interaction between the abutment and backwall. Further, isolation of the backwall from the abutment provides adequate space for inspection, maintenance, and replacement of bearings. However, isolation of the backwall from abutment requires developing specific design details to provide restraint to transverse movement of skew bridges. In that regard, placing the backwall over the abutment and restraining transverse movement by placing the wingwall against the backwall and deck, similar to current MDOT semi-integral details, provides many benefits if adequate measures are taken to minimize interface friction and infiltration of backfill material through the joints. One additional benefit of the current MDOT abutment-backwall configuration with different girder sizes is that restraint to lateral bridge movement is provided (Figure 2-53) equivalent to developing girder end restraint systems for skew bridges.

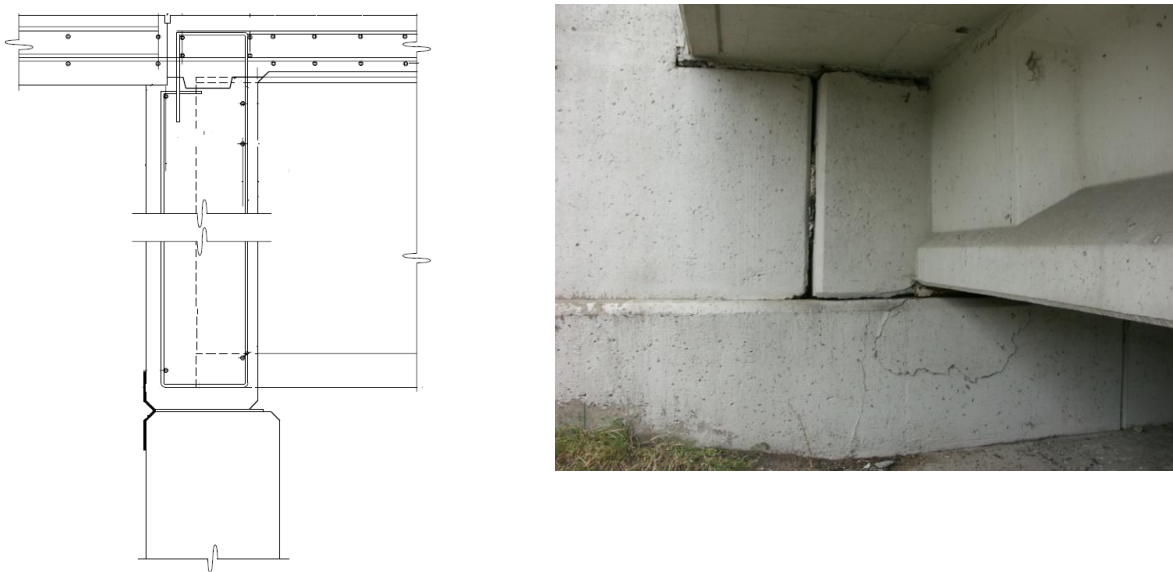


Figure 2-52. MDOT semi-integral abutment configuration



Figure 2-53. Backwall and abutment configuration of a bridge with different girder depths

2.4.7 Deck Reinforcement Details with Skew

According to Oesterle et al. (1999), reinforcement for skewed approach slabs should follow the skewed deck requirements of AASHTO LRFD (2010). The end of approach slab should be parallel to the abutment wall for both straight and skewed bridges.

AASHTO LRFD (2010) section 9.7.1.3 (Skewed Decks) for skew angle less than 25° , requires that the primary reinforcement to be placed in the direction of skew, otherwise placed normal to the girder axis (Figure 2-54). This provision is intended to prevent excessive deck cracking due to inadequate reinforcement in the direction of principal flexural stresses.

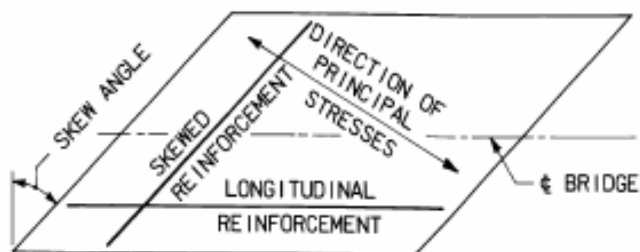


Figure 2-54. Reinforcement layout (AASHTO LRFD 2007)

According to section 9.7.2.5 (Reinforcement Requirements - Empirical Design) of AASHTO LRFD (2010), for a skew angle over 25° , the specified reinforcement in both directions shall be doubled in the end zones of the deck. Each end zone is the longitudinal distance equal to the effective length of the slab. This provision is also intended for crack control. It was documented that bridge decks with a skew greater than 25° have shown torsional cracks due to differential deflections in the end zone (OHBDC 1991). The extent of documented cracking was usually limited to a width equal to the effective length.

The MDOT Bridge Design Guide section 6.41.01 specifies bridge deck reinforcement layout when the deck is designed based on load factor method. “S along the skew” should be used to determine the slab reinforcement where S is the beam spacing minus the top flange width for slab on prestressed concrete I beams and beam spacing minus half flange width for slab on steel beams. If the angle of crossing is 70° or greater (i.e., skew is equal or less than 30°), transverse bars are placed parallel to the reference lines if “S along the skew” falls in the same beam spacing range as “S normal to the beams” or the next larger range.

According to the MDOT Bridge Design Guide section 6.41.02 (Standard Bridge Slabs – Empirical Design), transverse bars may be placed parallel to the reference lines if the angle of crossing is 65° or greater (i.e., skew is equal or less than 35°); they should otherwise be placed perpendicular to the bridge centerline. End zone reinforcement is required for both simply supported and continuous spans as shown in Figure 2-55.

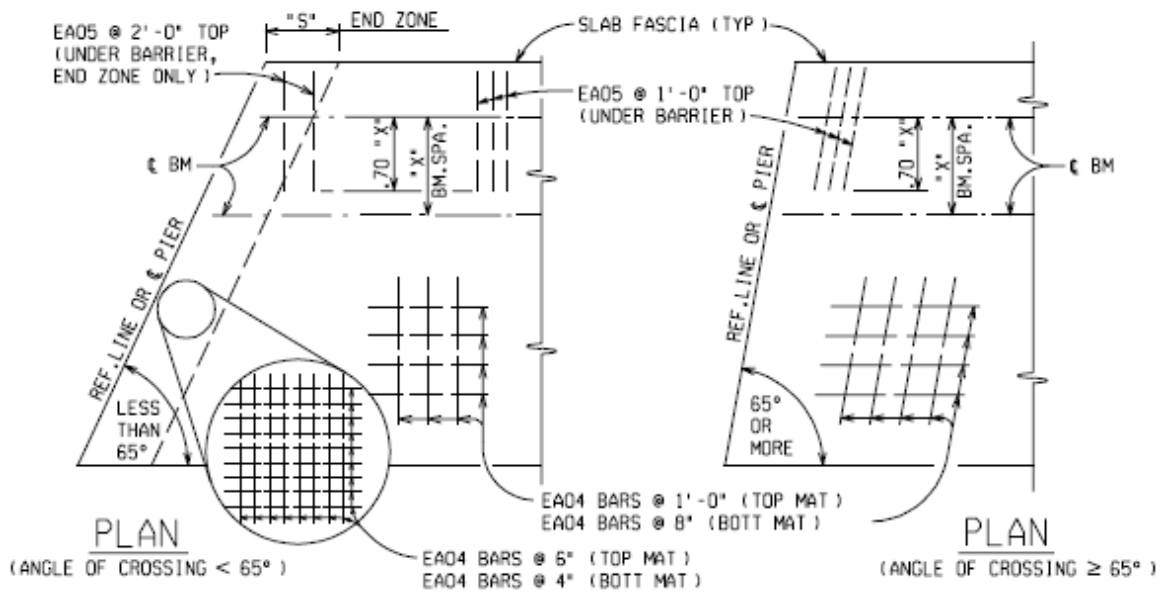


Figure 2-55. End zone reinforcement details (MDOT Bridge Design Guide 6.41.02)

2.5 FIELD PERFORMANCE OF SKEWED/JOINTLESS BRIDGES

The MDOT Structural Research Unit conducted field inspection of eight MDOT bridges that have link slab detail and were constructed between 2001 and 2003 (Gilani and Jansson 2004). Two of the bridges had moderate and high skew angles.

S08-63101 is a 26° skewed four-span steel bridge with a link slab over the center pier that was constructed in 2001 as part of a deck replacement project. Review of construction documents revealed that the longitudinal reinforcement was under-designed for HS-25 live loading. Inspection documented hairline cracks on the link slab within 1-2 feet of the saw cut region (Figure 2-56). Crack widths ranged between 0.002 and 0.004 inches. The rest of the link slab area was crack free.

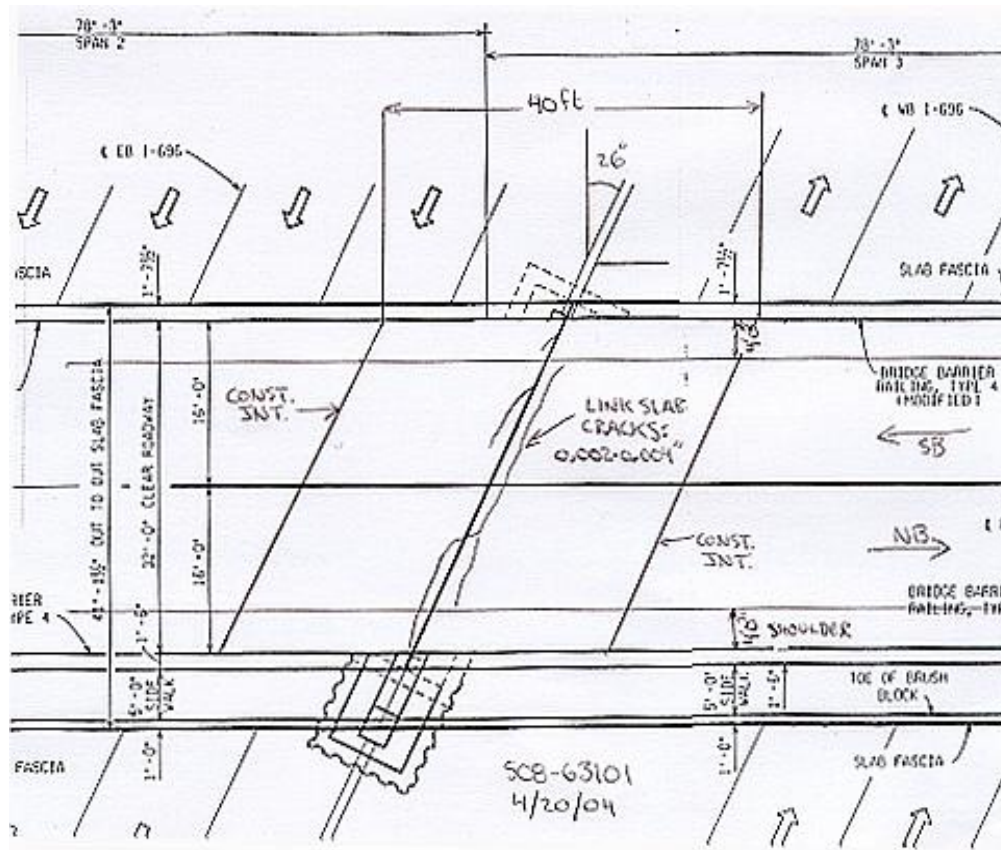


Figure 2-56. Link slab cracking on S08 of 63101 (Gilani and Jansson 2004)

S15-82025 is a four-span 45° skewed steel girder bridge. Link slab was constructed over the center pier in 2001 as part of a deck replacement project. Several pitfalls with design and construction were recorded: inadequate reinforcement, termination of the longitudinal reinforcement at the same location on both sides of the saw cut, unspecified pour sequence, and extra longitudinal reinforcement under the transverse reinforcement (Figure 2-57). The required area of longitudinal steel was calculated to be 1.40 in²/ft, and the quantity of as placed steel was 0.50 in²/ft. Despite the large difference in longitudinal steel between required and provided, the link slab in this structure appeared to be performing satisfactorily. ADT count on the bridge was only 600, with an ADTT count of zero. Despite the design and construction issues, typical link slab cracks were not documented during inspection (Gilani and Jansson 2004). It was believed that the light traffic with no truck loading might be the reason for the crack free link slab.

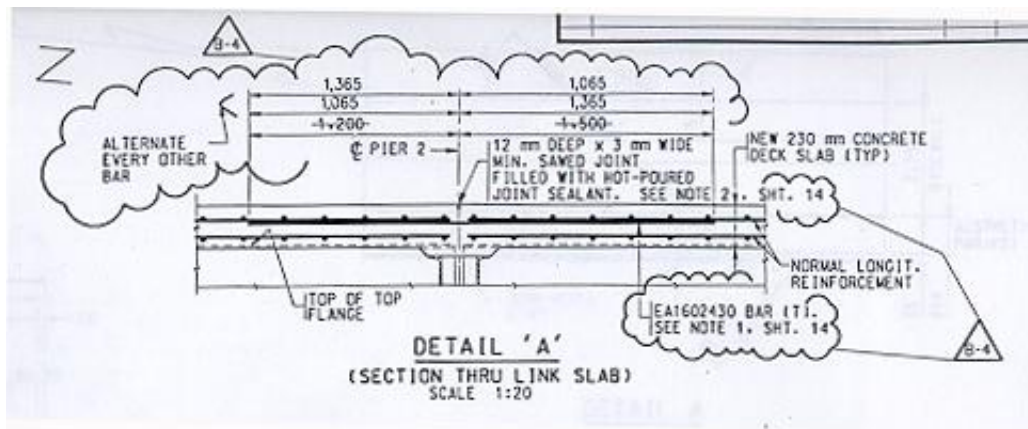


Figure 2-57. Link slab design detail and an inspection photo (Gilani and Jansson 2004)

North Carolina Department of Transportation (NCDOT) performed a follow up inspection to a high skew, 12-span bridge with link-slabs. The structure was opened to traffic for nearly two years. The link-slab saw cuts were filled with silicone. On the link slabs and the bridge deck only minor cracking parallel to the link slab was observed (NCDOT 2007).

The rotation of semi-integral bridges about its axis and its effects has been noted in the field (Sanford and Elgaaly 1993; Burke 1999; Van Lund and Brecto 1999). Indications of

significant transverse movement of abutments in bridges with high skews and/or horizontal curves were observed. Transverse movement of integral abutments should be accounted for in the design details for barrier walls, drainage structures, and the ends of the approach slabs (Tabatabai et al. 2005).

Figure 2-58 shows the abutment wall cracks near an acute corner of a two-span 45° skew bridge that sits on semi-integral abutments. The bridge was constructed in 1969 with an overall length of 292 ft and a width of 38 ft. The end-diaphragm moves with the superstructure that slides longitudinally, and it is guided transversely by relatively stiff abutments. Cracks in the abutment wall near the acute corner were perhaps caused by transverse forces (Nicholson et al. 1997 and Oesterle et al. 1999).

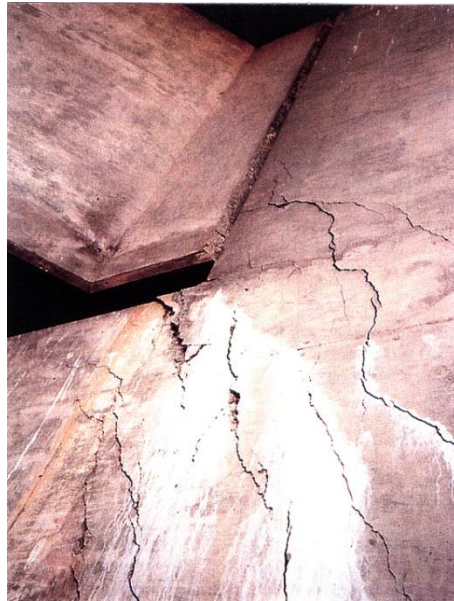


**Figure 2-58. Abutment wall cracking near an acute corner of the superstructure
(Nicholson et al. 1997 and Oesterle et al. 1999)**

The Ontario Ministry of Transportation (OMOT) utilized various semi-integral abutment configurations since late 1960s. The most recent configuration, superseded by the details shown in Figure 2-41 to Figure 2-44, is shown in Figure 2-59. Use of this configuration was discontinued because the neoprene or rubber bearing pads placed in between the backwall and abutment wall did not prevent ingress of backfill material (Husain and Bagnariol 1999).

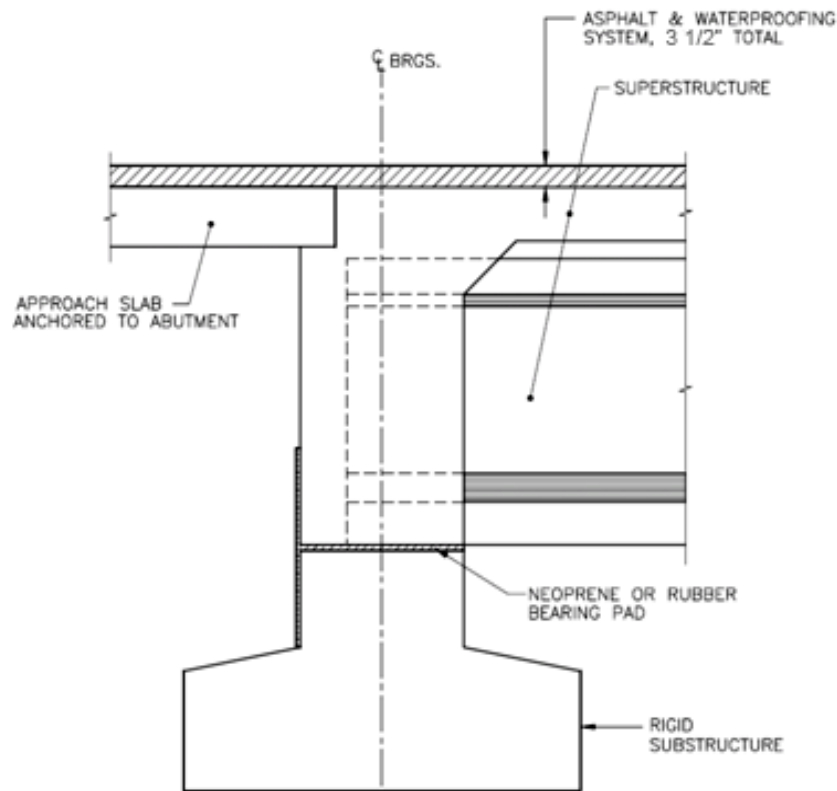


Figure 2-59. Semi-integral abutment configuration used by the Ontario MOT before most recent details

2.6 SUMMARY

A comprehensive literature review on the behavior, performance, and design details of skew/jointless bridges was presented. The summary below is developed to reemphasize key points identified through literature review:

1. Skewed bridges show clear distinctions in the behavior under both gravity and thermal loading than that of straight bridges. Skewed bridges up to a skew angle of 20° can be analyzed and designed as straight bridges. Refined analysis methods are recommended for bridges with a skew greater than 20° since their behavior is controlled by the skew angle, width to span ratio, and the type of deck and supports.
2. Characteristics of skewed bridges are reduction in maximum mid span moments compared to that of straight bridges under similar loads, negative moments near corners, torsional moments in the end zones, and redistribution of reaction forces. Skewed bridges develop high reactions and shear forces near obtuse corners and low

- reactions, and possibly uplift at acute corners. In general, negative moments are developed closed to obtuse corners; negative moments are a possibility at acute corners if uplift is prevented (Hambly 1991).
3. Skewed bridges with semi-integral abutments would tend to rotate about an axis normal to their horizontal plane. The rotation is due to the passive pressure developed behind the backwall under thermal expansion. Deck extensions also have a tendency to develop in-plane rotations but not as critical as semi-integral systems. In both deck extension and semi-integral systems, the rotation may be affected by the approach slab-subbase friction, the shearing resistance of the elastomers in the bearings, and by the compressive resistance of fillers used in the movable joints between the superstructure and wingwalls.
 4. The current MDOT deck sliding over backwall system uses EPS in between deck and backwall to introduce the sliding surface. The EPS elastic strain limit is very small and can deform beyond the elastic limit under deck self-weight and live loads. Further, peak and residual friction coefficients between EPS and concrete are 2.3 and 1.0, respectively. Because of these reasons, neoprene pads over the backwall may be used. In addition, a polyethylene sheet used under the approach should be extended to the backwall face on the span side to minimize friction at the interface.
 5. The current semi-integral configuration used by Ontario and several State Highway Agencies has the advantages of allowing the backwall to move independently from the abutment, providing access space for bearing inspection, maintenance, and replacement; and preventing backfill infiltration through the backwall.
 6. Isolation of the backwall from the abutment requires developing specific design details to constrain transverse movement of skew bridges. In that regard, placing the backwall over the abutment and restraining transverse movement by placing the wingwall against the backwall and deck, similar to current MDOT semi-integral details, provides many benefits if adequate measures are taken to minimize interface friction and infiltration of backfill material through the joints. Use of EPS from

- behind the backwall helps reduce passive earth pressure and prevents infiltration of backfill material.
7. One additional benefit of the current MDOT abutment-backwall configuration with different girder sizes is that restraint to lateral bridge movement is provided equivalent to developing girder end restraint systems for skew bridges. Adequate measures should be taken to minimize interface friction and infiltration of backfill material through the joints.
 8. Ontario uses EVA (Ethylene vinyl acetate, commonly known as expanded rubber or foam rubber) between the vertical faces of the backwall and abutment wall in order to allow the backwall to move independently from the abutment. EVA has a wider elastic range than EPS. On the other hand, the durability performance of EVA has not been documented.
 9. In order to allow the translation and rotation of skew bridges and provide sufficient load capacity, plain elastomeric pad (PEP), fiberglass-reinforced pad (FRP), and steel-reinforced elastomeric bearings or pads (SREB or SREP) are suitable for support bearings for semi-integral and deck sliding over backwall bridges. Also, PTFE sliding bearings can be combined with the support bearing types stated above to accommodate large superstructure movements. PTFE sliding bearings can be specified for most of the short and medium span bridges when girder end rotations are not critical.
 10. Rub plates, girder stops, or any other mechanism that is designed to resist large forces is needed to control lateral movement of skew bridges.
 11. With increasing backfill stiffness, forces at wingwalls of high skew bridges increase dramatically. EPS can be specified as a suitable backfill material for semi-integral bridges to reduce passive pressure. However, the approach slab should not be directly supported on EPS because of potential creep. EPS should also be protected using geotextiles and gasoline containment geomembranes.



MDOT RC-1563



High Skew Link Slab Bridge System with Deck Sliding over Backwall or Backwall Sliding over Abutments

FINAL REPORT – SEPTEMBER 2011

Part II



Western Michigan University
Department of Civil & Construction Engineering
College of Engineering and Applied Sciences

RESEARCH

Intentionally left blank

Technical Report Documentation Page

1. Report No. Research Report RC-1563	2. Government Accession No.	3. MDOT Project Manager Steve Kahl, P.E.	
4. Title and Subtitle High skew link slab bridge system with deck sliding over backwall or backwall sliding over abutments		5. Report Date September 30, 2011	
7. Author(s) Dr. Haluk Aktan, P.E., and Dr. Upul Attanayake, P.E.		6. Performing Organization Code WMU	
9. Performing Organization Name and Address Department of Civil and Construction Engineering College of Engineering and Applied Sciences Western Michigan University 1903 W. Michigan Ave, Kalamazoo, MI 49008		8. Performing Org Report No.	
12. Sponsoring Agency Name and Address Michigan Department of Transportation Construction and Technology Division PO Box 30049, Lansing MI 48909		Work Unit No.	
		11. Contract Number : 2006-0415	
		11(a). Authorization Number: 3	
15. Supplementary Notes		13. Type of Report and Period Covered Final Report, 2008-2011	
		14. Sponsoring Agency Code	
16. Abstract <p>A new bridge design and construction trend to help improve durability and rideability is to remove expansion joints over piers and abutments. One approach to achieve this is to make the deck continuous over the piers by means of a link slab while the girders remain simply supported. The need to implement link slabs is indicated by AASHTO LRFD section 2.5.2.4 which requires using a minimum number of expansion joints to improve rideability. Further, due to durability concerns associated with bridge deck joints, it is preferred to have a least number of joints or develop jointless decks. The expansion joints over the abutments can be removed by one of three methods: deck sliding over back wall, semi-integral abutments, and integral abutments. This results in expansion joints at either or both ends of the approaches. The design concerns other than link slab include backwall and wing-wall design and bearing movement. The behavior of a jointless bridge brings about many challenges to bridge designers. The complexity is augmented when skew is involved.</p> <p>This report complements an earlier report based on previous research on <i>Combining Link Slab, Deck Sliding Over Backwall and Revising Bearings</i> (Aktan et al., 2008) where the behavior of straight and moderately skew (skew < 20⁰) link slab bridges were investigated and design recommendations were developed. This report describes the behavior and performance of high skew (skew > 20⁰) jointless bridges with link slabs and two abutment configurations. These abutment configurations are deck sliding over backwall and backwall sliding over abutments (i.e. semi-integral abutments).</p> <p>Four tasks were performed in this project. The first task was to review and synthesize information related to the behavior, performance, design, and analysis of skew bridges. The second task was field assessment of skew bridge behavior under static truck loads and thermal loads. The third task was analytical and numerical analysis of skew link slabs. The final task was analytical and numerical analysis of skew sliding deck over backwall systems and semi-integral abutments.</p> <p>Design recommendations are developed based on literature, field assessment data analysis, finite element modeling, and subsequent simulations of the numerous models developed in this project. One recommendation deals with the skew link slab design and the remaining recommendations are for bearing selection and selection and design of a transverse restraint system at abutments of skew link slab bridges.</p>			
17. Key Words: Abutment, Concrete, Finite Element, Jointless Bridge, Link Slab, and skew.		18. Distribution Statement No restrictions. This document is available to the public through the Michigan Department of Transportation.	
19. Security Classification (report) Unclassified	20. Security Classification (Page) Unclassified	21. No of Pages 249	22. Price

Intentionally left blank

High Skew Link Slab Bridge System with Deck Sliding over Backwall or Backwall Sliding over Abutments

Project Manager: Mr. Steve Kahl, P.E.

Submitted to:



Submitted by

Dr. Haluk Aktan, P.E.
Professor & Chair
(269) – 276 – 3206
haluk.aktan@wmich.edu

Dr. Upul Attanayake, P.E.
Assistant Professor
(269) – 276 – 3217
upul.attanayake@wmich.edu



Western Michigan University
Department of Civil & Construction Engineering
College of Engineering and Applied Sciences
Kalamazoo, MI 49008
Fax: (269) – 276 – 3211

Intentionally left blank

DISCLAIMER

The content of this report reflects the views of the authors, who are responsible for the facts and accuracy of the information presented herein. This document is disseminated under the sponsorship of the Michigan Department of Transportation in the interest of information exchange. The Michigan Department of Transportation assumes no liability for the content of this report or its use thereof.

Intentionally left blank

ACKNOWLEDGEMENTS

This project is funded by the Michigan Department of Transportation. The authors would like to acknowledge the support and effort of Mr. Steve Kahl for initiating this research. The authors also wish to acknowledge the continuing assistance of the Research Advisory Panel (RAP) members in contributing to the advancement of this study. Contribution of graduate students Abdul Mohammed, Alp Servi, Duy Nguyen, Michael Romkema, and Mohamed Rusthi for the successful completion of this study is highly appreciated.

Intentionally left blank

3 MODELING AND FIELD TESTING OF A HIGH SKEW BRIDGE

3.1 OBJECTIVE AND APPROACH

The objective of this chapter is to document high skew bridge load response to truck and thermal loads. Reactions and deformations of the bridge are also obtained by finite element (FE) analysis and compared with the measured deflections and translations. Field measurements were made using a non-contact *Laser Tracker*. This chapter details the bridge configuration, instrumentation and measurement process, and FE bridge model development and analysis. The chapter also includes measurements and comparisons to the FE analysis results.

3.2 BRIDGE DESCRIPTION

The bridge (S12 of 03035) is located in Allegan, Michigan, and carries I-196 over Ottogan Street (one mile east of Holland city limits (Figure 3-1 and Figure 3-2)). The 120 ft long, 44 ft wide, single span simply supported bridge has a 42⁰ skew and carries two lanes of traffic (Figure 3-3). The bridge superstructure consists of seven steel built-up I-girders with cast-in-place concrete deck. The elevation and cross-section of the bridge is shown in Figure 3-4. The girders are connected transversely via “intermediate diaphragms” within the span and “end diaphragms” at both ends of the bridge. The diaphragm labels, locations, and cross-sections are shown in Figure 3-5 and Figure 3-6. The girders back into concrete backwalls at both ends as shown in Figure 3-7. The bridge is supported on the north abutment by a fixed bearing and on the south abutment by an expansion bearing (Figure 3-9), respectively. The expansion bearings are orientated along the bridge axis.

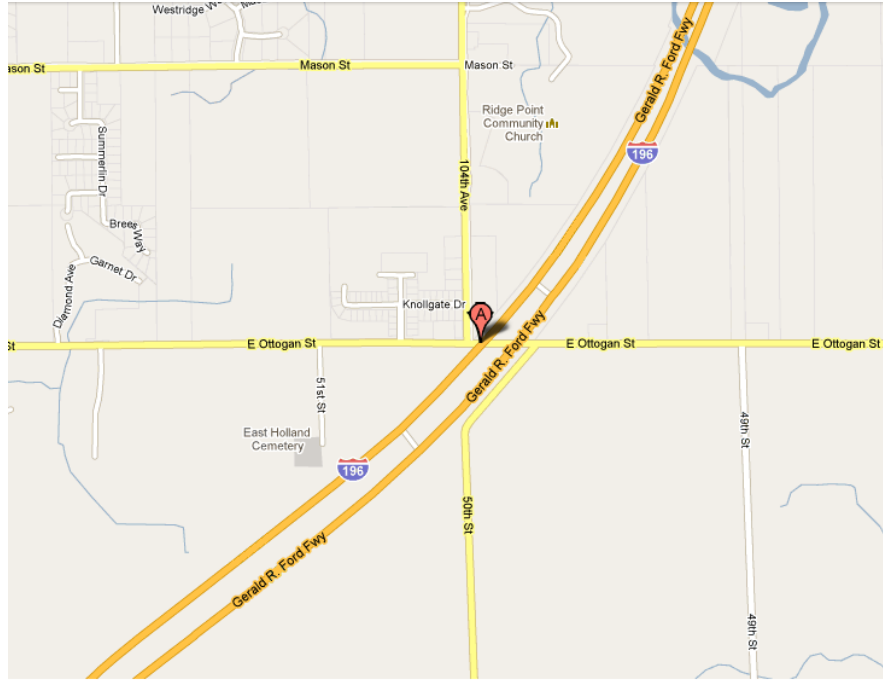


Figure 3-1. Bridge location (Source: Google map)



Figure 3-2. Aerial view of the bridge (Source: Google map)

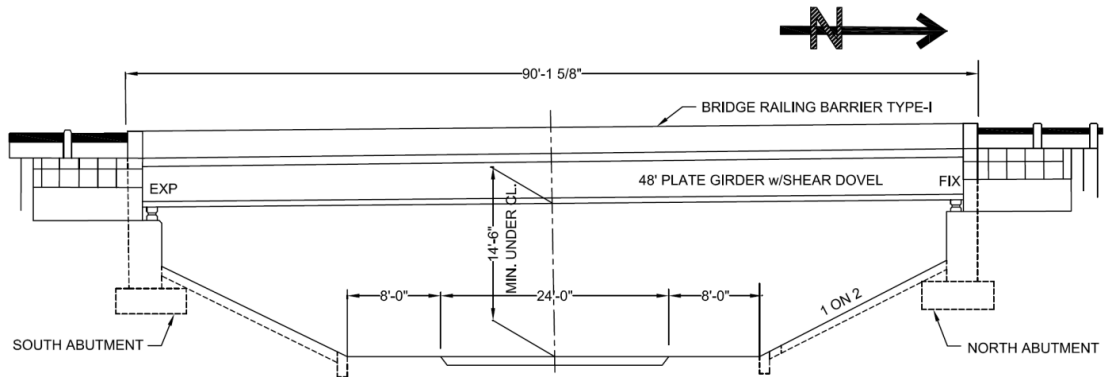


Figure 3-3. Isometric and elevation views of the bridge

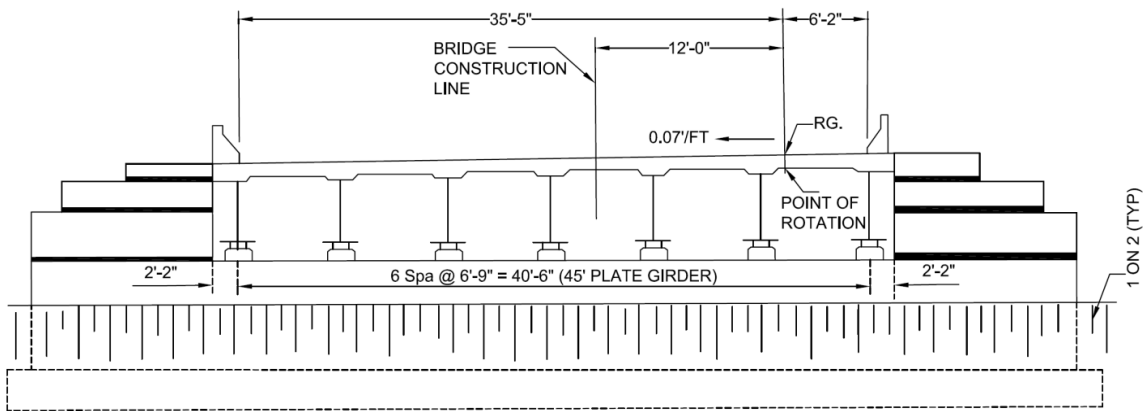


Figure 3-4. Schematic view of bridge cross section

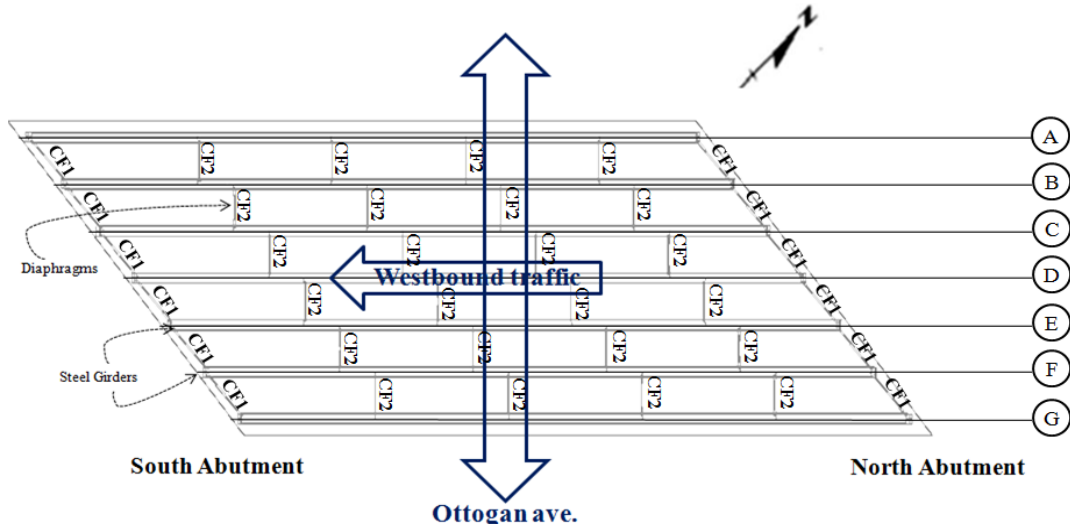


Figure 3-5. Schematic view of diaphragms and girders with labels

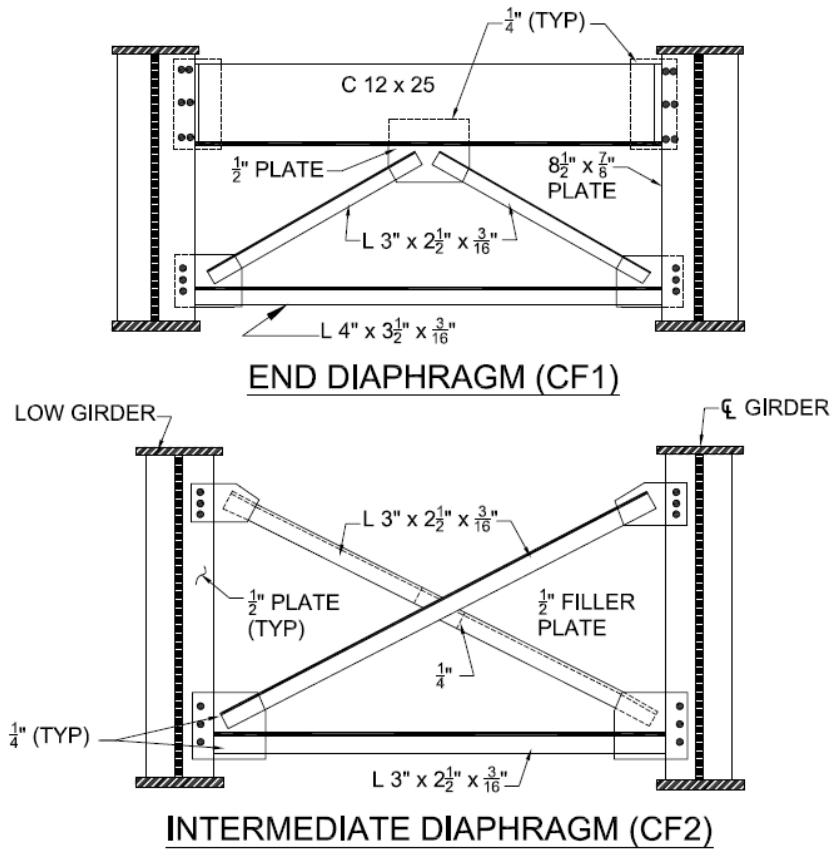


Figure 3-6. Schematic view of end and intermediate diaphragms (cross frames)

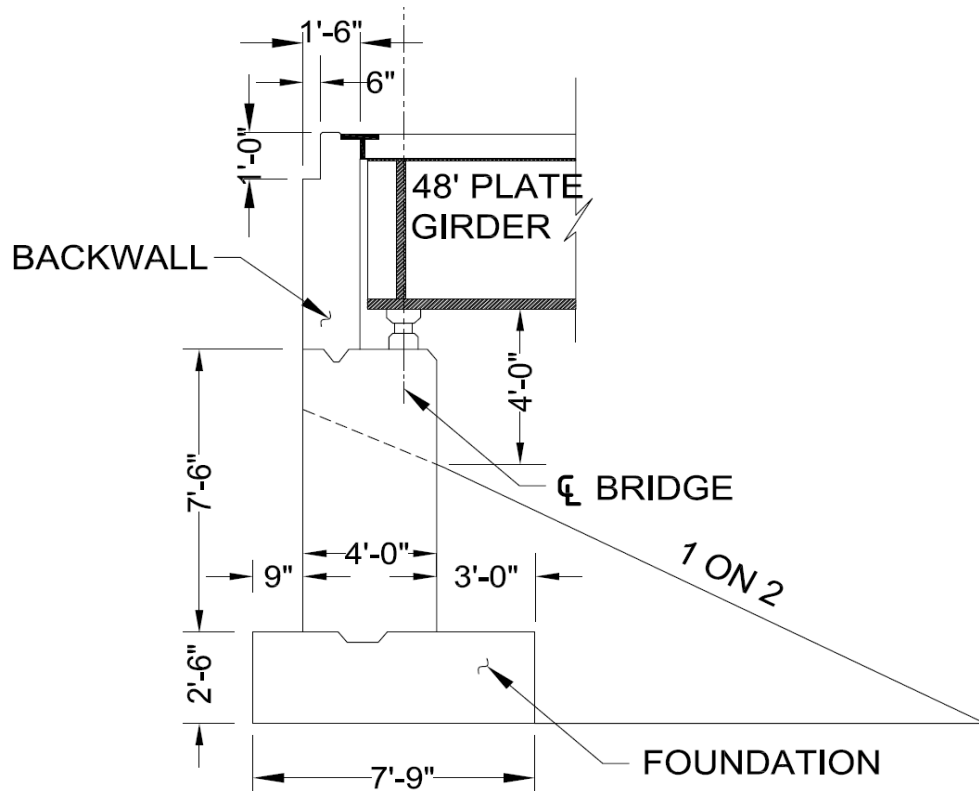


Figure 3-7. Schematic view of abutment section with backwall, girder and foundation

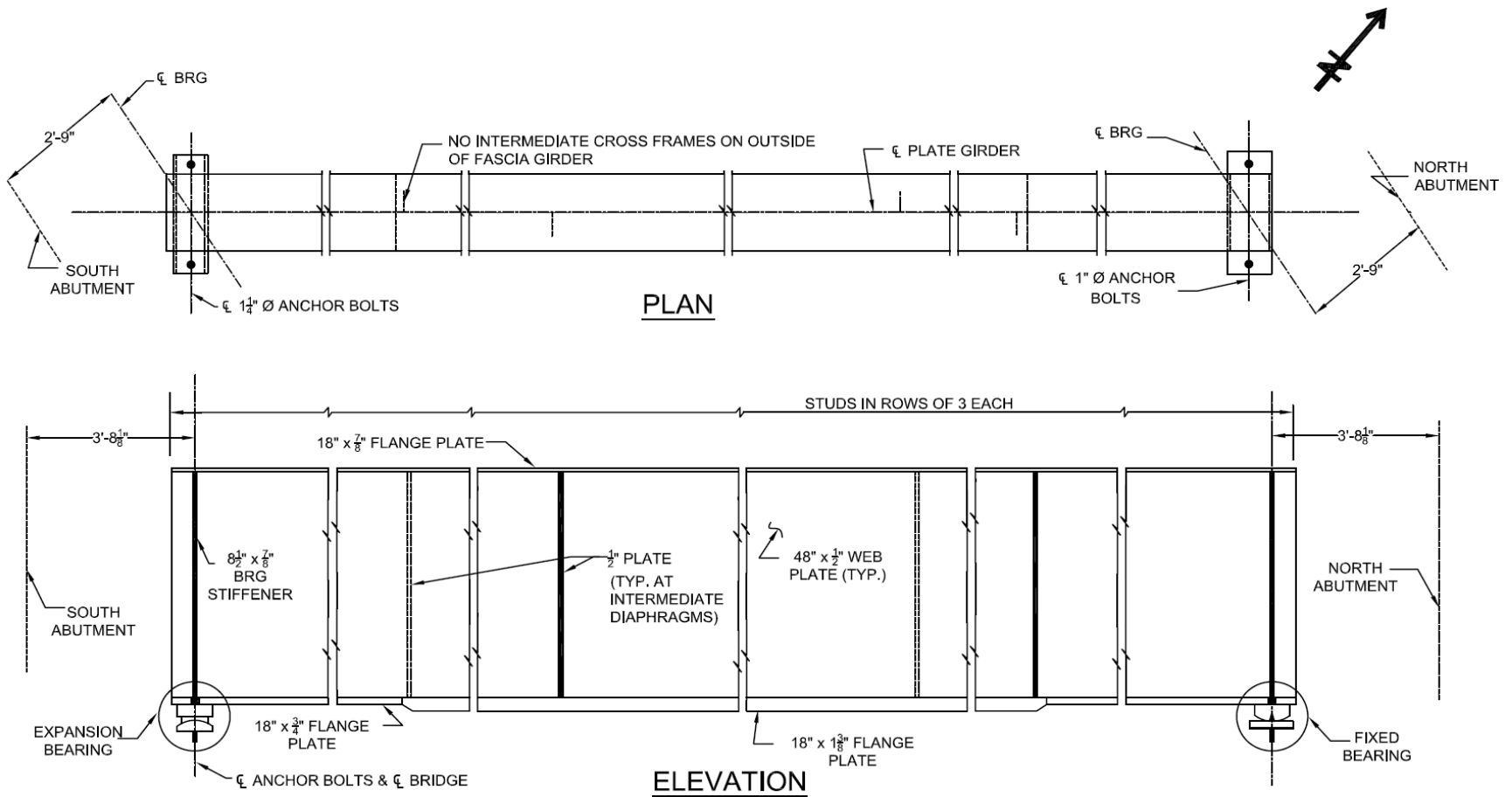
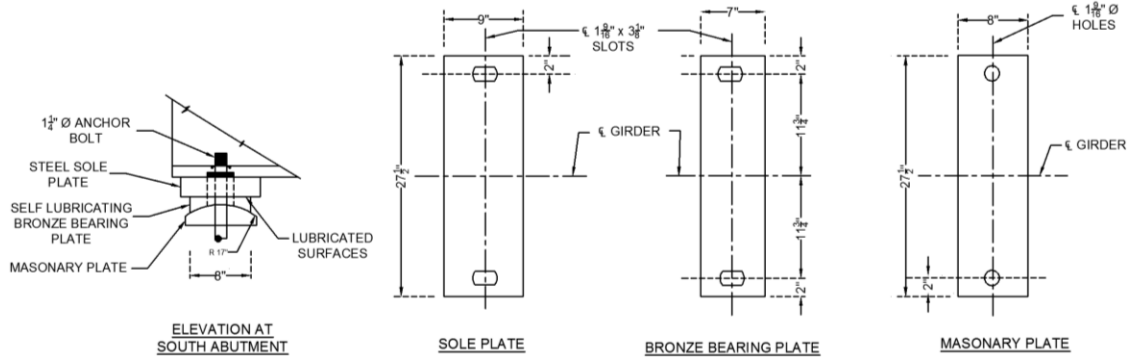
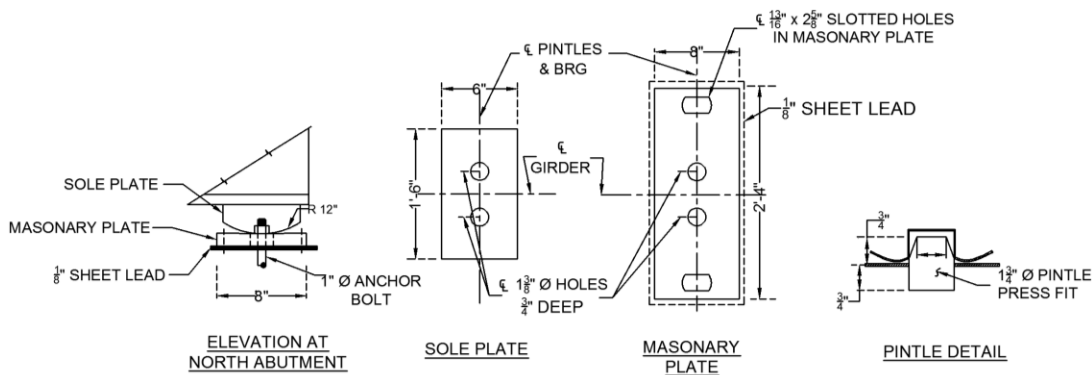


Figure 3-8. Schematic view of girder plan and elevation



(a) Expansion bearing details at south abutment



(b) Fixed bearing details at north abutment

Figure 3-9. Schematic view of respective bearing details

3.3 ABUTMENT, BEARING, AND DECK CONDITION

3.3.1 Abutment Condition

Abutments are in good condition with only a few vertical cracks.

3.3.2 Bearing Condition

Expansion and fixed bearings are used at south and north abutments, respectively (Figure 3-3 and Figure 3-8). Except for the bearings at fascia girders over north abutment, the bearings are in good condition (Figure 3-10). Steel on bronze plate bearings are used at the south abutment (Figure 3-3 and Figure 3-9a). Anchor bolt diameter of the expansion bearing is 1.25 in. The length of the sole plate slot is 3.125 in. Hence, 1.875 in. space is provided at the bearing to accommodate bridge movement due to thermal expansion and contraction. However, the majority of anchor bolts provided with expansion bearings are inclined indicating they have reached the slip limit (Figure 3-11 and Figure 3-12).



(a) Support bearing condition at interior girders (b) Support bearing condition at exterior girders

Figure 3-10. Interior and exterior bearing condition at north abutment



Figure 3-11. Expansion bearing and joint condition at south abutment

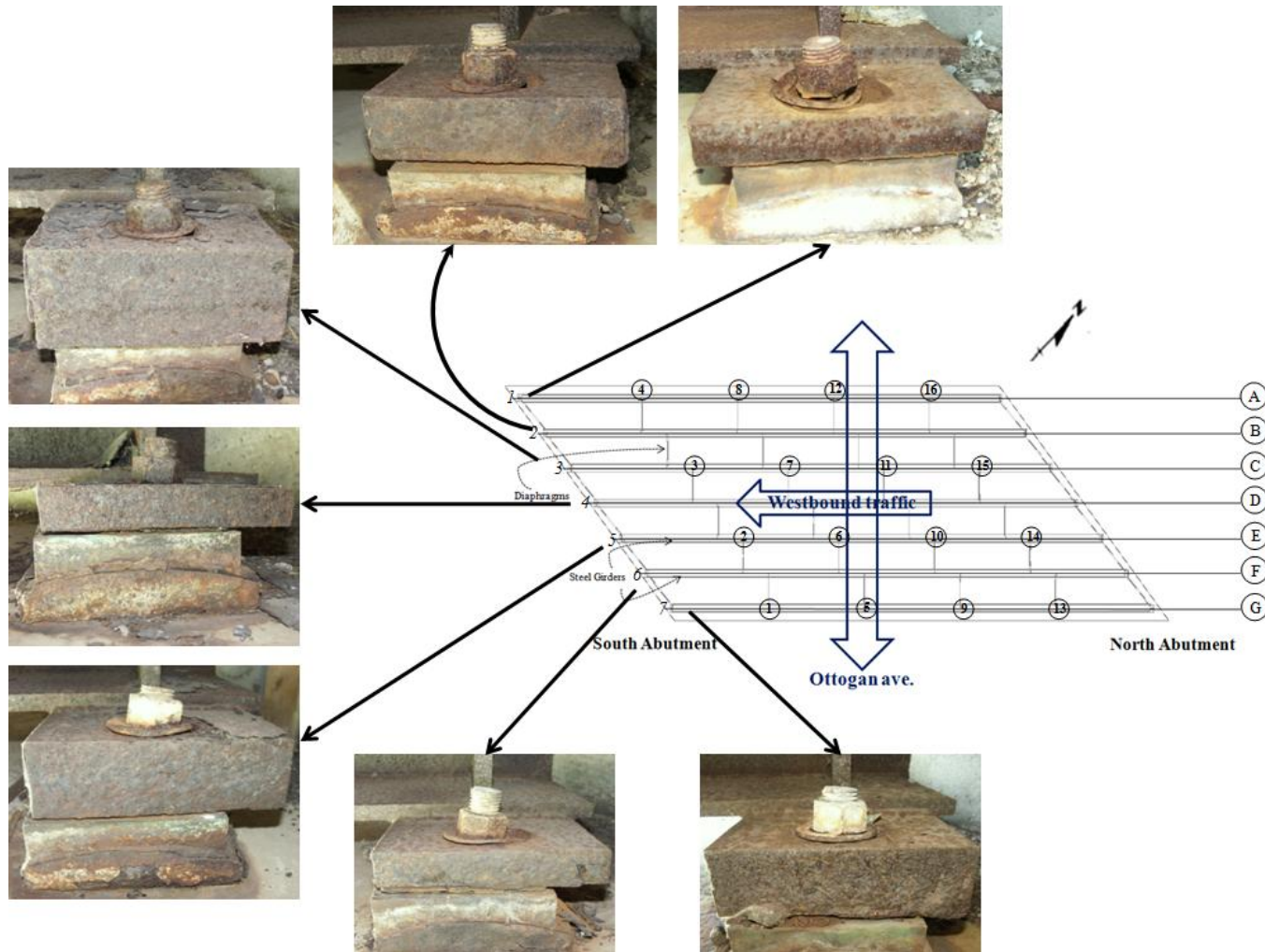


Figure 3-12. Expansion bearing condition at south abutment

3.3.3 Deck Condition

The deck is in good condition with minor areas of scaling and cracking. Repair history shows that expansion joints were replaced in 2004. During inspection, joint gaps were filled with fine debris. Minor cracking was observed adjacent to the joints (Figure 3-13).



(a) Joint over south abutment



(b) Joint over north abutment



(c) Deck cracking close to the obtuse corner of the deck over south abutment

Figure 3-13. Expansion joint and deck condition

3.4 FE MODELING AND PRELIMINARY ANALYSIS FOR LOAD TESTING

The objective of the preliminary analysis is to calculate the anticipated displacement of the girders and maximum girder and deck stresses during load testing.

3.4.1 Bridge FE Modeling

A detailed finite element model is developed with multiple element types (Figure 3-14). The element types used for the modeling of specific bridge components is included in Table 3-1.

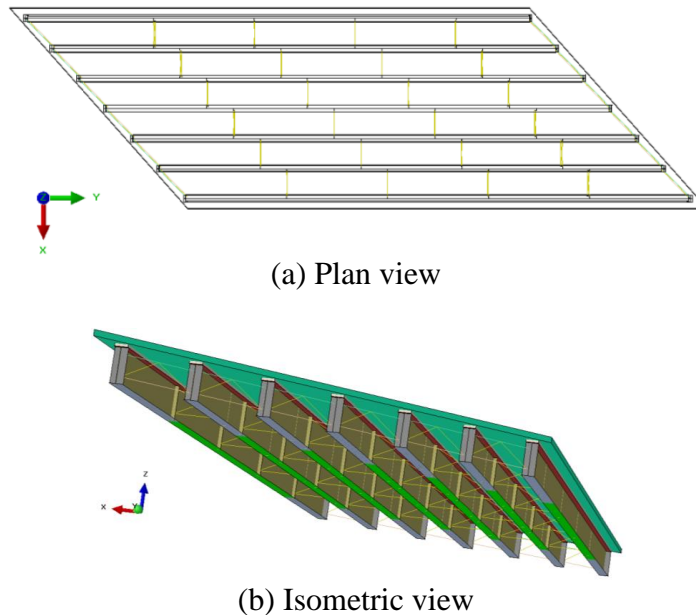


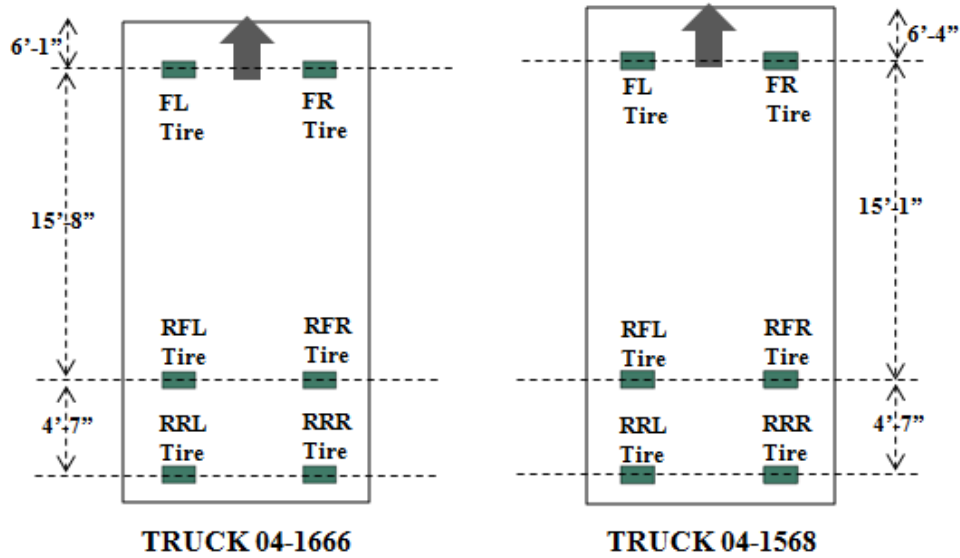
Figure 3-14. FE model configuration

Table 3-1. Bridge Components, Dimensions, and Element Types used in the Model

Component		Component Dimension (in.)	Element Types
Girder	Web	0.5	S4R (4-node general-purpose shell with reduced integration element)
	Intermediate stiffeners		
	Bearing stiffeners	0.875	
	Bottom flange	1.375	
		0.75	
Top flange	0.875		
Haunch		1.5	C3D8R (8-node linear brick with reduced integration) C3D6 (6-node linear triangular prism)
Deck		8	
Intermediate diaphragms		L 2.5 x 3.0 x 5/16	B31 (2-node linear beam element)
End diaphragms		C 12 x 25	
		L 3.5 x 4.0 x 5/16	

3.4.2 Truck Placement and Loading Configurations

The bridge is to be loaded using two trucks (Truck 04-1666 and Truck 04-1568 with axle dimensions and wheel loads shown in Figure 3-15) in four configurations as depicted in Figure 3-16 and Figure 3-17.



(a) Truck configuration

Truck Tire Position	Truck 04-1666 (GVW per Tire)	Truck 04-1568 (GVW per Tire)
Front Left (FL)	9000 lbs	9000 lbs
Front Right (FR)	9000 lbs	9000 lbs
Rear Front Left (RFL)	11500 lbs	11500 lbs
Rear Front Right (RFR)	11500 lbs	11500 lbs
Rear Rear Left (RRL)	11500 lbs	11500 lbs
Rear Rear Right (RRR)	11500 lbs	11500 lbs

(b) Wheel loads (GVW: Gross Vehicle Weight)

Figure 3-15. Truck configuration and wheel loads

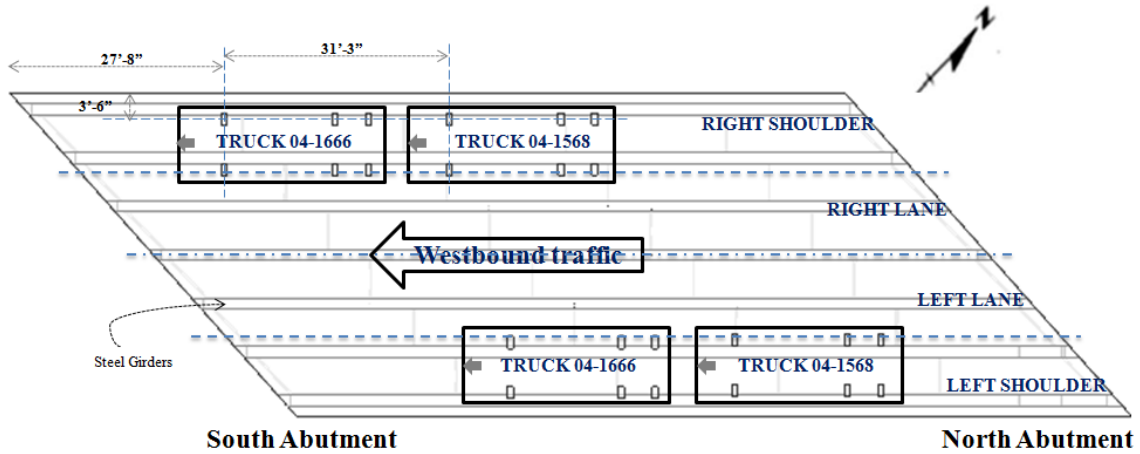


Figure 3-16. Truck positions and bridge configuration

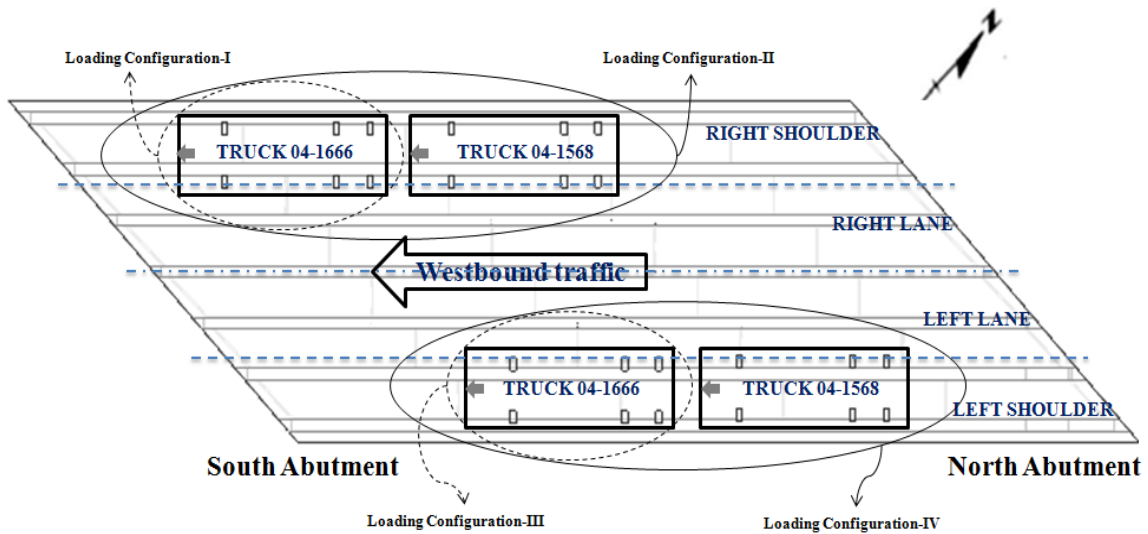


Figure 3-17. Mutually exclusive bridge loading configurations

3.4.3 Calculated Bridge Deflections and Translations

Girder ends over the south abutment are supported on expansion bearings while fixed bearings are used at the north abutment. Girder deflections and translations are calculated at girder ends and some intermediate diaphragm locations shown in Figure 3-18 . The bridge deflection profile was calculated for each loading configuration, as shown in Figure 3-19, Figure 3-20, Figure 3-21, and Figure 3-22. The figures show the girder bottom flange out of plane deformations and the color contours represent the value of vertical deflection under each loading configuration.

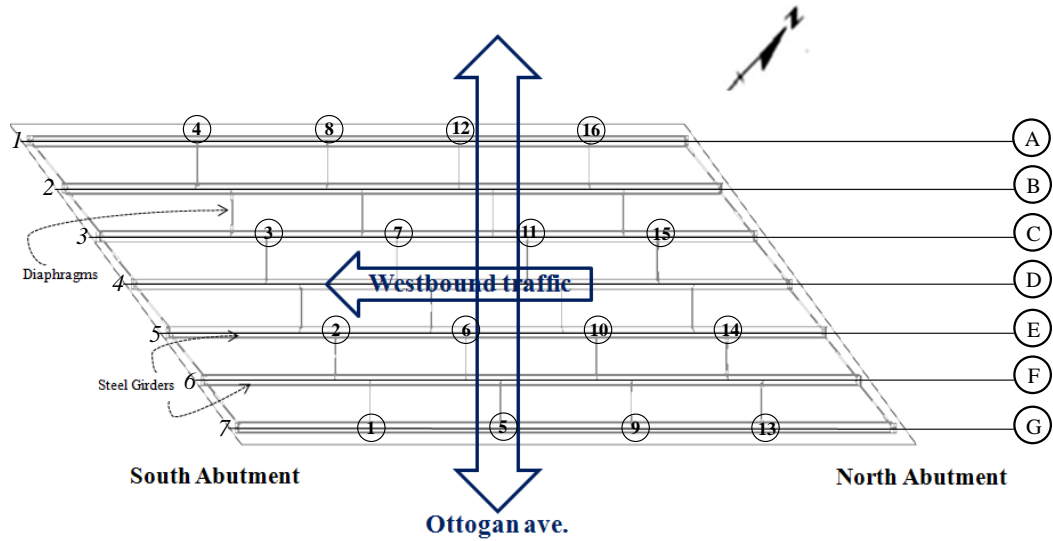


Figure 3-18. Girder labels and 16 displacement measurement points

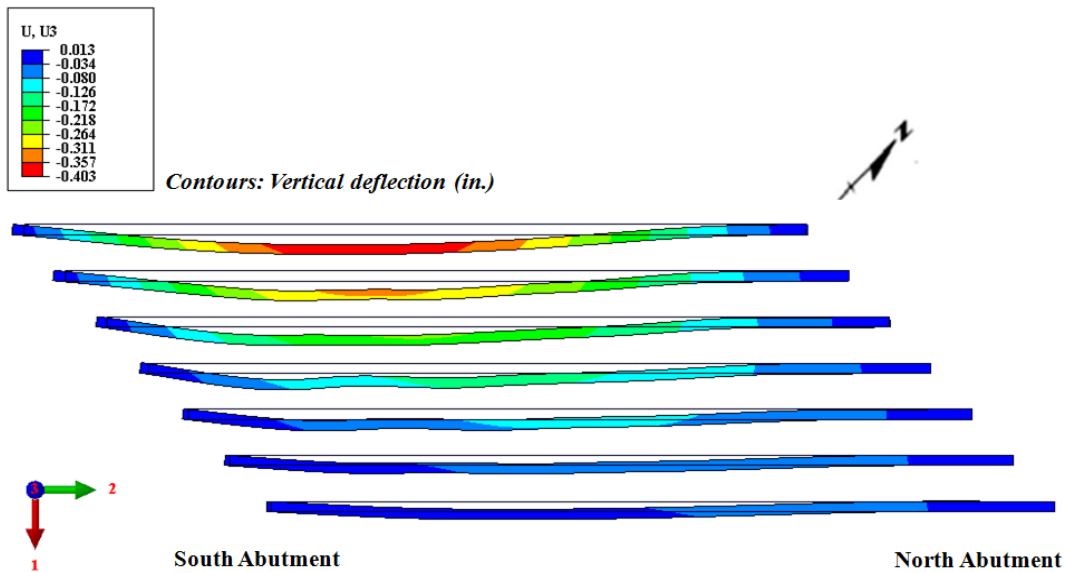


Figure 3-19. Girder bottom flange out of plane deformation, girder end translations, and vertical deflection contours under loading configuration-I

(Note: Color contours represent vertical deflection. Deformed shape depicts the girder bottom flange movement in 1-2 plane.)

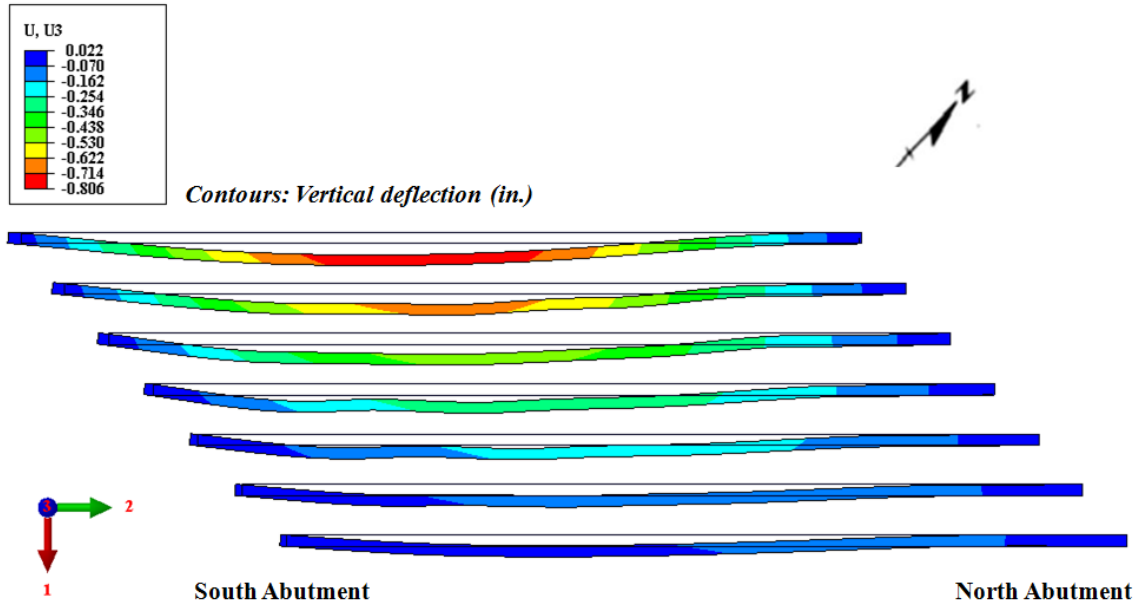


Figure 3-20. Girder bottom flange out of plane deformation, girder end translations, and vertical deflection contours under loading configuration-II

(Note: Color contours represent vertical deflection. Deformed shape depicts the girder bottom flange movement in 1-2 plane.)

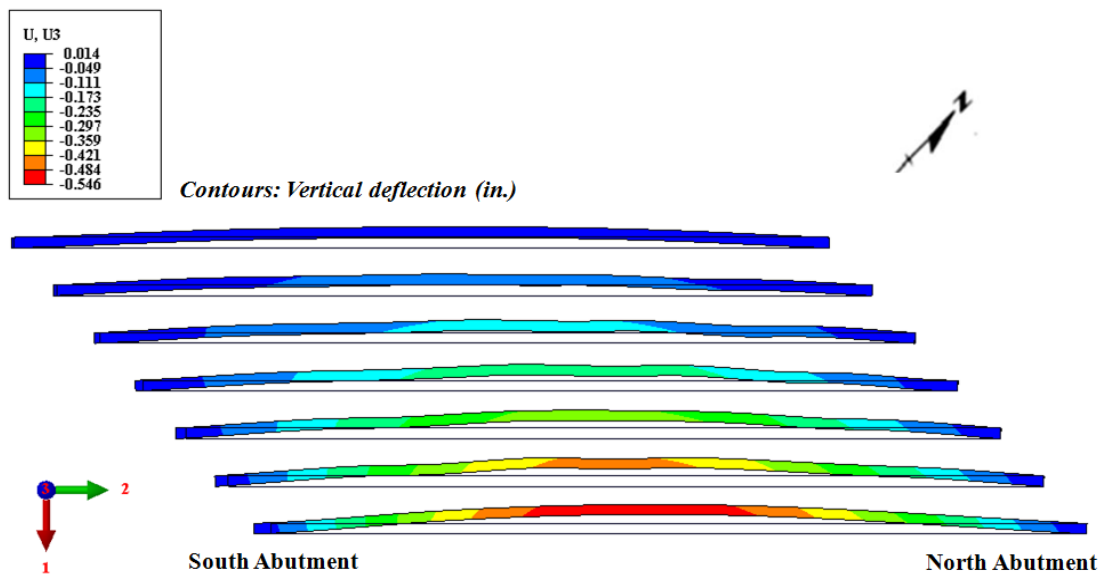


Figure 3-21. Girder bottom flange out of plane deformation, girder end translations, and vertical deflection contours under loading configuration-III

(Note: Color contours represent vertical deflection. Deformed shape depicts the girder bottom flange movement in 1-2 plane.)

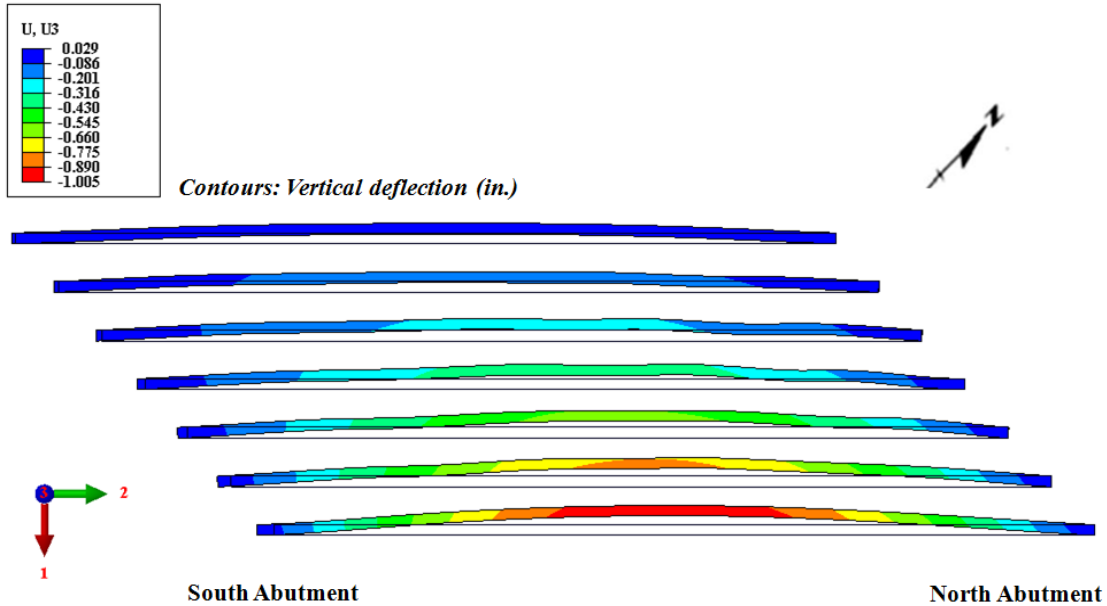


Figure 3-22. Girder bottom flange out of plane deformation, girder end translations, and vertical deflection contours under loading configuration-IV

(Note: Color contours represent vertical deflection. Deformed shape depicts the girder bottom flange movement in 1-2 plane.)

Girder stress representations are shown as the maximum von Mises stress under each load configuration. The maximum von Mises stress is 4.1 ksi calculated for loading configuration-I, 9.3 ksi for loading configuration-II, 3.7 ksi for loading configuration-III and 5.9 ksi for loading configuration IV.

3.5 MEASURED BRIDGE DEFLECTIONS AND TRANSLATIONS

3.5.1 Field Measurement Equipment and Procedures

3.5.1.1 Laser Tracker, Reflectors, and Meteorological Station

Displacement measurements are made using a laser-based device called Laser Tracker shown in Figure 3-23. For measuring the displacement of a point, first a target is placed at the point of interest. The displacement is measured by the tracker by generating a laser beam and computing the time of flight for the beam to be received by the tracker after reflecting back from a target. The measurement resolution is about 0.00003 in. Two types of targets (reflectors), shown in Figure 3-24a and Figure 3-24b, are used with the Laser Tracker. The first one is a 0.5 in. diameter glass prism reflector (Figure 3-24a) made of non-magnetic

anodized aluminum and can be attached to any surface using hot-glue. This reflector may have built in errors; hence, it is recommended to label and replace them accordingly when repeated measurements are made at different times. The 0.5 in. reflector has an acceptance angle of $\leq \pm 50^\circ$. The second type is a 1.5 in. diameter red-ring-reflector (RRR) (Figure 3-24b) made of surface-hardened magnetic stainless steel. This target is costly due to high precision manufacturing. The 1.5 in. reflector has an acceptance angle of $\leq \pm 30^\circ$. Having at least one of these red-ring reflectors is required with the equipment.

Field measurements require having at least one 1.5 in. reflector to guide the laser beam to help the tracker locate the 0.5 in. reflectors. A meteorological station (Figure 3-25) with temperature, humidity and pressure sensors is attached to the tracker for measuring ambient conditions as well as the structure temperature. The ambient weather data is used to make necessary compensations to the laser beam to improve measurement accuracy. A Laptop with Graphical user interface (GUI) is used to control the tracker (Figure 3-26).



Figure 3-23. Laser Tracker



(a) 0.5 in. glass prism reflector (b) 1.5 in. red-ring reflector (RRR)

Figure 3-24. Reflectors (targets) used with the Laser Tracker



Figure 3-25. AT MetroStation

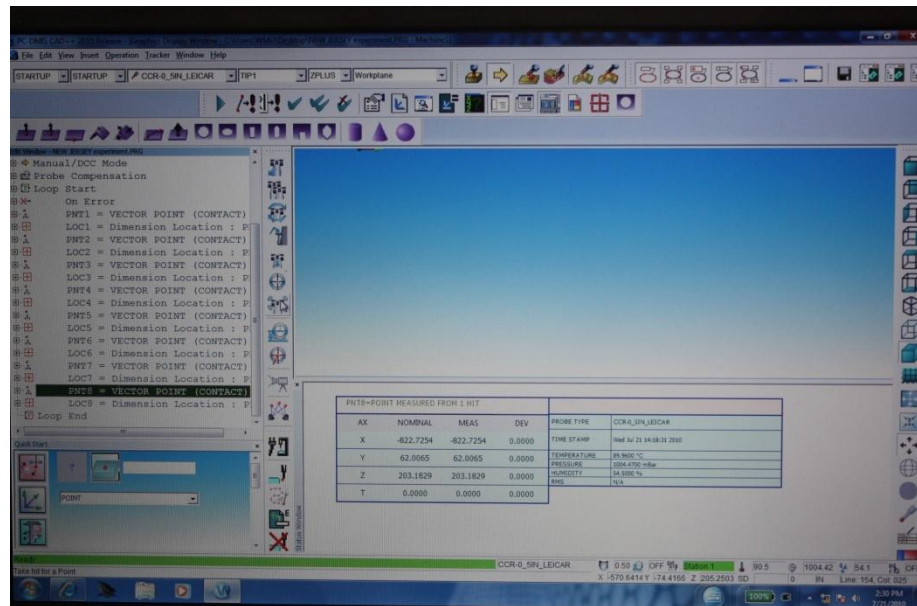


Figure 3-26. Graphical user interface (GUI) window

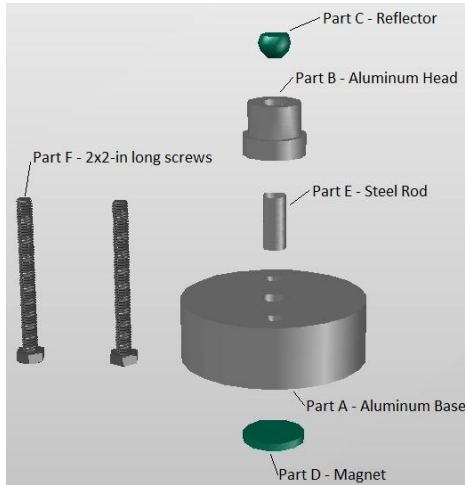
3.5.1.2 Target Locations and Placement

Monitoring the simple span bridge translation, under thermal load, relative to the abutments, requires mounting targets at girder ends as well as on abutments. Measurement of bridge translation under seasonal temperature changes requires mounting, removal, and remounting of targets as needed and aligning the laser tracker with respect to several fixed references (bench marks) every time the equipment is taken back to the field for making measurements. Targets on the abutments are used as benchmarks. A coordinate system is defined using the benchmarks so that the reference coordinate system is fixed for each measurement. Position coordinates of girder end targets are measured with respect to the reference coordinate system. Baseline measurements are taken after installing the targets. The other measurements are taken after several weeks or months (as needed) with respect to the reference coordinate system. The thermal deformations are calculated by subtracting the subsequent measurements on girder ends from the baseline measurements. The assumption in this measurement process is that the benchmark positions remain static during seasonal temperature changes.

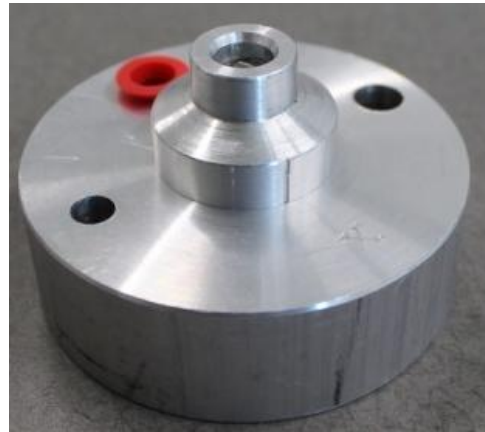
For mounting the targets, an aluminum base (part A) with a removable aluminum head (part B) was fabricated (Figure 3-27a). Reflector (part C) is placed in the removable aluminum head. The assembly is put together using a steel rod (part E) and a magnet (part D) attached to the back of the aluminum base. The target holder base is permanently attached to the abutments using 2-in. long cement screws (part F). At the girder end, they are mounted using high strength epoxy glue upon grinding and cleaning the girder surface.

Target holders on this particular bridge were mounted on December 16, 2011, and the ambient temperature was about 32 °F (Table 3-2). Cold weather conditions necessitate heating girder ends to promote curing of epoxy. However, use of regular heat guns to heat girder ends was not successful. Fortunately, having a magnet in the aluminum base helped hold the base against steel girders without using any clamping device until epoxy cured. The target is attached to the removable aluminum head using hot glue. All the removable aluminum heads are labeled to make sure the same target is connected to the aluminum base during the remounting process to control systemic errors. Following measurements part B is

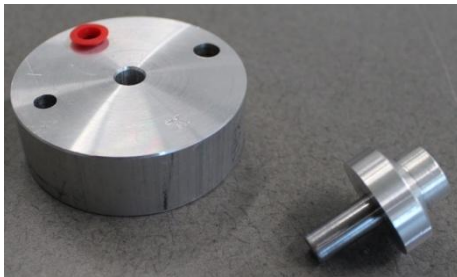
removed, and a plastic cap is placed over the hole in the aluminum base (part A) to keep it clean between measurements. Note that the plastic cap is mounted in an additional hole drilled in the aluminum base to avoid losing it during the reflector mounting/remounting process (Figure 3-27).



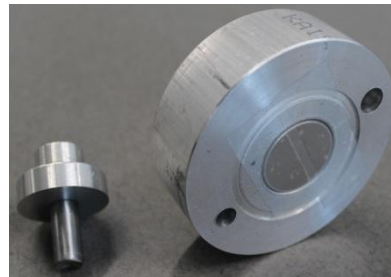
(a) Assembly



(b) Isometric view



(c) Top view



(d) Rear view

Figure 3-27. Accessories used for mounting girder end and abutment targets

Following the target installation, the Laser Tracker can be placed at a convenient location that is within the view of all targets (Figure 3-28).



Figure 3-28. Laser Tracker, server, and computer

The targets were mounted, and baseline measurements were taken on December 16, 2010. During that day four targets were mounted on each abutment (Figure 3-29 and Figure 3-30) as benchmarks. Also, eight more targets were mounted: four at each end of exterior girders and at the 3rd and 5th girders (Figure 3-29, Figure 3-30 and Figure 3-31). Fourteen more targets (3 @ the 1st diaphragm line, 4 @ the 2nd diaphragm line, 4 @ the 3rd diaphragm line, and 3 @ the 4th diaphragm line) were mounted to measure bridge deformations under static truckloads during load testing of the bridge (Figure 3-31). As seen from the figures, all the targets on the abutments and girder ends were labeled alphabetically while targets within the span used numerals. Target G, one of the benchmarks, was chosen as the origin of the coordinate system. The X-axis was defined along the exterior girder (on line A) while the Z-axis was defined in vertical direction (Figure 3-32). X-Y defined a horizontal plane. The position coordinates of the targets were measured on Dec. 16, 2010 with respect to the defined coordinate system. These coordinates serve as the baseline measurements to calculate bridge translations.

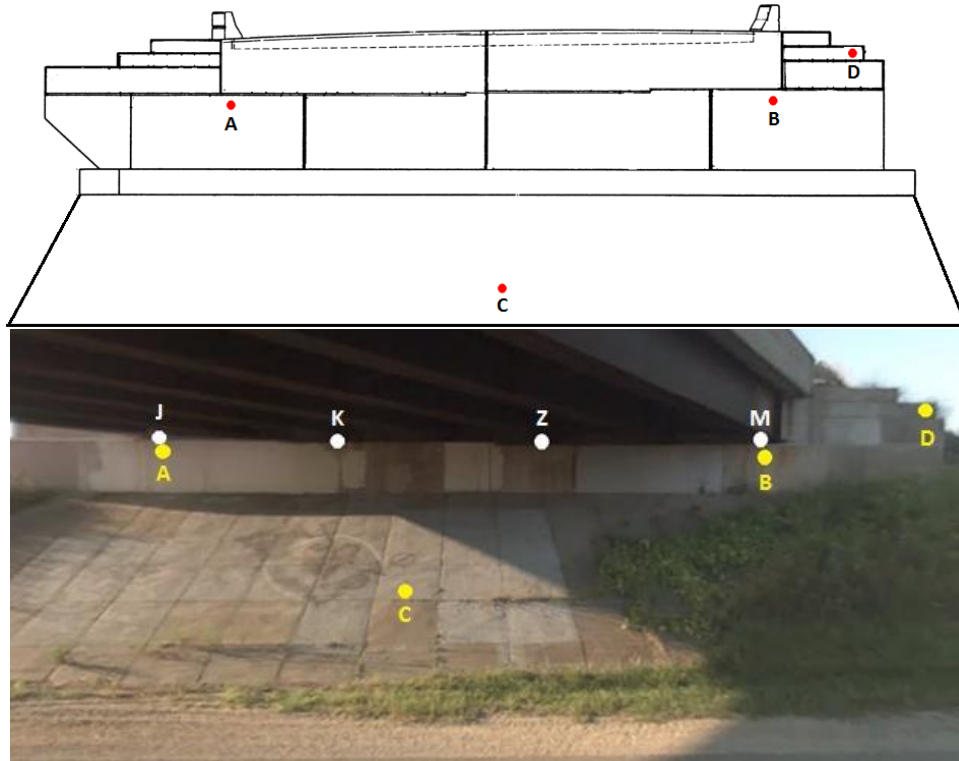


Figure 3-29. South abutment of the westbound bridge (targets on abutment and girder ends)

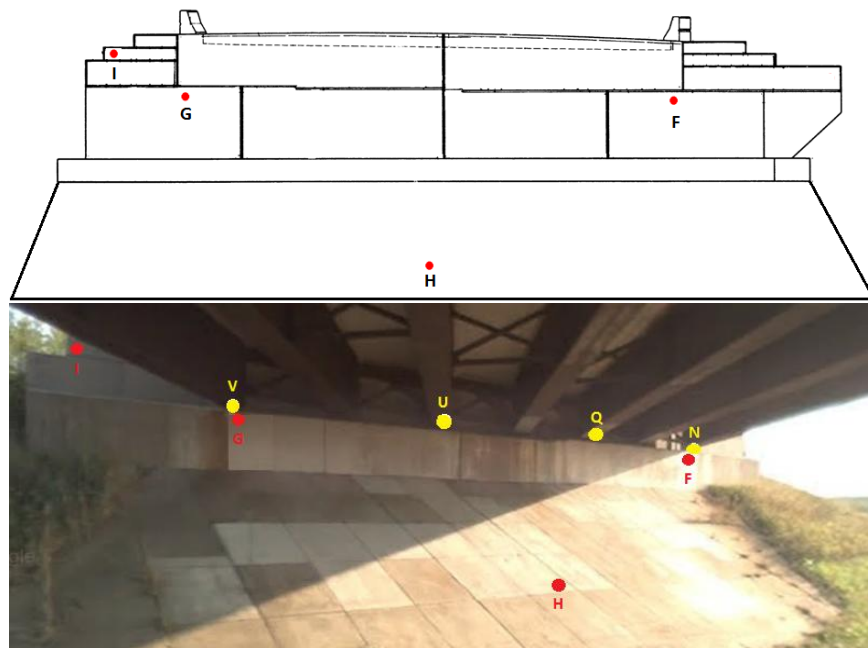


Figure 3-30. North abutment of the westbound bridge (targets on abutment and girder ends)

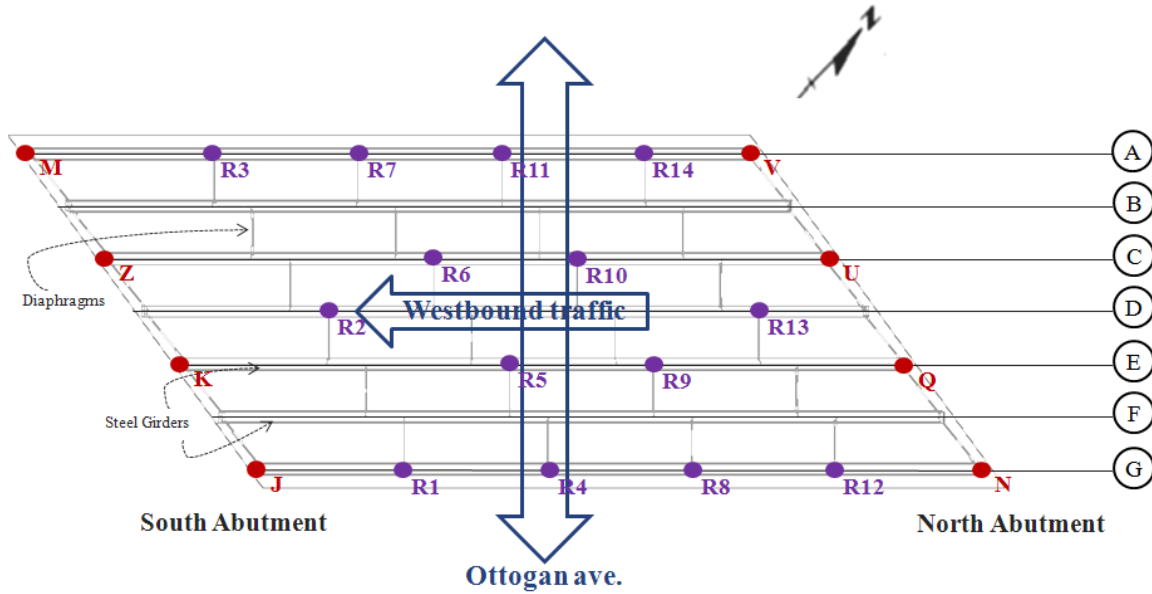


Figure 3-31. Target positions on girders

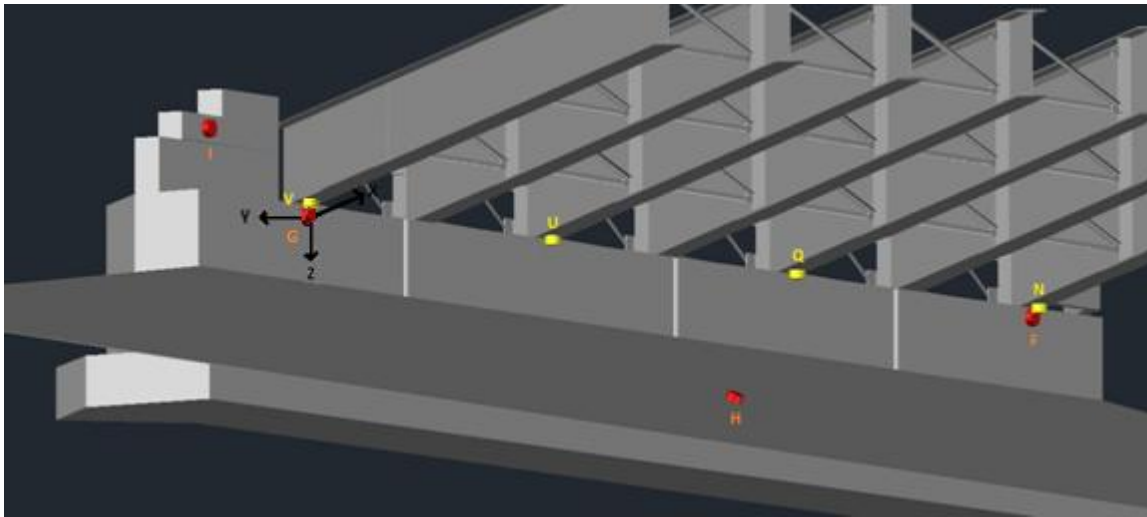


Figure 3-32. Coordinate system for Tracker measurements and target positions on north abutment and girder ends

Table 3-2. Ambient Conditions at 2:30pm on December 16 2010

Temperature (⁰ F)	32
Pressure (mmHg)	1181.91
Humidity (%)	51.7

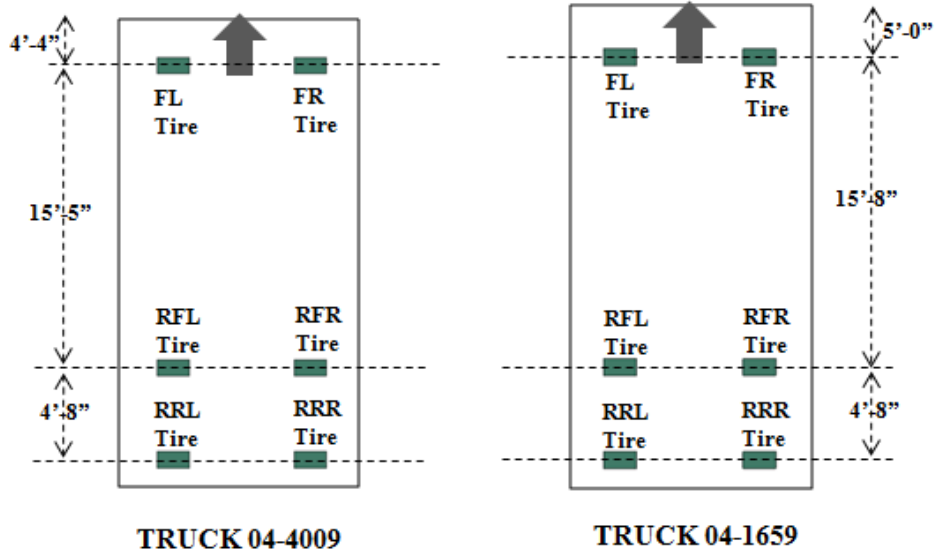
Table 3-3. Target Position Coordinates – Baseline Measurements (Dec. 16, 2010)

Reflector	Coordinates (in.)		
	X	Y	Z
A	892.5477	-472.3196	9.5949
B	1315.7579	4.0789	25.6603
C	965.7680	-166.5963	137.1540
D	1458.3465	119.4952	-18.3121
F	-434.1164	-488.0187	-11.3823
G	0	0	0
H	-78.4595	-313.7452	121.6880
I	42.8870	92.3908	-47.2806
J	884.1517	-486.8722	0.3646
K	1029.7024	-324.7426	5.3189
M	1310.6744	0.0678	16.0533
N	-432.4237	-482.4572	-23.9580
Q	-289.8550	-323.1314	-19.5721
U	-148.4056	-161.3447	-14.2191
V	-2.2858	2.6509	-9.2133
Z	1169.3041	-163.7294	10.6191

3.5.2 Bridge Deflection

3.5.2.1 Truck Configurations and Loading

The trucks, which were used for preliminary analysis, were not available on the day of load testing; hence, two similar trucks, shown in Figure 3-33 (Truck 04-4009 and Truck 04-1659), were used to serve the purpose. Four loading configurations similar to the preliminary analysis were used to load the bridge (Figure 3-34 and Figure 3-35).



(a) Truck configuration

Truck Tire Position	Truck 04-4009 (GVW per Tire)	Truck 04-1659 (GVW per Tire)
Front Left (FL)	8700 lbs	7650 lbs
Front Right (FR)	8900 lbs	7850 lbs
Rear Front Left (RFL)	10,650 lbs	10,150 lbs
Rear Front Right (RFR)	10,100 lbs	11,400 lbs
Rear Rear Left (RRL)	10,650 lbs	10,000 lbs
Rear Rear Right (RRR)	10,200 lbs	11,200 lbs

(b) Wheel loads (GVW: Gross Vehicle Weight)

Figure 3-33. Truck configurations and wheel loads

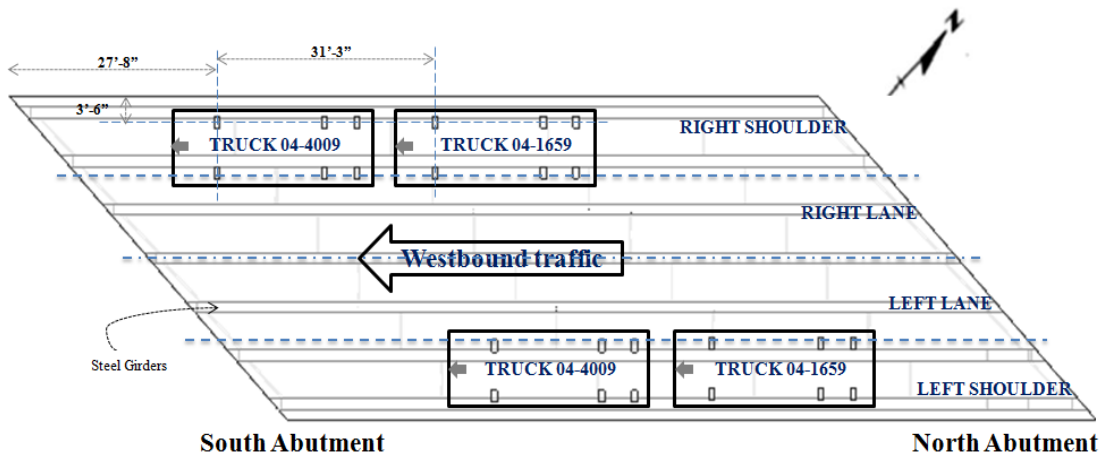


Figure 3-34. Truck positions and bridge configuration

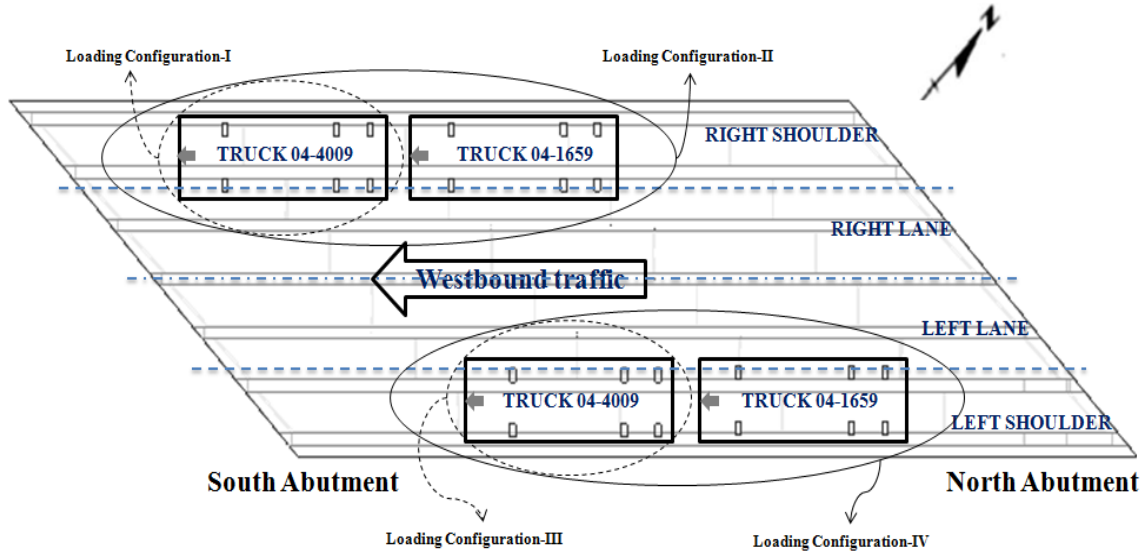


Figure 3-35. Mutually exclusive bridge loading configurations

3.5.2.2 Bridge Deflection

Deflections calculated from the FE model with ideal support conditions (i.e., girder ends over the north abutment are on fixed bearings and girder ends over the south abutment are on expansion bearings) are more than the measured values. The deflection calculated from the calibrated FE model, with support conditions incorporating frozen bearings, is more comparable to the measured displacements. The decision to include frozen bearing conditions in the FE model was based on visual inspection results detailed in section 3.3.2. Girder deflection comparisons from both FE analyses with field measurements are shown Figure 3-36 and Figure 3-37. All the raw data is presented in Appendix B. As seen from the figures, the forces developed at the girder ends due to static truck loads are not large enough to overcome the friction at the bearings; hence, bridge behavior under static truck loads resembles frozen bearing conditions.

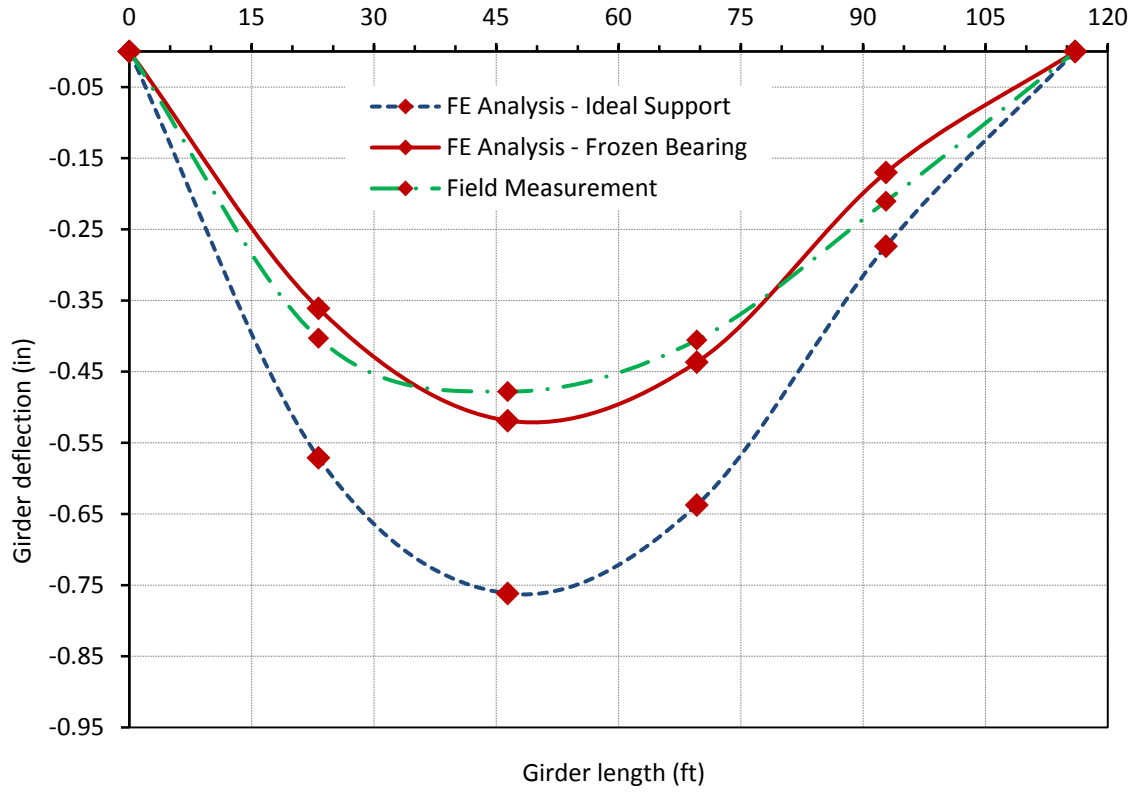


Figure 3-36. Girder A deflection under loading configuration II

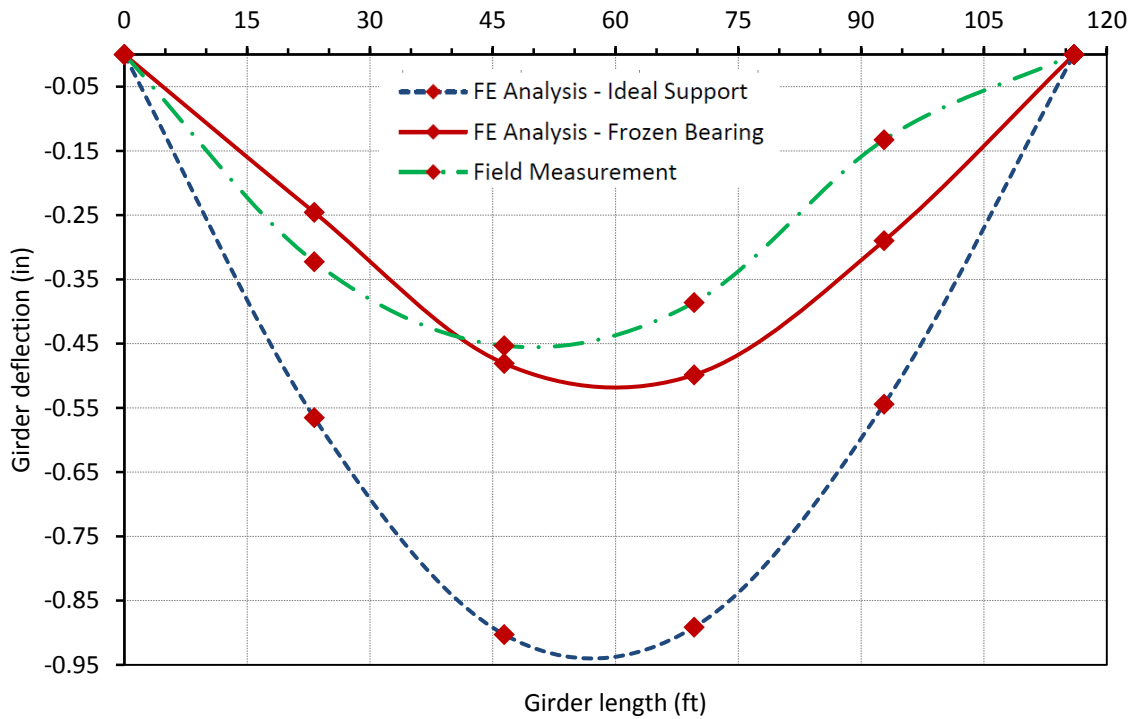


Figure 3-37. Girder G deflection under loading configuration IV

3.5.3 Bearing Translation

3.5.3.1 Bearing Translation under Truck Loads

Bearing movement over the south abutment is calculated using the FE model with ideal boundary conditions representing fixed and expansion bearings under each loading configuration and is depicted in Figure 3-38. Bearings move away from the bridge under truckloads because the neutral axis of the section is too close to the deck and pushes the girder bottom flange towards the abutment during bending as depicted in Figure 3-39. Under ideal boundary conditions (fixed and expansion), maximum bearing movement is less than 0.16 in., which is much smaller than the design movement.

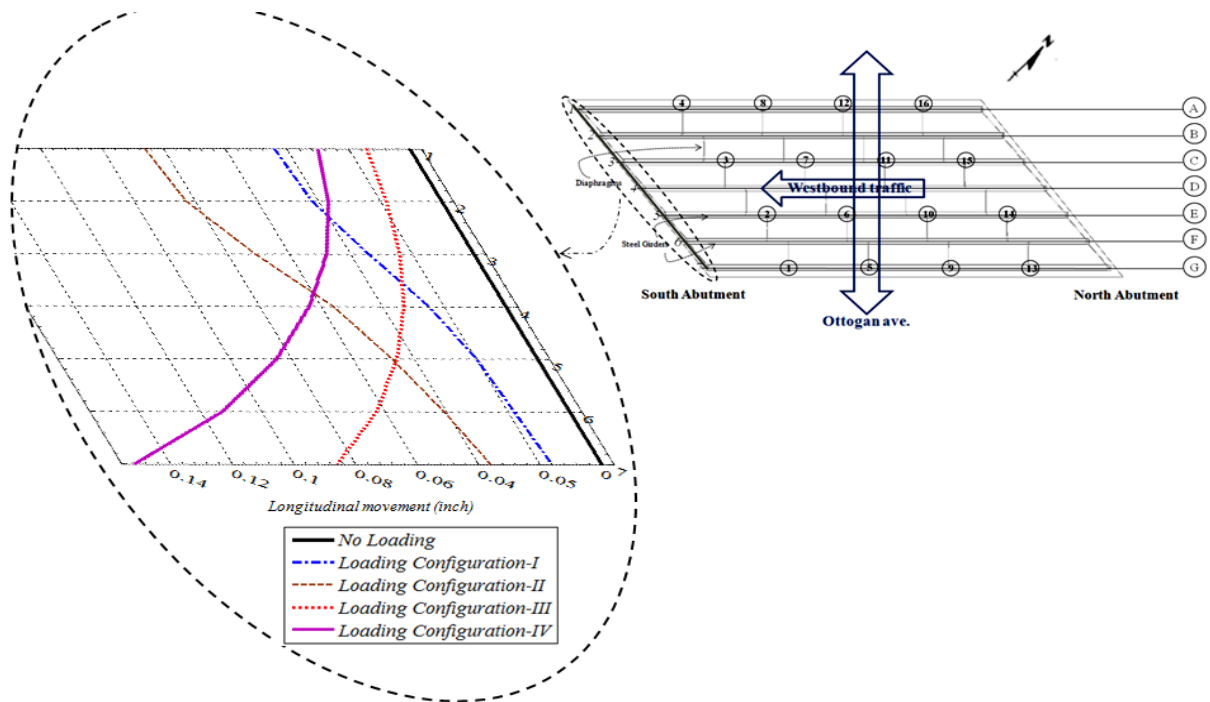
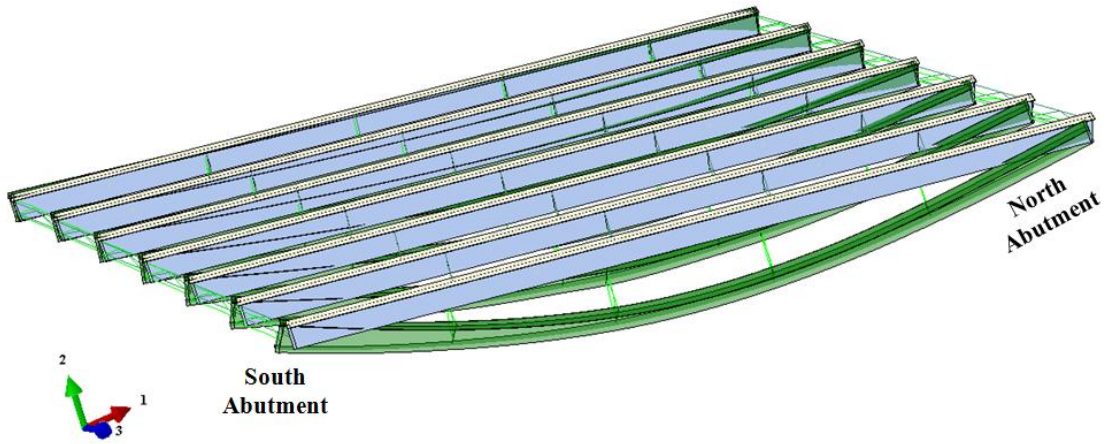
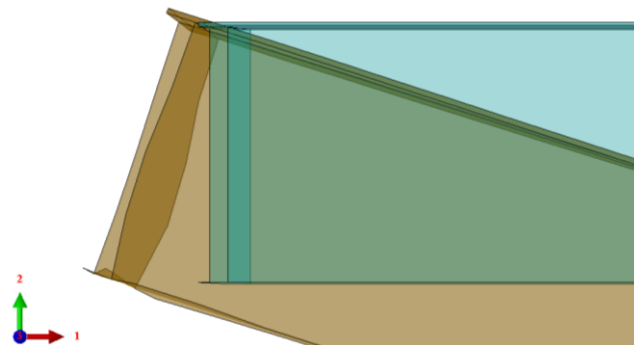


Figure 3-38. Bearing movement under truck loads (FE analysis)



(a) Isometric view of deformed and undeformed bridge



(b) Close-up of girder end movement

Figure 3-39. 3-D view of bearing movement (towards south abutment) under loading configuration IV

As measured bearing movements are depicted in Figure 3-40. The bearing movement measured for loading configurations I and II is in agreement predicted by FE analysis. It is worth stating that the maximum bearing movements under all loading configurations are very small. Tracker measurements show a similar trend in bearing movements as calculated from the FE model under loading configurations III and IV; but greater movements are measured at the acute corner (i.e., at target locations M and Z) than calculated from the FE model. Measured data, also shows that bearings do not slide back to their original positions at once upon the removal of live loads (Figure 3-41). The differences in measurements and FE analysis can be attributed to the bearing friction. These observations support the observations made during deflection calculation under static truckloads and calibration of the FE model using frozen bearing conditions.

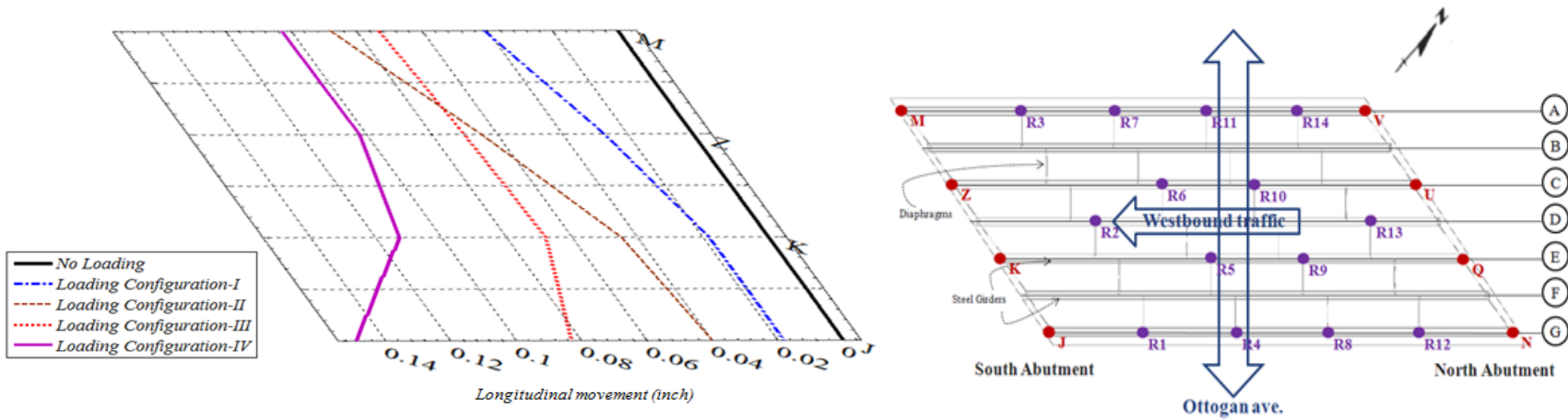


Figure 3-40. Bearing movement under truck loads (Tracker measurements)

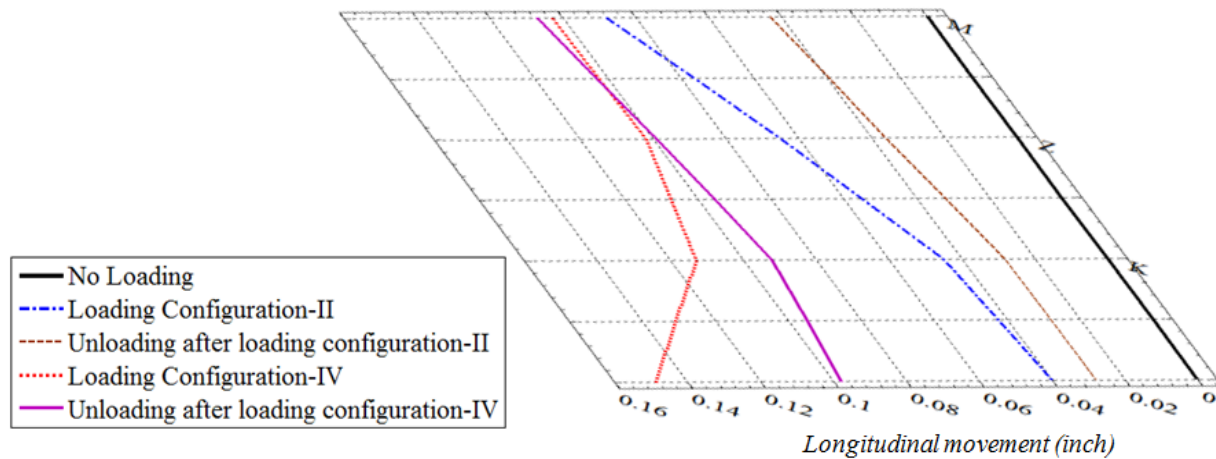


Figure 3-41. Bearing positions after loading and unloading following load configuration II and IV

3.5.3.2 Bearing Translation under Thermal Loads

Calculated bearing translations with the FE model under uniform thermal expansion and contraction as per AASHTO LRFD (2010) procedure B are given in Table 3-4 and shown in Figure 3-42. Calculated maximum bearing translation due to expansion ($\Delta T = 45^{\circ}\text{F}$) and contraction ($\Delta T = 70^{\circ}\text{F}$) occurs at the end of girder A. The bearing should allow 0.5 in. expansion and 0.77 in. contraction movement under girder A, which gives a total movement of 1.27 in. Though this movement is less than 1.875 in., shown in the bridge plans, the position of the dowel bar may not have been near the center. Also, dowel bar damage indicates lack of sufficient travel allowed for the bearing.

Tracker measurements were made to establish bearing travel over the south abutment under thermal changes. The initial measurements were made on December 16, 2010 and repeated on May 10, 2011 and again on July 13, 2011 (Figure 3-45). Ambient temperatures at the time of measurements on December 16, May 10, and July 13 are 32°F , 82.6°F , and 67.3°F . Bridge expansion is not due to daily temperature changes; it is due to the average temperature variation during a specific time period. Hence, maximum, minimum, and average temperature variation at the site from December to August are obtained from a nearby weather station, as shown in Figure 3-43 and Figure 3-44. According to Figure 3-44, average temperatures at the site on December 16, May 10, and July 13, are 27.5°F , 55°F , and 75°F , respectively. Hence, temperature difference from December 16 to May 10 and December 16 to July 13 are 25.7°F and 47.5°F , respectively. Calculated expansions at bearing from December 16 to May 10 and from December 16 to July 13 are 0.3 in. and 0.52 in. According to the calculations, the bearing at location M, shown in Figure 3-45, is expected to move 0.22 in. from May 10 to July 13. As shown in Figure 3-45, there was hardly any movement at bearing M (< 0.01 in.). However, there is 0.05 in. movement at bearing J, an indication that there is some rotation of the bridge deck about its normal axis. The observations indicate that there is significant restraint for movement.

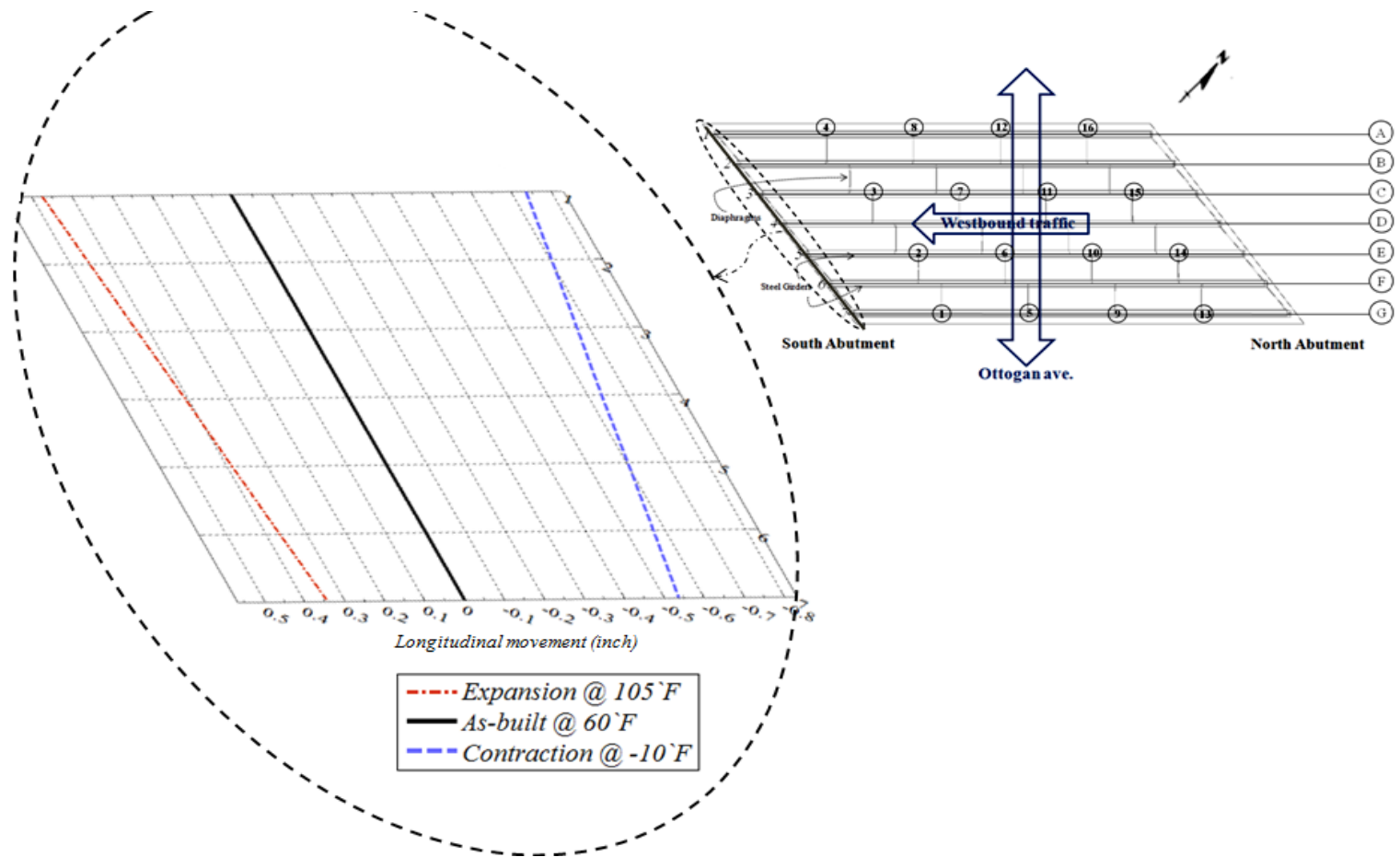


Figure 3-42. Bearing translation under uniform thermal loads (FE analysis)

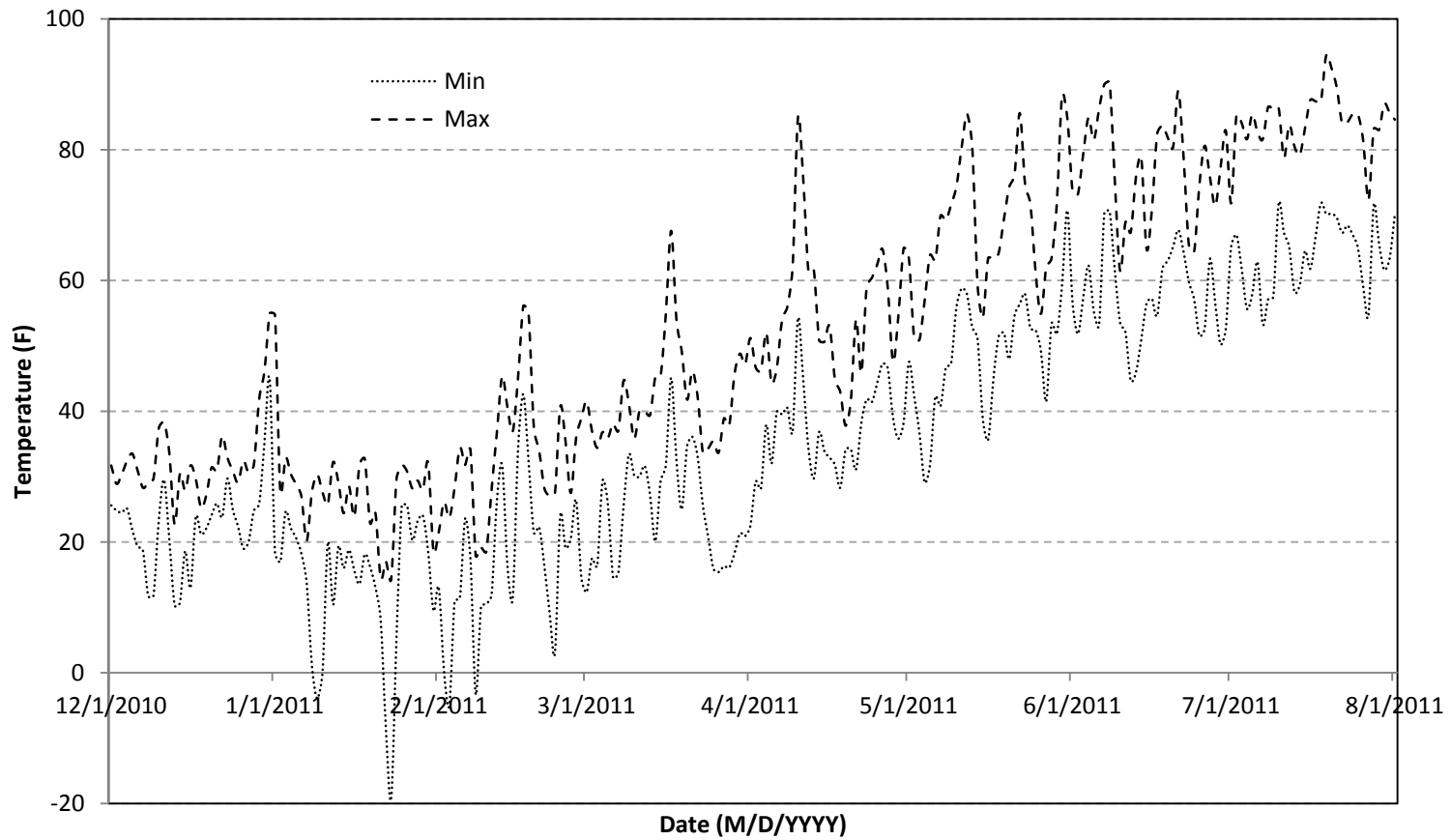


Figure 3-43. Maximum and minimum daily temperature variation at the site

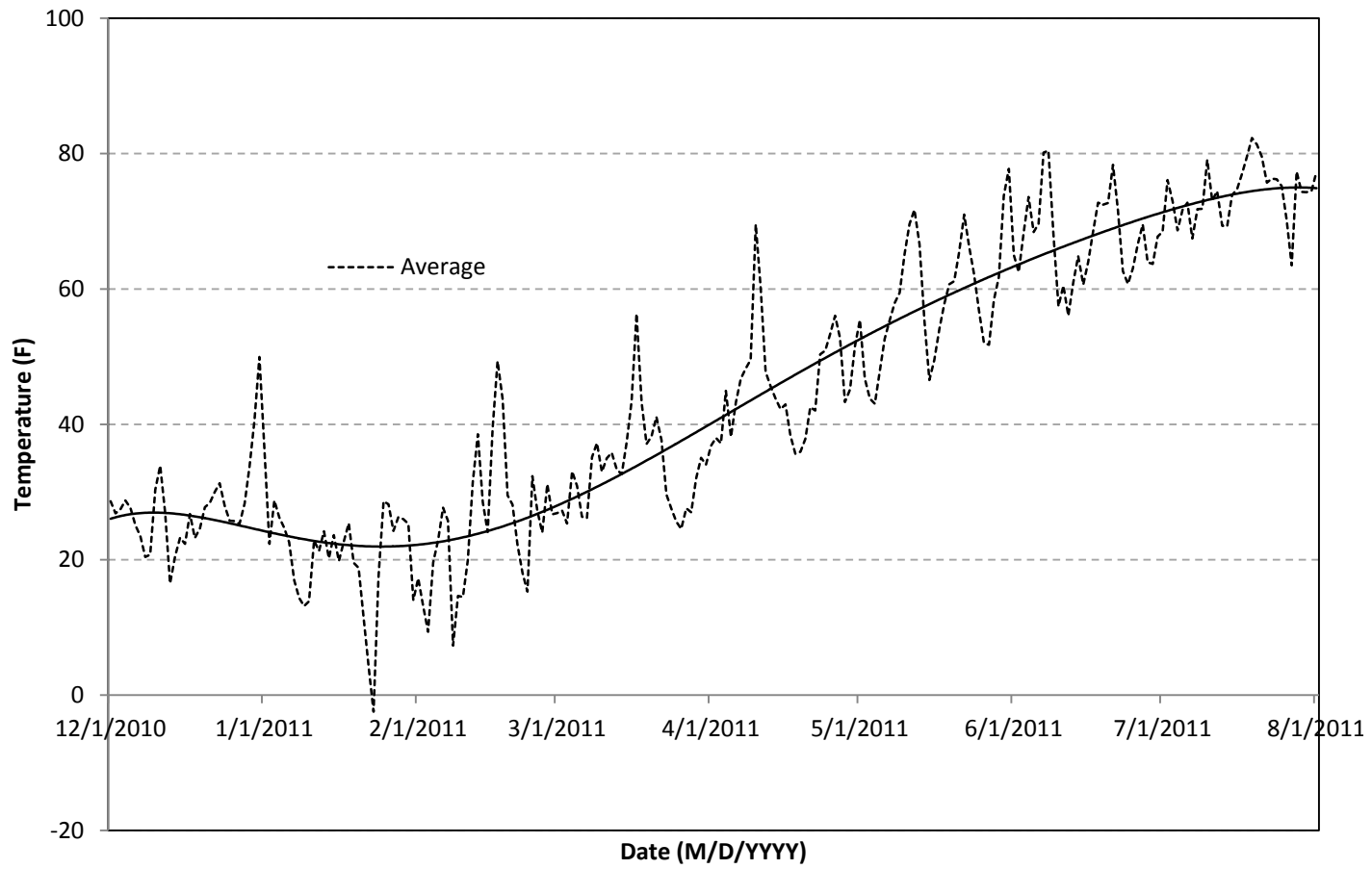


Figure 3-44. Average temperature variation at the site

Table 3-4. Girder-End Translations over South Abutment under Uniform Temperature Loading

Girder Label	FE Analysis (in.) ⁺	
	Expansion (in.) at 105 ^o F ($\Delta T = 45^{\circ}F$)	Contraction (in.) at -10 ^o F ($\Delta T = -70^{\circ}F$)
A	-0.474	0.737
B	-0.452	0.703
C	-0.430	0.669
D	-0.408	0.635
E	-0.387	0.602
F	-0.366	0.569
G	-0.344	0.535

+ Temperature at the time of construction is 60^oF

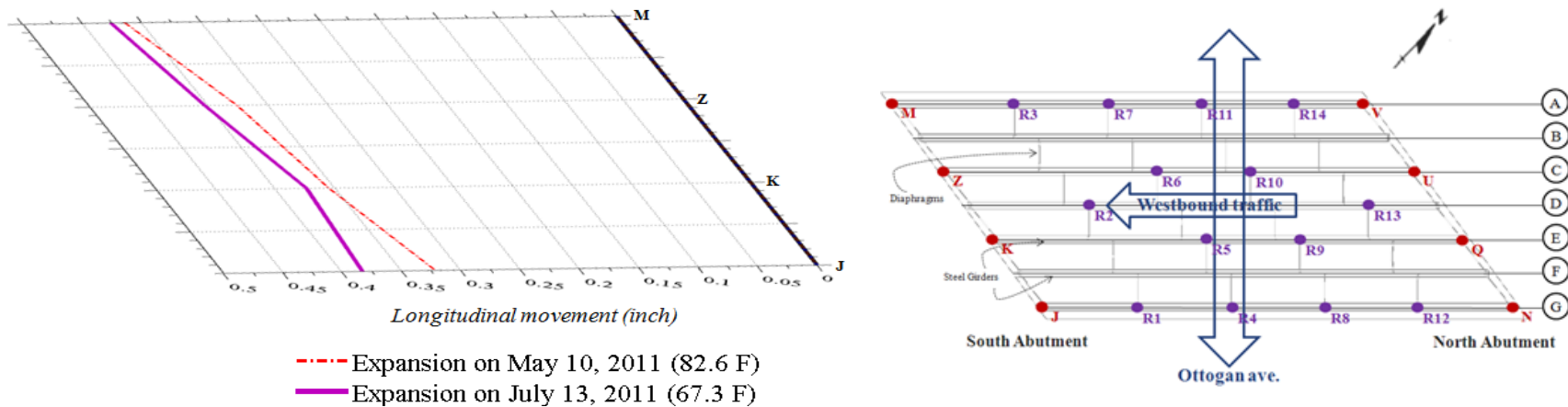


Figure 3-45. Bearing translation from Dec. 2010 to May 2011 and July 2011 (Tracker measurements)

3.6 SUMMARY

Bridge deflections and bearing translations were measured under static truck as well as thermal loads. Measured girder deflections showed that girder end movements were restrained due to friction. It is worth mentioning here that the bearing movements under static truck loads were very small compared to allowance made at the design for thermal expansion and contraction. The measured bearing movement under thermal expansion loads from May to July indicates that the bearings are frozen and the in-plane twist of the deck occurs due to bearing movement that is not expected at the design stage. Though there was no damage to the superstructure and substructure of this 120 ft long single span bridge, this behavior is critical when link slabs are implemented and the deck over the abutments is made continuous. The observations highlight the importance of using durable bearings that are capable of accommodating large deformation and a certain degree of rotation demands.

4 LINK SLAB ANALYSIS AND DESIGN GUIDELINES

4.1 OVERVIEW AND OBJECTIVES

The objective of this chapter is to present a detailed analysis of skew link slabs and moment and force demand envelopes with respect to the skew angle at the link slab section directly over the pier centerline. The analysis is performed for a specific bridge configuration (i.e., span length, width, and girder type), at various skew angles from 0° to 45° . The finite element (FE) models, for selected skew configurations, up to 45° , are analyzed under loads and configurations specified in AASHTO (2010). Further, the influence of different bearing configurations on the link slab moment and force resultants are also investigated. Finally, the design recommendations are developed for the utilization of links slabs in high skew bridges. The design recommendations are developed based on literature review, analysis results, and AASHTO (2010) requirements on strength and service load combinations.

4.2 CONTACT SIMULATION

The full-bridge FE models are developed using a detailed model of the link slab, deck, and girders. Unfortunately when doing so, differences in the mesh densities prevent nodes on different components from coinciding, thus preventing a way to “tie” the components together. Fortunately, the contact surface options available in Abaqus/Standard version 6.10.1 are available to overcome this challenge (Abaqus 2010). Table 4-1 summarizes contact surface option syntax used. For further information on the functions and use of each option can be found in Romkema et al. (2010).

Table 4-1. ABAQUS Syntax for Various Contact Options

Row	Contact Definitions	ABAQUS Syntax
a	General contact (automatic option)	*CONTACT *CONTACT INCLUSIONS, ALL EXTERIOR
b	General contact (user defined option)	*CONTACT *CONTACT INCLUSIONS surface_1, surface_2
c	Contact pair with separation	*CONTACT PAIR, INTERACTION=interaction1, ADJUST=nodes_to_adjust_to slave_surface, master_surface *SURFACE INTERACTION, NAME=interaction1
d	Contact pair with tied option	*CONTACT PAIR, INTERACTION=interaction1, TIED, ADJUST=nodes_to_adjust_to slave_surface, master_surface *SURFACE INTERACTION, NAME=interaction1 *SURFACE BEHAVIOR, NO SEPARATION
e	Contact pair with friction	*CONTACT PAIR, INTERACTION=interaction1 slave_surface, master_surface *SURFACE INTERACTION, NAME = interaction1 *FRICTION 1.0, 0.0, 0.0, 0.0

4.3 MODELING AND ANALYSIS OF A LINK SLAB BRIDGE

4.3.1 Overview and Objectives

The objective is to design and analyze high-skew bridges that meet current design standards. A prototype bridge is identified and modified so that it complies with current standards. Next, the bridge is modeled with contact surface options so that the link slab debonding from the girders is accurately represented. Boundary conditions are prescribed, and the AASHTO LRFD specified loads and combinations are applied. Lastly, the results are extracted, post-processed, and presented in graphical/tabular format.

4.3.2 Prototype Bridge

An in-service bridge, S12-7 of 25042, is identified for finite element (FE) modeling (Figure 4-1). The bridge carries eastbound I-69 over I-75 in Flint, Michigan. The bridge consists of two 69 ft 6 in. spans with a 1 in. gap between girders at the center pier for a total length of 139 ft 1 in. The bridge features a 9 in. thick concrete deck with five PCI Type III girders spaced at 66 in. The bridge was designed in 1966 to handle two lanes of traffic and does not meet current design standards; specifically the shoulder width is narrow. As a result, additional girders are added to make the bridge comply with the current standards.

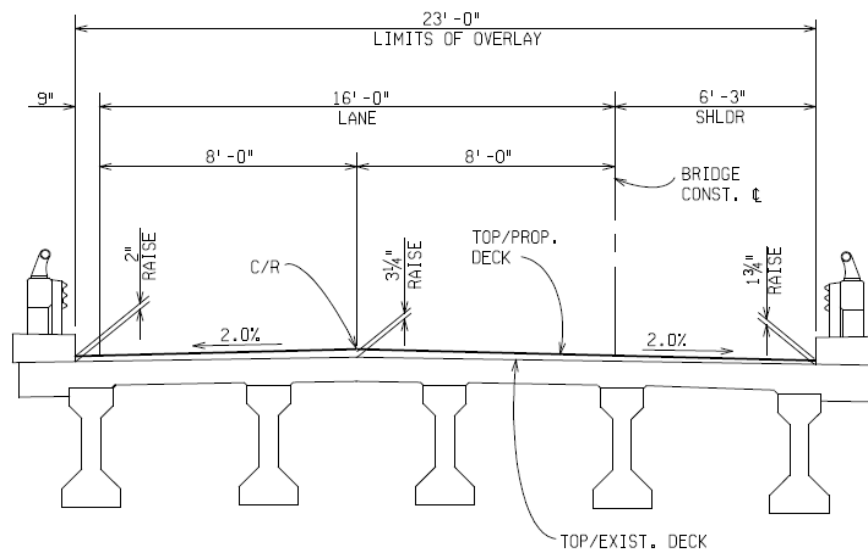


Figure 4-1. Cross section of Bridge S12-7 of 25042

4.3.3 Material Properties

The girder and deck concrete properties are assumed the same. Bridge deck concrete strength specified in MDOT design (f'_c) is 4500 psi (MDOT 2009). The modulus of concrete is calculated using Eq. 4-1 as per AASHTO Section 5.4.2.4 (AASHTO 2010). The unit weight of concrete (w_c) is assumed to be 0.15 kcf. The Poisson's ratio of 0.2 is used per AASHTO Section 5.4.2.5. Thermal expansion coefficient of $6.00 \times 10^{-6} / ^\circ\text{F}$ is used (AASHTO 2010, section 5.4.2.2).

$$E_c = 33,000 \times w_c^{1.5} \times \sqrt{f'_c} \quad (4-1)$$

4.3.4 Bridge Model Geometry

The current MDOT bridge design guide requires different shoulder widths depending on the number of traffic lanes. The existing bridge has two lanes of traffic. Each traffic lane width is 12 ft, as required for highways. A median shoulder of 8 ft and an outside shoulder of 8 ft plus 2 ft, or 10 ft, are required for an average daily traffic volume of 2000 vehicles per day or above (Figure 4-2) (MDOT 2011).

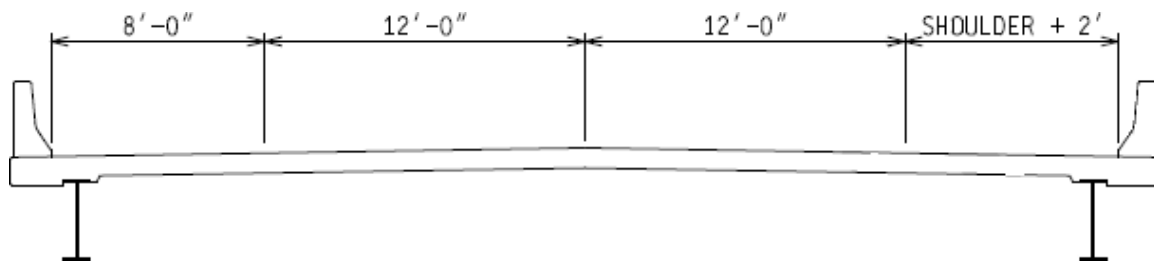


Figure 4-2. Current MDOT requirements for two-lane highway bridges

Bridge barriers are assumed to be MDOT New Jersey Type 4 (Figure 4-3) (MDOT 2011). In addition, the deck is to extend 1.5 in. beyond the barrier per drawings but is modeled as 2.25 in. to be compatible with the smallest FE mesh increment.

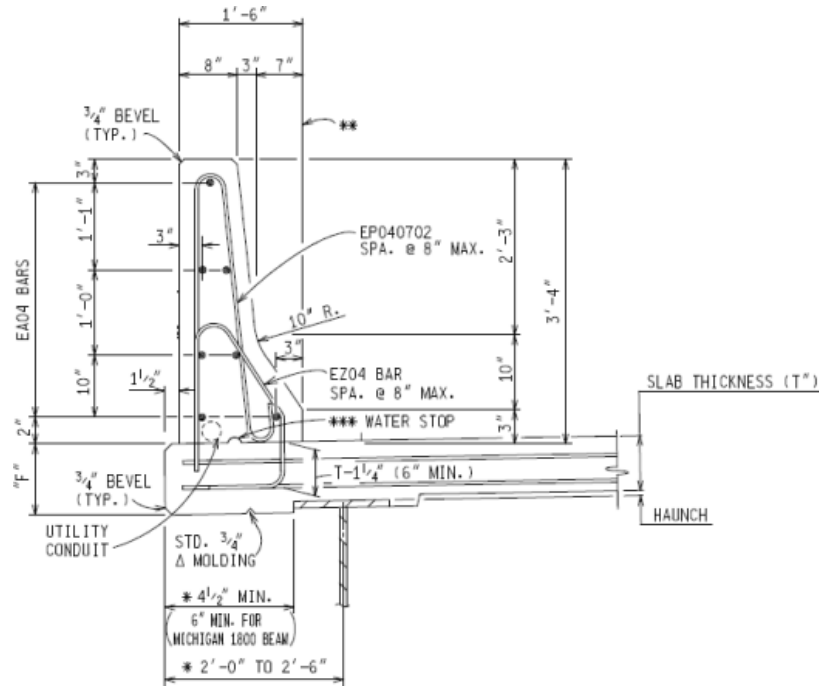


Figure 4-3. MDOT New Jersey Type 4 barriers

The deck thickness is kept at 9 in., and the crown is neglected. With girders spacing at 66 in., the final bridge cross section is shown in Figure 4-4. The FE model does not include barriers except as dead load as they are assumed not to contribute to structural capacity. The FE bridge model length is 139 ft 1 in. The model consists of two 69 ft 6 in. spans and a 1 in. gap between girder ends at the center pier (Figure 4-5).

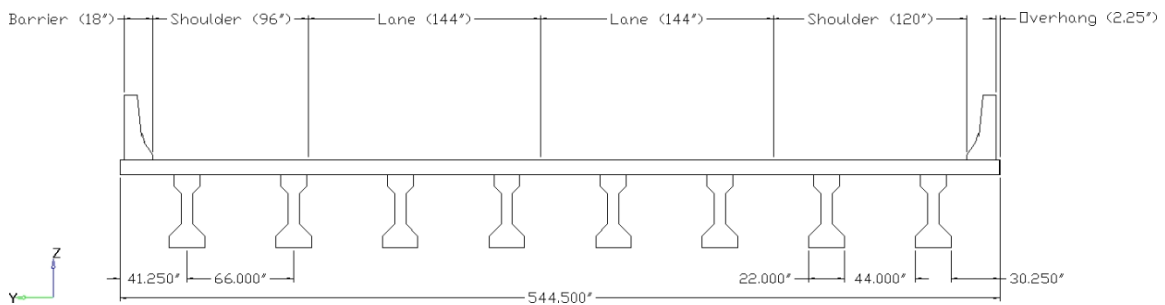


Figure 4-4. Cross section of bridge

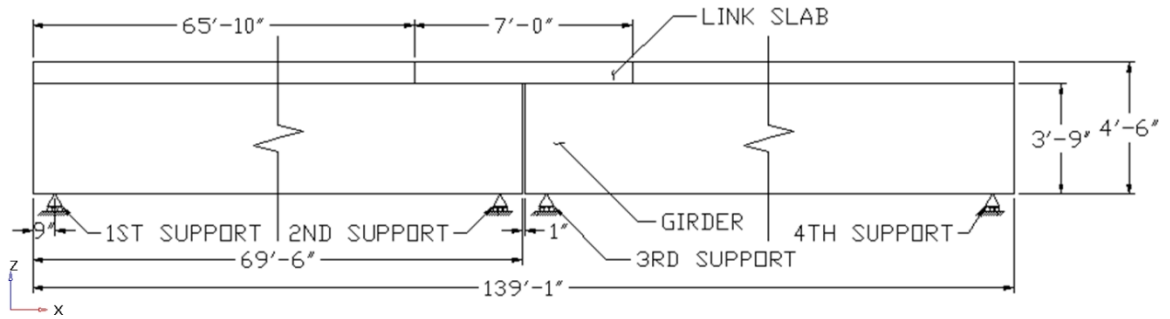


Figure 4-5. Elevation view of FE bridge

4.3.5 Bridge Model Orientation

The longitudinal axis of the bridge, along the direction of traffic, is defined as the X-axis. The transverse direction of the bridge is along the Y-axis, and gravity loads act along the negative Z-axis. A labeling system is also devised. The bridge orientation is assumed to run from south to north where the “South” end of the bridge lies at the origin along the X-axis. The span closer to the south end of the bridge is named “Span A,” and the remaining span as “Span B.” Girders are then numbered 1 to 8 with increasing index from east to west. Axis layout and the bridge labeling system are shown in Figure 4-6.

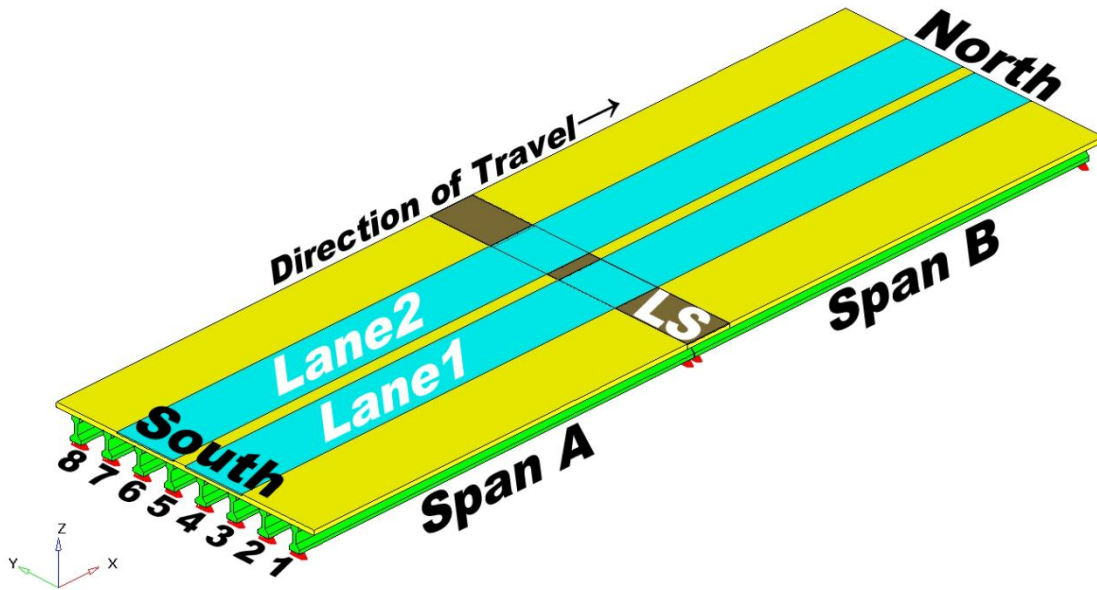


Figure 4-6. Bridge model orientation and labeling system

4.3.6 Link Slab Length

Ulku et al. (2009) recommends a link slab length of 5% of the span length. The link slab length would then be 5% of 69 ft 6 in. multiplied by 2 spans plus 1 in. for the gap between girders (i.e., 84.4 in.). The link slab length of 84 in. is used in the model for compatibility with the FE mesh.

4.3.7 FE Discretization of the Bridge Model

4.3.7.1 Discretization of the Link Slab

Element width (along the y-axis) of 4.125 in. is selected for the deck and link slab. Mesh needed to be refined at the link slab region for improved accuracy of the stresses. An element height (along the z-axis) of 1.5 in. is used to allow for a node line along the mid-height of the link slab. The length (along the x-axis) of the link slab elements must be determined in such a way that a node line lies along the middle of the gap between the girder ends. This is to allow calculation of the forces and moments along that middle section. Hence, an element length of 2 in. is selected for the link slab region. Finally, the element length adjacent to the deck is increased to 2.5 in. to satisfy the link slab length requirement. The resulting FE mesh is shown in Figure 4-7 and Figure 4-8.

4.3.7.2 Discretization of the Deck

Uniform element width of 4.125 in. is chosen for the deck. Since stresses in the deck are not of focus in this research, a coarser mesh with an element length of 10 in. is used for the remainder of the deck outside the link slab region. A deck element thickness of 2.25 in is used.

4.3.7.3 Discretization of the Girders

A coarser mesh with 10 in. long elements is chosen for the girders since accurate girder stresses are not required. Mesh length near the bearings is reduced to 4.5 in. for accurate placement of support restraints.

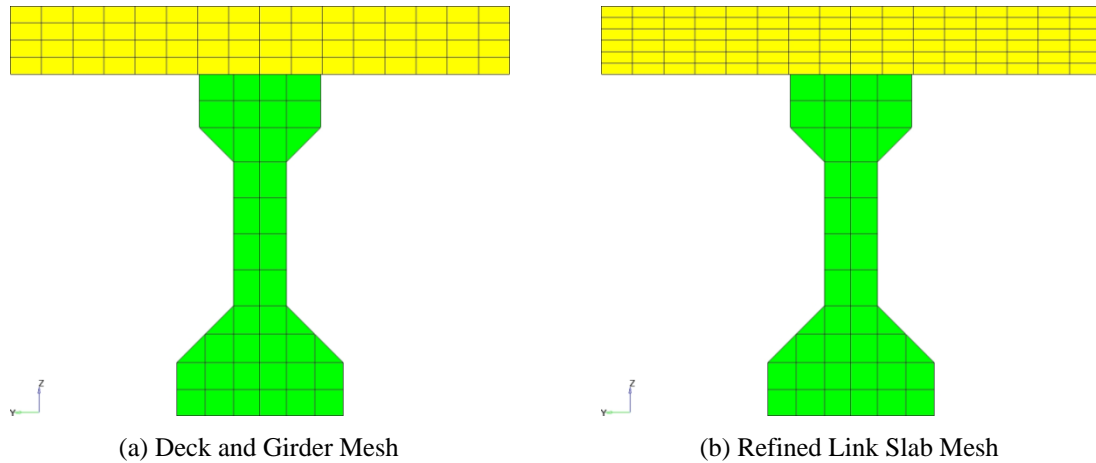


Figure 4-7. Cross section view of single girder and deck

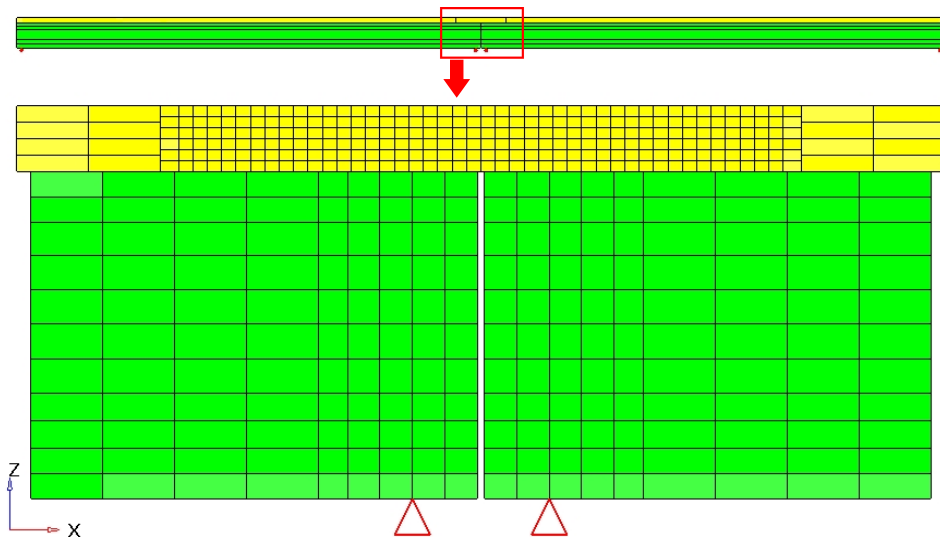


Figure 4-8. Elevation view of mesh at link slab region

4.3.8 Skew Mesh

The FE mesh is first developed for a straight bridge. The mesh is altered to generate bridge models with the same structure and with skew angles of 20°, 30°, and 45°. Link slab and deck element skew match bridge skew so that a surface parallel to the skew angle directly over the pier centerline is generated to calculate the link-slab force resultants. The MDOT Bridge Design Manual (2009) requires the concrete I-beam ends to be square for all angles of skew. As a result, girder elements are not skewed, but rather the entire girder is offset so that the center of the girder end is along the angle of skew. The FE models for all skews are shown in Figure 4-9, and mesh details are shown in Figure 4-10.

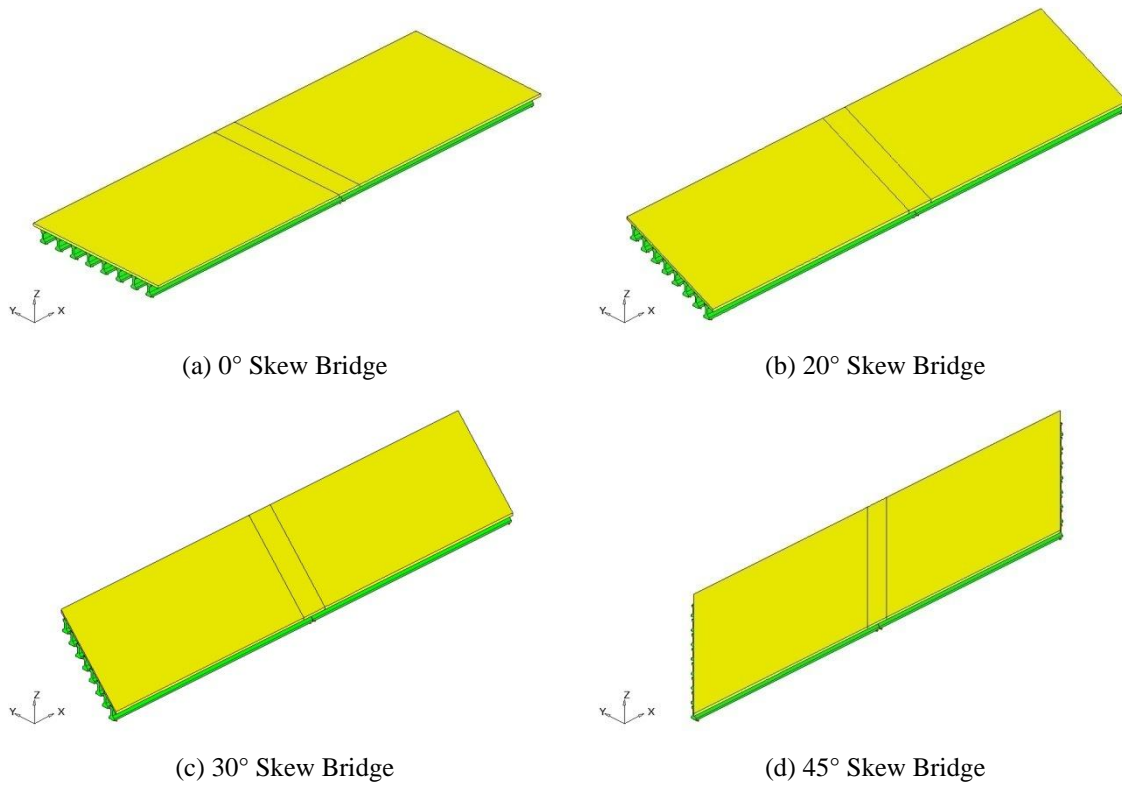


Figure 4-9. Isometric view of bridge models

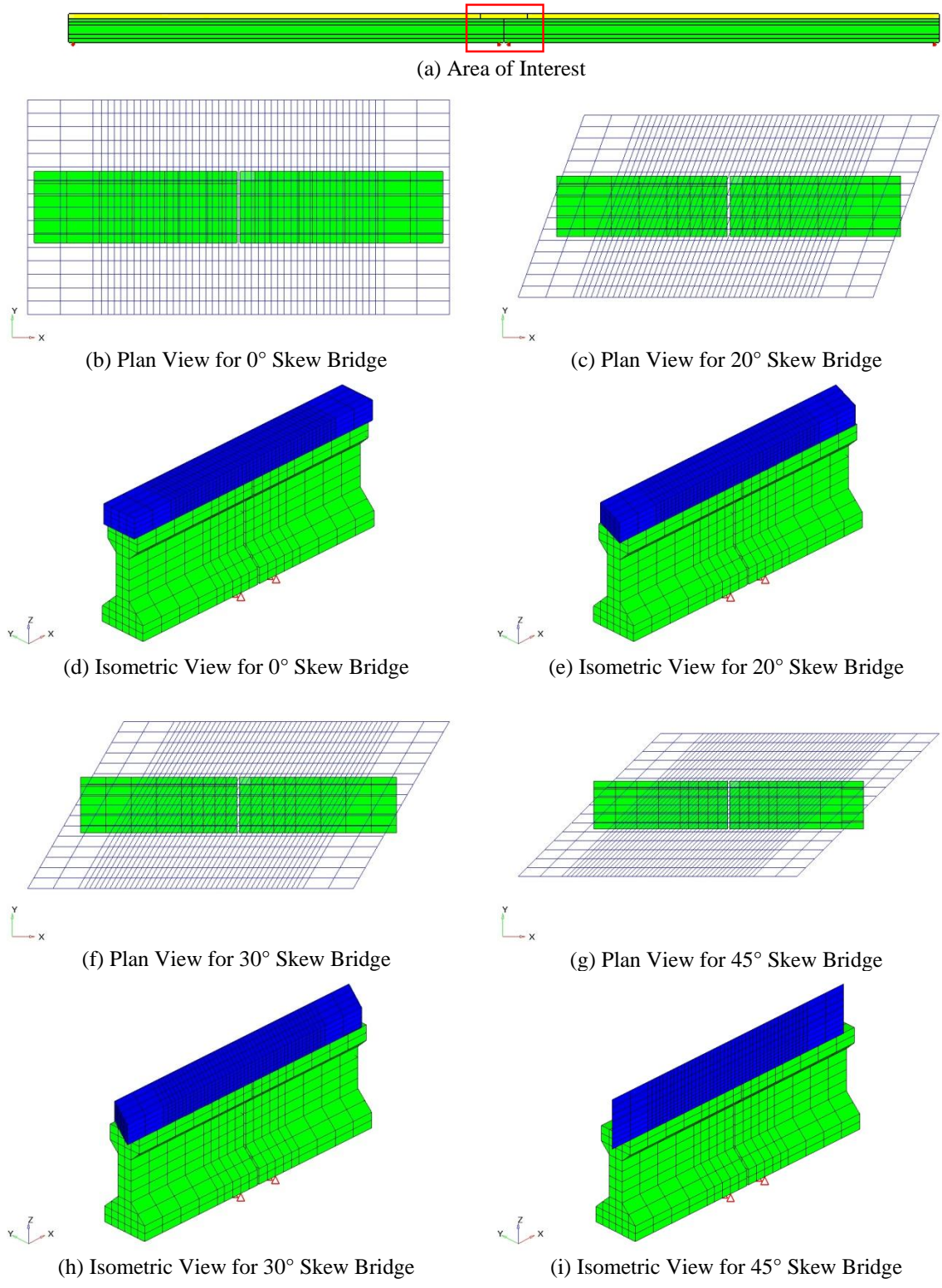


Figure 4-10. Skew link slab mesh

4.3.9 Contact Surfaces in the FE Model

Contact surfaces are created at the interfaces between each section: link slab and deck, link slab and girders, and deck and girders. The surface-to-surface option is used for optimized stress accuracy on the surface. The top surface of the girder is defined as the master surface and the link slab and deck as slave surfaces. Between the deck and the link slab interface, the deck is defined as the master surface. The surfaces are shown in Figure 4-11. The ‘NO SEPARATION’ with ‘TIED’ option is used for the contact between the deck and girders as well as the deck and the link slab. The contact between the link slab and the girders is established without the ‘TIED’ option in order to allow separation of the link slab from the girders. Contact surface definitions are given in Figure 4-12.

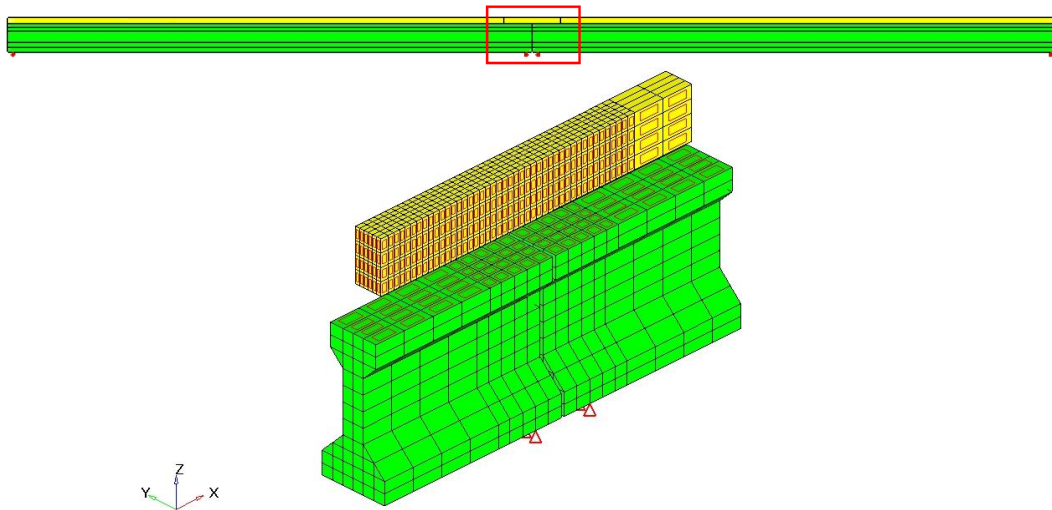


Figure 4-11. Contact surfaces in the FE models

```
*SURFACE INTERACTION, NAME = int_sep
*SURFACE INTERACTION, NAME = int_nosep
*SURFACE BEHAVIOR, NO SEPARATION
**
*CONTACT PAIR, INTERACTION=int_sep, TYPE=SURFACE TO SURFACE
surf-ls_bot, surf-girder_top
*CONTACT PAIR, INTERACTION=int_nosep, ADJUST=nset-girder_adj, TIED,
TYPE=SURFACE TO SURFACE
surf-deck_bot, surf-girder_top
*CONTACT PAIR, INTERACTION=int_nosep, ADJUST=nset-girder_adj, TIED,
TYPE=SURFACE TO SURFACE
surf-ls_south, surf-spana_north
*CONTACT PAIR, INTERACTION=int_nosep, ADJUST=nset-girder_adj, TIED,
TYPE=SURFACE TO SURFACE
surf-ls_north, surf-spanb_south
```

Figure 4-12. Abaqus syntax used in FE bridge model

4.3.10 Boundary Conditions

Elastomeric bearing pads supporting girder ends allow movement and rotation of the girder ends while providing limited restraint. Research conducted by Ulku et al. (2009) identified that the difference between the restraining effects of the bearing pads and the ideal support conditions on the link slab stresses are negligible. Accordingly, the ideal boundary conditions are specified in the models.

Three different bearing configurations are investigated: hinge-roller-roller-roller (HRRR), roller-hinge-hinge-roller (RHHR), and roller-roller-hinge-roller or roller-hinge-roller-roller (RRHR or RHRR). The first support (roller or hinge) is the boundary condition over the first abutment, the second support is the boundary condition over the pier, and so forth. This can be visually seen in Figure 4-13 and Table 4-2.

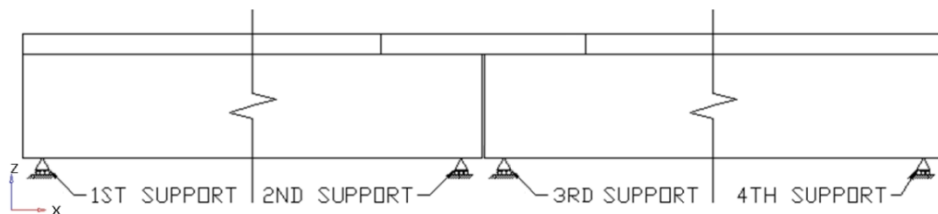


Figure 4-13. Bearing configuration layout

Table 4-2. Bearing Configurations and Corresponding Support Conditions

Bearing Configuration	1 st Support (Abutment)	2 nd Support (Pier)	3 rd Support (Pier)	4 th Support (Abutment)
HRRR	H	R	R	R
RHHR	R	H	H	R
RRHR (RHRR)	R (R)	R (H)	H (R)	R (R)

R = roller, H = hinge

4.3.11 Loads

The purpose here is to establish the design moment and axial force envelopes in the link slab under various skew conditions. Five load cases are defined for this purpose. The first four cases are truck and lane loads (i.e., AASHTO HL-93), and the last two cases are thermal gradient loads. Deck and girder self weight effects on the link slab are often eliminated when link slab placement is the last activity. In addition, barrier load effects are eliminated when link slabs are implemented as part of a repair activity.

4.3.11.1 Live Loads

The AASHTO HL-93 live load, consisting of a truck load and a lane load, is used. Loading patterns are shown in Figure 4-14 with detailed dimensions in Figure 4-15. Wheel loads, shown in Figure 4-15, include the dynamic amplification factor of 1.33. In addition, a 640 pound per linear foot lane load is applied. The load is represented as a pressure load over a 10 ft wide lane. However, due to mesh resolution, the lane width load is applied over 9 ft 11.625 in.

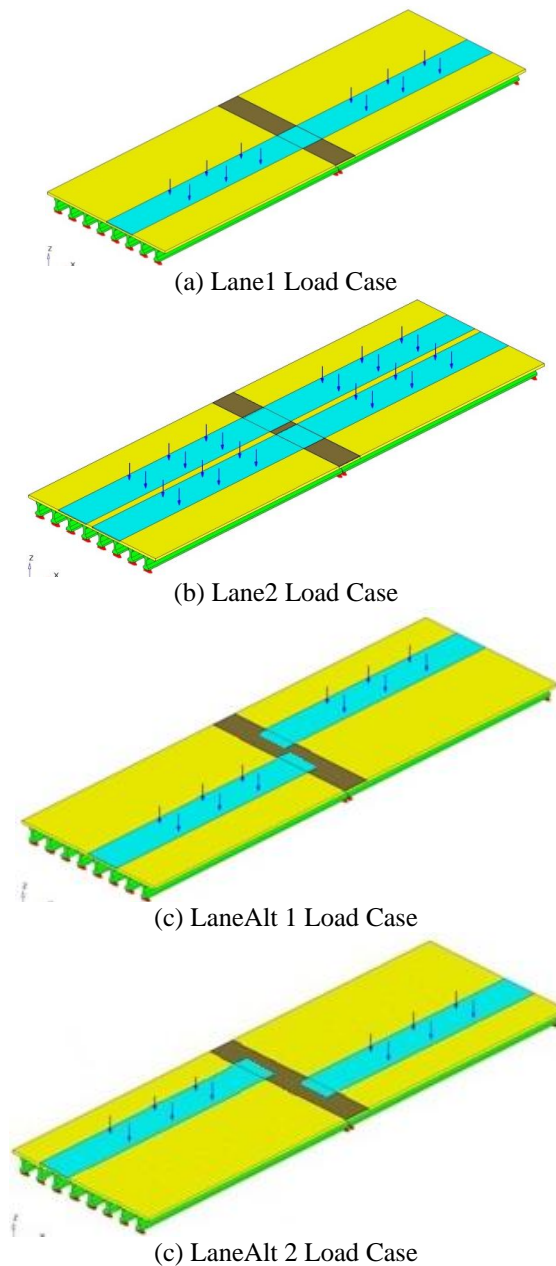


Figure 4-14. Live load cases

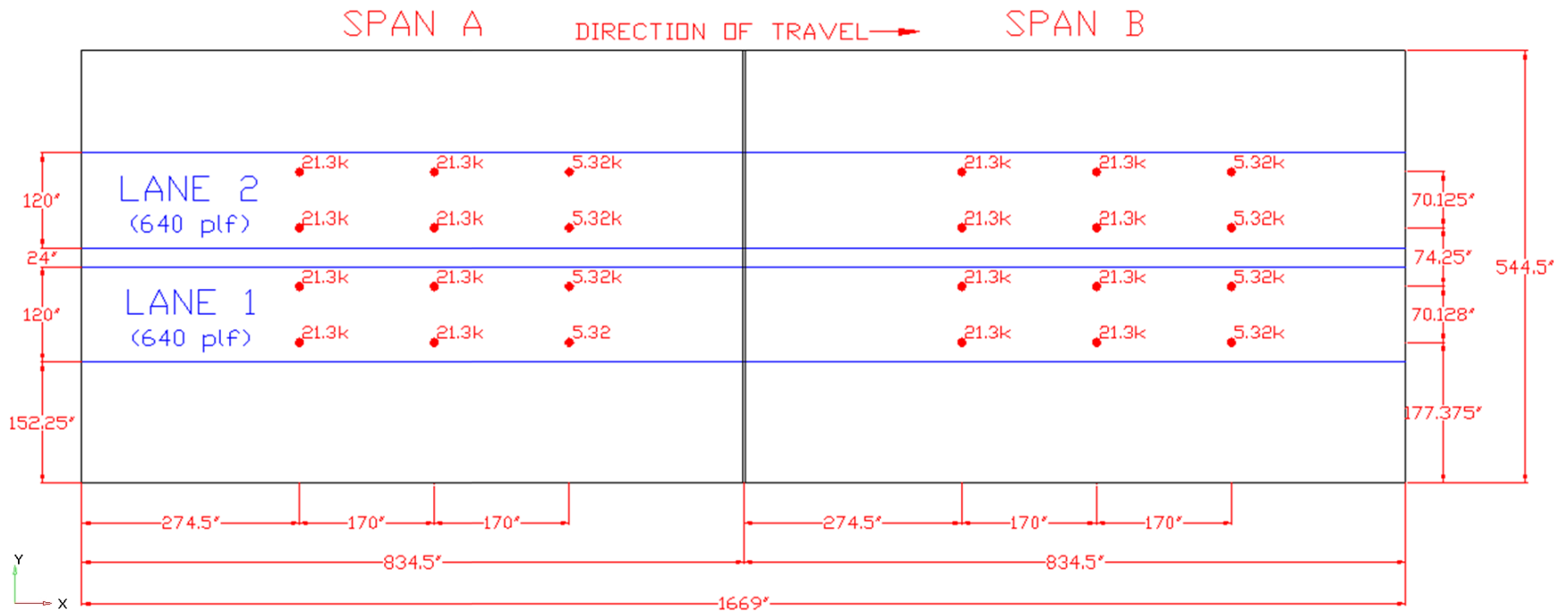


Figure 4-15. Truck and lane load locations

4.3.11.2 Temperature Gradient

The AASHTO (2010) Specification divides the United States into four zones based on solar radiation. Each zone is assigned a temperature for the top of the deck and a temperature 4 in. below the top of the deck. For Michigan, these are 41°F and 11°F for the positive temperature gradient (PTG). The resulting temperature gradient is shown in Figure 4-16a. The negative temperature gradient (NTG) values are obtained by multiplying the PTG values by -0.30 for plain concrete and -0.20 for a deck with asphalt overlay. The value of -0.30 is selected and the resultant temperature gradient profile is shown in Figure 4-16b.

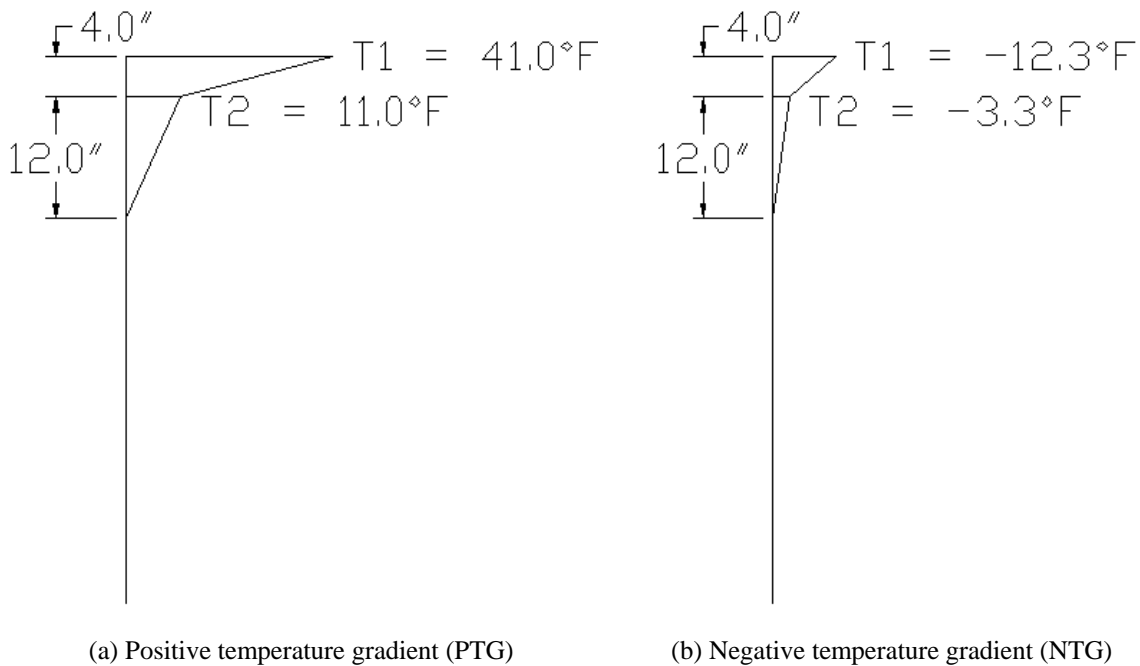


Figure 4-16. Temperature gradient

4.4 SIGN CONVENTION, MODEL VERIFICATION, AND RESULTS

4.4.1 Overview

The objective of analysis is to develop design recommendations for link slabs; hence, stresses in the link slab are required. Envelopes of moments and forces that are needed for link slab design are calculated from the link slab stresses. Abaqus allows for stresses to be averaged at nodes so that they may be interpreted by the user. In addition, Abaqus has an option to calculate forces and moments about a user-defined section. This option is utilized at the center of the link slab where such a section is defined. The section provides the total force and moment at the user-defined section along the center of the link slab. Finally, the reaction forces are checked to assure FE model equilibrium.

4.4.2 Sign Convention

A sign convention is defined as shown in Figure 4-17. The longitudinal axis of the bridge lies along X-axis. Link slab force in the X-direction is the axial force (F_x). Moment about the X-axis is the torsion (M_{xx}). The transverse axis of the bridge is along the global Y-axis. Force in the link slab in this direction is the transverse shear (F_y), and moment about this axis is the bending moment (M_{yy}). The vertical axis of this bridge is along the global Z-direction, the opposite direction gravity acts. Force in this direction is the vertical shear (F_z), and moment about this axis is the in-plane twist (M_{zz}). Force in tension has a negative sign. A negative bending moment generates tension at the link slab top fiber.

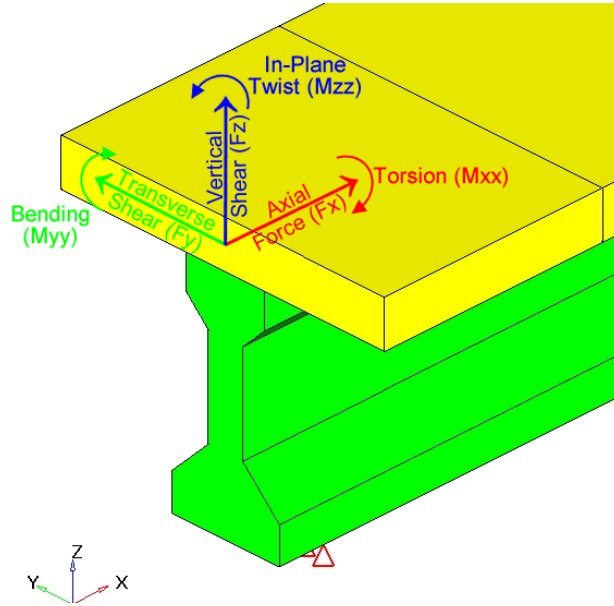


Figure 4-17. Sign convention

4.4.3 FE Model Verification

Equilibrium checks are performed to verify the model accuracy. Loads are applied only in the vertical direction so the net longitudinal and transverse reactions must be zero. The reaction forces in the vertical direction are the sum of the lane load plus truck load (HL-93). Models with thermal loads develop a null net vertical reaction. For each load case under gravity loads, the vertical reaction forces are calculated using Eq. 4-2 through Eq. 4-4.

$$R.F_{.lane1} = (1 \text{ lane})(0.640 \text{ k/ft/lane})(139.083 \text{ ft}) + (2 \text{ trucks})(1.33(72\text{k/truck})) \quad (4-2)$$

$$\mathbf{R.F_{.lane1} = 250.533k}$$

$$R.F_{.lane2} = (2 \text{ lanes})(0.640 \text{ k/ft/lane})(139.083 \text{ ft}) + (4 \text{ trucks})(1.33(72\text{k/truck})) \quad (4-3)$$

$$\mathbf{R.F_{.lane2} = 561.067k}$$

$$R.F_{.lanealt} = (2 \text{ lanes})(0.640 \text{ k/ft/lane})(69.5 \text{ ft}) + (2 \text{ trucks})(1.33(72\text{k/truck})) \quad (4-4)$$

$$\mathbf{R.F_{.lanealt} = 280.48k}$$

The reaction forces calculated from analytical and FE models are compared. The forces at the center of the link slab are verified by the state of equilibrium at the section along the center of the link slab.

4.4.4 Results

Resultant forces and moments are calculated at a section defined as a surface. This feature is utilized to calculate total force and moment acting at the user-defined surface along the midspan of the link slab. Forces at a section are useful to draw general conclusions about the effect of the angle of skew. In designing the section, a designer requires the effective force and moment for a unit width. Both results are calculated and discussed below.

4.4.4.1 Cross Sectional Moments and Forces

Moments and forces are generated by the FE software about the local coordinate system of the surface along the center of the link slab. Each angle of skew has a different orientation, thus a local coordinate system of this surface. To have comparable forces for all skew cases, the moments and forces about the local coordinate system are transformed into the global coordinate system. The transpose of the transformation matrix between the local and global systems is multiplied by vector of displacements, forces, moments, etc. in the local coordinate system to obtain the values in relationship to the global coordinate system (Nelson and McCormac2003). This relationship is given in Eq. 4-5.

$$\{f\} = [T]^T \{f'\} \quad (4-5)$$

where

$$\begin{aligned} \{f\} &= \text{Vector of forces in global coordinates} \\ [T] &= \text{Transformation matrix} \\ \{f'\} &= \text{Vector of force in local coordinates} \end{aligned}$$

As an example, a straight bridge with an HRRR boundary condition and *Lane1* load case is selected. Eq.4-6 shows the link slab moments in the local coordinate system. The first term in the force vector shown in Eq.4-6 is the moment about the local x-axis (torsion), the second is about the local y-axis (bending moment), and the third is about the local z-axis (in-plane twist). The transformation matrix is shown in Eq. 4-7. The first row of the transformation matrix is the direction cosines of local x-axis with respect to the global coordinates. Similarly, row 2 and row 3 represent direction cosines of local axes y and z.

From here, the transformation matrix is transposed and multiplied by the moments about the local coordinate system as shown in Eq. 4-8. Lastly, the moments about the global coordinate system are shown in Eq. 4-9. This process is performed for all the models so that the results allow direct comparison of forces and moments in all cases of changing skew.

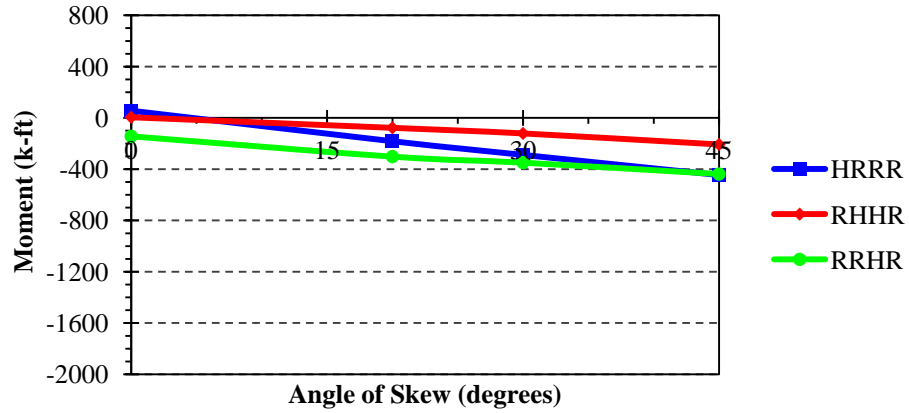
$$\{f\}' = \{47 \quad -501 \quad 190\} \text{ kip} - ft \quad (4-6)$$

$$[T] = \begin{bmatrix} 1 & 0 & 0 \\ 0 & 0 & 1 \\ 0 & -1 & 0 \end{bmatrix} \quad (4-7)$$

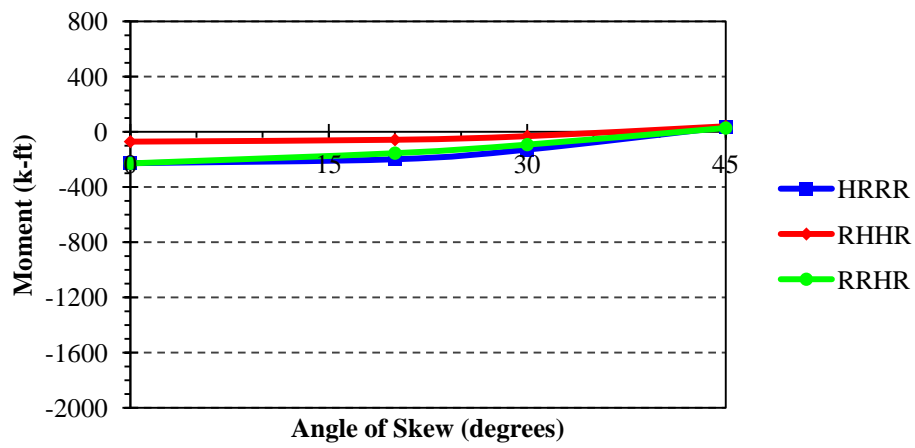
$$[T]^T = \begin{bmatrix} 1 & 0 & 0 \\ 0 & 0 & 1 \\ 0 & -1 & 0 \end{bmatrix}^T \{47 \quad -501 \quad 190\} \quad (4-8)$$

$$\{f\} = \begin{pmatrix} 47 \\ -190 \\ -501 \end{pmatrix} \text{ kip} - ft \quad (4-9)$$

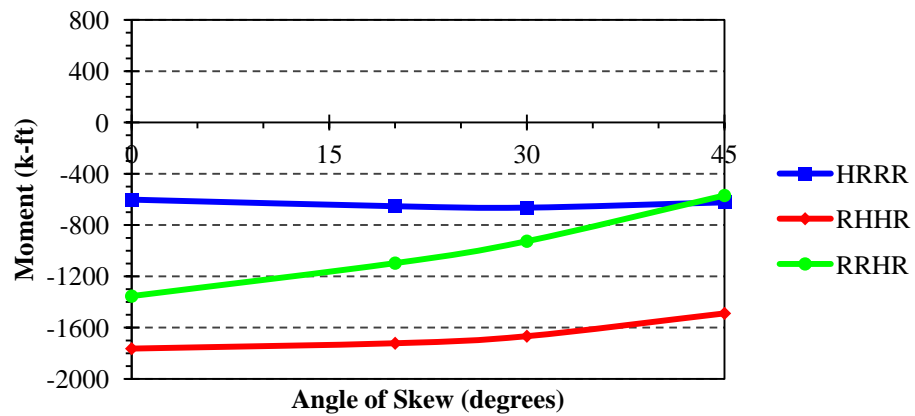
The total sectional moments and forces, with respect to the global coordinate system, are shown graphically in Figure 4-18 through Figure 4-29 with respect to each load case.



(a) Link slab torsion (M_{xx})

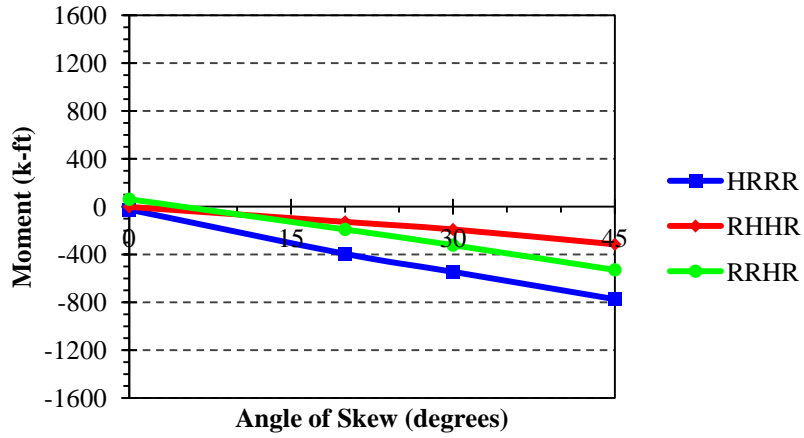


(b) Link slab bending moment (M_{yy})

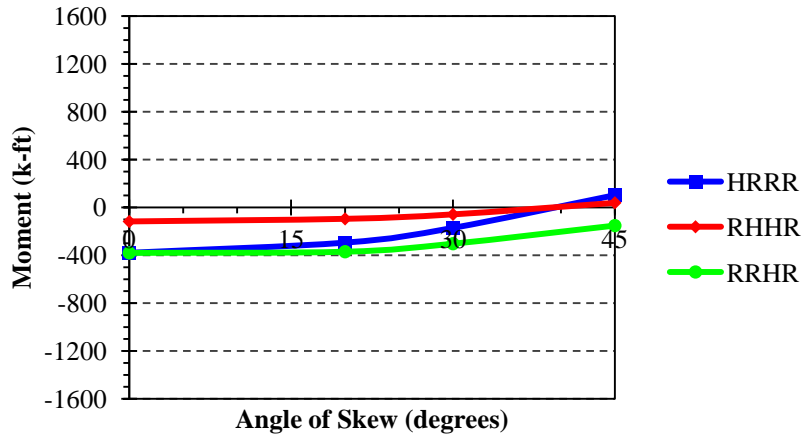


(c) Link slab in-plane twist (M_{zz})

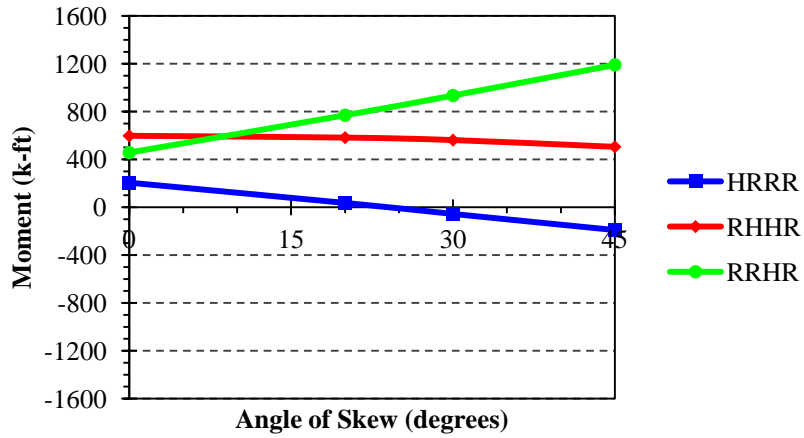
Figure 4-18. Total sectional moment - Lane1 load case



(a) Link slab torsion (M_{xx})

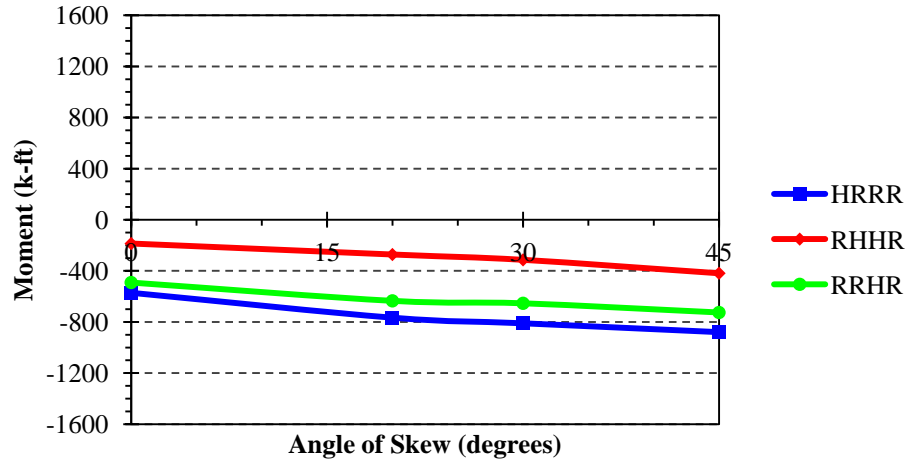


(b) Link slab bending moment (M_{yy})

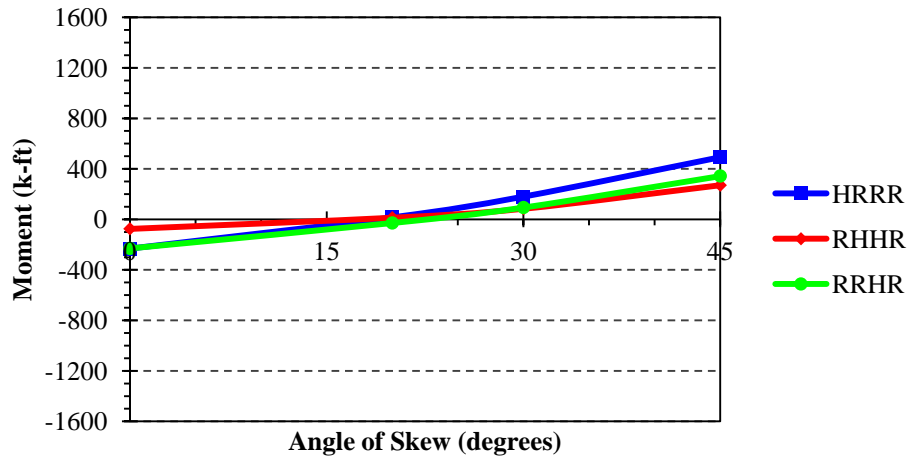


(c) Link slab in-plane twist (M_{zz})

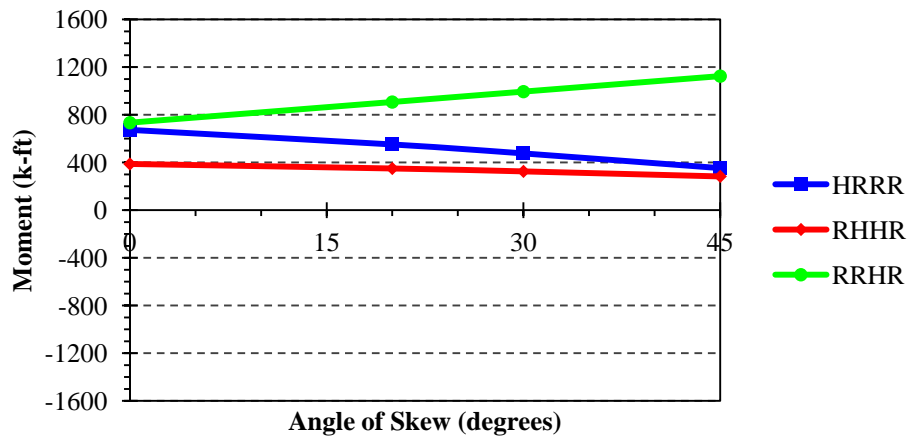
Figure 4-19. Total sectional moment - Lane2 load case



(a) Link slab torsion (M_{xx})

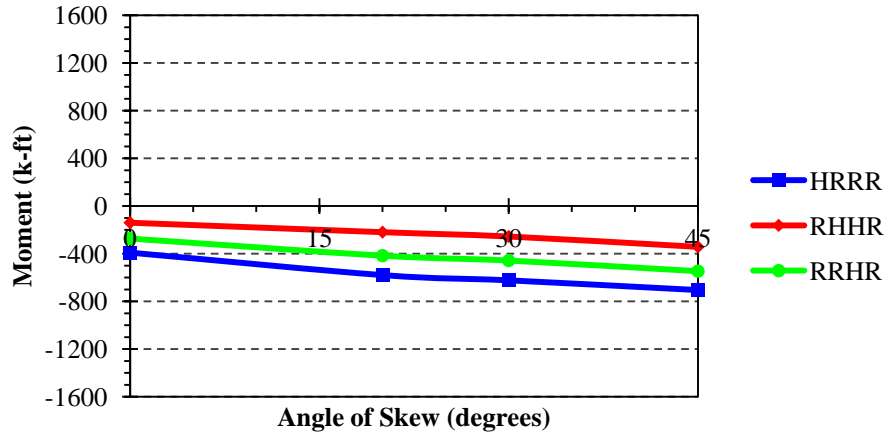


(b) Link slab bending moment (M_{yy})

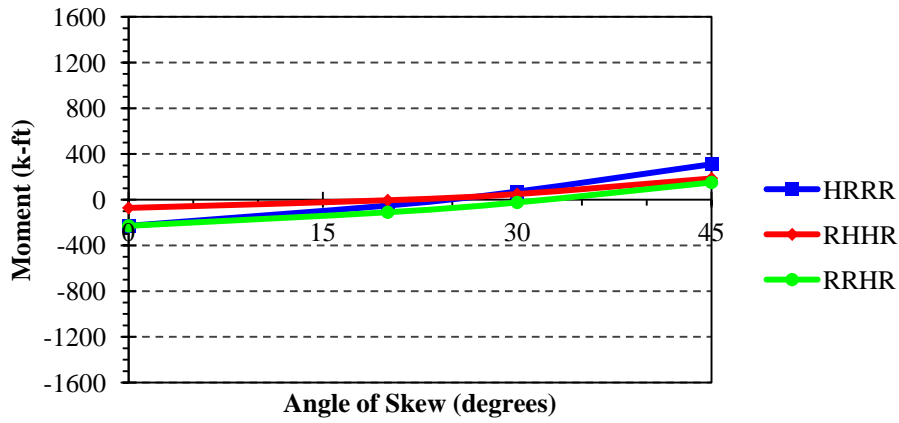


(c) Link slab in-plane twist (M_{zz})

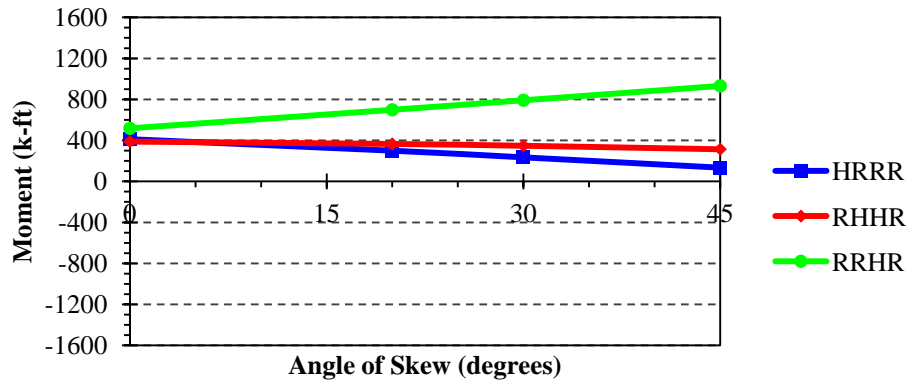
Figure 4-20. Total sectional moment – LaneAlt1 load case



(a) Link slab torsion (M_{xx})

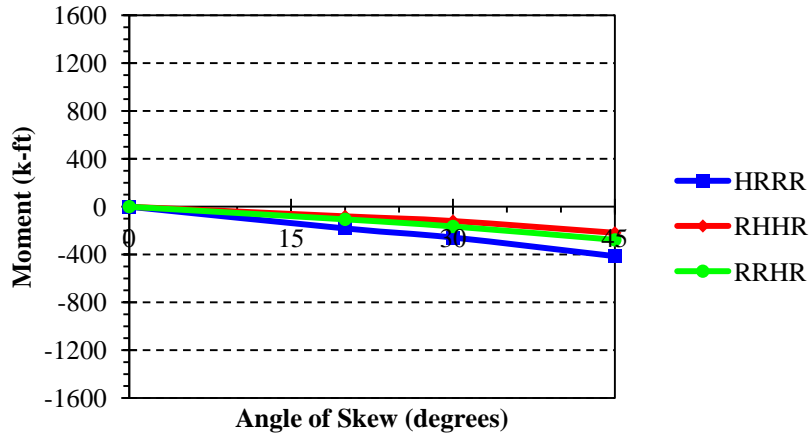


(b) Link slab bending moment (M_{yy})

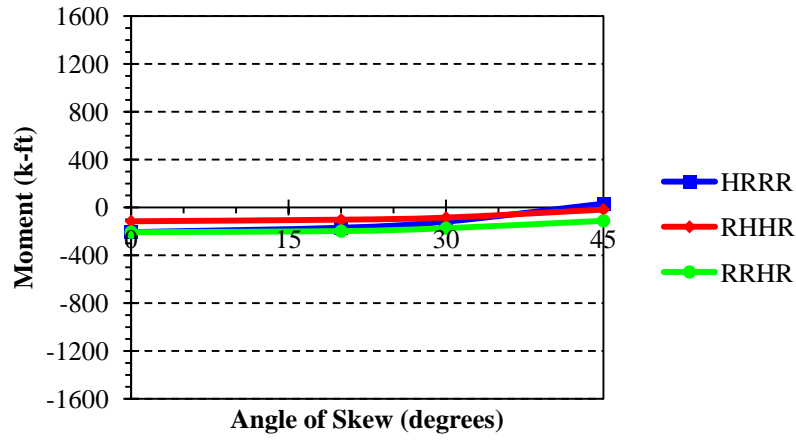


(c) Link slab in-plane twist (M_{zz})

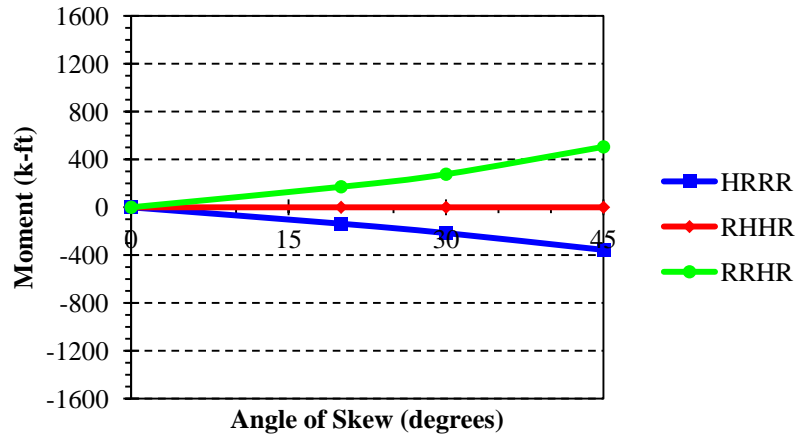
Figure 4-21. Total sectional moment – LaneAlt2 load case



(a) Link slab torsion (M_{xx})

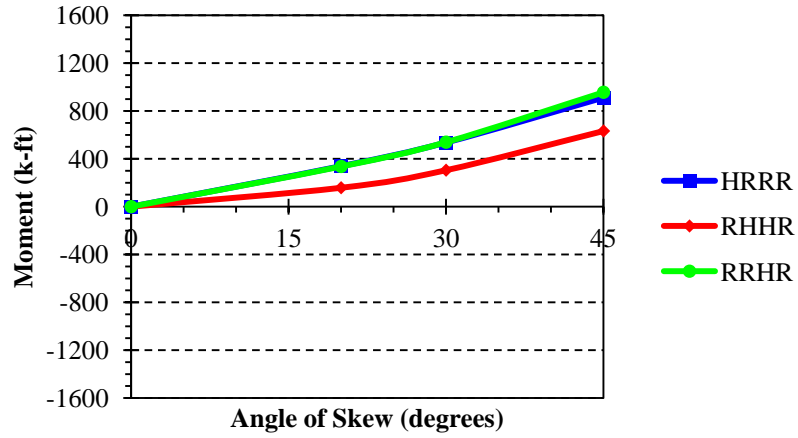


(b) Link slab bending moment (M_{yy})

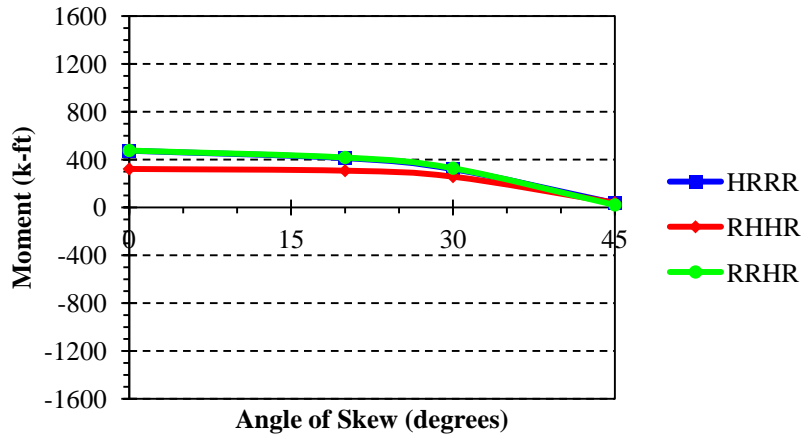


(c) Link slab in-plane twist (M_{zz})

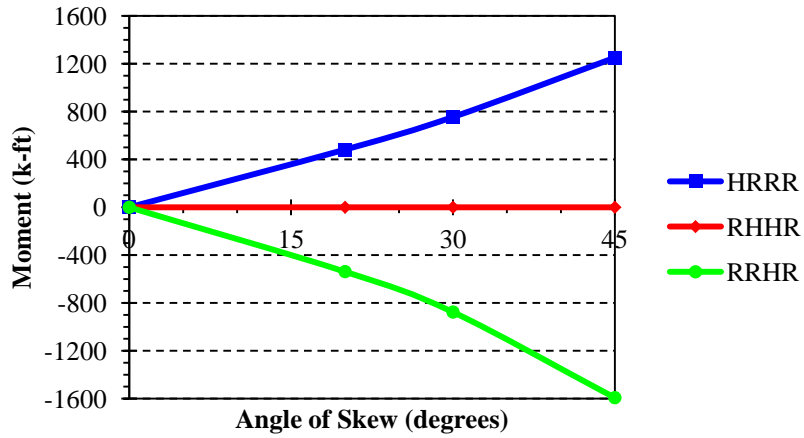
Figure 4-22. Total sectional moment - NTG load case



(a) Link slab torsion (M_{xx})

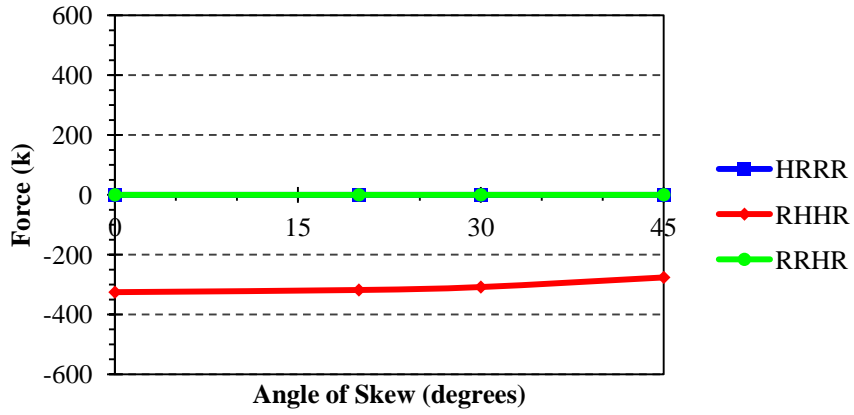


(b) Link slab bending moment (M_{yy})

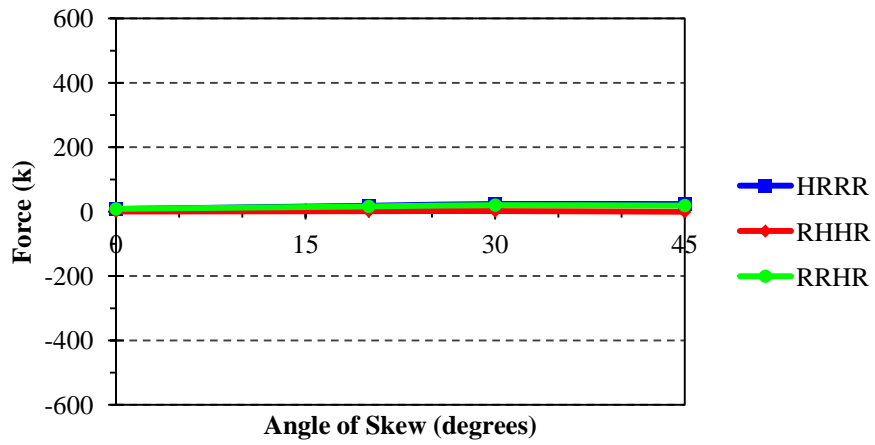


(c) Link slab in-plane twist (M_{zz})

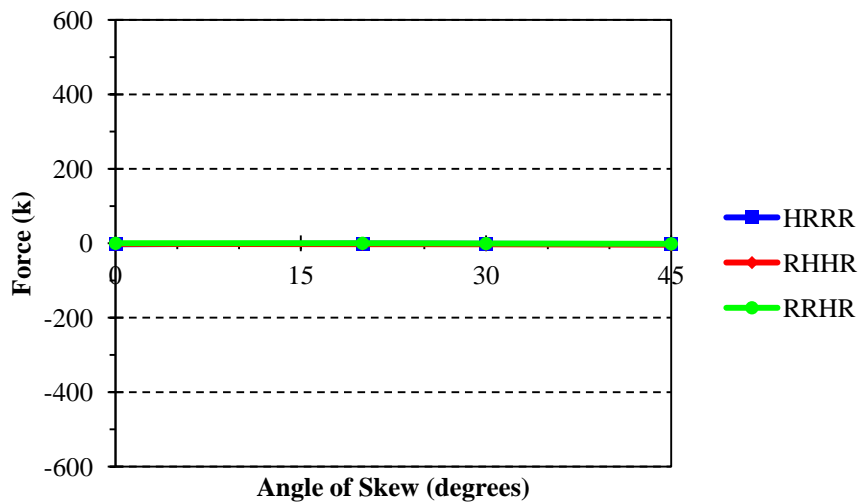
Figure 4-23. Total sectional moment - PTG load case



(a) Link slab axial force (F_x)

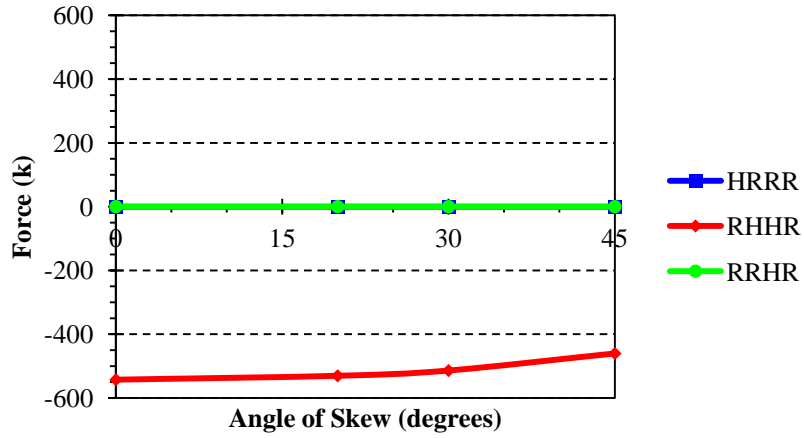


(b) Link slab transverse shear (F_y)

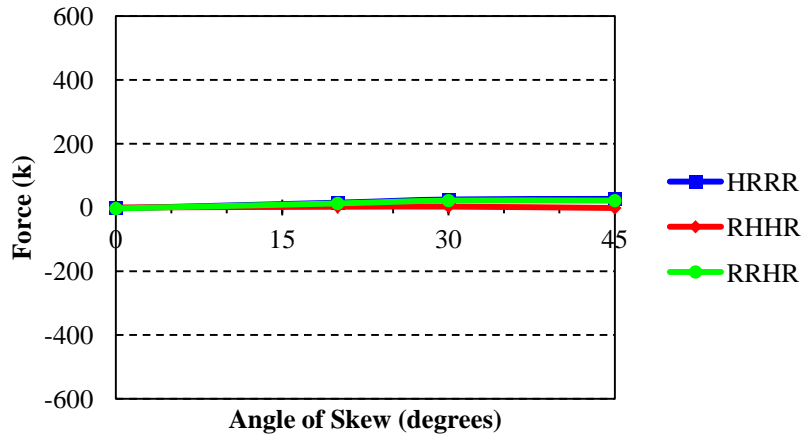


(c) Link slab vertical shear (F_z)

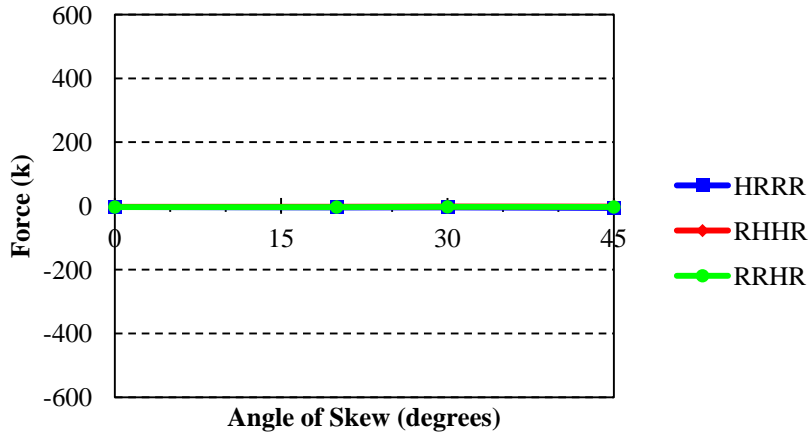
Figure 4-24. Total sectional force - Lane1 load case



(a) Link slab axial force (F_x)

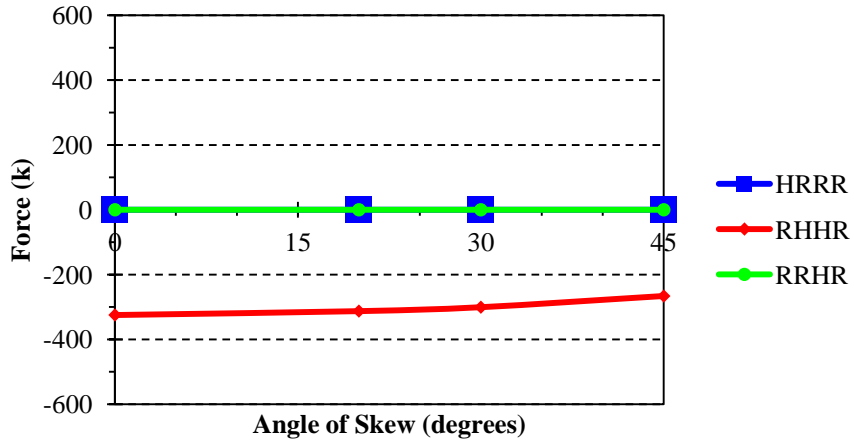


(b) Link slab transverse shear (F_y)

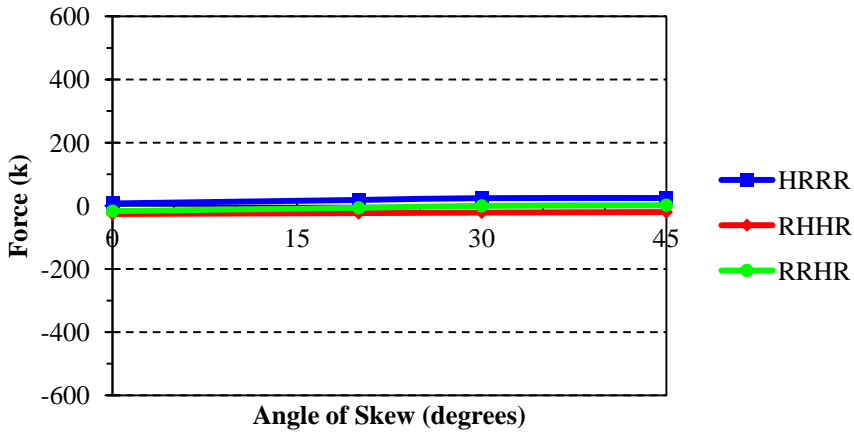


(c) Link slab vertical shear (F_z)

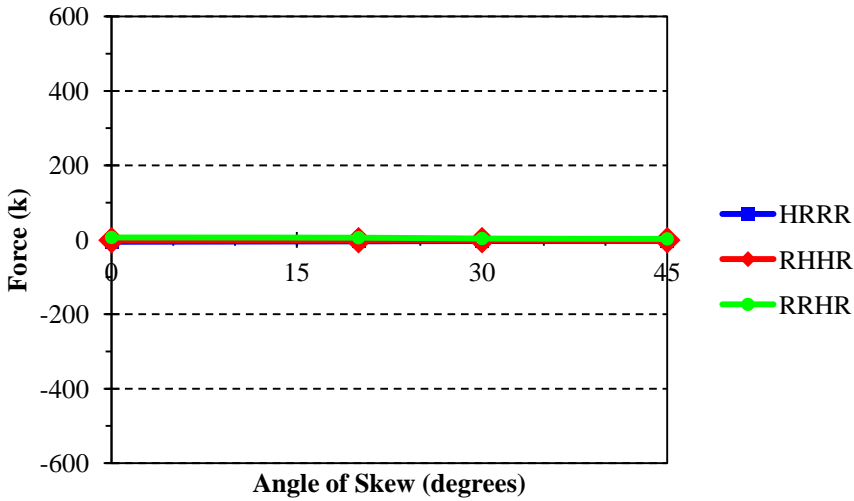
Figure 4-25. Total sectional force - Lane2 load case



(a) Link slab axial force (F_x)

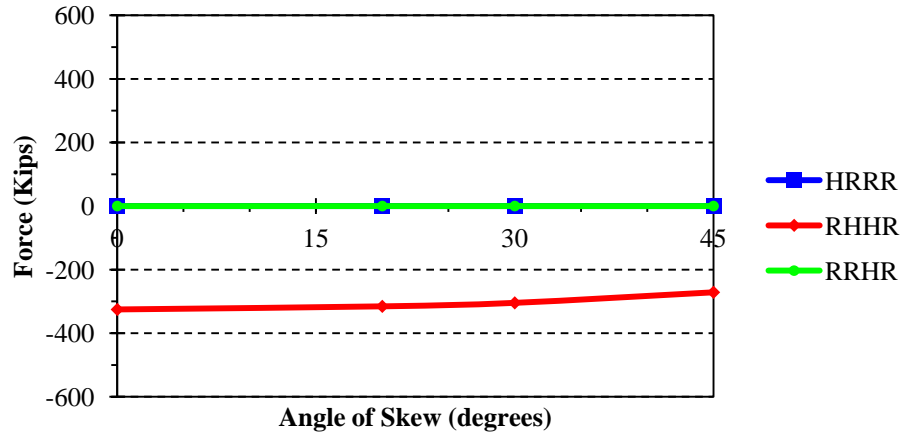


(b) Link slab transverse shear (F_y)

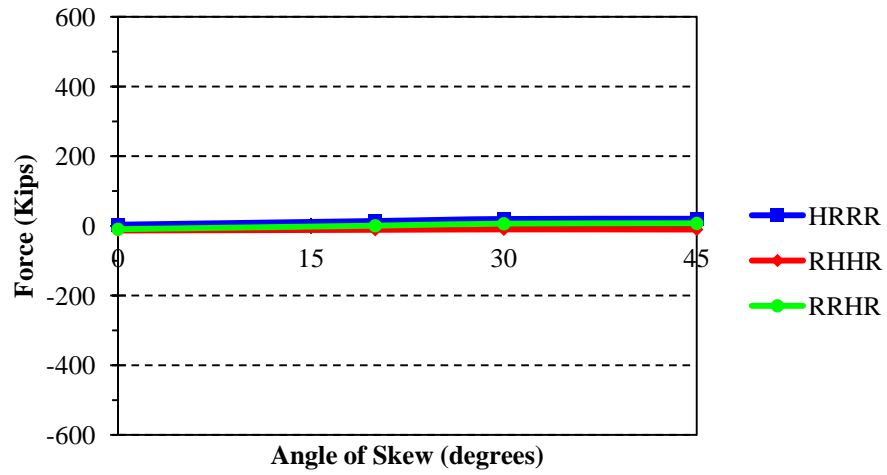


(c) Link slab vertical shear (F_z)

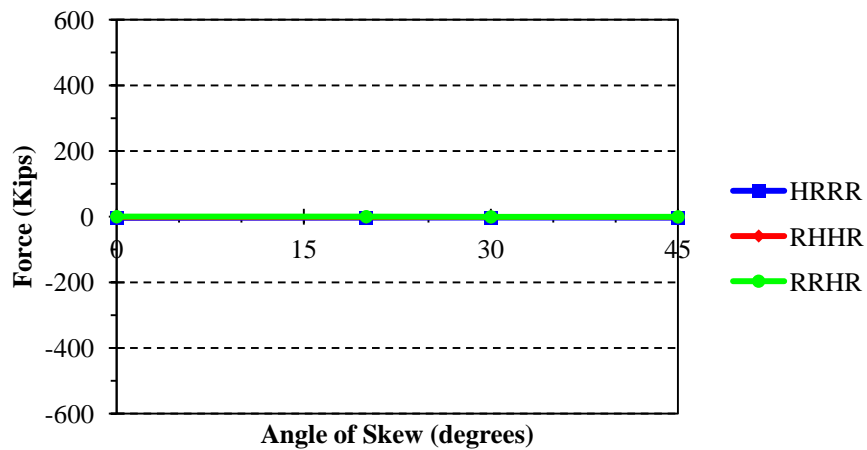
Figure 4-26. Total sectional force – LaneAlt1 load case



(a) Link slab axial force (F_x)

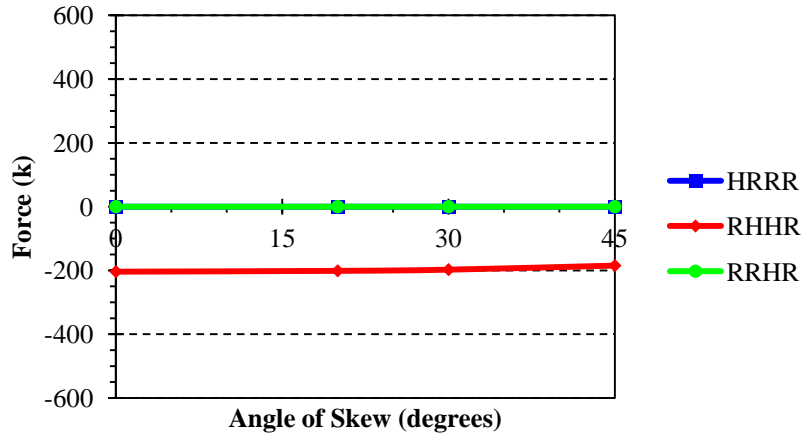


(b) Link slab transverse shear (F_y)

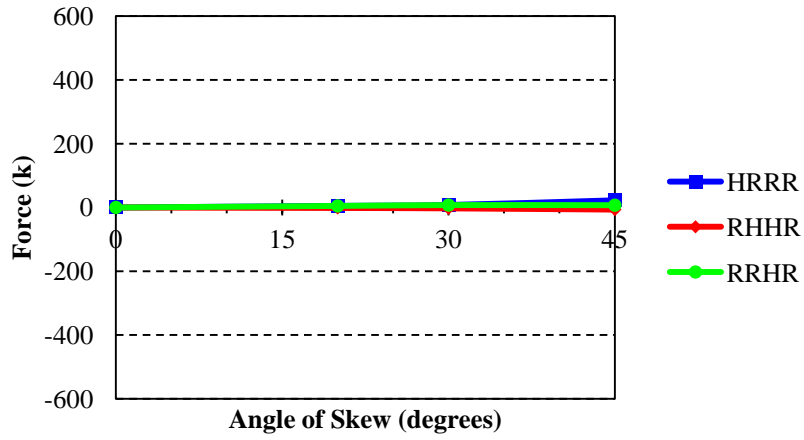


(c) Link slab vertical shear (F_z)

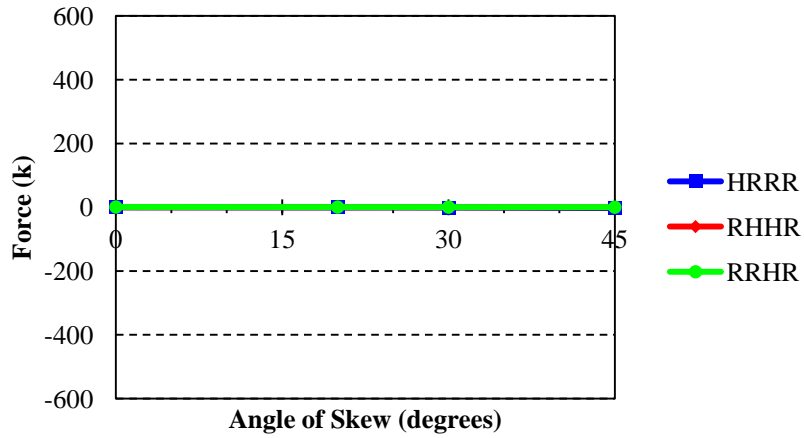
Figure 4-27. Total sectional force – LaneAlt2 load case



(a) Link slab axial force (F_x)

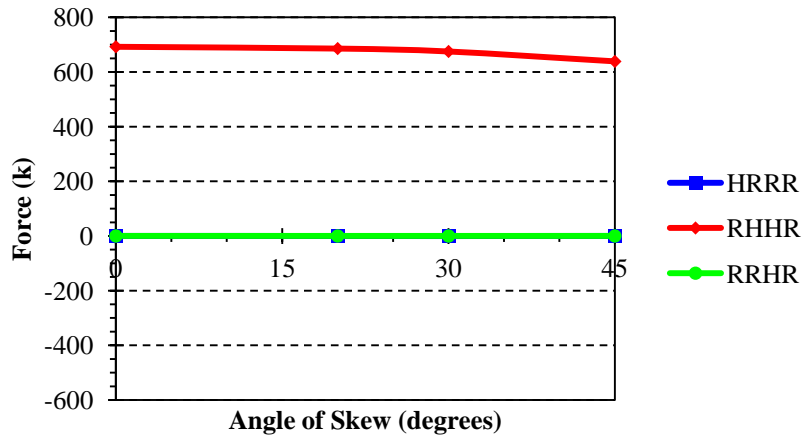


(b) Link slab transverse shear (F_y)

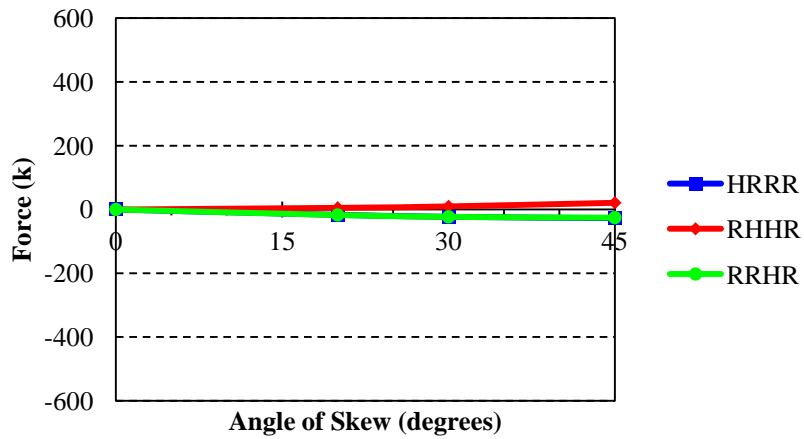


(c) Link slab vertical shear (F_z)

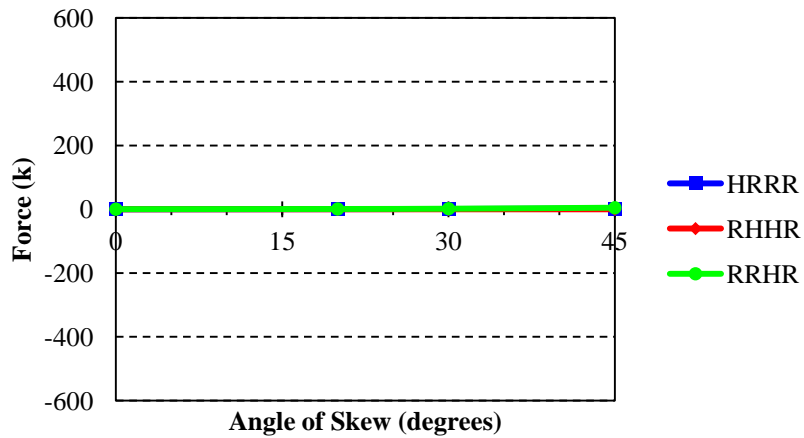
Figure 4-28. Total sectional force - NTG load case



(a) Link slab axial force (F_x)



(b) Link slab transverse shear (F_y)



(c) Link slab vertical shear (F_z)

Figure 4-29. Total sectional force - PTG load case

Table 4-3 presents a summary of the total sectional moments and forces shown in Figure 4-18 through Figure 4-29. From Table 4-3, the following general conclusions are derived.

- 1) The torsion (M_{xx}) magnitude in the link slab increases as the angle of skew increases for all load cases and boundary conditions. The RHHR boundary condition generates the lowest torsion.
- 2) The bending moment, under the *LaneAlt 1 and 2* load cases, reverses from negative to positive. The bending moment magnitude decreases as the angle of skew increases in load cases *Lane1* and *Lane2* as well as both positive temperature gradient (PTG) and negative temperature gradient (NTG). The lowest bending moment magnitude is developed with RHHR boundary condition while magnitudes are the same for HRRR and RRHR boundary conditions.
- 3) The link slab with an RHHR support configuration does not develop in-plane twist (M_{zz}) under PTG or NTG, irrespective of bridge skew. Twist remains constant under live loads with RHHR support configuration. Under PTG or NTG, significant twist is developed with HRRR and RRHR support configurations. Link slab twist shows mixed behavior under live loads with HRRR or RRHR support configurations.
- 4) Axial force in the link slab slightly decreases under all load cases with increasing skew and with RHHR boundary conditions. The largest axial force is developed under the PTG.
- 5) Axial force is zero under HRRR and RRHR boundary conditions. Vertical or transverse shear forces developed in the link slab are insignificant irrespective of loads, support configurations, or skew.

The above conclusions are based on the moments and forces developed at the entire cross-section of the link slab. These moments and forces are helpful in understanding the link slab behavior with changing skew. Design forces and moments will be calculated combining forces and moments within an effective width of a link slab. Hence, such forces and moments are calculated and presented in the following section.

Table 4-3. Total Sectional Moment and Force Variation Trend with Increased Skew under Various Load and Support Configurations

Load	Support Configuration	Moment (kip-ft)			Force (kip)		
		M _{xx}	M _{yy}	M _{zz}	F _x	F _y	F _z
Lane 1	HRRR	↑ (0 - -400)	↓ (-200-0)	~ (-600)	~ 0	~ 0	~ 0
	RRHR	↑ (-100 - -400)	↓ (-200-0)	↓ (-1400--600)	~ 0	~ 0	~ 0
	RHHR	↑ (0 - -100)	↓ (-100-0)	↓ (-1800--1500)	↓ (-300--250)	~ 0	~ 0
Lane 2	HRRR	↑ (0 - -800)	↓↑ (-400-100)	↑↓ (200--200)	~ 0	~ 0	~ 0
	RRHR	↑ (0 - -500)	↓ (-400--200)	↑ (400 - 1200)	~ 0	~ 0	~ 0
	RHHR	↑ (0 - -300)	↓ (-100-0)	↓ (600-500)	↓ (-550--450)	~ 0	~ 0
LaneAlt 1	HRRR	↑ (-600 - -900)	↓↑ (-200-500)	↓ (700-400)	~ 0	~ 0	~ 0
	RRHR	↑ (-500 - -700)	↓↑ (-200-400)	↑ (700 - 1100)	~ 0	~ 0	~ 0
	RHHR	↑ (-200 - -400)	↓↑ (-100-200)	↓ (400-300)	↓ (-300--250)	~ 0	~ 0
LaneAlt 2	HRRR	↑ (-400 - -700)	↓↑ (-200-300)	↓ (400-100)	~ 0	~ 0	~ 0
	RRHR	↑ (-300 - -600)	↓↑ (-200-100)	↑ (500 - 900)	~ 0	~ 0	~ 0
	RHHR	↑ (-200 - -400)	↓↑ (-100-100)	↓ (400-300)	↓ (-300--250)	~ 0	~ 0
NTG	HRRR	↑ (0 - -400)	↓ (-200-0)	↑ (0 - -400)	~ 0	~ 0	~ 0
	RRHR	↑ (0 - -300)	↓ (-200--100)	↑ (0 - 500)	~ 0	~ 0	~ 0
	RHHR	↑ (0 - -300)	↓ (-100-0)	~ 0	~ -200	~ 0	~ 0
PTG	HRRR	↑ (0 - 900)	↓ (500-0)	↑ (0 - 1200)	~ 0	~ 0	~ 0
	RRHR	↑ (0 - 900)	↓ (500-0)	↑ (0 - -1600)	~ 0	~ 0	~ 0
	RHHR	↑ (0 - 600)	↓ (300-0)	~ 0	↓ (700-650)	~ 0	~ 0

Note: ↑ - Increase; ↓ - Decrease; ↓↑ - Change from (-) to (+); ↑↓ - Change from (+) to (-); ~ - No significant change

4.4.4.2 Effective Section Axial Force and Bending Moment

In order to calculate the forces and moments within an effective width of a link slab, the full bridge cross-section is divided into eight segments as shown in Figure 4-30. The force and moment within an effective width of a link slab are referred to as the effective force and effective moment.

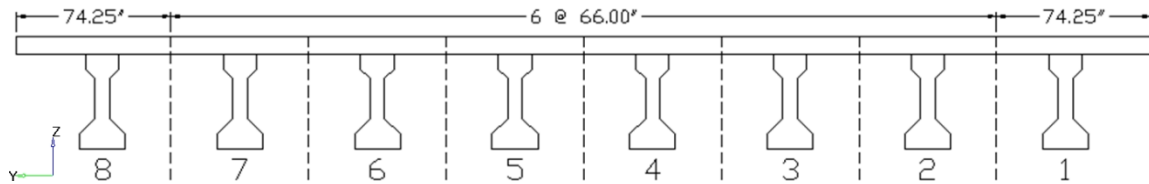
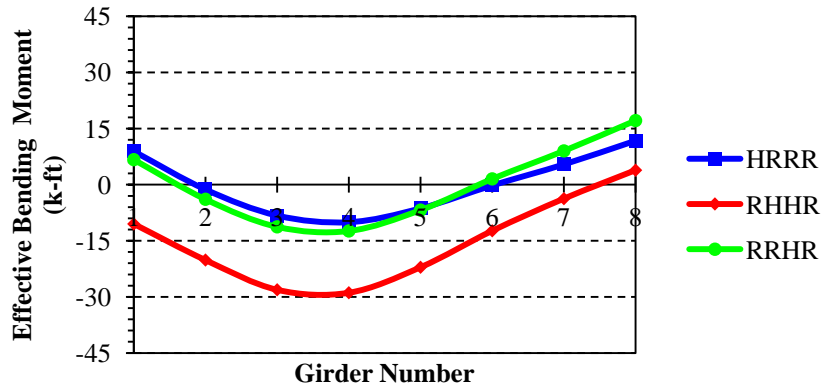
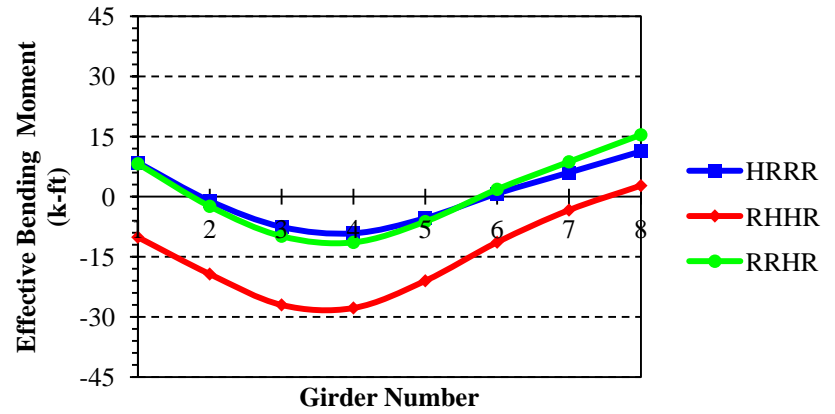


Figure 4-30. Effective width segments

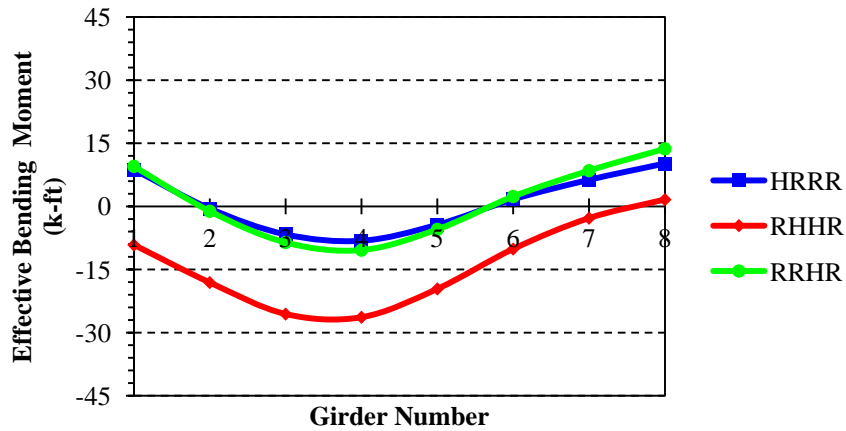
The effective axial force for each segment is calculated from summation of average nodal axial stress multiplied by the projected area of each node. The effective bending moment for each segment is computed by summation of nodal axial forces multiplied by the vertical distance from the neutral axis of the link slab to the node. Effective moments versus skew, under different load configurations are presented in Figure 4-31 through Figure 4-42, and effective forces are presented in Figure 4-37 through Figure 4-42. In these figures, segments are defined by the associated girder index.



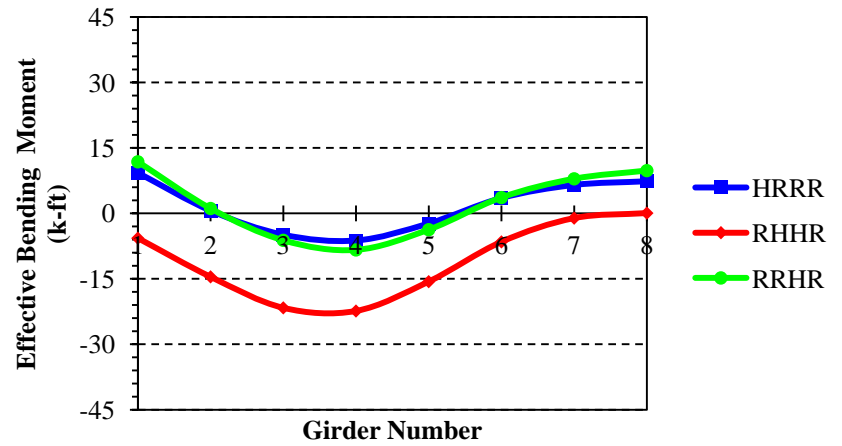
(a) Skew angle of 0°



(b) Skew angle of 20°

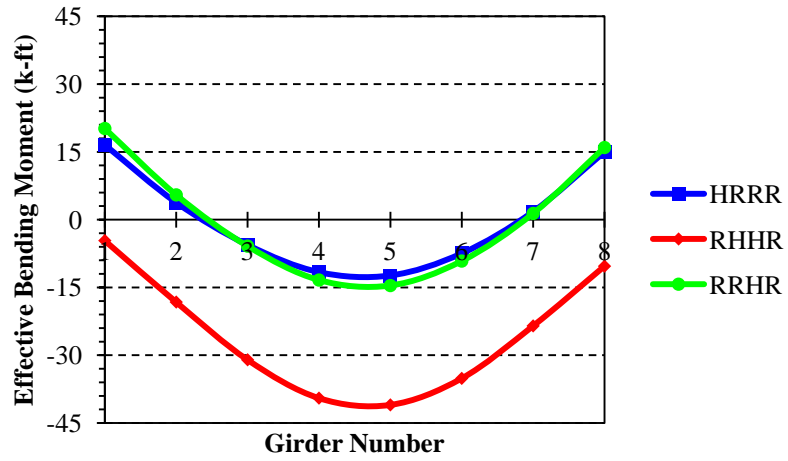


(c) Skew angle of 30°

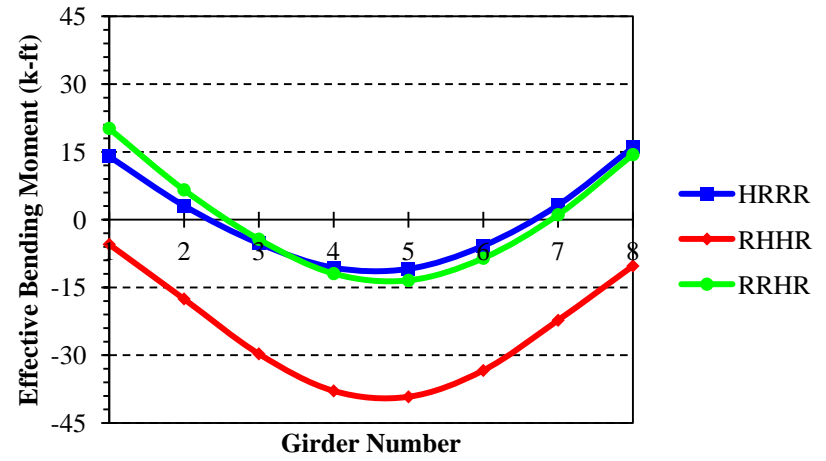


(d) Skew angle of 45°

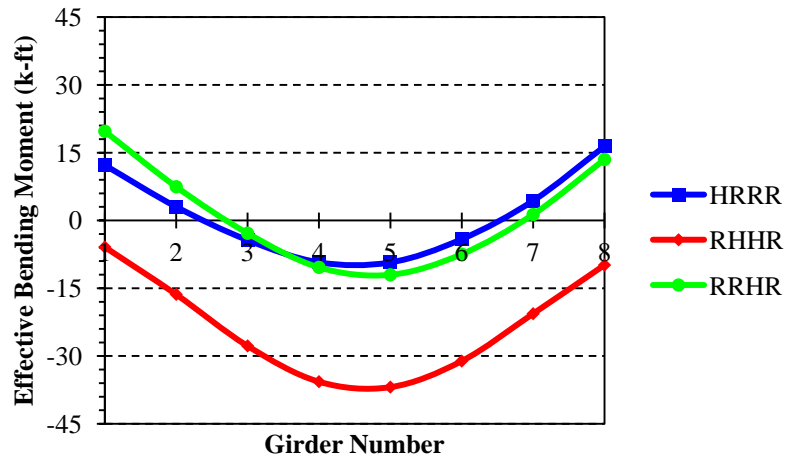
Figure 4-31. Effective moment - Lane1 load case



(a) Skew angle of 0°



(b) Skew angle of 20°

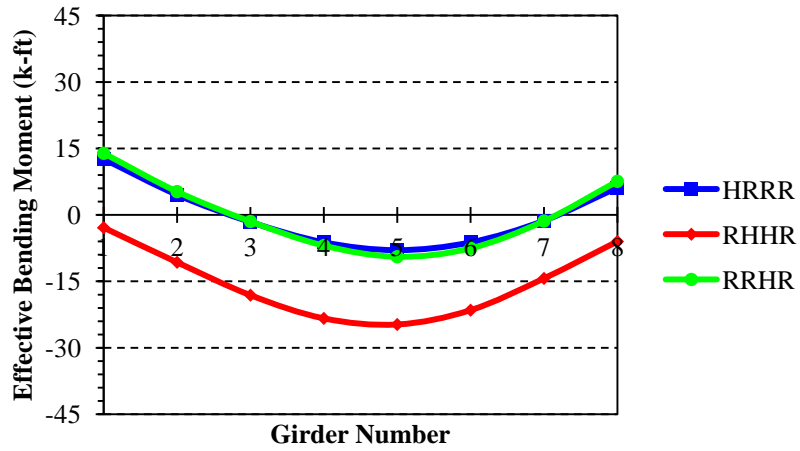


(c) Skew angle of 30°

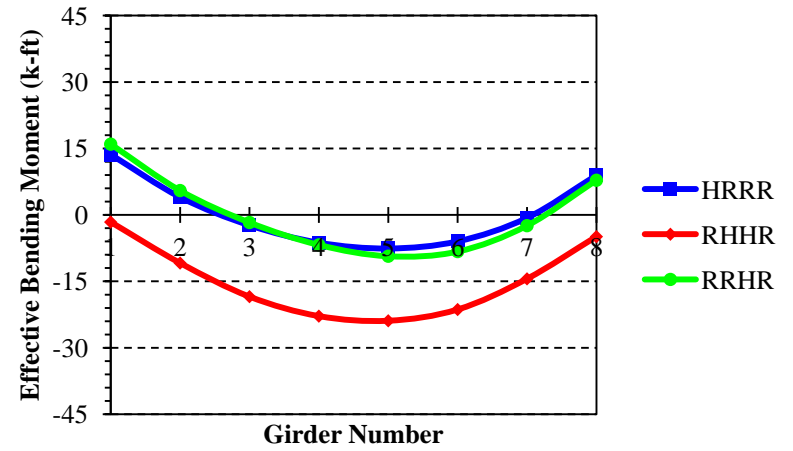


(d) Skew angle of 45°

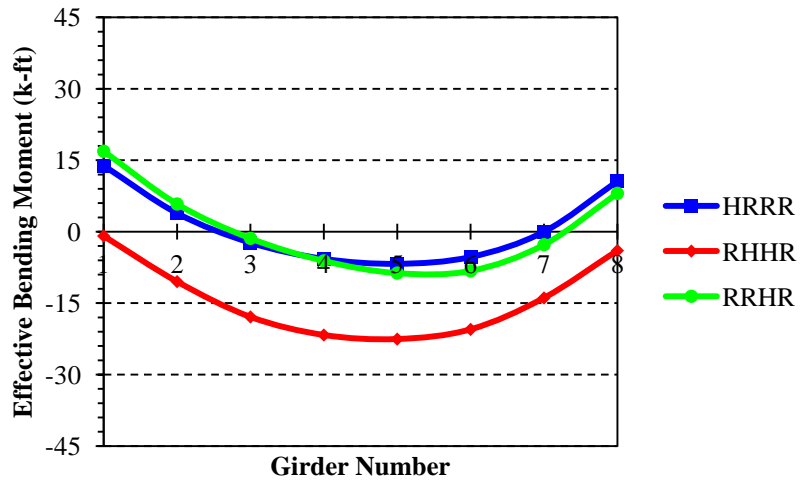
Figure 4-32. Effective moment - Lane2 load case



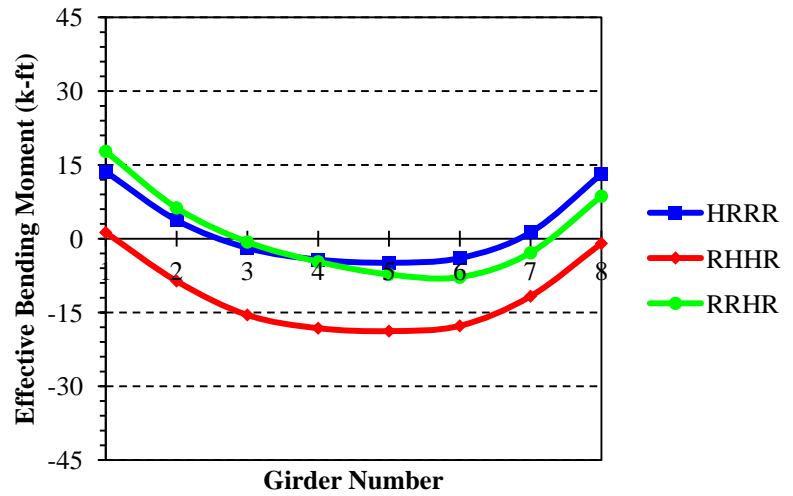
(a) Skew angle of 0°



(b) Skew angle of 20°

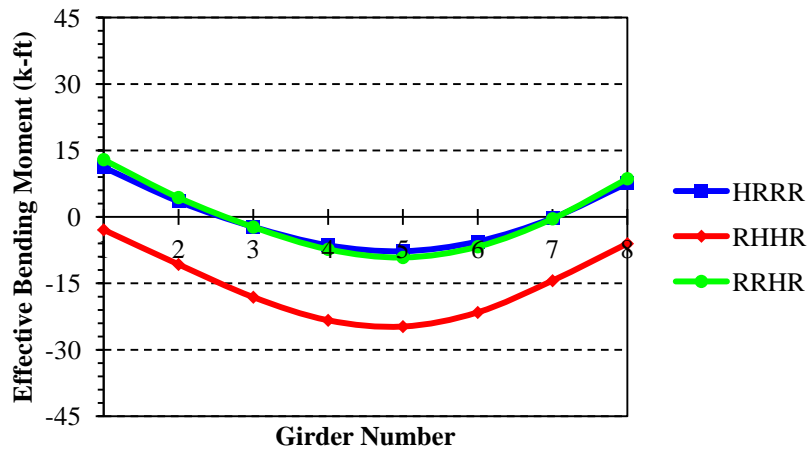


(c) Skew angle of 30°

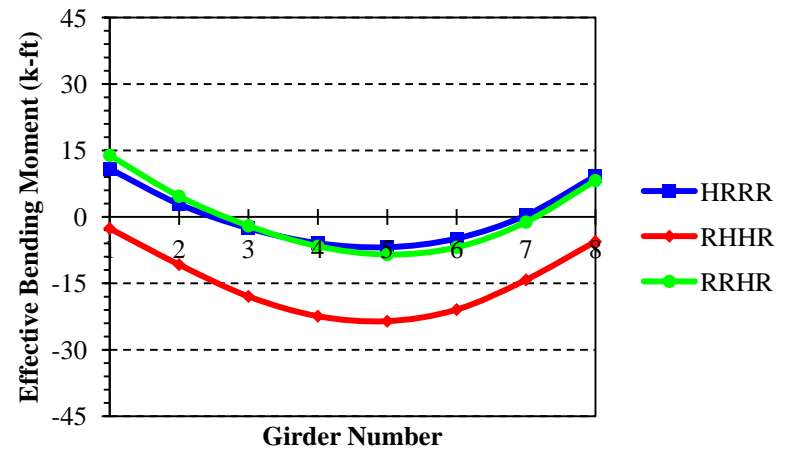


(d) Skew angle of 45°

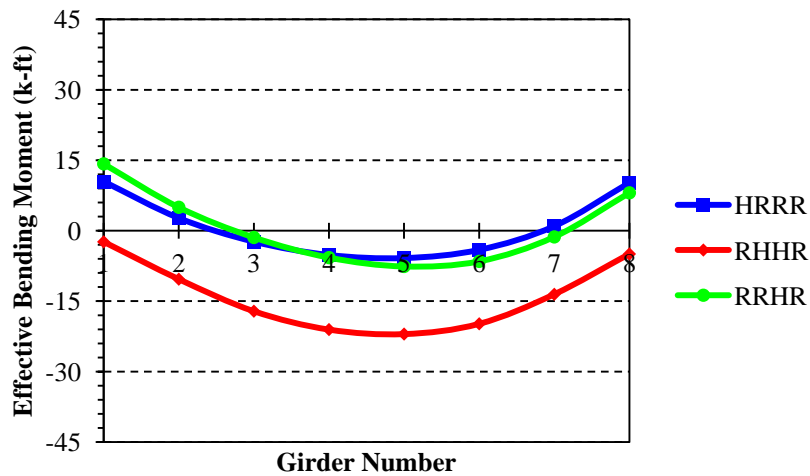
Figure 4-33. Effective moment – LaneAlt1 load case



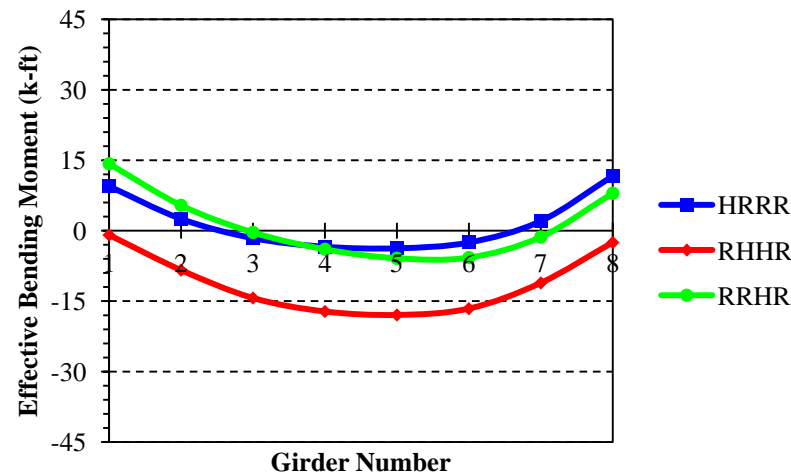
(a) Skew angle of 0°



(b) Skew angle of 20°

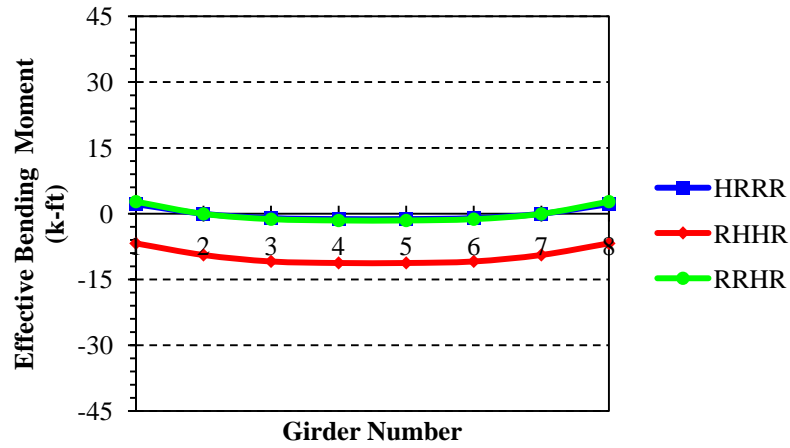


(c) Skew angle of 30°

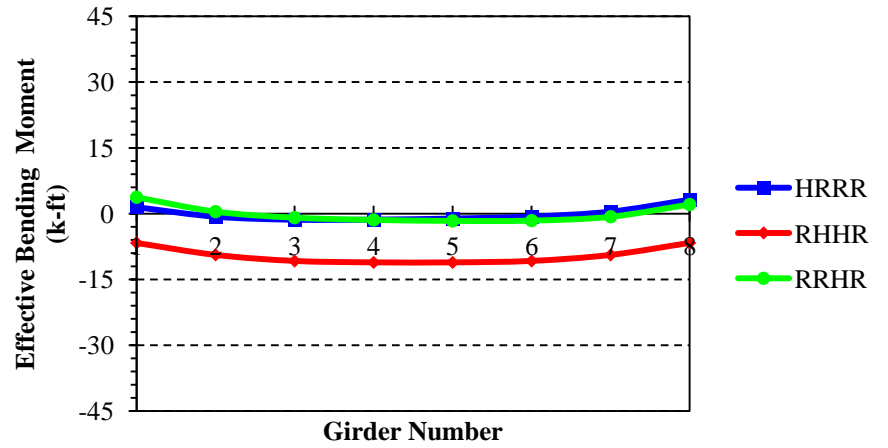


(d) Skew angle of 45°

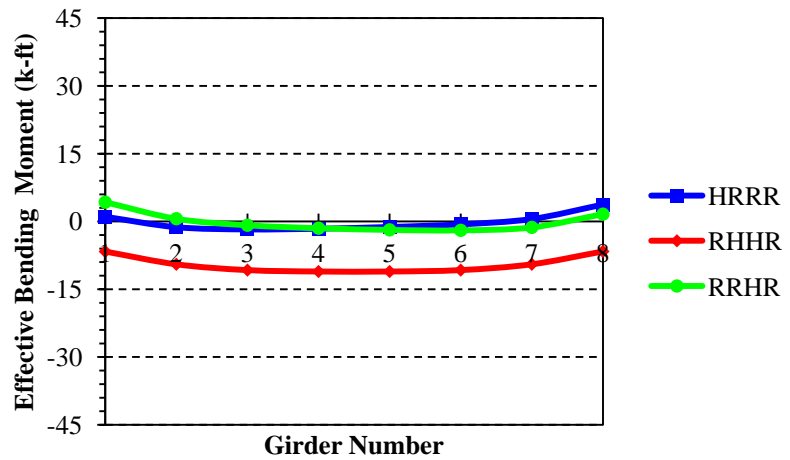
Figure 4-34. Effective moment – LaneAlt2 load case



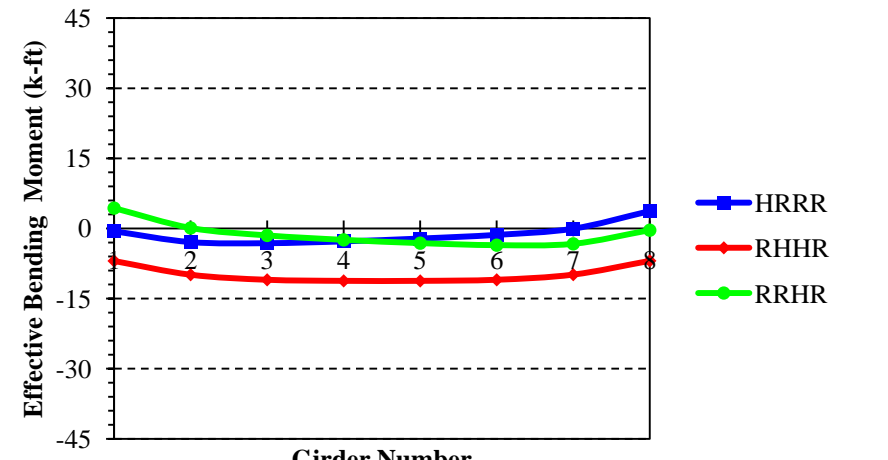
(a) Skew angle of 0°



(b) Skew angle of 20°



(c) Skew angle of 30°

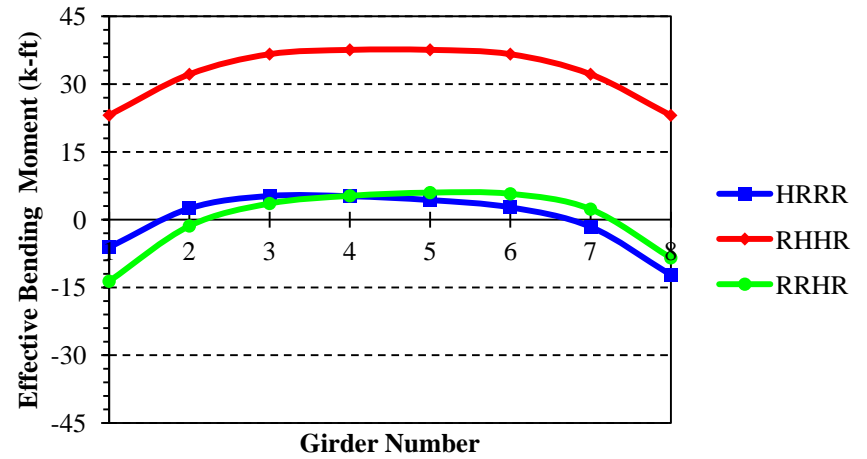


(d) Skew angle of 45°

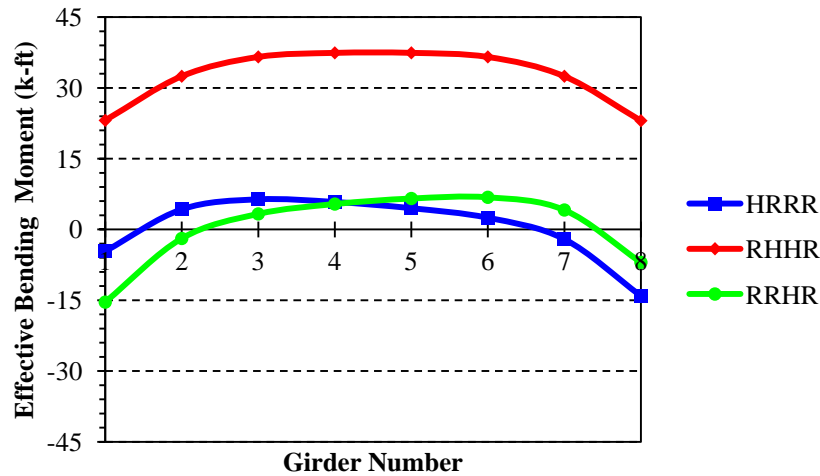
Figure 4-35. Effective moment - NTG load case



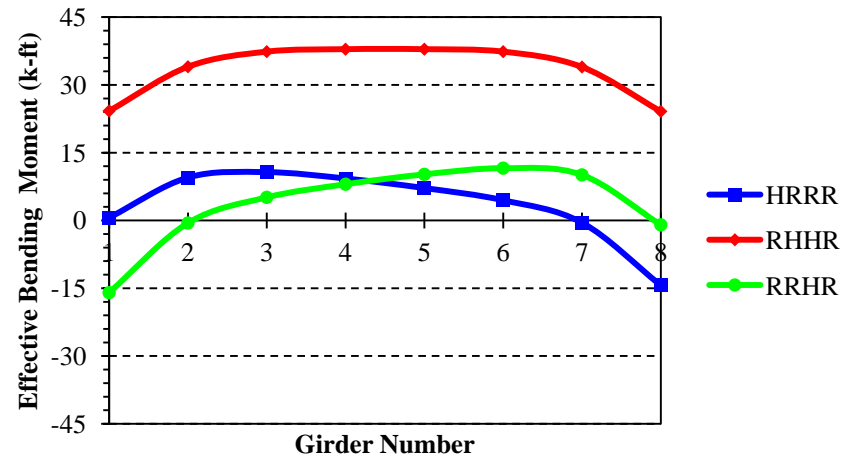
(a) Skew angle of 0°



(b) Skew angle of 20°

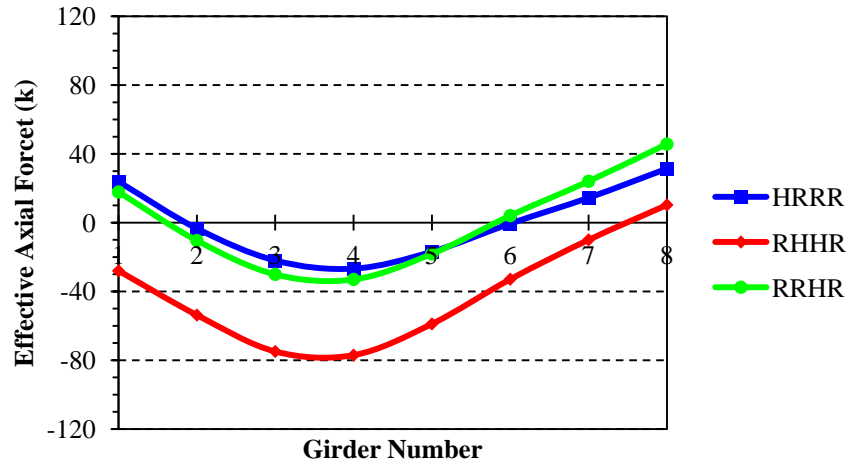


(c) Skew angle of 30°



(d) Skew angle of 45°

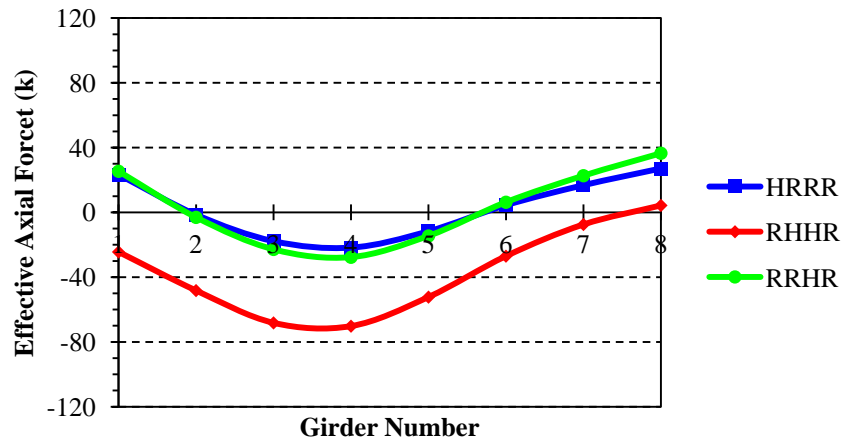
Figure 4-36. Effective moment - PTG load case



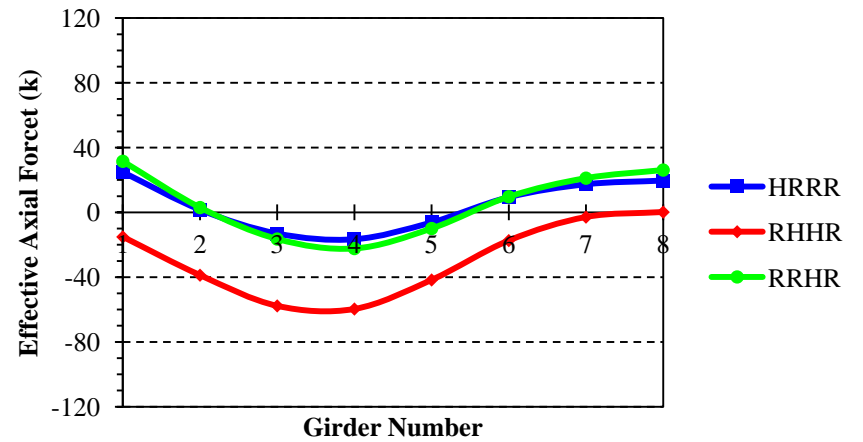
(a) Skew angle of 0°



(b) Skew angle of 20°

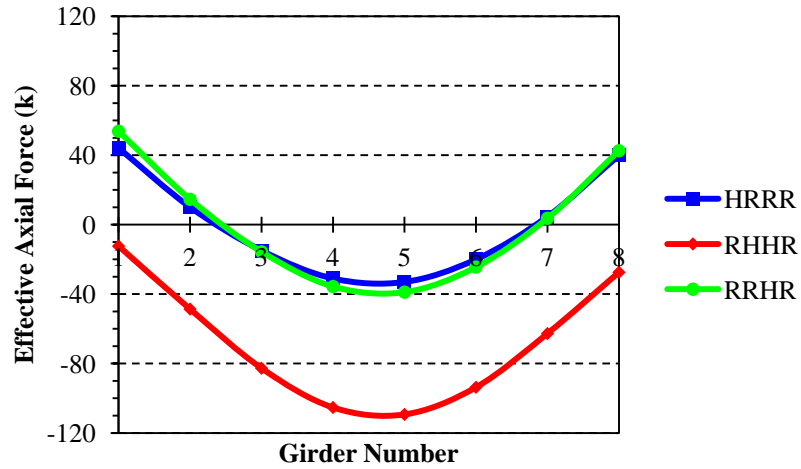


(c) Skew angle of 30°

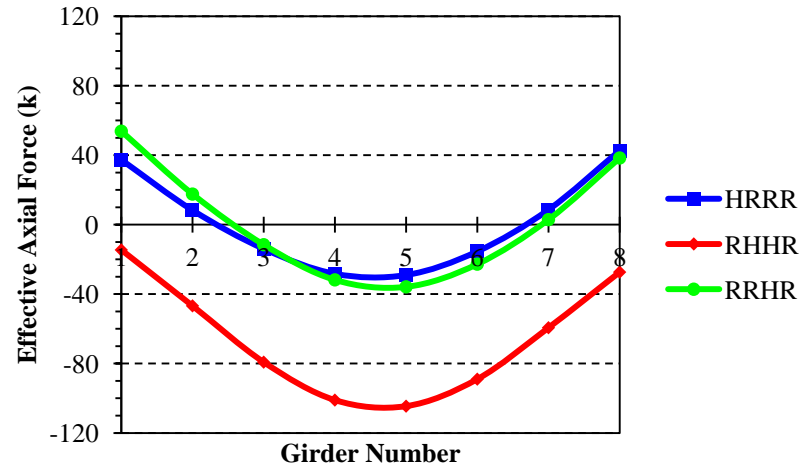


(d) Skew angle of 45°

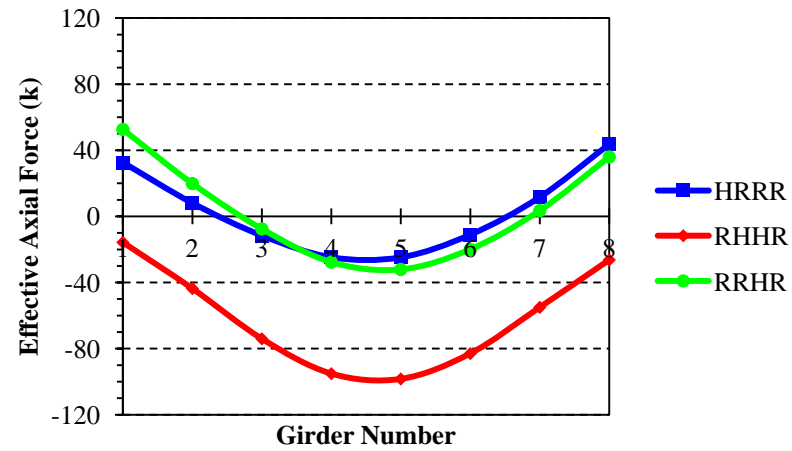
Figure 4-37. Effective force - Lane1 load case



(a) Skew angle of 0°



(b) Skew angle of 20°

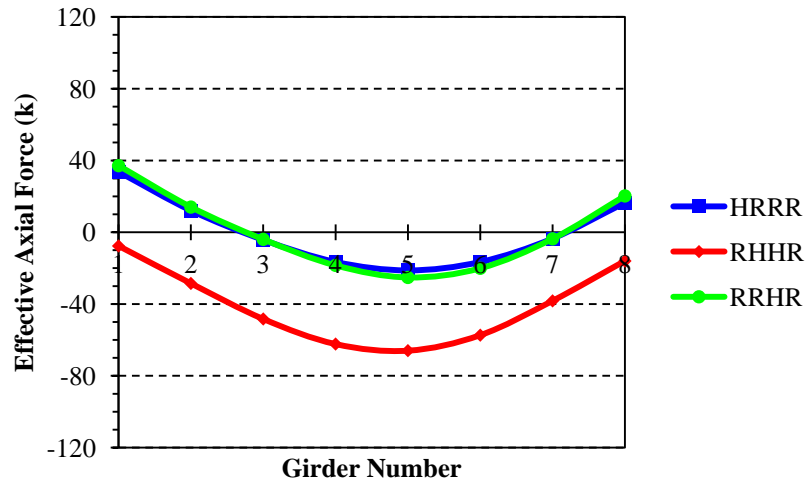


(c) Skew angle of 30°

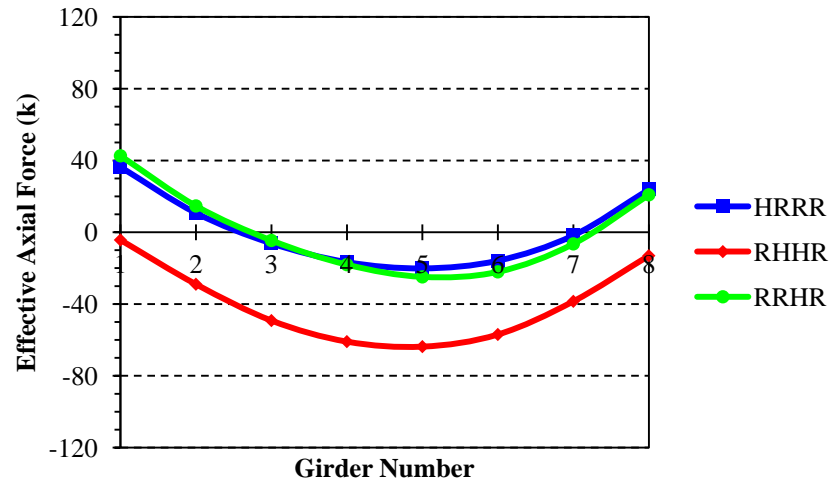


(d) Skew angle of 45°

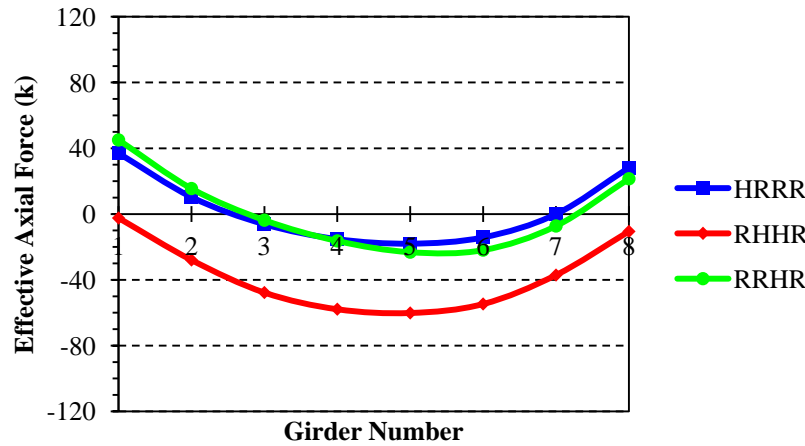
Figure 4-38. Effective force - Lane2 load case



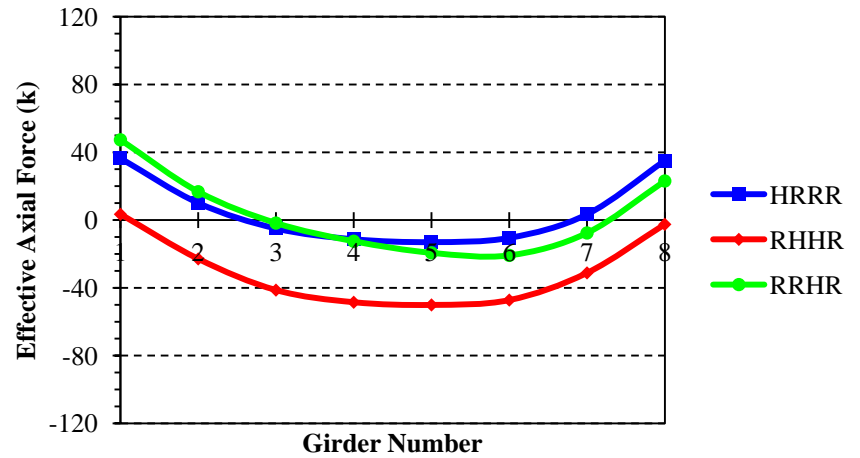
(a) Skew angle of 0°



(b) Skew angle of 20°

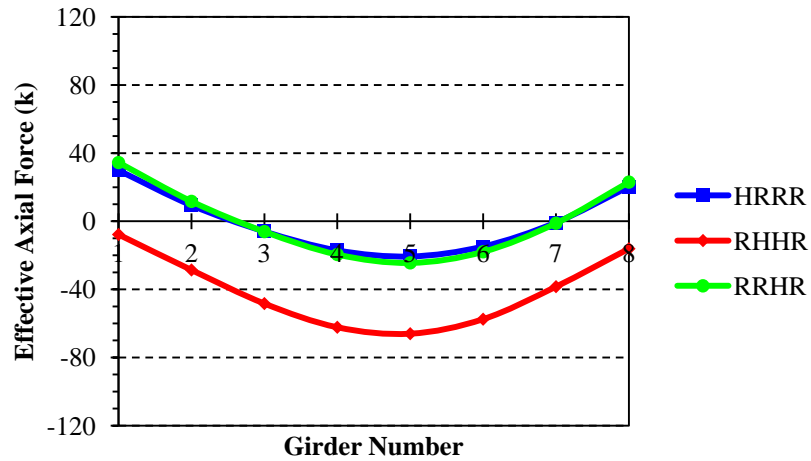


(c) Skew angle of 30°



(d) Skew angle of 45°

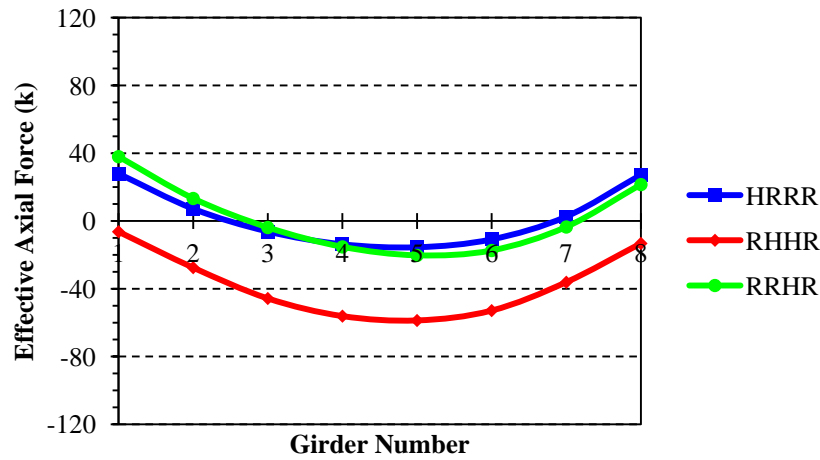
Figure 4-39. Effective Force – LaneAlt1 load case



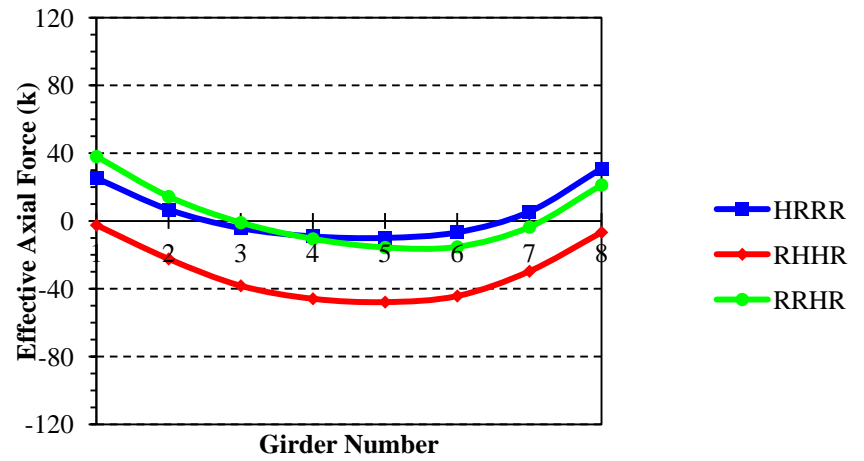
(a) Skew angle of 0°



(b) Skew angle of 20°



(c) Skew angle of 30°

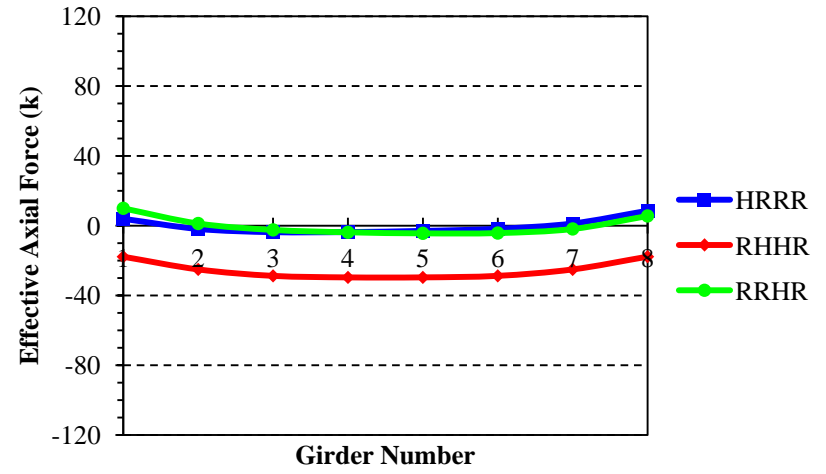


(d) Skew angle of 45°

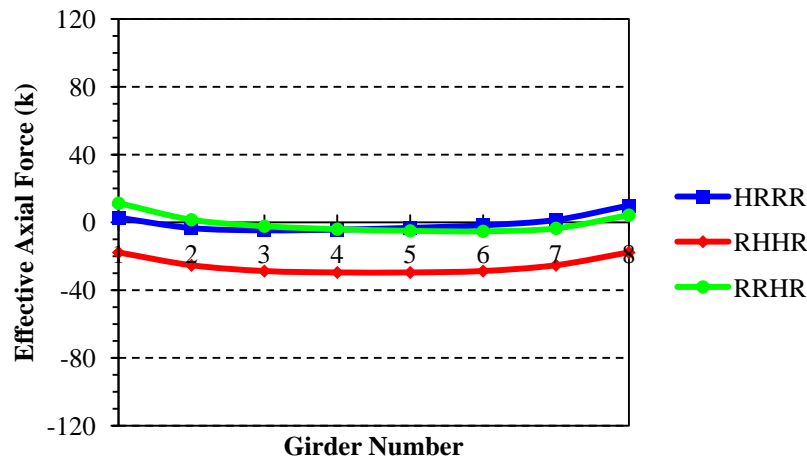
Figure 4-40. Effective Force – LaneAlt2 load case



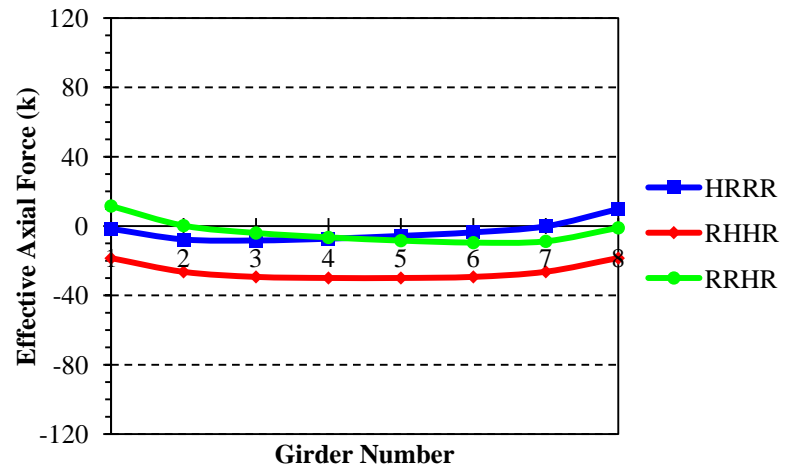
(a) Skew angle of 0°



(b) Skew angle of 20°

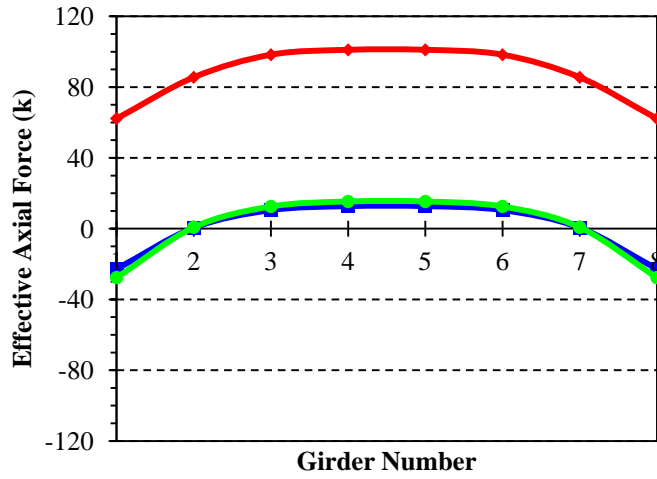


(c) Skew angle of 30°

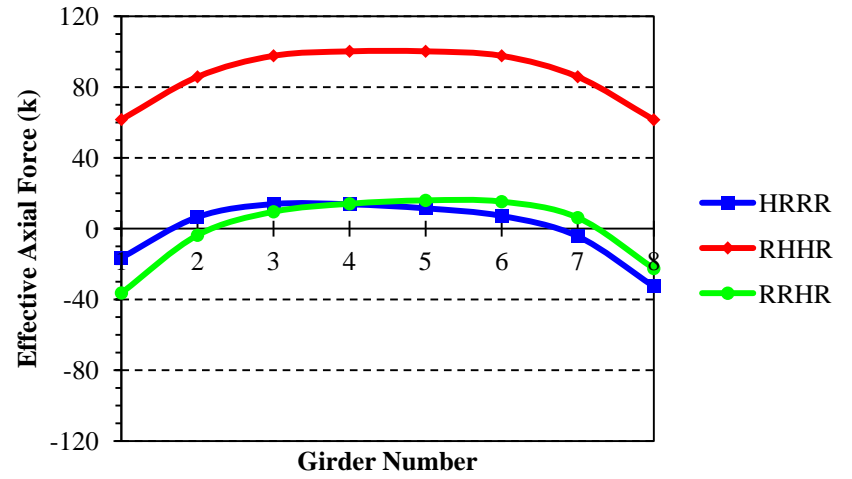


(d) Skew angle of 45°

Figure 4-41. Effective force - NTG load case



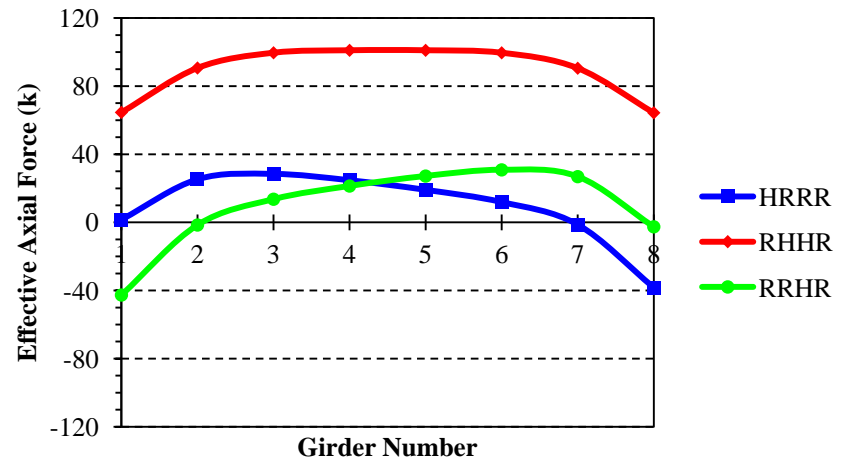
(a) Skew angle of 0°



(b) Skew angle of 20°



(c) Skew angle of 30°



(d) Skew angle of 45°

Figure 4-42. Effective force - PTG load case

The following are the key findings of the effective moment and force results:

- 1) Effective bending moments and axial forces decrease as the angle of skew increases.
- 2) Live load on both lanes (*Lane2*) is the critical load case for a two-lane bridge, effective link-slab negative moment and axial force.
- 3) Under NTG, with HRRR and RRHR boundary conditions, link-slab axial force is negligible
- 4) PTG with RHHR boundary condition is the critical load case for effective positive moments and effective forces.
- 5) The RHHR support configuration generates negative moments under live and NTG loads developing tensile stresses at the top fiber of the link slab.
- 6) Under live and NTG loads, with HRRR or RHHR support configurations, the effective link slab sections closest to the deck edges develop positive moment which increases with skew angle while the rest of the sections develop negative moments. Conversely, under PTG, negative moments develop at link slab sections close to the deck edges and increase with skew angle while the rest of the sections develop positive moments.
- 7) The effective axial force for each segment is calculated from summation of average nodal axial stress multiplied by the projected area of each node. The effective bending moment for each segment is computed by summation of nodal axial forces multiplied by the vertical distance from the neutral axis of the link slab to the node. Hence, variation of effective axial force with respect to loads, boundary conditions, and skew resembles the variation of the effective moment.
- 8) As per the results presented in Figure 4-31 through Figure 4-42, live and NTG load develop the critical load combination for negative moment whereas PTG load is critical for positive moment design.

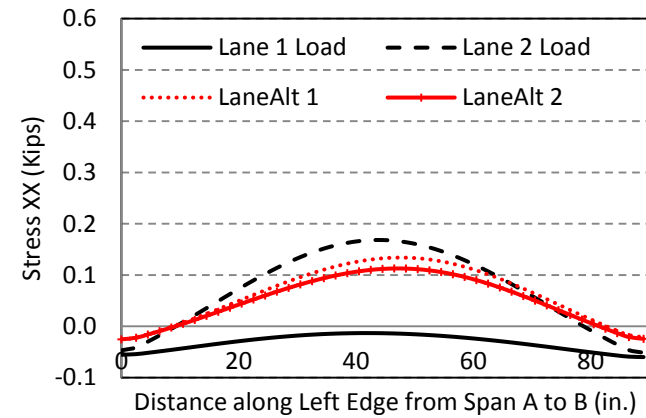
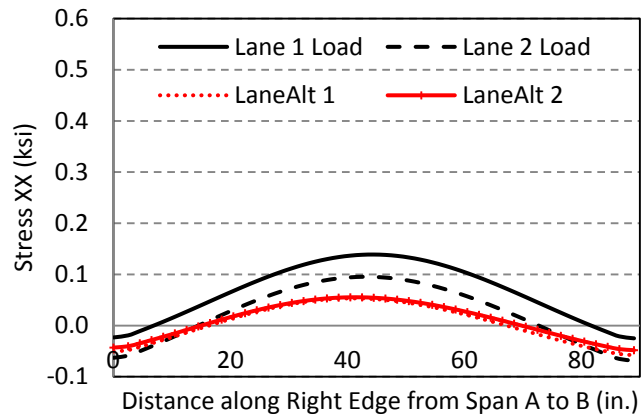
- 9) Effective moments and axial forces calculated from 3D analyses show that moment-axial force interaction should be included in the link slab design for RHHR support configuration.
- 10) In addition to axial force and moment effects, the design of high skew link slabs may need to consider additional effects of link slab torsion and in-plane twist.

4.4.4.3 *Link Slab Edge Stresses under In-plane Twist*

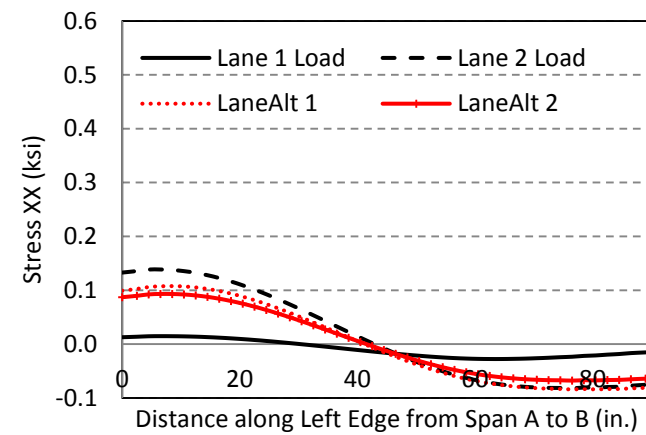
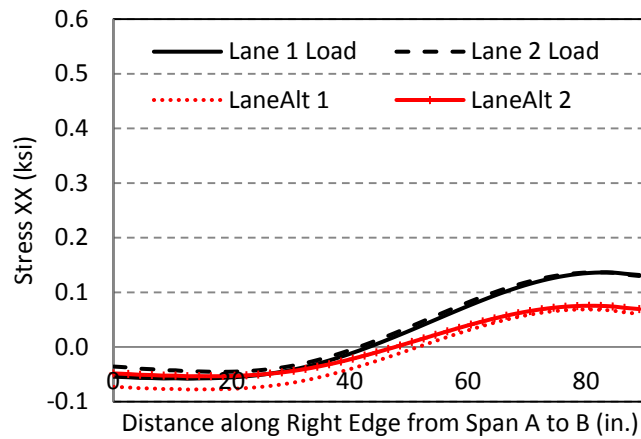
HRRR and RRHR support conditions under PTG load develop the critical in-plane twist (M_{zz}) in the link slab with increasing skew. The link slab develops axial loads under M_{zz} linearly increasing towards the outside edges of the slab. Link slab edge stresses due to twist are calculated along the right and left edges (note: right and left edges are defined based on the vehicle traveling direction, i.e., from span A to span B, shown in Figure 4-6). Live loads and NTG develop the largest tensile stresses at the edge top fiber while PTG develops the largest stresses at the link slab bottom fiber. Top fiber stresses are calculated for live loads and NTG loads are shown in Figure 4-43 and Figure 4-44. Bottom fiber stresses are calculated for PTG and shown in Figure 4-45.

The debonded length of the link slab is measured from span A to span B as defined in Figure 4-6. In skew bridges, the maximum longitudinal stresses are developed near link slab ends (i.e., at the point of debonding). The stresses developed under PTG are greater than the stresses developed under live loads and NTG. In this particular bridge with HRRR support conditions, stress developed under PTG is about 600 psi and exceeds tensile strength of grade D concrete used in bridge decks (i.e., $0.24\sqrt{f'_c}$). Deck concrete compressive strength is 4500 psi.

In order to accommodate high stresses developed along the link slab edges along the debonded zone, a joint near the link slab end is provided allowing rebars to resist the entire load. The joint needs to be saw cut and sealed for durability. Link slab reinforcement designed for moment should be checked for twist developed at the edge segments. Additional longitudinal reinforcement should be provided along the link slab edges if found inadequate.

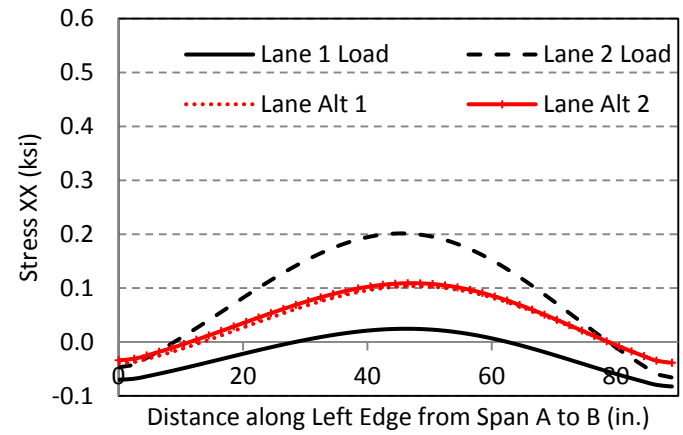
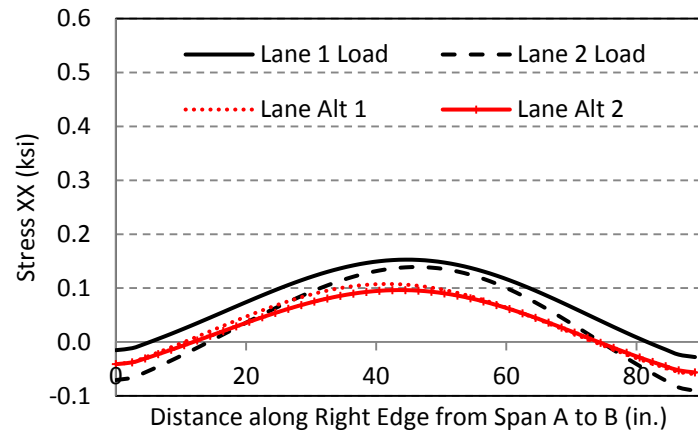


(a) Straight bridge

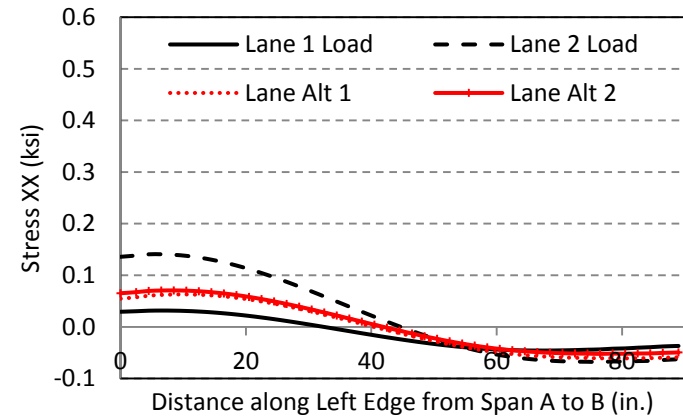
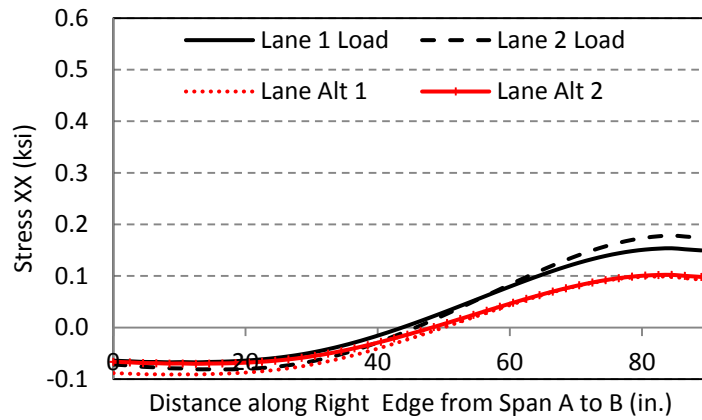


(b) 45° skew bridge

Figure 4-43. Edge stresses of link slab with HRRR support conditions under live loads



(a) Straight bridge



(b) 45° skew bridge

Figure 4-44. Edge stresses of link slab with RRHR support conditions under live loads

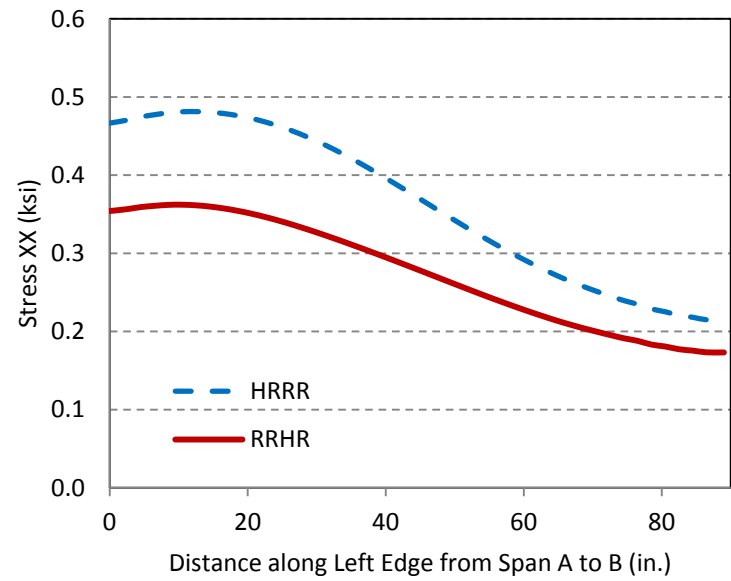
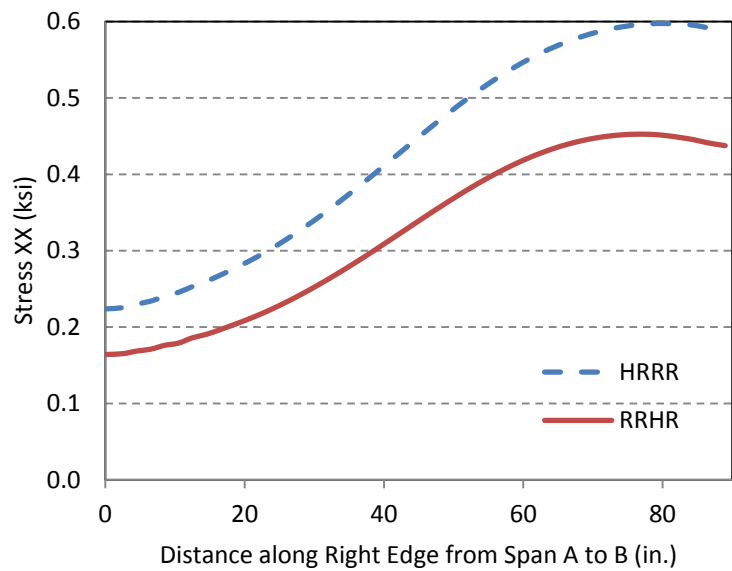
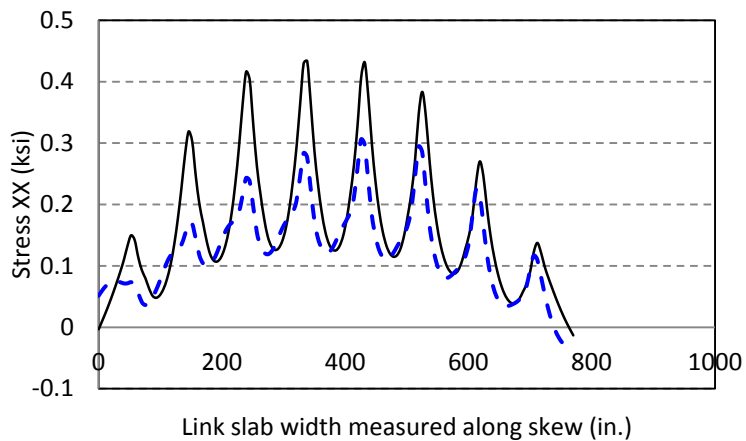


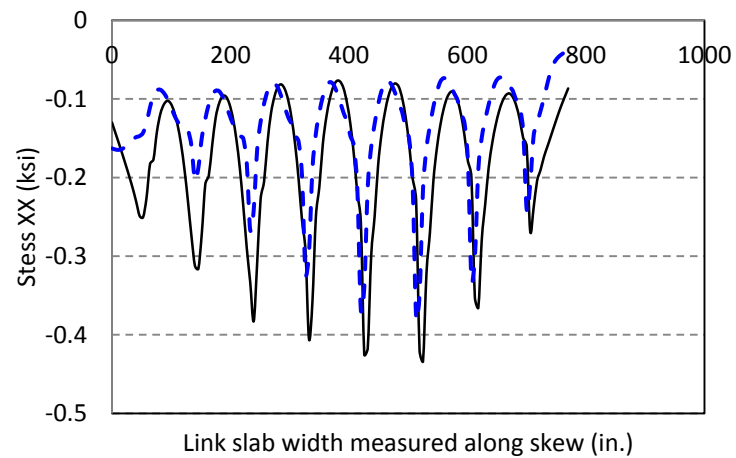
Figure 4-45. Edge stresses of a 45° skew link slab under PTG

4.4.4.4 *Link-Slab Torsion with Skew*

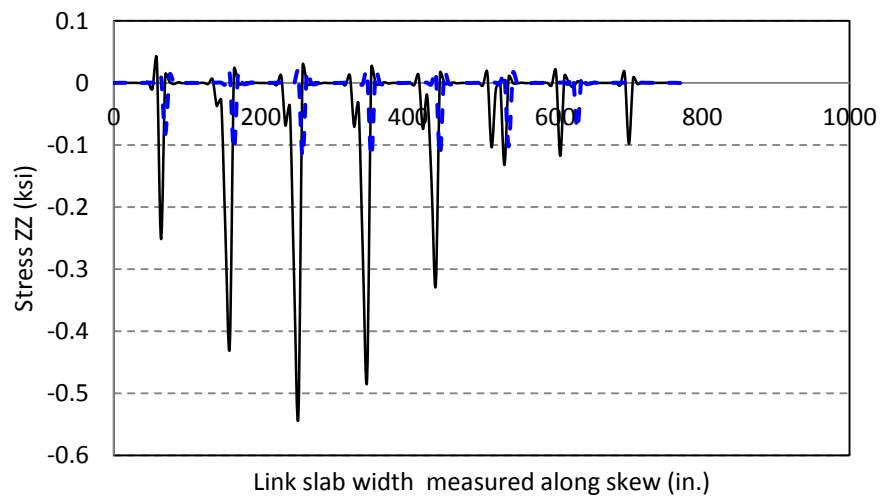
As skew increases, link slab torsion (M_{xx}) is developed under the LaneAlt1 load case (Figure 4-20). One way to deal with the torsion would be by providing cushioning between the girder ends and the link slab. For this purpose, use of a *soft* material like neoprene or Styrofoam over the girder ends underneath the link slab is investigated. The most critical case of a 45^0 skew link slab is analyzed under the LaneAlt1 load case, and the results are presented below. As shown in Figure 4-46, longitudinal tensile stresses and contact stresses developed underneath the link slab-girder contact points are reduced from the case without cushioning. Further, resultant gross-section moments are reduced when cushioning materials are introduced in between girder ends and the link slab (Figure 4-47).



(a) Longitudinal stress at top fiber



(b) Longitudinal stress at bottom fiber



(c) Vertical stress along bottom fiber

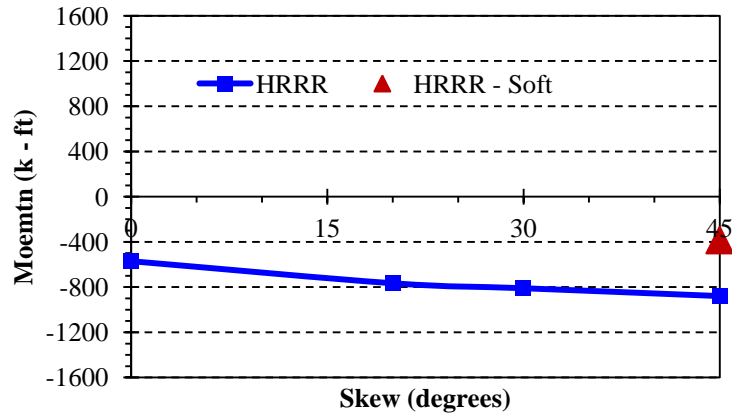
Note: The *soft* material emulates the properties similar to neoprene

Legend:

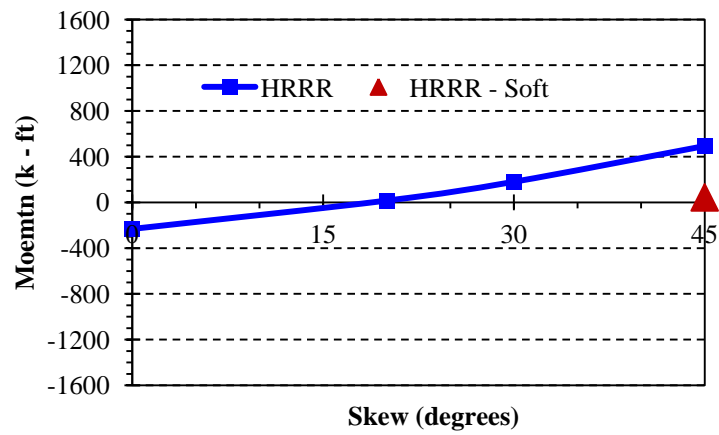
———— Without *Soft* material

- - - - - With *Soft* material

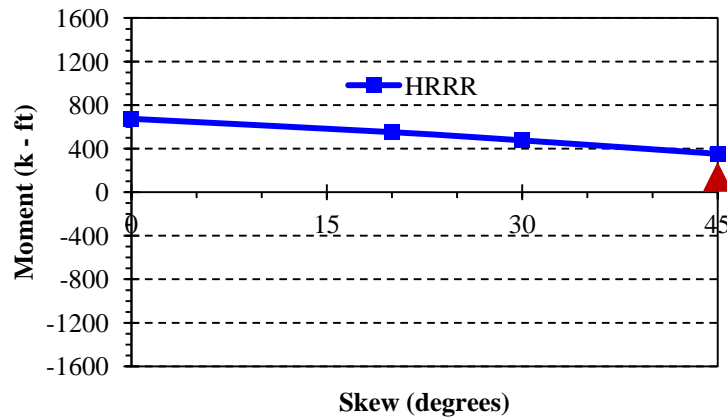
Figure 4-46. Stresses developed in 45° skew link slab with HRRR support conditions under LaneAlt1 load case



(a) Link slab torsion (M_{xx})



(b) Link slab bending moment (M_{yy})



(c) Link slab in-plane twist (M_{zz})

Note: The *soft* material emulates the properties similar to neoprene.

Figure 4-47. Gross section moment with and without soft material – LaneAlt1 load case

Placing cushioning material between girder ends and the link slab reduces torsion and resultant moments. However, there is no significant reduction in longitudinal stresses developed along the link slab edge near the transition zone at the start of the debonded region. There is a benefit in reducing contact stresses (stress z_z in Figure 4-46) by using cushioning material. Also, providing construction joints between the link slab and the deck near the deck edges and additional reinforcement along the link slab's outside edges needs to be incorporated for link slabs with HRRR and RRHR support configurations. Additional reinforcement is not required for a link slab with RHHR support configuration because there is no in-plane twist (M_{zz}) under PTG (Figure 4-36).

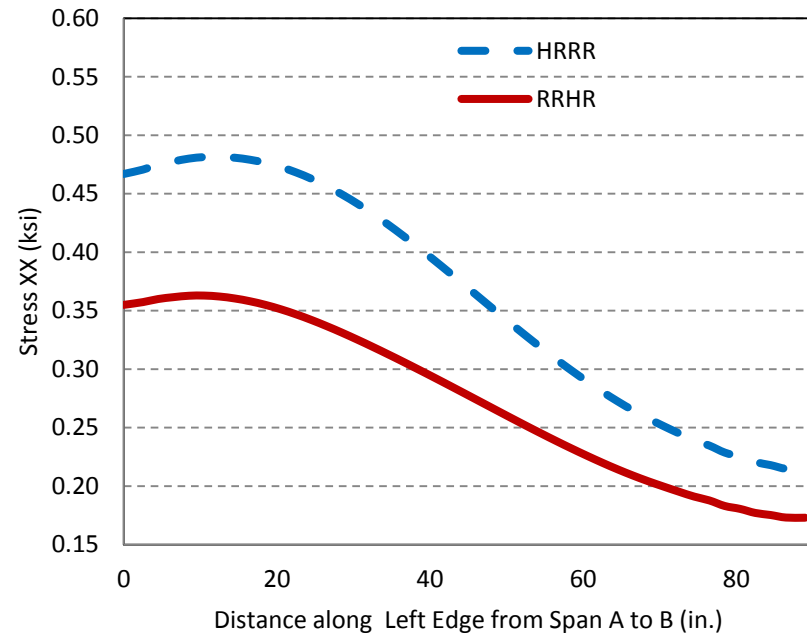
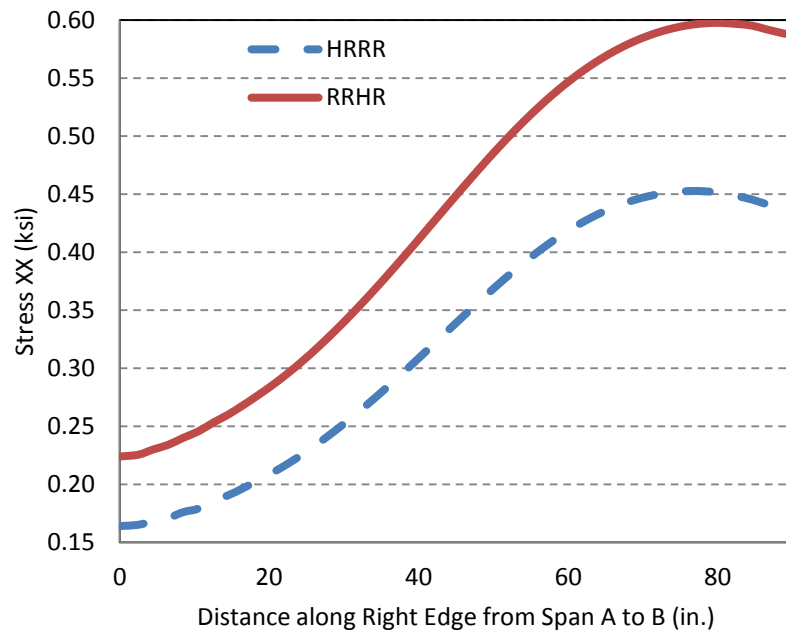


Figure 4-48. Edge stresses developed under PTG - 45° skew link slab with soft material over girder ends

4.4.4.5 Link Slab Stresses at the Transition Zone

Positive temperature gradient (PTG), with HRRR and RRHR support configurations, generate large tensile stresses at the link slab bottom fibers near the end of the link slab debonded region. Stress magnitude significantly increases directly over the girders (Figure 4-49). Longitudinal stress along the link slab bottom fiber at the end of the link slab debonded region is shown in Figure 4-50 and Figure 4-51. As seen in the figures, the stresses are greater than the tensile strength of concrete. Potential cracking can be dealt with by introducing construction joints at the boundary of debonded and fully bonded regions. Also, additional reinforcement may be required to resist the axial force.

Axial force developed within the tension region over the girders is calculated from the stresses. Elements with tensile stresses are identified and shown in Figure 4-52. The resultant tensile forces are the summation of incremental forces calculated by the stress multiplied by the associated area. The maximum tensile forces calculated for HRRR and RRHR support configurations are 33.3 kips/ft and 36.3 kips/ft. Adequacy of provided reinforcement to resist such forces should be checked. See the link slab design example provided in Appendix C for the methodology of checking the adequacy of link slab reinforcement to resist the axial load developed in the link slab.

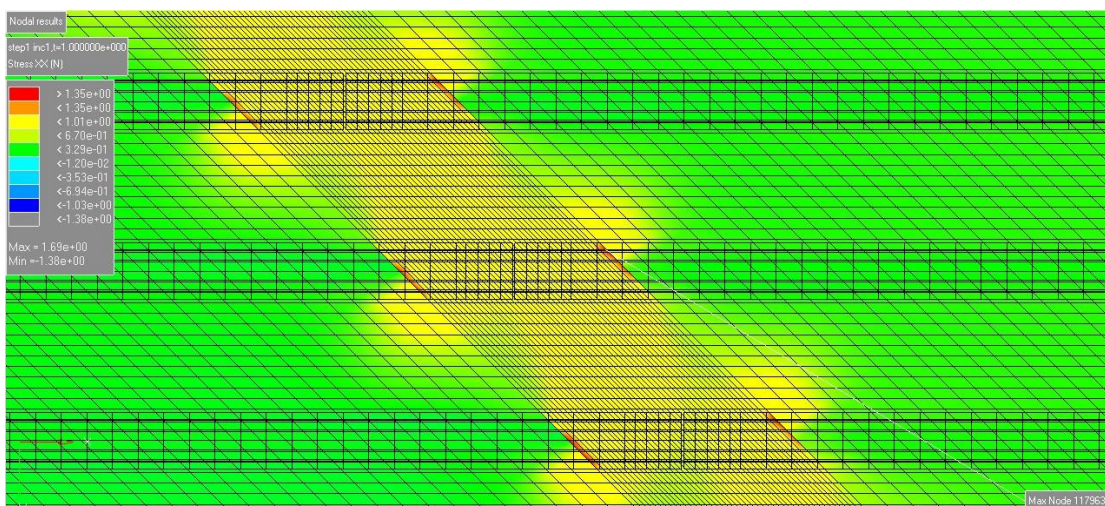


Figure 4-49. Link slab bottom fiber stresses under PTG load

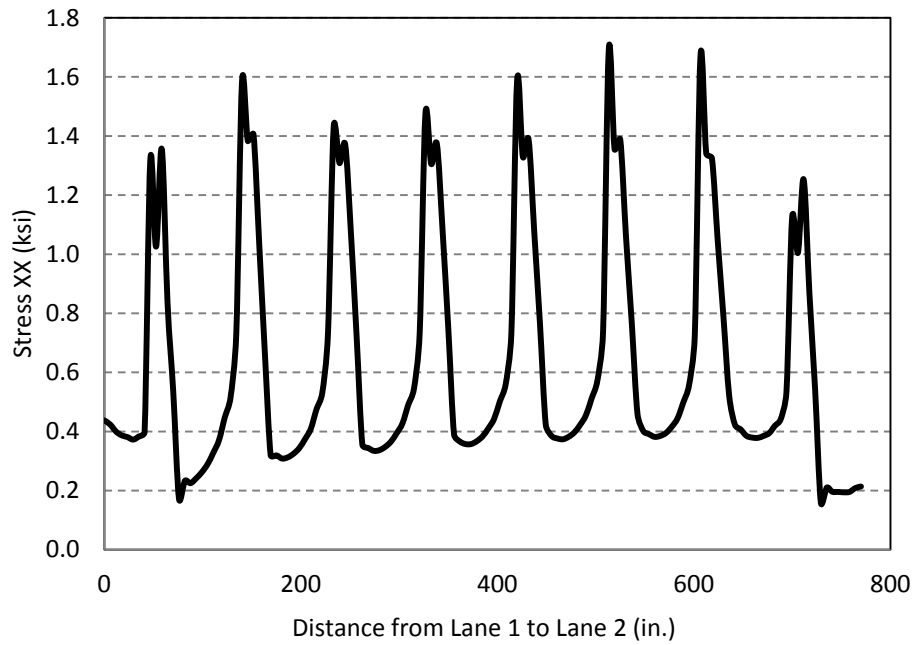


Figure 4-50. Longitudinal stress distribution across north end of the 45° skew link slab bottom fiber under PTG with HRRR support configuration

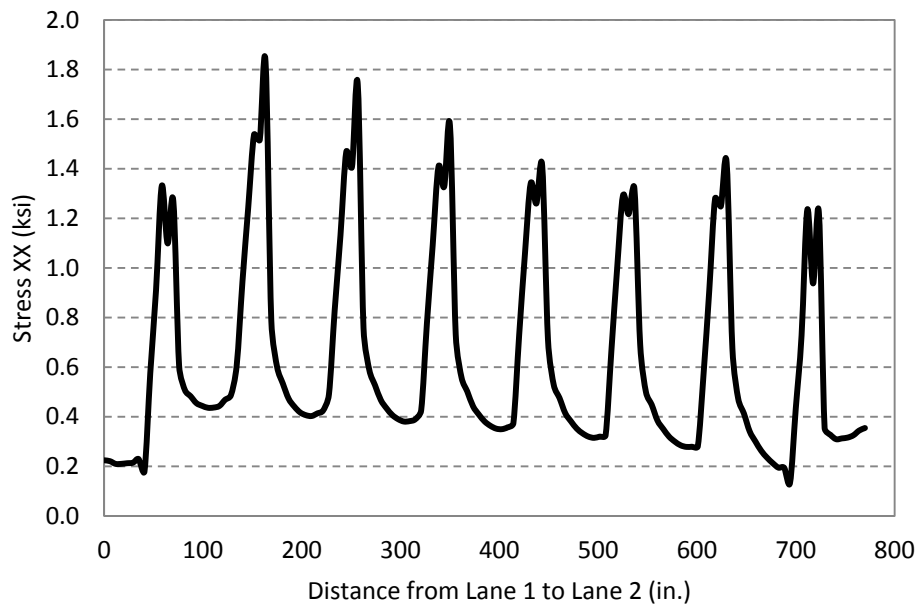


Figure 4-51. Longitudinal stress distribution across south end of the 45° skew link slab bottom fiber under PTG with RRHR support configuration

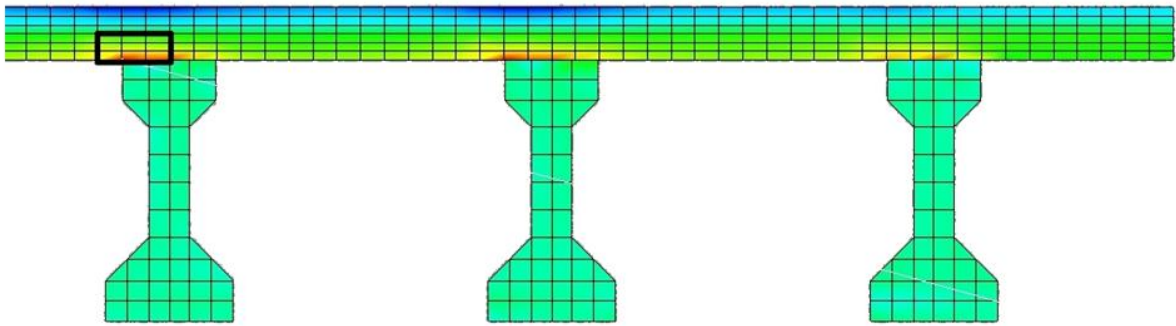


Figure 4-52. Stresses in link slab with HRRR under PTG

4.4.4.6 *Moment Reduction Factors based on Skew*

The moment demand on skew link slabs is calculated as follows. First, the maximum positive and negative moments per unit length of link slab are calculated by extracting maximum effective moments from respective figures (Figure 4-31 - Figure 4-36) and dividing them by the effective width of 66 in. (Figure 4-30). Second, the unit moment ratios with respect to the moment of link slab with zero skew (skew reduction factors) are calculated. The moment ratios for each load case are presented for all support conditions in Table 4-4, Table 4-5, and Table 4-6.

Similarly, this calculation process is duplicated for the axial force demands. Since, moments are calculated by multiplying forces by the moment arm, the axial force ratios will be the same of unit moment ratios. Thus, the ratio tables describing the skew effects will be valid for bending moments as well as axial forces.

The following conclusions are additional observations from the analysis results:

1. In general, moment demand on the link slab due to live load decreases as skew increases, irrespective of the support configuration (columns a, b, and c of Table 4-4, Table 4-5, and Table 4-6)
2. Moment demands under negative temperature gradient (NTG) and positive temperature gradient (PTG) on the link slab with RHHR (roller-hinge-hinge-roller) support configuration remains constant independent of skew (column e and f of Table 4-6).

3. The maximum effective negative and positive moment envelope patterns across the link slab under live (*Lane 2*) and NTG loads are similar (Figure 4-31 - Figure 4-36). Both load effects should be combined.
4. The link slab maximum effective positive and negative moment locations under PTG are different from NTG (Figure 4-31 - Figure 4-36). PTG should be considered independent from live loads and NTG.
5. *Lane 2* is the governing live load case for this specific bridge configuration, for all support configurations (column b of Table 4-4, Table 4-5, and Table 4-6).
6. The link slab moment with HRRR and RRHR support configuration is much less than the cracking moment capacity; additional reinforcement may be required to resist large tensile stresses developed along link slab bottom fibers within the end of the link slab debonded region (Figure 4-45 and Figure 4-48 - Figure 4-52).

Table 4-4. Skew Reduction Factors for HRRR

HRRR						
Load Case						
	Lane 1 (a)	Lane 2 (b)	Lane Alt 1 (c)	Lane Alt 2 (d)	NTG (e)	PTG (f)
Maximum Effective Positive Moment of Zero Skew Link Slab (kip – ft)/ft	2.1	3.0	1.9	2.0	0.4	0.9

Skew (Degree)	Ratio of Maximum Positive Link-Slab Effective Moment (Skew/Zero Skew) (Skew Reduction Factors)					
0	1.00	1.00	1.00	1.00	1.00	1.00
20	0.76	0.88	0.95	0.74	1.11	1.43
30	0.68	0.75	0.85	0.63	1.40	1.65
45	0.52	0.52	0.61	0.40	2.51	1.68

HRRR						
Load Case						
	Lane 1	Lane 2	Lane Alt 1	Lane Alt 2	NTG	PTG
Maximum Effective Negative Moment of Zero Skew Link Slab (kip - ft)/ft	-1.8	-2.2	-1.2	-1.4	-0.2	-1.6

Skew (Degree)	Ratio of Maximum Negative Link-Slab Effective Moment (Skew/Zero Skew) (Skew Reduction Factors)					
0	1.00	1.00	1.00	1.00	1.00	1.00
20	0.79	≈1.00	1.08	0.81	1.47	1.09
30	0.72	≈1.00	1.10	0.78	1.73	1.33
45	0.66	≈1.00	1.08	0.87	1.71	2.23

Table 4-5. Skew Reduction Factors for RRHR

	RRHR					
	Load Case					
	Lane 1 (a)	Lane 2 (b)	Lane Alt 1 (c)	Lane Alt 2 (d)	NTG (e)	PTG (f)
Maximum Effective Positive Moment of Zero Skew Link Slab (kip - ft)/ft	2.6	3.7	2.1	2.0	0.5	1.0

Skew (Degree)	Ratio of Maximum Positive Link-Slab Effective Moment (Skew/Zero Skew) (Skew Reduction Factors)					
0	1.00	1.00	1.00	1.00	1.00	1.00
20	0.92	0.92	0.99	0.93	1.05	1.32
30	0.84	0.83	0.92	0.83	1.25	1.49
45	0.68	0.63	0.83	0.64	2.29	1.54

	RRHR					
	Load Case					
	Lane 1	Lane 2	Lane Alt 1	Lane Alt 2	NTG	PTG
Maximum Effective Negative Moment of Zero Skew Link Slab (kip - ft)/ft	-1.9	-2.7	-1.4	-1.4	-0.3	-1.9

Skew (Degree)	Ratio of Maximum Negative Link-Slab Effective Moment (Skew/Zero Skew) (Skew Reduction Factors)					
0	1.00	1.00	1.00	1.00	1.00	1.00
20	0.90	1.00	1.15	1.08	1.36	1.04
30	0.80	0.98	1.21	1.10	1.56	1.18
45	0.69	0.90	1.28	1.10	1.59	2.01

Table 4-6. Skew Reduction Factors for RHHR

	RHHR					
	Load Case					
	Lane 1 (a)	Lane 2 (b)	Lane Alt 1 (c)	Lane Alt 2 (d)	NTG (e)	PTG (f)
Maximum Effective Zero Skew Link Slab Moment (kip - ft)/ft	-4.4	-7.5	-3.7	-3.7	-2.0	4.2
Skew (Degree)	Ratio of Maximum Link-Slab Effective Moment (Skew/Zero Skew) (Skew Reduction Factors)					
0	1.00	1.00	1.00	1.00	1.00	1.00
20	0.96	0.96	0.97	0.95	≈ 1.00	≈ 1.00
30	0.91	0.90	0.91	0.89	≈ 1.00	≈ 1.00
45	0.77	0.74	0.76	0.72	≈ 1.00	≈ 1.00

4.4.4.7 Skew Reduction Factors based on Girder-End Rotations

Girder-end rotations are calculated from nodal displacements at the North end of each girder in Span A. These results are shown in Table 4-7 through Table 4-12, columns a-c. The ratios of the maximum girder-end rotation to the maximum girder-end rotation from the model with no skew, much like what was done for the effective bending moment, are calculated and presented in Table 4-7 through Table 4-12, columns d-f.

For the live load cases, rotations decrease for the HRRR and RRHR boundary conditions and for angles of skew greater than 30°. The RHHR boundary condition has no appreciable difference in the girder-end rotations under live loads even with an angle of skew of 45°. Lane2 load case is the controlling load configuration for a two lane bridge as demonstrated by the girder-end rotations under live loads shown in Table 4-7 through Table 4-12. The HRRR and RRHR boundary conditions show a decrease in girder-end rotations of 24% and 25%, respectively for the 45° skew bridge with the Lane2 load case. When the Lane2 load case and RHHR boundary conditions are considered, there is only 3% reduction in the girder rotations in the 45° skew bridge compared to that of the straight bridge.

In the design process girder-end rotations are calculated from simple beam analysis considering the girder-end displacement in the global X-direction; hence they fail to represent resultant girder-end rotation calculated from a 3D model. For this reason, the use of skew reduction factors calculated using the moment ratio is recommended (Table 4-4, Table 4-5, and Table 4-6).

Table 4-7. Girder-End Rotations and Skew Reduction Factors - Lane1 Load Case

Angle of Skew	Girder-End Rotation (radians)			Skew Reduction Factors		
	HRRR (a)	RRHR (b)	RHHR (c)	HRRR (d)	RRHR (e)	RHHR (f)
0	0.000562	0.00601	0.000196	1.0000	1.0000	1.0000
20	0.000562	0.000593	0.000200	0.9995	0.9870	1.0173
30	0.000548	0.000574	0.000201	0.9744	0.9549	1.0221
45	0.000481	0.000494	0.000194	0.8554	0.8230	0.9884

Table 4-8. Girder-End Rotations and Skew Reduction Factors - Lane2 Load Case

Angle of Skew	Girder-End Rotation (radians)			Skew Reduction Factors		
	HRRR (a)	RRHR (b)	RHHR (c)	HRRR (d)	RRHR (e)	RHHR (f)
0	0.000926	0.000984	0.000263	1.000	1.000	1.000
20	0.000873	0.000926	0.000259	0.943	0.942	0.985
30	0.000834	0.000881	0.000261	0.900	0.896	0.993
45	0.000699	0.000732	0.000254	0.755	0.745	0.967

Table 4-9. Girder-End Rotations and Skew Reduction Factors – LaneAlt1 Load Case

Angle of Skew	Girder-End Rotation (radians)			Skew Reduction Factors		
	HRRR (a)	RRHR (b)	RHHR (c)	HRRR (d)	RRHR (e)	RHHR (f)
0	0.000562	0.00601	0.000196	1.000	1.000	1.000
20	0.000562	0.000593	0.000200	0.9995	0.9870	1.0173
30	0.000548	0.000574	0.000201	0.9744	0.9549	1.0221
45	0.000481	0.000494	0.000194	0.8554	0.8230	0.9884

Table 4-10. Girder-End Rotations and Skew Reduction Factors – LaneAlt2 Load Case

Angle of Skew	Girder-End Rotation (radians)			Skew Reduction Factors		
	HRRR (a)	RRHR (b)	RHHR (c)	HRRR (d)	RRHR (e)	RHHR (f)
0	0.000492	0.000148	0.000526	1.000	1.000	1.000
20	0.000468	0.000148	0.000497	0.9501	0.9955	0.9442
30	0.000454	0.000151	0.000472	0.9219	1.0149	0.8971
45	0.000397	0.000150	0.000407	0.8068	1.0084	0.7735

Table 4-11. Girder-End Rotations and Skew Reduction Factors - NTG Load Case

Angle of Skew	Girder-End Rotation (radians)			Skew Reduction Factors		
	HRRR (a)	RRHR (b)	RHHR (c)	HRRR (d)	RRHR (e)	RHHR (f)
0	0.000264	0.000273	0.000064	1.000	1.000	1.000
20	0.000257	0.000261	0.000079	0.975	0.958	1.225
30	0.000255	0.000249	0.000086	0.966	0.912	1.341
45	0.000234	0.000223	0.000095	0.886	0.818	1.483

Table 4-12. Girder-End Rotations and Skew Reduction Factors - PTG Load Case

Angle of Skew	Girder-End Rotation (radians)			Skew Reduction Factors		
	HRRR (a)	RRHR (b)	RHHR (c)	HRRR (d)	RRHR (e)	RHHR (f)
0	-0.000989	-0.001019	-0.000220	1.000	1.000	1.000
20	-0.000982	-0.000994	-0.000271	0.993	0.975	1.230
30	-0.000978	-0.000963	-0.000298	0.989	0.946	1.351
45	-0.000930	-0.000901	-0.000335	0.940	0.885	1.523

4.4.5 Skew Link Slab Design Procedure

4.4.5.1 Overview

The skew link slab design is based on the bending moment and axial force calculated from analysis that incorporates the effects of skew under specific load combinations. The simplified analysis procedure for bridges with no skew was presented in Ulku et al. (2009). The analysis procedure assumes that the link slab does not provide any continuity between spans. Therefore, the spans are analyzed as simply supported. The girder-end rotations are calculated from the design load combinations. Imposing compatibility, the link slab is subjected to a rotation equal to the girder-end rotation. The link slab moment is calculated from Eq. 4-10 by substituting the beam end rotation.

$$M = \frac{2E_c I_{LS} \theta}{L_{LS}} \quad (4-10)$$

where

M = Link slab bending moment (k-in)

E_c = Elastic modulus of concrete (ksi)

I_{LS} = Moment of inertia of the link slab (in⁴)

L_{LS} = Length of link slab (in)

θ = Girder-end rotation (radians)

The simplified link-slab design procedure by Caner and Zia (1998) was updated by Ulku et al. (2009) to incorporate the effects of bearing configurations and thermal gradient loads, also for bridges with zero skew. The procedure developed here is the modification of the procedure by Ulku et al. (2009) to incorporate the effects of link-slab skew.

The load demand calculation based on the modified procedure and link slab design is described below on a numerical example with the geometry of the specific bridge used in the FE analysis. Geometric and material property data used in this section as well as in the design example presented in Appendix C are given in Figure 4-53 and Table 4-13.

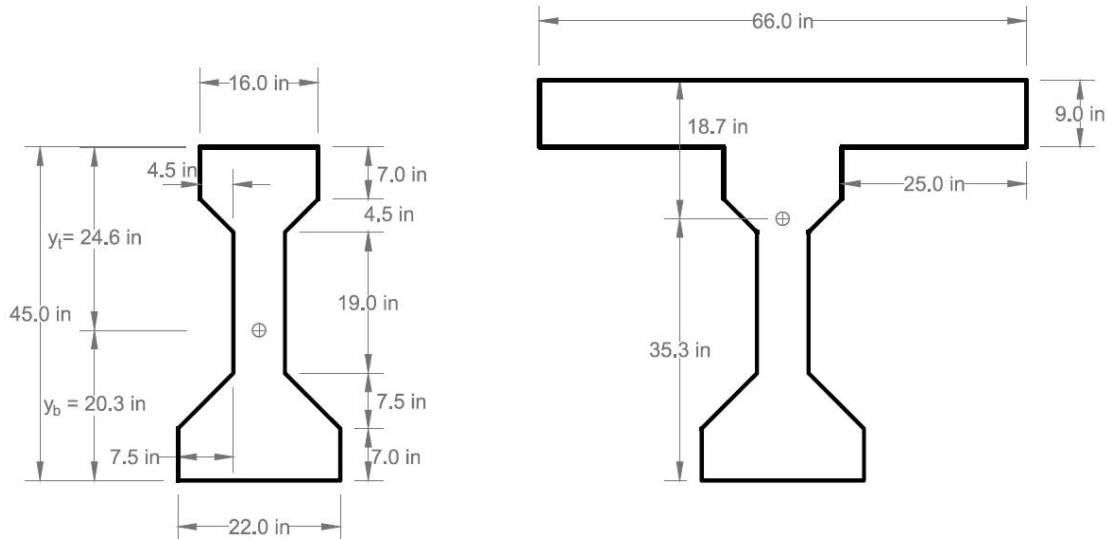


Figure 4-53. AASHTO Type III girder and composite section geometric properties

Table 4-13. Material and Geometric Properties used in Link Slab Design Example

Boundary condition	RHHR
Skew (θ)	45 deg.
Compressive strength of concrete (f_c')	4,500 psi
Unit weight of concrete (w_c)	0.15 kcf
Concrete modulus of elasticity (E_c) (AASHTO LRFD Section 5.4.2.4)	4,067 psi
Reinforcement yield strength (f_y)	60 ksi
Steel modulus of elasticity (E_s)	29,000 ksi
Link slab length (L_{LS})	84.4 in.
Effective deck width (B) ⁺	66 in.
Link slab thickness	9 in.
Moment of inertia of link slab (I_{LS})	4,009.5 in ⁴
Deck overhang (on either side of the beam)	25 in.
Moment of inertia of the girder (I_{girder})	125,390 in ⁴
Moment of inertia of the composite section ($I_{composite}$)	375,678 in ⁴

+ Link slab section perpendicular to bridge longitudinal axis is considered in the example because design moments are calculated perpendicular to bridge longitudinal axis (Figure 4-31 - Figure 4-42).

4.4.5.2 Live Load and Thermal Gradient Moments

In the analysis procedure for the skew link slab, girder-end rotation of 3.47×10^{-3} radians is calculated under HL-93 load on a 69.5 ft span of a zero-skew bridge as per AASHTO LRFD (2010). An impact factor of 1.33 is included with the truck load. The live load distribution factor for the zero-skew bridge is calculated as 0.508. The girder end rotation used in Eq. 4-10 (i.e., analytical design rotation) is calculated by multiplying 3.47×10^{-3} radians with 0.508 (Table 4-14).

Girder-end rotations for thermal gradient loads are calculated following the procedure presented by Ulku et al. (2009). (Design example in Appendix C is included for more details; a MathCAD calculation sheet is also included in Appendix D.) The analytical rotations and analytical design moments for all three loads are shown in Table 4-14. Thermal gradient load effects are not subjected to distribution factors; hence, the analytical-girder end rotations are directly used as design rotations. Lastly, analytical design moments under thermal gradient loads are calculated from Eq. 4-10 as shown in Table 4-14.

Table 4-14. Analytical Rotation and Analytical Design Moment Magnitudes

Load Case	Analytical Rotation (Radians)	Distribution Factor	Analytical Design Rotation	Analytical Design Moment (k-ft)/ft
Live	0.003470	0.508	0.001763	10.32
NTG	0.000484	N/A	0.000484	2.83
PTG	0.001613	N/A	0.001613	9.44

Note: NTG – negative temperature gradient; PTG – positive temperature gradient

4.4.5.3 Moment Reduction due to 3D Effect

The design moments calculated by this analytical procedure are significantly greater than the moments calculated from FE analysis. Design moments from FE analysis and the simplified analytical procedure are compared in Table 4-15 as the moment ratios obtained by the two procedures.

Table 4-15. Ratios of 3D FE to Analytical Design Moment for a Straight Bridge

Load Case	HRRR	RRHR	RHHR
Live	0.218	0.257	0.887
NTG	0.092	0.111	0.967
PTG	0.080	0.100	0.961

As observed in Table 4-15 , the maximum link slab live load moments calculated by FE analysis with RHHR support configuration is about 90% of the design moments calculated by the simplified analytical procedure. The maximum link slab live load moments calculated by FE analysis with HRRR and RRHR supports are approximately 22% and 26% of the design moments calculated by the simplified analytical procedure.

4.4.5.4 Span Effect on Link Slab Moment

Another parametric study was conducted to evaluate the span effect on link slab design moments. Spans ranging from 70 ft to 120 ft were identified by analyzing the Michigan bridge inventory. According to the data provided in Table 4-16, only moment due to live load increases with increasing span. The link slab moment due to temperature gradient load remain constant (Table 4-16 column y and z) because the curvature remains constant. According to Eq. C-9 and C-10, the length cancels and design moment due to temperature gradient is not a function of span.

Table 4-16. Analytical Rotation and Analytical Design Moment Magnitudes for Different Spans

Span (ft)	Analytical Rotation (rad)			DF*	Analytical Design Rotation (rad)			Analytical Design Moment (k-ft/ft)		
	LL	NTG	PTG		LL	LL	NTG	PTG	LL	NTG
	(a)	(b)	(c)	(d)	(a)*(d)= (e)	(b) = (f)	(c) = (g)	(x)	(y)	(z)
70	0.00347	0.00048	0.00161	0.51	0.00176	0.00048	0.00161	10.32	2.83	9.44
80	0.00475	0.00055	0.00185	0.49	0.00233	0.00055	0.00185	11.95	2.84	9.46
90	0.00627	0.00062	0.00208	0.48	0.00299	0.00062	0.00208	13.63	2.84	9.47
100	0.00803	0.00069	0.00231	0.46	0.00373	0.00069	0.00231	15.29	2.84	9.48
110	0.01005	0.00076	0.00254	0.45	0.00455	0.00076	0.00254	16.99	2.85	9.48
120	0.01236	0.00083	0.00277	0.44	0.00548	0.00083	0.00277	18.74	2.85	9.49

*No distribution factor (DF) used for NTG and PTG

The span effect on the ratio of 3D FE moment to analytical design moment for straight bridge was calculated and shown in Table 4-17. According Table 4-17, the ratios for both PTG and NTG remain approximately constant with span. Thus, the link slab moment due to temperature gradient is independent of span.

As observed from Table 4-17, live load (LL) moment ratio decreases with increasing span. However, from the simple calculation procedure, the LL moment increases with increasing

span (Table 4-16). This discrepancy is because the simple procedure uses girder end rotation to calculate the link slab moment. In doing so, the loads acting on the link slab are not considered. In 3D FE analysis, lane load is placed on both spans as per the AASHTO LRFD (2010) specifications is continuous over the link-slab. With increasing span the link slab length also increases; hence, the load on the link slab cantilevering from the beam reduces the link slab rotation. The link slab design moment with increasing span should be based on rotations calculated from the simple beam analysis. Increasing span results in increasing link-slab length. Consequently, increasing rotation will not increase the link slab-moment and providing minimum reinforcement will be adequate for bridges with span up to 110 ft.

Table 4-17. Ratio of 3D FE to Analytical Bending Moment for Straight Bridge with Different Spans

Span (ft)	LL			PTG			NTG		
	HRRR	RRHR	RHHR	HRRR	RRHR	RHHR	HRRR	RRHR	RHHR
70	0.218	0.257	0.887	0.092	0.111	0.967	0.080	0.100	0.961
80	0.171	0.215	0.798	0.082	0.106	1.015	0.066	0.093	1.006
90	0.141	0.178	0.791	0.093	0.117	1.032	0.075	0.103	1.022
100	0.113	0.144	0.768	0.099	0.123	1.042	0.080	0.107	1.031
110	0.093	0.120	0.768	0.101	0.125	1.048	0.081	0.109	1.037

4.4.5.5 Skew Effect on Link Slab Moment

Also of interest is skew effects on link slab moments. Skew reduction factors were calculated using moment ratios and were presented in Table 4-4, Table 4-5, and Table 4-6. Skew reduction factors presented in Table 4-4, Table 4-5, and Table 4-6 vary significantly with the live loads configurations, support configurations under the link slab, and whether the moment is negative or positive. For the specific bridge configuration used in the FE analysis, *Lane 2* is the governing live load configuration. Skew reduction factors show that load demand decreases with increasing skew.

A detailed link slab design example is included in Appendix C. The bridge in this example is with RHHR support configuration, which develops the largest link slab moments and axial forces under applied loads. Yet, the amount of required link slab reinforcement is governed by the minimum reinforcement amount requirements of AASHTO LRFD (2010).

4.4.5.6 Summary of Link Slab Analysis Results

The following are further key summary observations on analysis results:

1. The RHHR boundary condition develops significantly larger link-slab moments compared to other support conditions.
2. NTG can be excluded from design load combination with HRRR and RRHR support conditions.
3. NTG load case moments that develop in the link slab of bridges with zero skew and RHHR support configuration, should be directly used in design without any reduction for skew.
4. The negative moment design of a link slab with the RHHR support configuration is governed by the combined effect of live and NTG loads.
5. Positive moment design of a link slab with the RHHR support configuration is governed by a PTG load.
6. Moment developed in a link slab under thermal gradient loads (PTG and NTG) remains constant irrespective of span.
7. Providing the minimum reinforcement amount required in AASHTO LRFD Section 5.7.3.3.2 is adequate for the majority of skew link slabs with HRRR or RRHR support configuration for spans up to 110 feet. However, additional reinforcement at the bottom layer is needed to resist large tensile stresses developed near the boundaries of the debonded region. A top layer of #6 bars at 4 in. spacing and bottom layer of #6 bars at 4 in. spacing are adequate for high skew link slabs. Proposed detail in standard MDOT Bridge Design Guide format is presented in Appendix E.
8. Simplified analysis models are not able to represent three dimensional effects such as positive moments under live load or negative moments under PTG. New analysis models and procedures are required.

5 SKEW ABUTMENT ANALYSIS AND DESIGN GUIDELINES

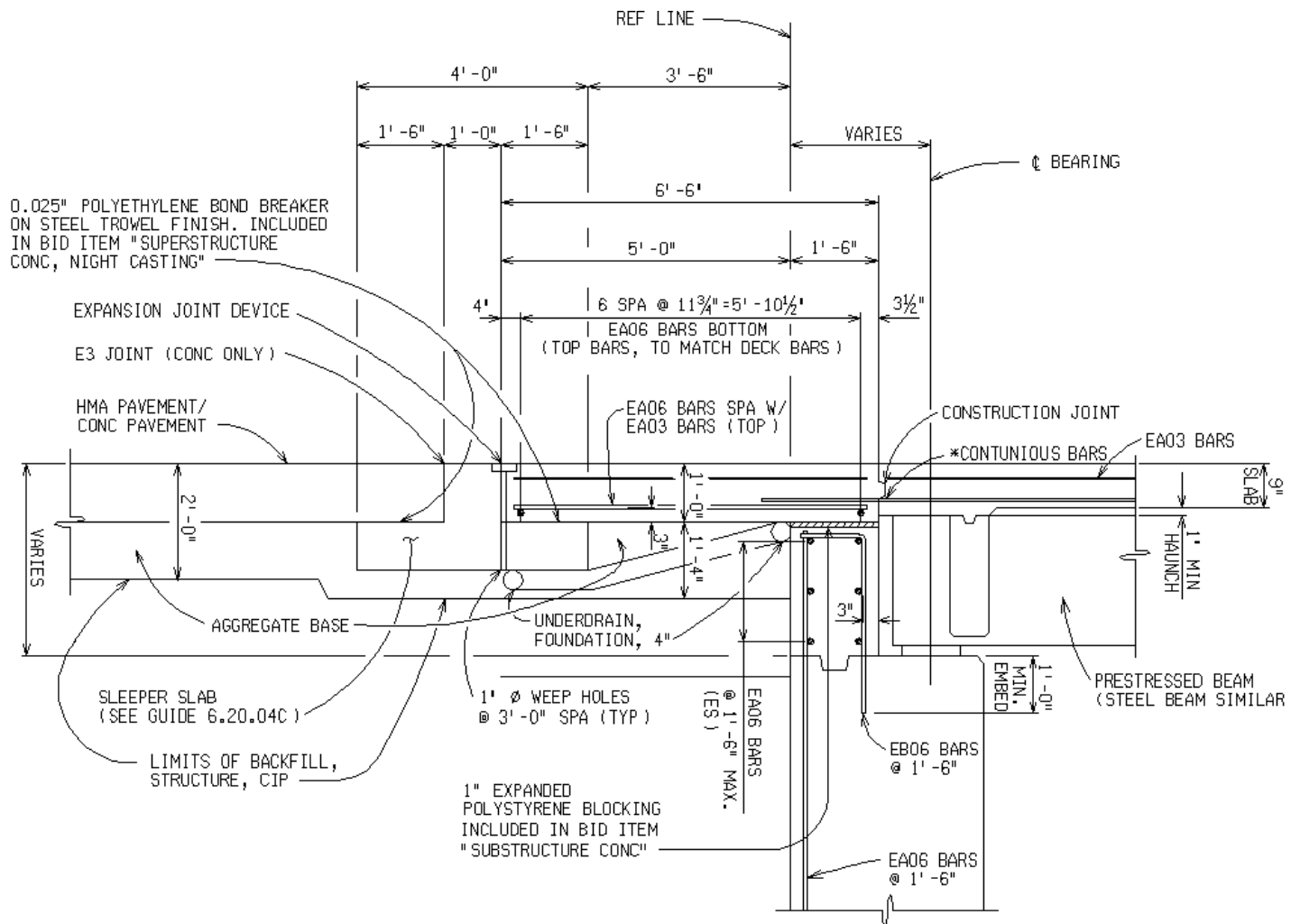
5.1 OVERVIEW AND OBJECTIVES

This chapter presents the detailed analysis of (1) two skew abutment configurations namely deck sliding over backwall and semi-integral systems, (2) deformation and rotation demands at bearings with respect to the skew angle, and (3) forces at girder ends and other components with respect to skew angle. The analysis was performed for a specific bridge (i.e., span length, width, and girder type) modeled for two different abutment configurations, and with various angles of skew from 0° to 45° . The finite element (FE) models, for selected skew configurations, were analyzed under loads and configurations as specified in AASHTO (2010) and the Michigan Bridge Design Manual (MDOT 2005). Design recommendations and design details were developed based on literature review, analysis results, and AASHTO (2010), AASHTO (2008), and MDOT (2005) requirements on strength and service load combinations.

5.2 ABUTMENT CONFIGURATIONS AND ANALYSIS MODELS

Deck sliding over backwall and semi-integral abutment details presented in Aktan et al. (2008) were considered in this analysis. Figure 5-1 shows the details of the deck sliding over backwall abutment configuration. Wingwalls were not included in the model.

The semi-integral abutment detail with backwall placed directly over the abutment is shown in Figure 5-2. This configuration was analyzed with and without wingwalls. Additional configuration considered in the analysis was the backwall offset from the abutment wall as depicted in Figure 5-3. Strictly speaking, the analysis models of the configurations shown in Figure 5-2 and Figure 5-3 are practically the same when adequate space is provided between the abutment and backwall, and the vertical load transfer from backwall to abutment is prevented.



* CONTINUE BOTTOM BARS 24" PAST CONSTRUCTION JOINT INTO THE APPROACH SLAB

Figure 5-1. Deck sliding over backwall details

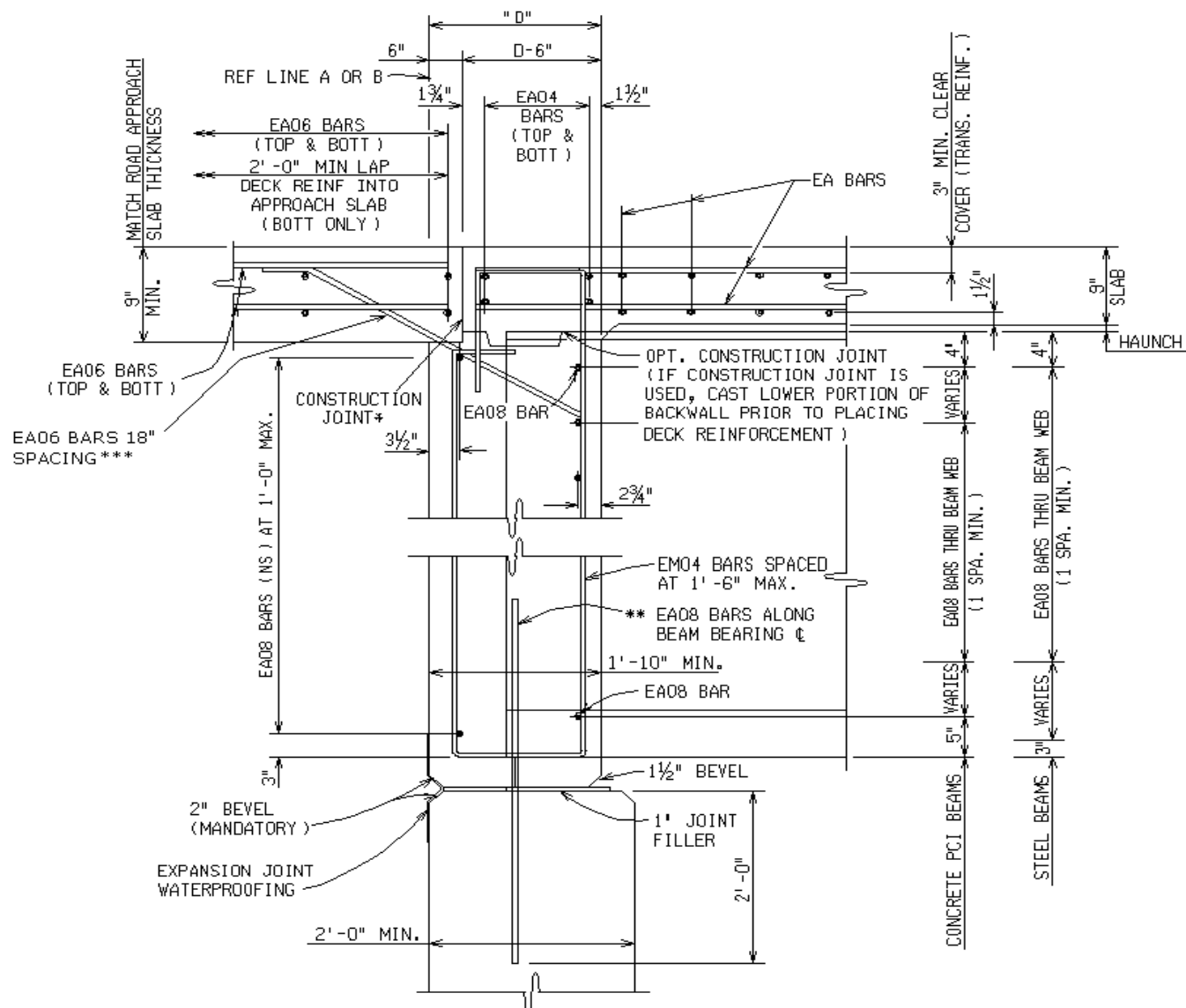


Figure 5-2. Semi-integral abutment details

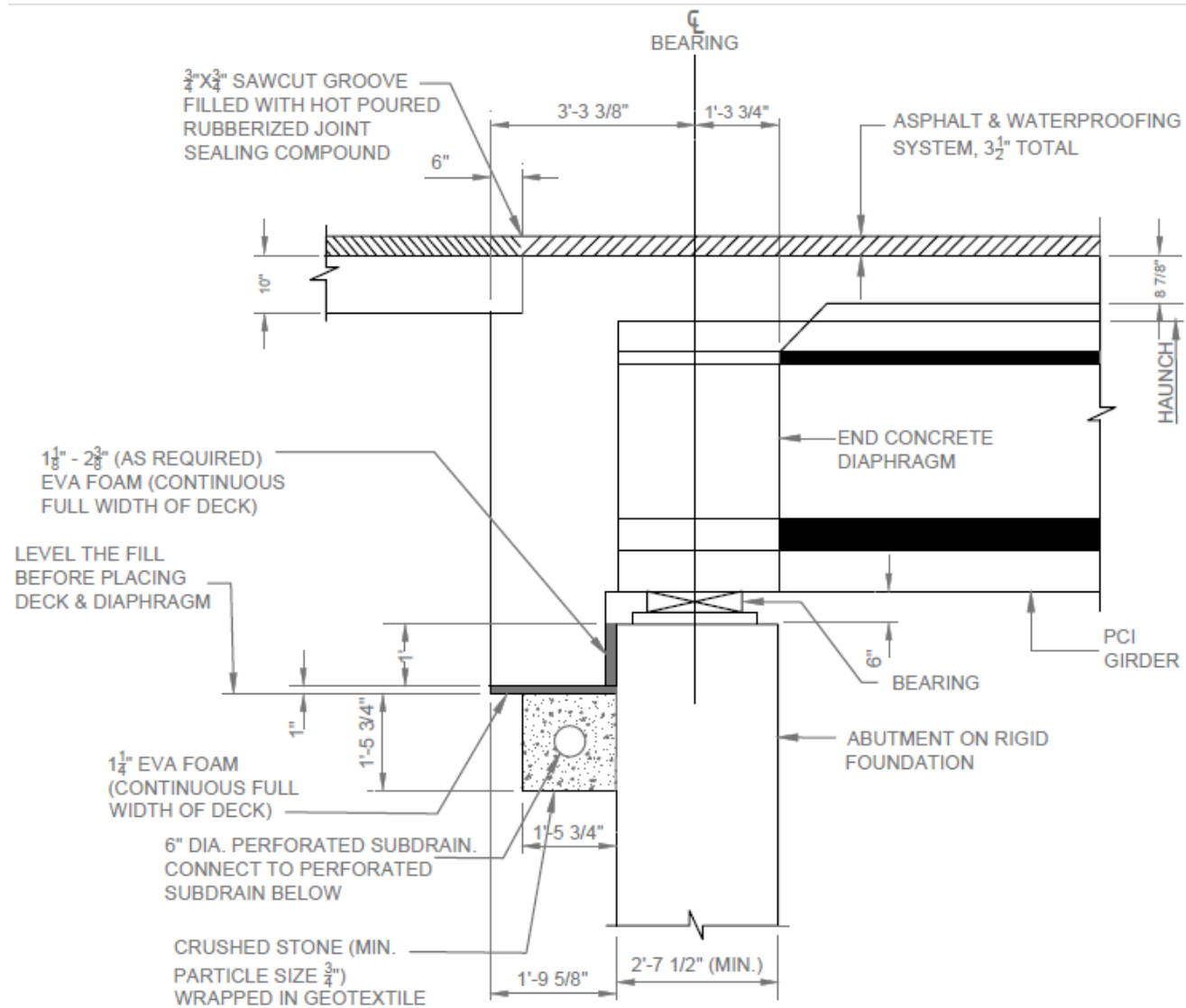


Figure 5-3. Semi-integral abutment detail used in Ontario and several other states

5.3 LATERAL RESTRAINT SYSTEMS IN SKEW BRIDGES

Various restraint systems are utilized for controlling transverse movement of skew bridge superstructures. A few examples are:

1. Sliding surfaces between the backwall and wingwall (rub plates) (Figure 5-4)
2. Sliding surfaces between the deck and wingwall (rub plates) (Figure 5-5)
3. Single angle bearing retainers against the steel plate of the bearing (Figure 5-6a)
4. Two-single angle bearing retainers against the steel plate of the bearing (Figure 5-6b)
5. Dowels in a slotted hole (Figure 5-7)
6. Concrete key system with rub plates (Figure 5-8)

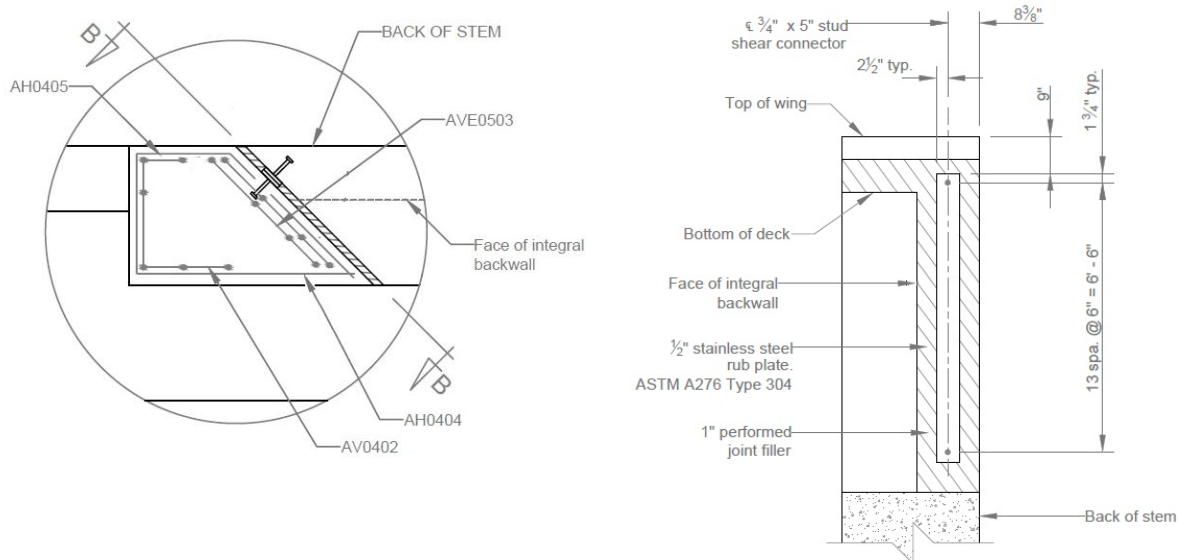


Figure 5-4. Rub plates at backwall - wingwall interface (Source: VDOT 2010)

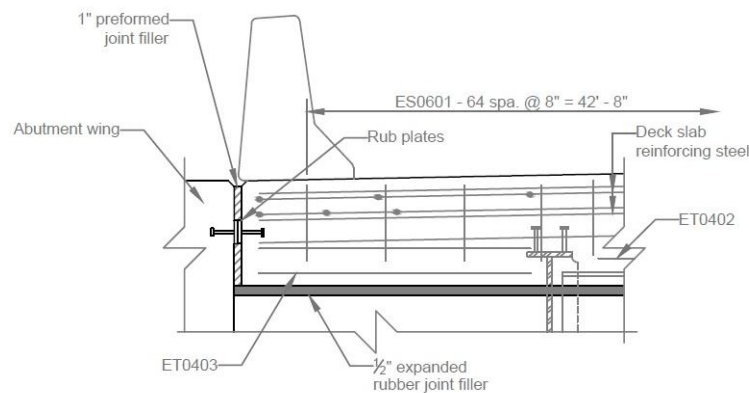


Figure 5-5. Rub plates at deck-wingwall interface (Source: VDOT 2010)

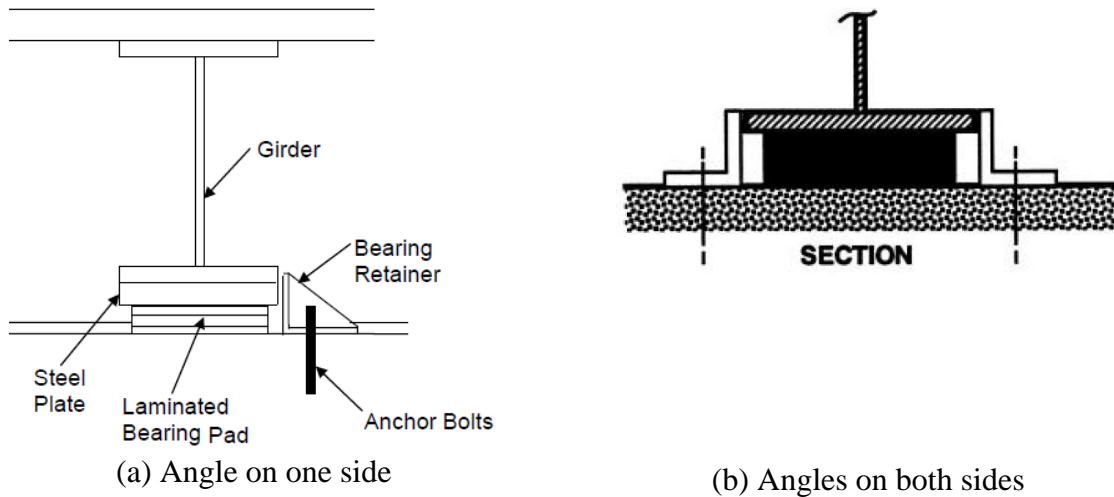


Figure 5-6. Bearing retainer detail (Source: Steinberg and Sargand 2010; Roeder and Stanton 1996)

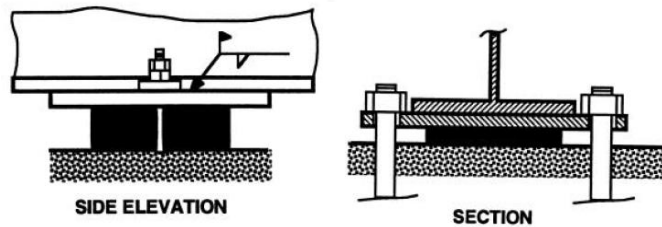


Figure 5-7. Dowel bar details for resisting lateral loads on shallow bearing (Source: Roeder and Stanton 1996).

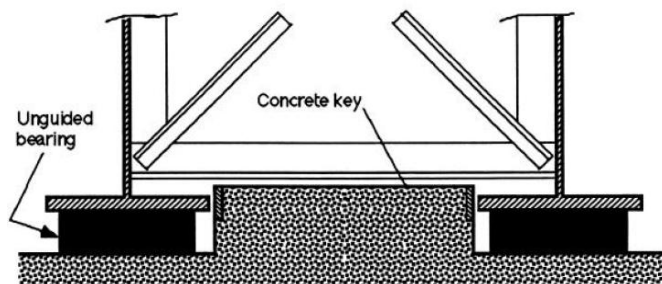


Figure 5-8. Concrete key system for resisting lateral forces (Source: Roeder and Stanton 1996).

Most viable configurations among these are those shown in Figure 5-4, Figure 5-5, and Figure 5-8. Still, utilizing these restraint systems in deck sliding over backwall and semi-integral systems with link slabs presents specific challenges.

5.3.1 Restraint Systems at the Abutment

5.3.1.1 Deck Sliding over Backwall System

Placing rub plates between the wingwall and deck at the acute corner of the deck poses several challenges. Rub plates should be placed on the span side of the deck with respect to the construction joint, if transverse movement is to be a restraint at the deck level. Also, the corner of the deck should be adequately detailed to accommodate the forces generated due to restraint. For deck sliding over backwall system, the most promising later load restraint system is the use of concrete key system shown in Figure 5-8.

5.3.1.2 Semi-Integral Backwall System

Semi-integral abutment details given in Figure 5-2 provide several advantages if adequate measures are taken to prevent backfill ingress through the abutment-backwall interface and load transfer between the backwall and abutment. A lateral movement restraint system can be developed by using the details shown in Figure 5-4. Forces on wingwalls can be minimized by providing transverse movement restraints at girders and/or providing EPS as a backfill material. Similar details can be developed to restrain transverse movement of the configuration given in Figure 5-3 by providing restraint against the diaphragm rather than the backwall.

5.3.2 Restraint System over the Pier

Deck level restraints cannot be implemented over the pier with the link slab. In addition, the restraint system that extends from the pier cap to the deck level has to accommodate a large moment. Considering these, an option to restrain transverse movement of the bridge superstructure is to provide concrete keys with a configuration similar to that shown in Figure 5-8 .

5.4 ANALYSIS OF HIGH SKEW BRIDGE WITH DECK SLIDING OVER BACKWALL AND SEMI-INTEGRAL ABUTMENTS

The objective of the analysis is to investigate the behavior of high skew bridge spans with specific abutment details presented in Figure 5-1, Figure 5-2, and Figure 5-3. The analysis results will establish the design load calculation procedures.

5.4.1 Material Properties

The girder and deck concrete properties are assumed to be the same. The bridge deck concrete strength specified in MDOT design (f'_c) is 4500 psi (MDOT 2009). The modulus of concrete is calculated using Eq. 4-1 as per AASHTO Section 5.4.2.4 (AASHTO 2010). Unit weight of concrete (w_c) is assumed to be 0.15 k/ft³. The Poisson's ratio of 0.2 is used per AASHTO Section 5.4.2.5. The thermal expansion coefficient of 6.00×10^{-6} /°F is used (AASHTO 2010 section 5.4.2.2).

An expanded polystyrene (EPS) layer is placed in between the sliding deck and backwall. The use of EPS behind the backwall in semi-integral abutments will reduce passive pressure acting on the backwall during bridge expansion. The modulus of elasticity and Poisson's ratio of EPS are 0.2 ksi and 0.09, respectively. The peak and residual friction coefficients between EPS and concrete are 2.3 and 1, respectively. The peak friction coefficient value is used in the deck sliding over backwall abutment configuration for generating the extreme bearing forces under expansion and contraction loads.

5.4.2 Loads

5.4.2.1 Live Load

HL-93 loading with an impact factor of 1.33 is used in conjunction with wheel load as per AASHTO (2010) Section 3.6.1.2.3 and 3.6.2. Section 3.6.1.2.5 of AASHTO (2010) requires distributing wheel load over an area of 10×20 in.

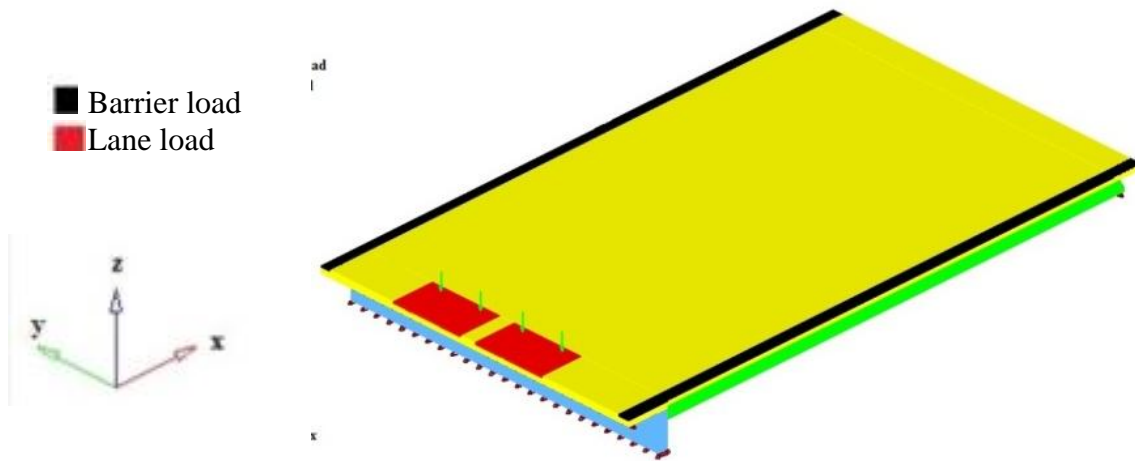
The MDOT Bridge Design Manual (2005) Section 7.03.01 specifies that abutment is designed for multiple load configurations. For the abutment models discussed in this report, the following load cases are considered:

CASE II: Bridge open to traffic with truck loading on the approach only.

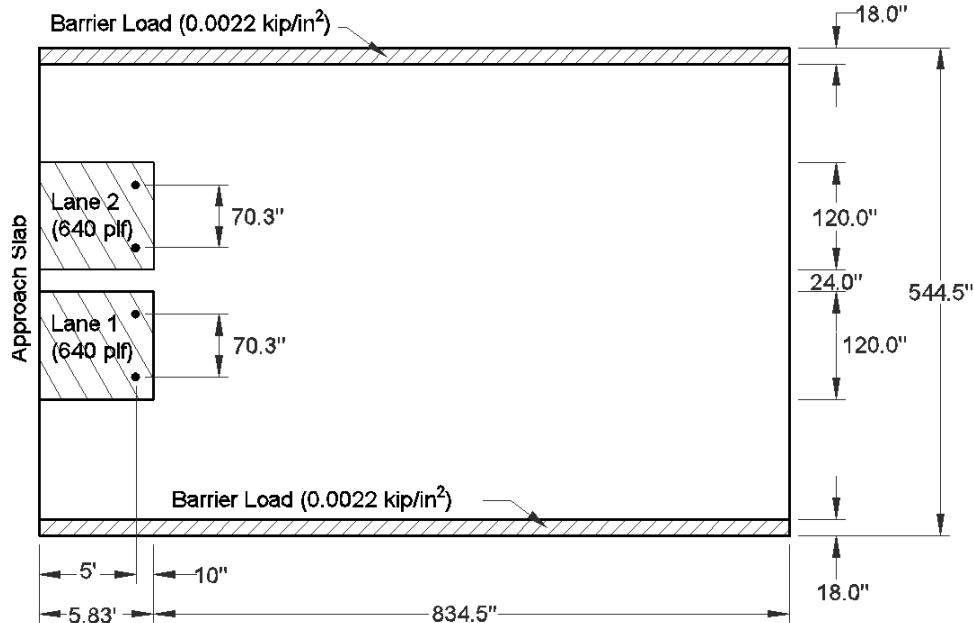
CASE III: Bridge with traffic on it and no load on approach.

CASE IV: Contraction – Case II loading plus the effects of uniform negative thermal in the deck transmitted to the abutment. Expansion – for integral abutments Case IV instead assumes the Case III loading plus the effect of uniform positive thermal transmitted from the deck.

Figure 5-9 shows the live load application for the *CASE IV Contraction* configuration; rear axles of the truck are placed on approach directly over the backwall and lane load is applied only on the approach. Figure 5-10 shows the live load application for the *CASE IV Expansion* configuration; two trucks are placed on the span such that the rear axle is over the bearings and the lane load is applied over the entire span. Wheel loads applied on the model include the dynamic impact factor of 33%.



(a) Isometric view



(b) Plan view

Figure 5-9. Live load configuration for *CASE IV Contraction*

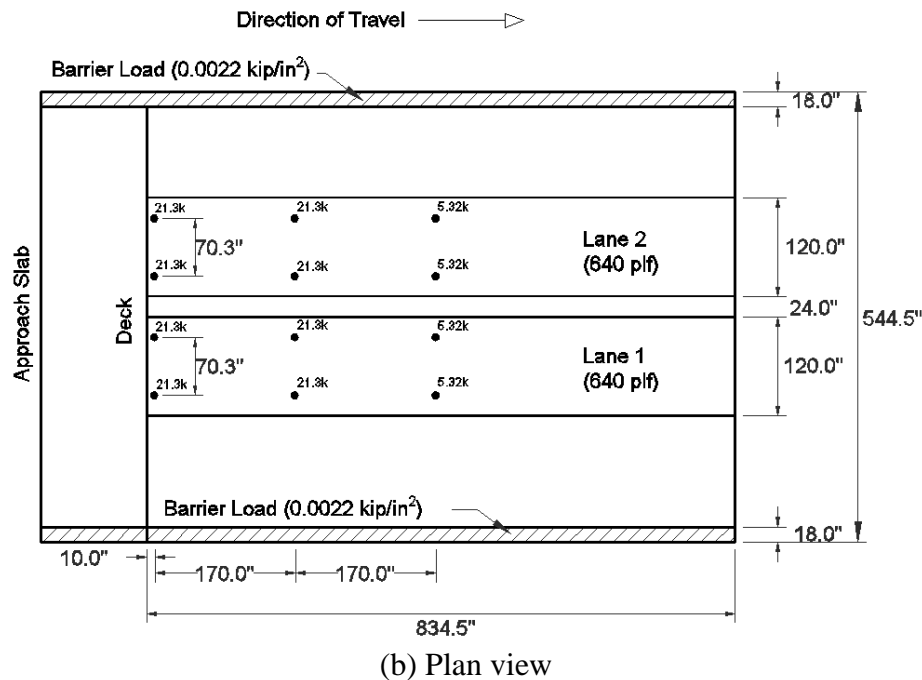
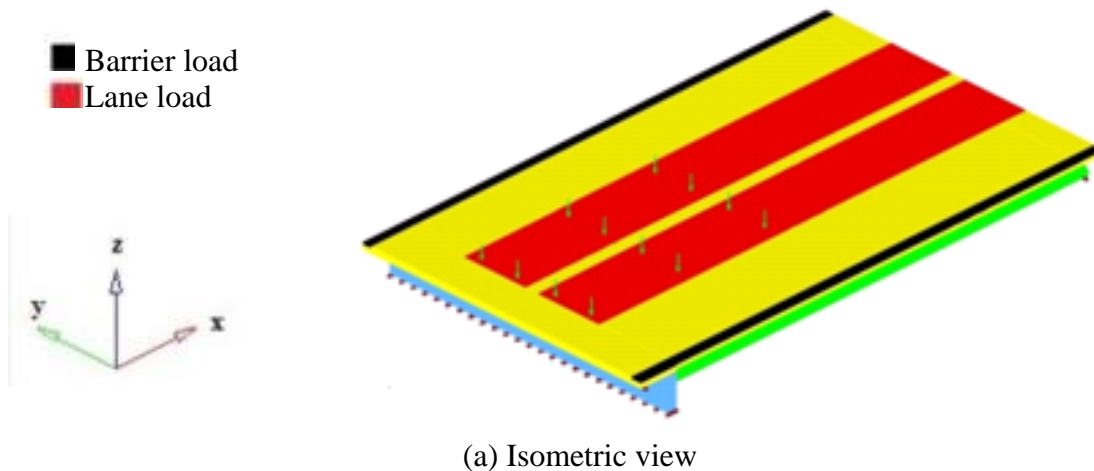


Figure 5-10. Live load configuration for CASE IV Expansion

Bearing type selection is controlled by the rotation, deformation, and load demands. Live load configurations specified were used to calculate bearing load and deformations. A parametric study was conducted to identify a live load position that generates maximum girder end rotation. As shown below, the trucks were placed at three different locations, and the girder end rotations were calculated. Two trucks were used and placed in each lane in opposite traffic direction. Trucks were placed on each lane such that one wheel line of each truck was directly above a girder. In this case, girder 8 and girder 1 were selected (Figure 5-11).

- Truck Position 1 –the trucks were placed as near as possible to the obtuse corner of the skew bridge (Figure 5-12). One of the rear wheels of the truck was placed approximately on the diagonal between the obtuse corners (load path).
- Truck Position 2 – the center of gravity of the trucks was placed at 1/3 of the span measured along the lane from the obtuse corners (Figure 5-13).
- Truck Position 3 – the center of gravity of the trucks was close to midspan of the girders (Figure 5-14). The trucks were positioned at locations that generate the maximum midspan moment of the girder.

Table 5-1 summarizes the girder 1 and 8 end rotations under above stated positions of the trucks. It is clear from the results that the girder end rotations increase as the trucks move towards the acute corner of the bridge. Hence, Truck Position 3 was used for further analysis in conjunction with dead and thermal gradient loads to calculate the girder end rotation. Additionally, girder end rotation values validate that the load path is along the diagonal between obtuse corners (i.e., the end rotation of girder 8 at the obtuse corner is larger than girder 1 for all the load cases).

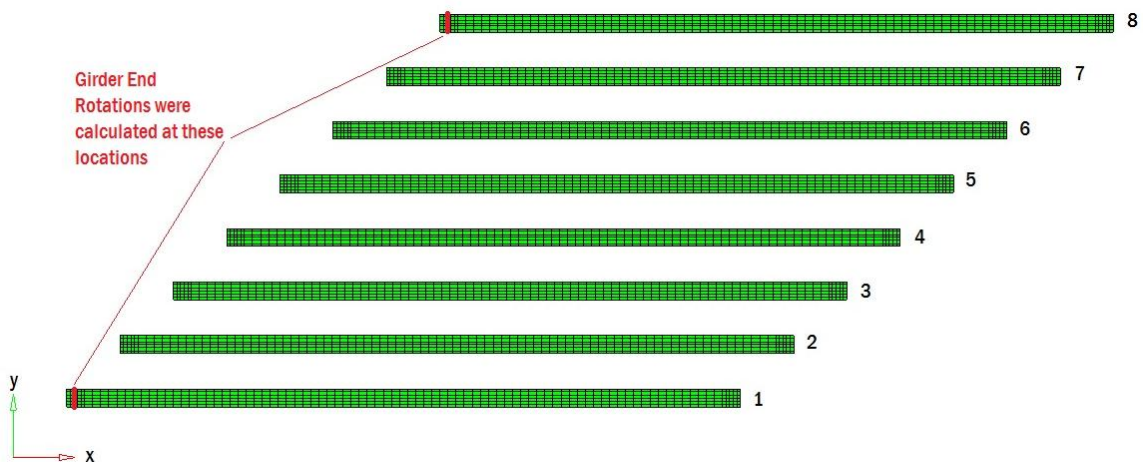


Figure 5-11. Location of girder 1 and 8 where girder end rotation was calculated

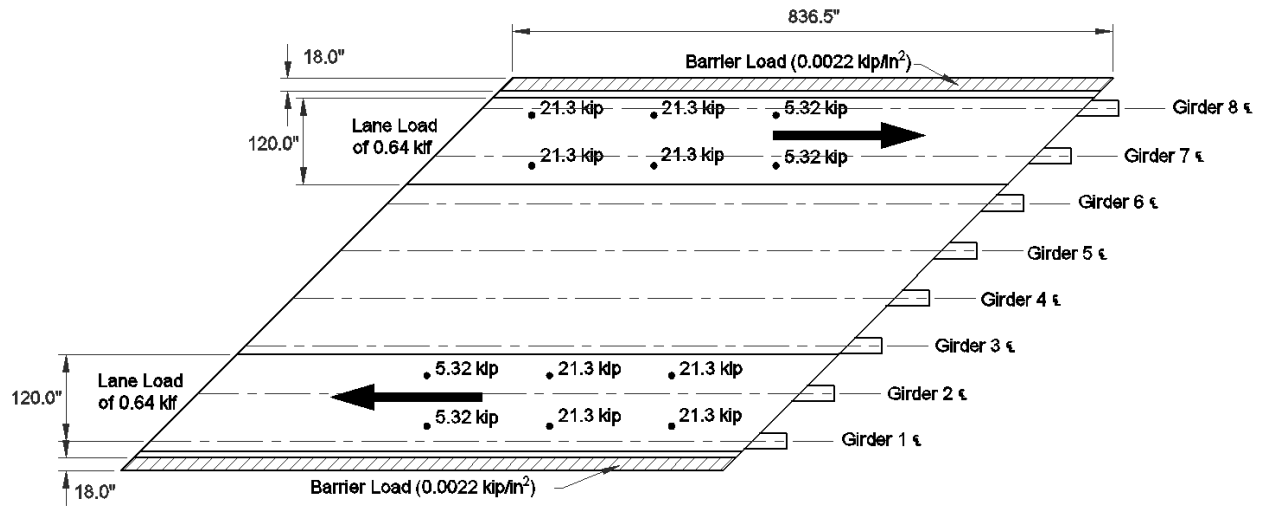


Figure 5-12. Truck position 1 for girder end rotation calculation

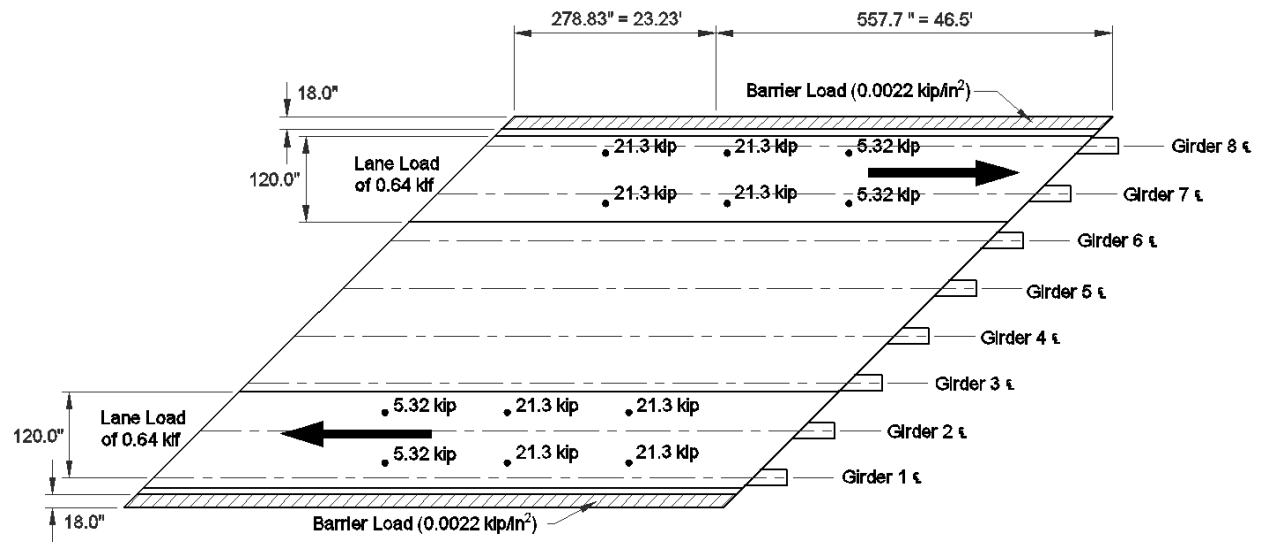


Figure 5-13. Truck position 2 for girder end rotation calculation

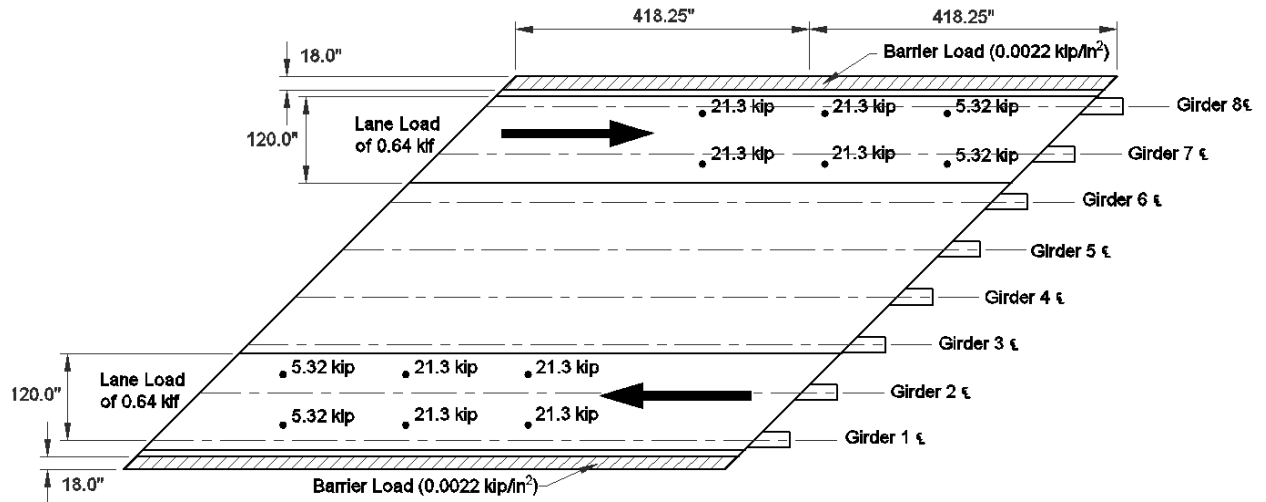


Figure 5-14. Truck position 3 for girder end rotation calculation

Table 5-1. Girder End Rotations against Different Truck Positions on Skew Bridge

	Girder1	Girder 8
Truck Position 1	0° 15' 56"	0° 19' 28"
Truck Position 2	0° 16' 38"	0° 20' 15"
Truck Position 3	0° 17' 10"	0° 20' 37"

5.4.2.2 Dead Load

The selfweight of the bridge components is included in the model. A New Jersey Type 4 barrier is selected. The selfweight of the barrier is 475 lb/ft. Instead of modeling the barrier, an area load of 2.2 lb/in² was applied within a 18 in. strip [i.e., 475 lb/ft / (18 in. x 12 in.) = 2.2 lb/in²] along the edge of the deck (Figure 5-9 and Figure 5-10).

5.4.2.3 Thermal Load

Uniform thermal loads that cause expansion and contraction of the bridge were calculated by Aktan et al. (2008) and used in this analysis. The values are summarized in Table 5-2. Negative and positive temperature gradient profiles and values are given in section 4.3.11.2 of the report.

Table 5-2. Thermal Load for Bridge Expansion and Contraction

Minimum Temperature (°F)	-10
Maximum Temperature (°F)	105
Base Temperature (°F)	62.7
Expansion (°F)	42.3
Contraction (°F)	-72.7

5.4.3 Load Combinations

Considering the construction sequence of a deck sliding over backwall, as a worst case scenario, only the approach slab and barrier loads will be acting on the backwall. The remaining loads are transferred through the bearings. In the case of semi-integral bridges, the entire superstructure loads including the approach are transferred through the bearings. Considering AASHTO (2010) strength and service limits, construction sequence of the bridge, and the load configurations suggested in the MDOT Bridge Analysis Guide, the following load combinations are used to calculate girder end rotations and translations and load demand on bearings and wingwalls.

Bridge Expansion (Deck sliding over backwall):

Strength 1-1: $1.25 DL_A + 1.75 LL_S + 1.2 UT_E$ Transverse forces at bearings
 Service 1-1: $1.0 DL_A + 1.0 LL_S + 1.2 UT_E$ Transverse forces at bearings

Bridge Contraction (Deck sliding over backwall):

Strength 1-1: $1.25 DL_A + 1.75 LL_A + 1.2 UT_C$ Transverse forces at bearings
 Service 1-1: $1.0 DL_A + 1.0 LL_A + 1.2 UT_C$ Transverse forces at bearings

Bearing Forces and Girder Rotation (Deck sliding over backwall):

Strength 1-1: $1.25 DL_{A+S} + 1.75 LL_S$ Vertical bearing forces
 Service 1-1: $1.0 DL_{A+S} + 1.0 LL_S$ Vertical bearing forces
 Service 1-2: $1.0 DL_{A+S} + 1.0 NTG + 1.0 LL_{S-mid}$ Girder rotation

Bridge Expansion (Semi-integral):

Strength 1-1: $1.25 DL_{A+S} + 1.75 LL_S + 1.2 UT_E + 1.0 EH$ Transverse forces at bearings and wingwall
 Service 1-1: $1.0 DL_{A+S} + 1.0 LL_S + 1.2 UT_E + 1.0 EH$ Transverse forces at bearings and wingwall

Bridge Contraction (Semi-integral):

Strength 1-1: $1.25DL_{A+S} + 1.75LL_A + 1.2 UT_C + 1.0EH$ Transverse forces at bearings and wingwall

Service 1-1: $1.0DL_{A+S} + 1.0 LL_A + 1.2 UT_C + 1.0EH$ Transverse forces at bearings and wingwall

Bearing Forces and Girder Rotation (Semi-integral):

Strength 1-1: $1.25DL_{A+S} + 1.75LL_S$ Vertical bearing forces

Service 1-1: $1.0DL_{A+S} + 1.0LL_S$ Vertical bearing forces

Service 1-2: $1.0DL_{A+S} + 1.0NTG + 1.0 LL_{S-mid}$ Girder rotation

Where DL_A – Dead load of approach

DL_{A+S} – Dead load of the entire superstructure including the approach

EH – Earth pressure

LL_A – Live load on approach (Figure 5-9)

LL_S – Live load on span (Figure 5-10)

LL_{S-mid} – Live load for maximum girder rotation

NTG – Negative temperature gradient

UT_C – Uniform temperature - contraction

UT_E – Uniform temperature - expansion

5.4.4 Boundary Conditions

An ideal boundary condition was used with all the abutment configurations. Ideal boundary condition generates maximum translations and rotations at the bearings. Bearing translations over the abutments are restricted to the bridge's longitudinal axis. Hence, reaction forces are developed in transverse and vertical directions and will be useful for bearing and girder end restraint design. In models with deck sliding over backwall configuration, friction between EPS and approach was included. Semi-integral models were analyzed with and without wingwalls to evaluate the forces at the bearings. As a worst case representation, transverse bearing restraint at the abutment is removed in order to calculate the maximum force on the wingwall. Further, forces at the wingwall are calculated with respect to the skew angle of the deck. The sliding surface between the deck and the wingwall is assumed friction free.

5.4.5 Deck Sliding over Backwall Abutment

The FE model of the deck sliding over backwall configuration shown in Figure 5-15 is based on the details provided in Figure 5-1. Models with different skew angles (i.e., 0, 20, 30 and 45 degrees) were developed and analyzed under strength and service loads to calculate the forces on the bearings. Interaction between approach and base and approach and sleeper slab were not incorporated into the models. Polyethylene sheets can be placed underneath the approach and at the interface between the approach and the sleeper slab of deck sliding over backwall system to minimize friction. Further, there is a potential for subgrade settlement and use of new material such as EPS as a backfill. Ideal boundary conditions were assigned at the end of the approach slab and girder ends. Friction at the deck and EPS interface over the backwall was included following literature recommendations though level of friction can be minimized by extending the polyethylene sheet that is placed underneath the approach over the EPS layer.

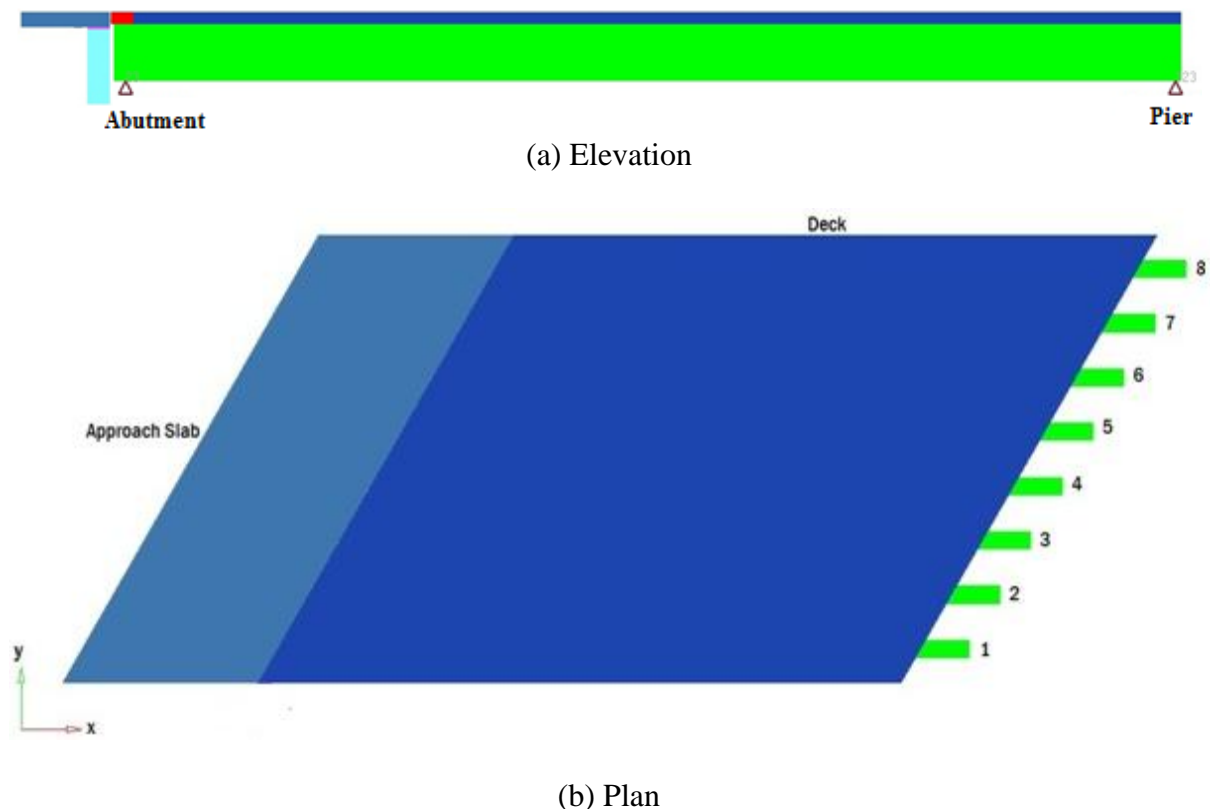


Figure 5-15. Deck sliding over backwall model description

5.4.5.1 Analysis Results – Girder End Rotations

Girder end rotations over the abutment of the deck sliding over backwall system were calculated under service loads. The maximum girder end rotations were calculated from the straight bridge model (Figure 5-17). As the skew increases, girder end rotation decreases.

The details provided in Figure 5-1 allow the span to act as simply supported. Hence, assuming the span is simply supported, the procedures given in Chapter 4 and Appendix C can be used to calculate girder end rotations under dead, live, and NTG loads. As discussed in step 2 of the Appendix C example, girder end rotation of a straight bridge under live load is calculated as 1.763×10^{-3} radians. The selfweight of an AASHTO Type II girder (0.583 k/ft) and self weight of an effective flange width of 66-in. deck (0.619 k/ft) generated a maximum dead load moment of 725.6 k-ft at the deck-girder composite section. Using this moment in conjunction with the section properties of the deck-girder composite section listed in Appendix C, girder end rotation was calculated as 2.4×10^{-3} radians. The girder end rotation, due to the negative temperature gradient load, was 4.84×10^{-4} radians (Table C-1). Hence the service rotation calculated at the girder end due to the combined effect of dead, live, and negative thermal gradient of a straight bridge is about 0.005 radians. This rotation is 60 percent greater than 0.003 radians calculated from the 3D FE model of a straight bridge.

AASHTO (2010) section 14.4.2.1 requires including 0.005 radians to the girder end rotation calculated from the service loads to account for uncertainties. The difference between the girder end rotation calculated from analytical methods described in Chapter 4 and Appendix C, and the FE models provide an adequate buffer for the uncertainties described in the AASHTO (2010). This is because the analysis procedure presented here accounts for all the possible loads except construction tolerances and intrinsic loads such as creep and shrinkage. Strong conclusions and recommendations can be derived for end rotation calculations after analyzing a large bridge population by incorporating various parameters such as span length and width, girder type, girder spacing, etc.

Following AASHTO recommendation, FE results plus 0.005 radians (i.e., 0.008 radians) is defined as the design rotation. The rotation of 0.008 radians is less than the maximum rotation limit of plain elastomeric pads given in Section 2.4.6 of Chapter 2 (i.e., 0.01 radians;

Table 2-3). Hence, plain elastomeric pads are recommended. The use of polytetrafluorethylene (PTFE) sliding bearing is not a viable option for bridges with such dimensions or longer. The use of sliding bearings in such bridges constraints girder end rotations and may result in girder end cracking, abutment D-cracking, and/or backwall cracking (Figure 5-16).



Figure 5-16. Abutment and girder end distress

Another option is the steel-reinforced elastomeric bearings. Use of plain elastomeric pads or steel-reinforced bearings should be carefully evaluated because vertical deformation of the bearings may result in reactions transferred through the backwall, instead of the bearings. Use of neoprene pads in between the approach and backwall is also an option to minimize the potential for the alternate load path. Another option for supporting the deck over the backwall is the use of EPS with a large elastic range as stated in Hoppe and Bagnall (2008). The special provisions presented in Hoppe and Bagnall (2008) require EPS with linear elastic stress-strain behavior up to 10 percent strain and linear proportional stress-strain behavior up to 30 percent strain.

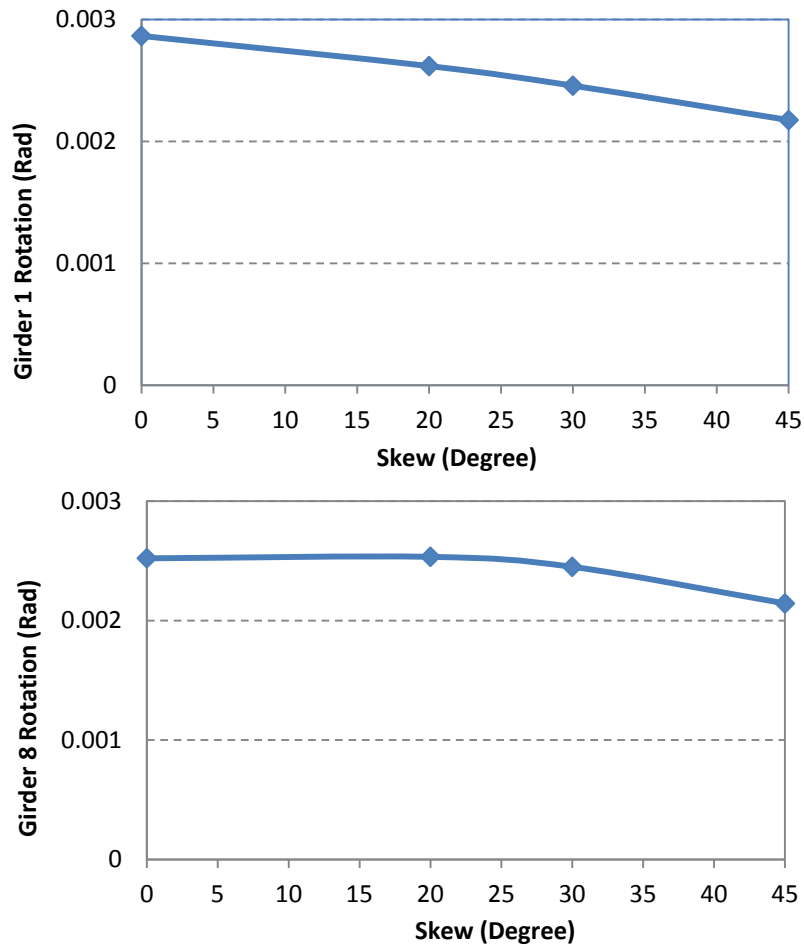


Figure 5-17. Girder 1 and 8 end rotation over abutment

5.4.5.2 Analysis Results – Bearing Translation

Uniform expansion and contraction temperatures are defined in Table 5-2. The length and width of the bridge deck are 834.5 in. and 544.5 in. Skew angle (θ), effective length of thermal movement (L_{th}), and angle between bridge longitudinal axis and L_{th} (β) are defined in Figure 5-18. The expansion or contraction is the greatest along the effective length of thermal movement, L_{th} (Hoppe and Bagnall 2008). For a 45° skew bridge with dimensions similar to what is defined above, the theoretical contraction and expansion in the longitudinal direction under the temperature values defined in Table 5-2 are calculated as 0.6 in. and 0.35 in.

The longitudinal bearing translation over the abutments was calculated from 3D FE models (Figure 5-19). Though FE results mirror the skew bridge behavior, the expansion and contraction values are reduced due to the model's ability to represent the three-dimensional

(3D) behavior of the structure. The friction force at the sliding surface is small because the vertical load at the backwall is very small, and the majority of superstructure load in the model was transferred through the bearings. However, for these unremarkable bridges, calculation of longitudinal expansion and contraction by analytical methods is sufficient to determine the deformation demands at the bearings. As per the limitations given in Table 2-3, a plain elastomeric pad is not a viable option for the calculated maximum deformation of 0.6 in. Considering both rotation and translation demand, the steel-reinforced elastomeric bearing is the most suitable bearing type. The 45^0 skew bridge considered in the analysis is only 69.5 ft long and 45 ft wide, which resulted in an effective length of thermal movement (L_{th}) of 123 ft, of which the effective length for horizontal bearing translation ($L_{th} \times \cos\beta$) is 115 ft long. Bridges with effective length for horizontal bearing translation greater than 115 ft will require reinforced elastomeric bearings to accommodate rotation and deformation demands. Further, implementation of link slabs, depending on the bearing configuration, increases the effective length of longitudinal expansion.

The maximum longitudinal expansion of the deck sliding over backwall and semi-integral systems is limited by the effective movement rating of the bearings or the expansion joints provided at the sleeper slab. Published data on preliminary bearing selection shows that the maximum translation up to 5 in. can be accommodated with available bearing types. According to Roeder and Stanton (1996), the maximum translation that steel reinforced elastomeric bearings (SREB) can accommodate, based on the total compressive force and rotation demand, ranges from 2 in. to 4 in. Greater translations can be accommodated with flat PTFE or combined systems. However, the maintenance cost of PTFE is greater than that of SREB.

According to the Michigan Bridge Design Manual (MDOT 2005), modular expansion joint devices are required when the expansion joint opening, in the direction of traffic, is greater than 4 in. However, according to Purvis (2003), modular joints are complex and recommend avoiding whenever possible. Instead, he recommends using strip seal joints of which the effective movement rating is 4 in. In deck sliding over backwall and semi-integral systems expansion joints are placed at the sleeper slab. Hence, in addition to the bridge superstructure movement due to thermal loads, the expansion joints should accommodate fit-

in tolerances, approach slab expansion/contraction, deformation of substructure due construction loads and sequence, and superstructure deformations due to creep and shrinkage in prestressed girders and selfweight. When strip seals are used, it is reasonable to assume available expansion range of 3 in. at the joint to accommodate thermal movement of a bridge superstructure.

According to published data, performance of expansion joints is well below expected (Purvis 2003). Further, expansion joint maintenance and replacement cost is much greater than that of bearings due to shorter service life of joints. Hence, expansion joint effective movement rating should be considered when bridge expansion length is specified. Bridge expansion length (i.e., L in Figure 5-18) is defined as the distance along the longitudinal axis measured from abutment to the nearest fixed bearing.

Bridge expansion length recommendations are developed considering width and skew ranges of single span steel and prestressed concrete bridges under the MDOT jurisdiction as shown in Figure 5-20 and Figure 5-21. Also assumed are a maximum strip seal joint width of 3 in., and an expansion and contraction thermal load of 115 °F. For example, from Figure 5-20, a straight concrete bridge superstructure expansion length should not exceed 300 ft. For a 45° skew concrete bridge of 100 ft wide superstructure expansion length should be limited to 200 ft. From Figure 5-21, when steel girder bridges are considered, expansion length should not exceed 275 ft for straight and 175 ft for a 100 ft wide 45° skew bridge (Figure 5-21).

On the other hand, transverse deformations of a bridge under uniform expansion and contraction thermal loads are only a function of the bridge width. Bridge width is measured perpendicular to the longitudinal axis of the bridge. The girder deformations and associated forces developed in a skew system due to transverse bearing restraint can be minimized by increasing bearing fit-in tolerances. As an example, when bearings are arranged in such a way that a bridge is allowed to expand in the transverse direction symmetrical to the longitudinal axis, a maximum of 0.5 in transverse movement can be expected under the exterior girder bearing of a 100 ft wide steel or concrete bridge that is exposed to a 115 °F expansion and contraction thermal range.

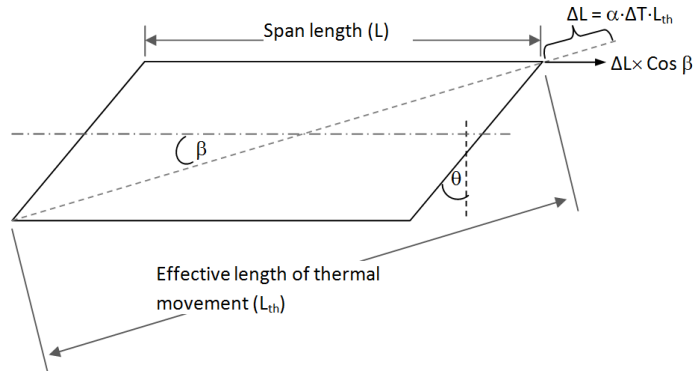
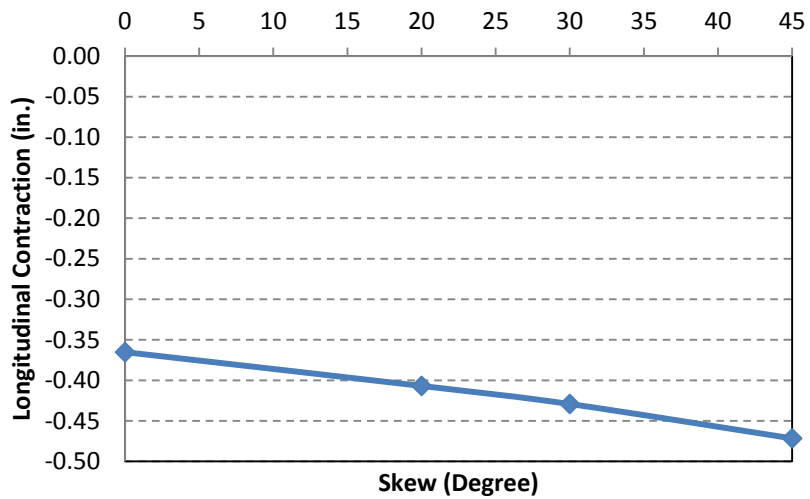
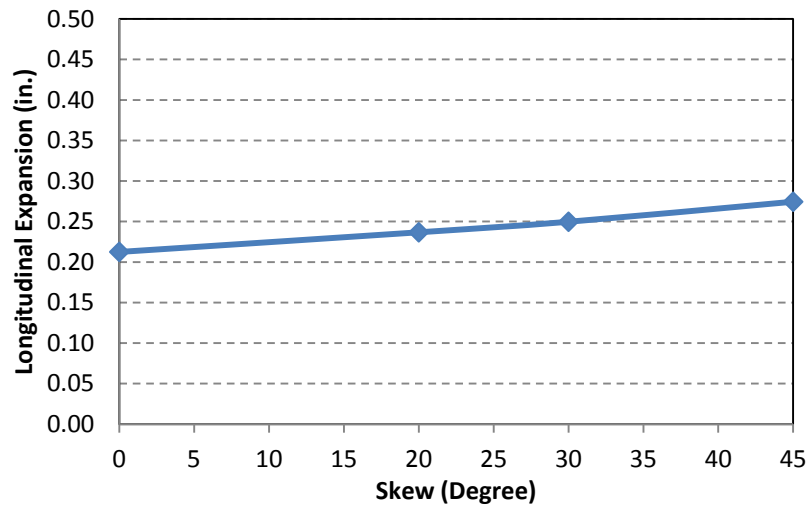


Figure 5-18. Thermal expansion of a skew bridge



(a) Maximum contraction in the longitudinal direction



(b) Maximum expansion in the longitudinal direction

Figure 5-19. Maximum longitudinal bridge contraction and expansion

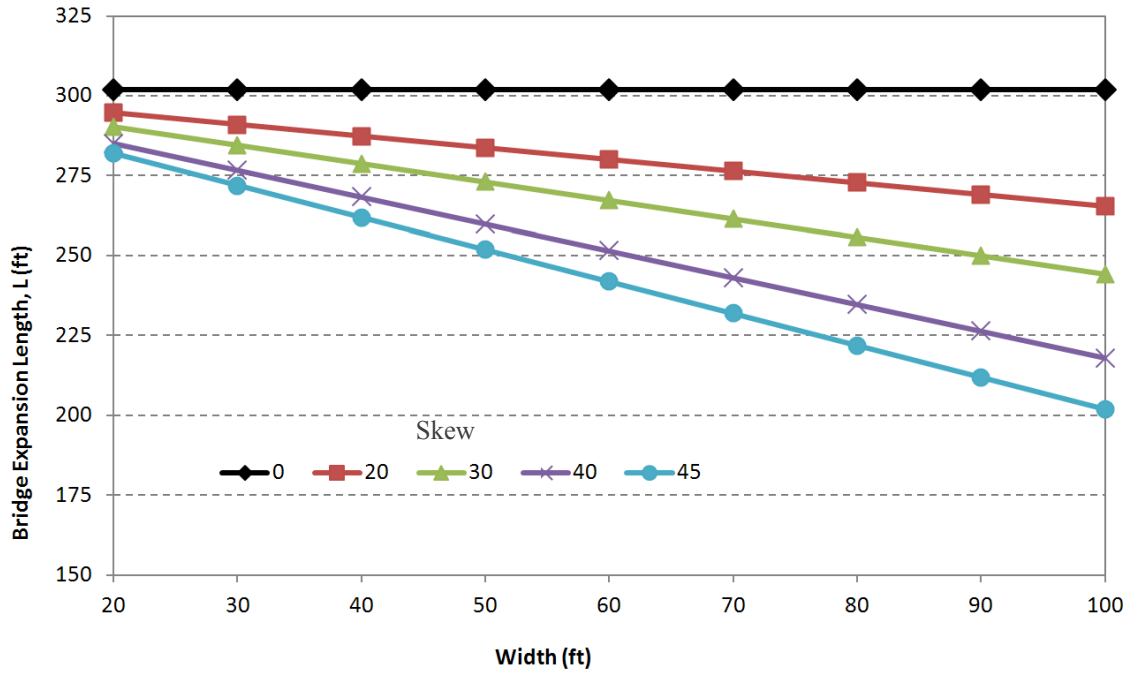


Figure 5-20. Variation of concrete bridge expansion length against width and skew when strip seal joint width of 3 in. available for thermal movement

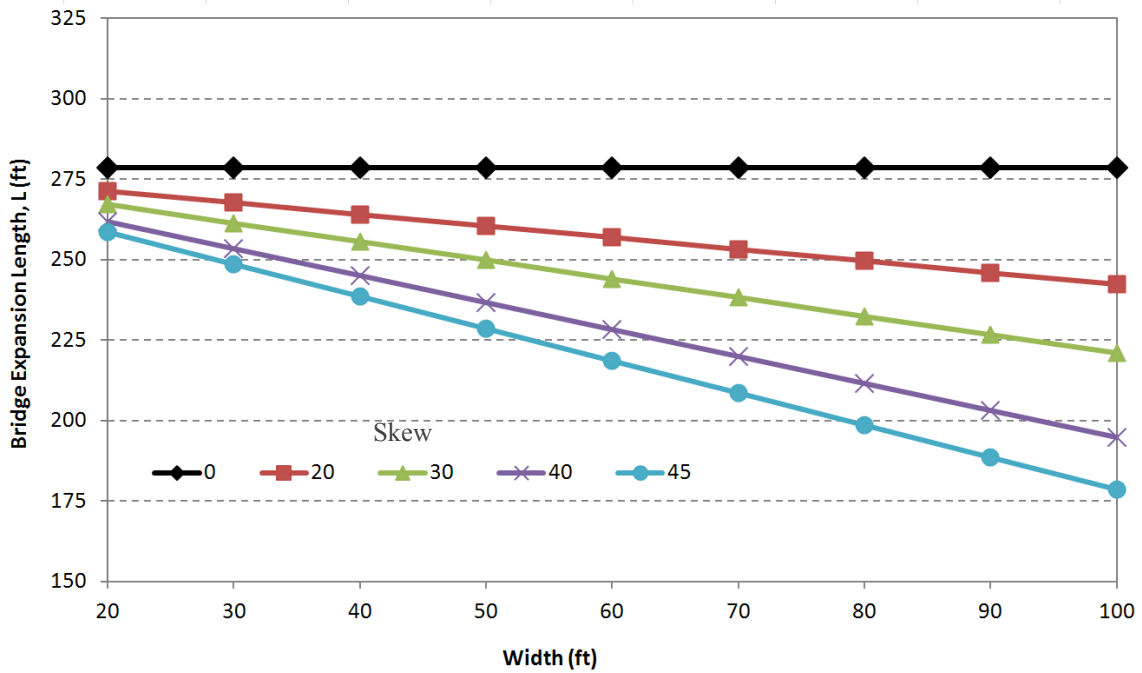
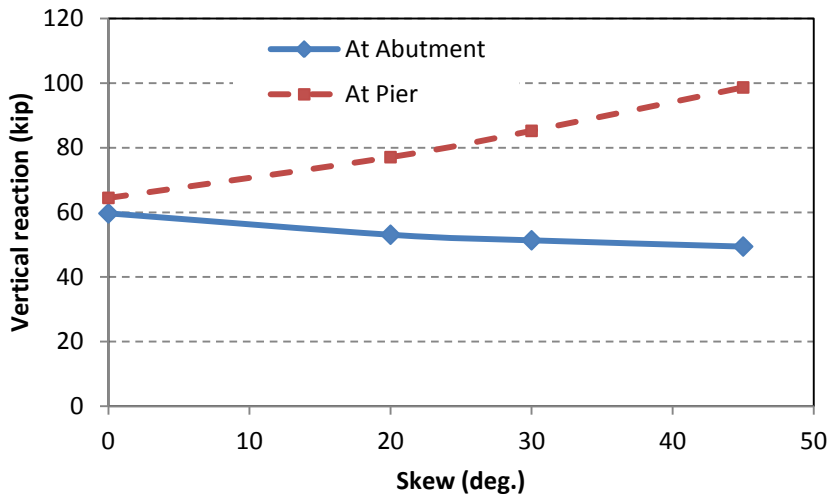


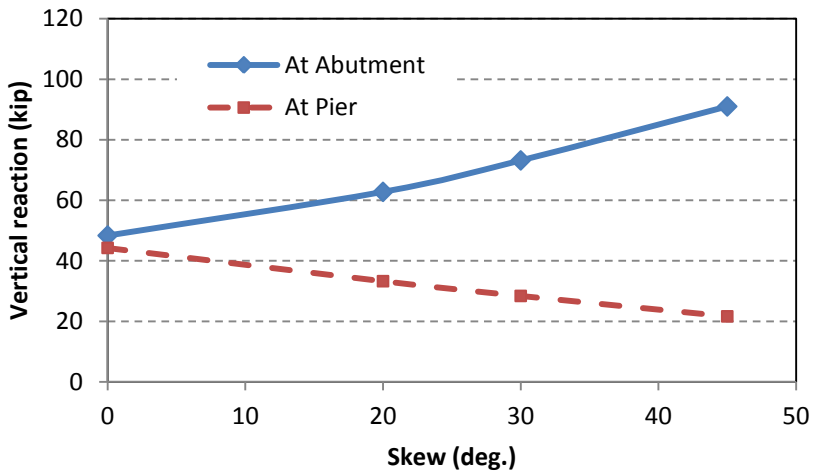
Figure 5-21. Variation of steel girder bridge expansion against width and skew when strip seal joint width of 3 in. available for thermal movement

5.4.5.3 Analysis Results – Vertical Bearing Forces

Bridge FE models were analyzed under the critical service load combination that generates the maximum vertical bearing forces. Results shown in Figure 5-22 show that the bridge response duplicates the skew behavior of a simple span, where girder end reactions reduce under the acute corner and increase under the obtuse corner with increasing skew. Vertical forces that develop on the bearing of this particular bridge are not a concern for any of the bearing types up to a 45⁰ skew. This is because the maximum load recommended for a plain elastomeric pad, which is the lowest among other bearing types, is 100 kips. The two-lane bridge considered in the analysis is only 69.5 ft long. As the bridge length increases, the load demand on bearings will increase. Especially, the load demand on the bearings underneath the obtuse corner of wide high skew bridges will increase dramatically. Considering all these factors, reinforced elastomeric bearings are recommended for skew deck sliding over backwall configurations. This recommendation is supported by the translation and rotation demands presented in previous sections. Hence, the designer can use the simple span model to calculate the reactions and deformations of the bridge with deck sliding over backwall for the bearing design.



(a) Girder 1 vertical reaction variation over abutment and pier



(b) Girder 8 vertical reaction variation over abutment and pier

Figure 5-22. Girder 1 and 8 reaction variation over the abutment and pier

5.4.5.4 Analysis Results – Transverse Bearing Forces at Abutment

Transverse bearing forces were calculated at each bearing over the abutment under strength load combinations that include thermal contraction loads (Figure 5-23). Similarly, transverse bearing forces were calculated at each bearing over the abutment under strength load combinations that include thermal expansion loads (Figure 5-24). In both cases, no other transverse restraints were considered. As shown in the figures, in the transverse direction, thermal contraction generates the greatest forces on bearings. According to AASHTO LRFD (2010) section 14.7.9 *guides and restraints shall be designed using strength limit state load*

combinations for the larger of either (a) the factored horizontal design force or (b) 10 percent of the total factored vertical force acting on all the bearings at the bent divided by the number of guided bearings at the bent. Though the AASHTO recommendation is for the bearings over the bent, this can also be applied to the design of bearings over the abutment of the deck sliding over backwall configuration since there is no backfill pressure effect on the structure. The total vertical force on the abutment bearings that was calculated from strength load combinations is 1000 kips. According to AASHTO, if two girder ends are restrained in the transverse direction, the design load is 50 kips which is less than the 10% of the forces generated under thermal loads.

The bearing forces shown in Figure 5-23 and Figure 5-24 were calculated without any allowance for bearing movement in the transverse direction. Transverse bearing forces can be minimized or eliminated by increasing fit-in tolerances between position dowel and the sole plate. This is a practical solution for the deck sliding over backwall system once the friction at interfaces between approach-EPS, approach-base, and approach-sleeper slab is minimized by providing a polyethylene sheet. Bridge plans generally require a 0.125 in. fit-in tolerance between the position dowel bar and the slot in the sole plate (Figure 5-25). Further, AASHTO LRFD Bridge Construction Specification (2008) provides manufacturing and installation tolerances. With the tolerances achieved during manufacturing and installation, there is a great possibility of the total transverse force not being equally shared by all of the bearings. Providing adequate tolerance for transverse movement of the bearings and constraining a single or a two middle girder ends should be considered. The transverse expansion of a 40 ft wide concrete bridge under differential uniform thermal load of 80 °F is about 0.23 in. whereas the allowable tolerance specified in the specifications is 0.125 in. Most of the analysis and design examples in the literature have dealt with other structural systems such as semi-integral or integral abutments that are subjected to thermal expansion loads. This is because the passive earth pressure built up at the backwall tends to rotate the superstructure and increases the bearing forces than those developed under contraction thermal loads. In the case of deck sliding over backwall, for expansion thermal loads, only restrain force is from the interface friction which can be minimized as suggested above.

Implementation of some of the bearing configurations discussed in Chapter 2 section 2.3 can release girder end forces developed under thermal expansion and contraction loads. Because of the link slab over the pier, the only possible bearing configuration is the radial from center (Figure 2-17 c). The recommendation is to restrain the transverse movement of the middle girder end (if odd number of girders) or two middle girder ends (if even number of girders) using concrete keys with rub plates (shown in Figure 5-8) and to increase the tolerance of the slot in the sole plate and bearing to accommodate transverse movement of unrestrained girder ends. Once the middle girder(s) is restrained in the transverse direction, the transverse movement the bearing needs to accommodate is proportional to only half of the bridge width. For example, the required tolerance for a 40 ft wide bridge under differential uniform thermal load of 80 °F is about 0.12 in. This is less than the allowable tolerance of 0.125 in. recommended for the position dowels by the AASHTO LRFD Bridge Construction Specification (2008).

It is recommended the maximum bearing tolerance in the transverse direction is limited to 0.25 in. until further investigations are carried out investigating the impact of the increased fit tolerances on the girder position dowels on the rest of the bridge components. The maximum limit was established as the summation of fit-in tolerance provided with general bearing details (Figure 5-25) and the AASHTO Bridge Construction Specification tolerance of $|+0.125|$ or $|-0.125|$ in.

Further, friction at the approach-EPS, approach-base, and approach-sleeper slab has a great influence on link slab stresses. The analysis discussed in Chapter 4 used three different support configurations, HRRR, RRHR, and RHHR, where H and R represent hinge (i.e., fixed bearing) and roller (i.e., expansion bearing). In the case of HRRR, the bearings underneath the link slab are expansion bearings (R) while the bearings over the abutments are fixed (H) and expansion (R) types. If large frictional forces develop at the approach of the abutment with expansion bearings, large stresses will develop at the link slab. This is because the restrains that develop at the supports will result in an HRRR support system to approach HRRH. As discussed, this support configuration is not recommended for link slab bridges. In order to reduce the friction forces, providing a polyethylene sheet underneath the entire surface of the approach is recommended (MnDOT 2011). Reducing the friction force

at interfaces and providing adequate tolerances for girder end movement under thermal expansion and contraction releases the restraint forces developed at the supports.

Details of the bearings over the abutment and independent backwall abutment configuration were developed to accommodate the reduced restraint forces. Proposed detail in standard MDOT Bridge Design Guide format is presented in Appendix F. All the required mathematical relationships and variables are presented with the drawings. The rub plate design procedure was adopted from VDOT Bridge Design Manual section 20.04 (2010) with some modifications and presented in Appendix G.



Figure 5-23. Transverse bearing force over abutment under thermal contraction strength load combination

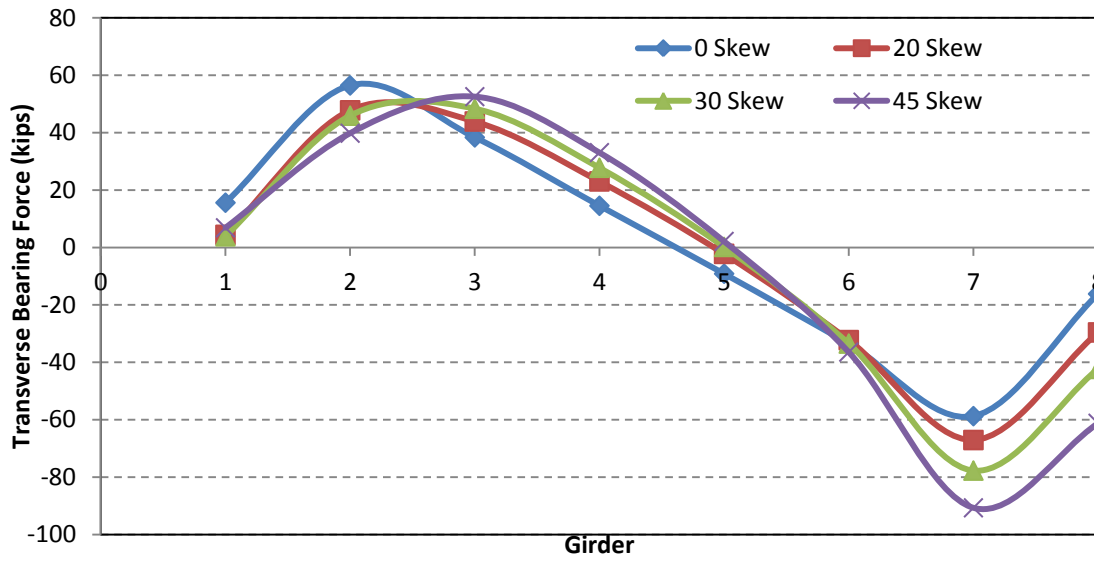


Figure 5-24. Transverse bearing force over abutment under thermal expansion strength load combination

5.4.6 Semi-Integral Abutment

Two different configurations shown in Figure 5-2 and Figure 5-3 were analyzed. Even though there is a difference in the position of backwalls in these two configurations, the same FE model is applicable for both configurations because the load transfer is only through the bearings. FE models were developed with and without wingwalls (Figure 5-26) and analyzed under the load combinations listed above to calculate translation, rotation, and force demand at the bearing as well as the forces that develop at the wingwalls. EPS was included as the backfill material.

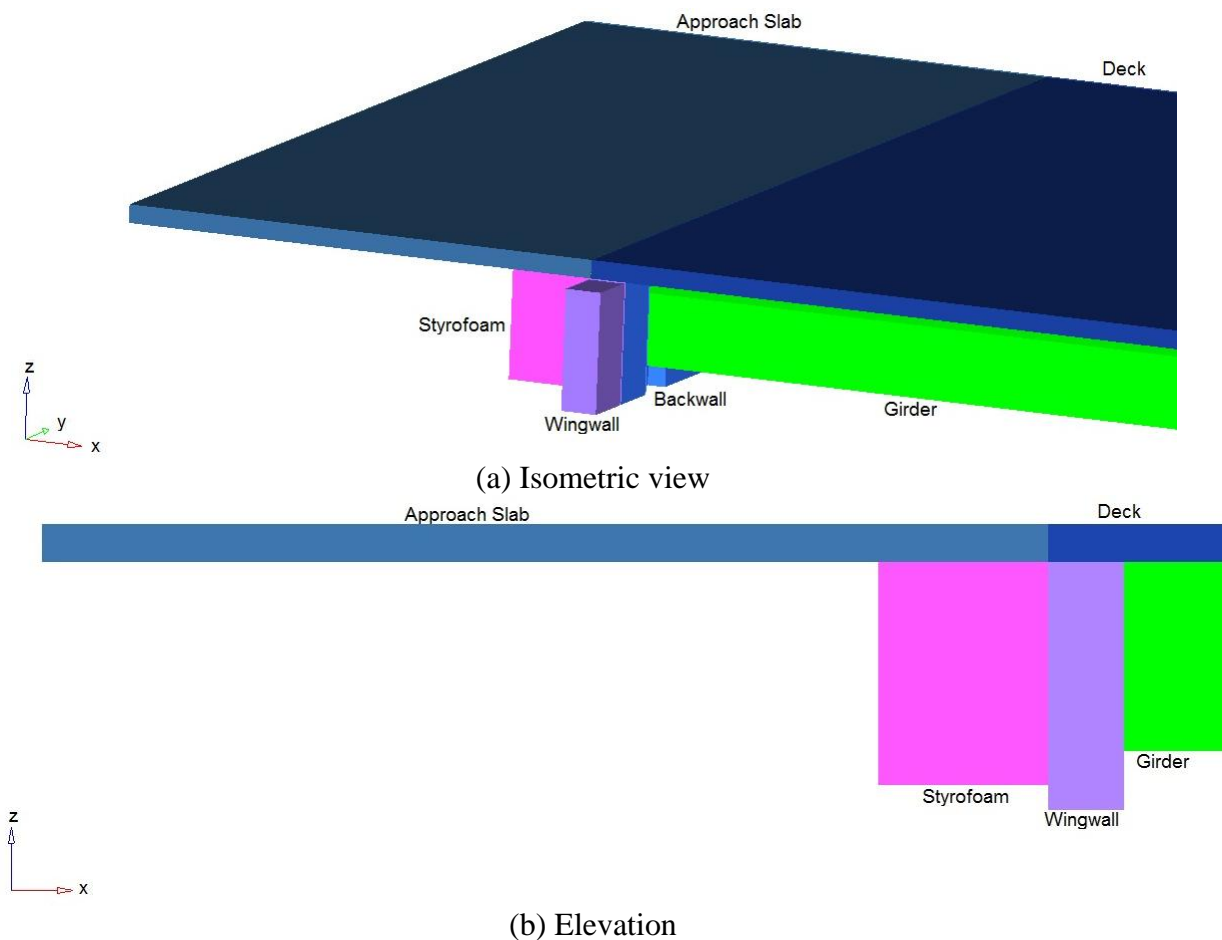


Figure 5-26. Semi-integral bridge model with wingwalls (not drawn to scale)

5.4.6.1 Analysis Results – Girder End Rotations

Girder end rotations were calculated over the abutment under the 1.0 DL_{A+S} + 1.0 NTG + 1.0 LL_{S-mid} load combination. Beyond a 25° skew, girder end rotations decrease as skew increases (Figure 5-27). Girder 1 rotation was calculated to be the largest. As shown in Figure 5-2, the approach slab is connected to the backwall by a diagonal reinforcement. This detail is assumed as a hinge, and the moment is not transferred across the connection. The bridge span can then be modeled conservatively as a simply supported system. The girder end rotations are similar to from the results of the deck sliding over backwall system. Subsequently, the analytical calculations and recommendations for the bearing selection provided in section 5.4.5.1 are also applicable for semi-integral system.

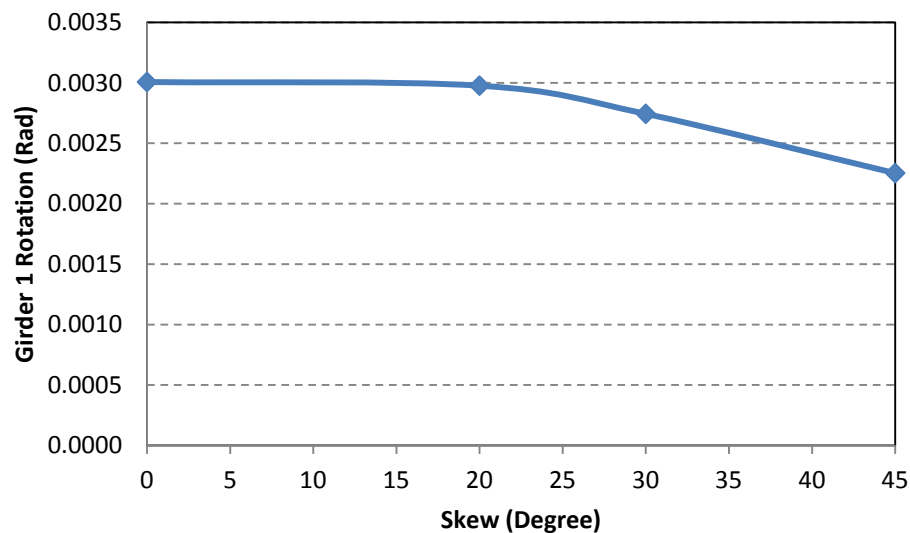


Figure 5-27. Girder 1 rotation of semi-integral bridge

5.4.6.2 Analysis Results - Bearing Translation

Theoretical bridge contraction and expansion in the longitudinal direction calculated in section 5.4.5.2 as 0.6 in. and 0.35 in. are applicable to the semi-integral configuration when backfill and bearings do not restrain the longitudinal movement. As discussed in section 5.4.5.2, bridge expansion length limitations due to expansion joint movement rating should be considered when link slabs are implemented in semi-integral bridges. Bridge expansion and contraction in the longitudinal direction at girder 1 over the abutment is shown in Table 5-3. The results are also similar to those calculated for the deck sliding over backwall

configuration. The idealized boundary conditions were assumed in order to calculate the maximum beam end translations. The FE model includes EPS backfill material but provides very limited constraint to the expansion of the structure due to its low stiffness ($K_p = \nu/(1 + \nu)$; $\nu = 0.09$; $K_p = 0.08$). The difference in analytical and 3D analysis is due to the 3 dimensional effects as discussed in section 5.4.5.2. The model without wingwalls slightly overestimates the deformations due to the uncontrolled movement of the deck.

Hoppe and Bagnall (2008) indicated that to minimize forces on the backwall and wingwalls, EPS with desired properties can be procured for placement at the backwall by incorporating special provisions to the project documentations. The Virginia DOT has developed special provisions for inclusion of EPS and geotextile. These special provisions are provided in Hoppe and Bagnall (2008).

Table 5-3. Expansion and Contraction of Girder 1 End over Semi-Integral Abutment

		FE Model	
		Without Wingwall	With Wingwall
Skew		Δx (in.)	Δx (in.)
Contraction	0	-0.36	-0.37
	20	-0.40	-0.40
	30	-0.42	-0.42
	45	-0.49	-0.45
Expansion	0	0.21	0.21
	20	0.23	0.25
	30	0.24	0.26
	45	0.26	0.27

5.4.6.3 Analysis Results – Transverse Bearing and Wingwall Forces at Abutment

Transverse bearing forces were calculated at each bearing over the abutment under strength load combinations that include thermal contraction loads (Figure 5-28). Similarly, transverse bearing forces were calculated at each bearing over the abutment under strength load combinations that include thermal expansion loads (Figure 5-29). In both cases, no other transverse restraints on the bridge deck were considered. As shown in the figures, thermal contraction generates the largest force on bearings in the transverse direction in the absence of backfill pressure under expansion loads. The forces are developed due to expansion or contraction in the transverse direction because of girder restraints in that direction. These

forces are generated when supports do not accommodate transverse movement. These forces are much greater than the ones developed in the deck sliding over backwall system with similar dimensions. This is mainly due to the expansion and contraction of the stiff concrete mass consisting of the backwall at the girder end.

As discussed earlier, according to AASHTO LRFD Bridge Construction Specifications (2008), construction and manufacturing tolerances are specified up to 0.125 in. Incorporating the tolerances, the forces developed at the girder ends, especially under thermal contraction loads, will be reduced. Transverse forces under thermal contraction can be reduced substantially by specifying an increased tolerance for transverse movement. However, thermal expansion also develops bearing forces due to backfill pressure. This backfill pressure effect can be minimized by using an EPS layer in between the backwall and the backfill. EPS is a very soft material, and the passive pressure coefficient can be as low as $K_p = 0.08$ (see section 5.4.6.2). After monitoring a 45° skew bridge for about two years, Hoppe and Bagnall (2008) estimated K_p to be 1.2, which is much lower than the VDOT (2010) recommended value of $K_p = 4$. After all, the benefits of inclusion of an EPS layer are obvious and have a great potential to minimize the forces developed in the transverse restraint systems of skew bridges.

Three dimensional models were analyzed under thermal expansion loads to calculate transverse forces on the wingwall. Transverse restraint at the bearings over the abutment was released to calculate the resultant force on the wingwall. EPS with K_p of 0.08 was used as the backfill. The resultant wingwall force variation with skew is presented in Figure 5-30. The calculated force on the wingwall is smaller than the values presented in literature for different backfill material. For this reason, using an EPS layer in between the backwall and backfill material and providing adequate tolerances at the bearings over the abutment is recommended to release girder end forces that are developed under uniform thermal loads. It is also recommended to use geotextile filter fabric in between EPS and backfill for protection. Due to lack of data on passive pressure coefficient of EPS, it is recommended to use the values suggested in VDOT (2010), i.e., $K_p = 4$, for design. Further, due to lack of guidelines, the equation given in VDOT (2010) section 20-06-6 can be used to calculate EPS

layer thickness (i.e., Eq. 2-2 in Chapter 2 section 2.4.4). Transverse force on the wingwall should be calculated following the procedure described in VDOT (2010).

Wingwalls are not effective under thermal contraction. Hence, it is recommended that wingwalls are used in conjunction with a concrete key to assure stability of the bridge with the increased alignment pin slot tolerances to accommodate thermal movement.

Further, minimizing friction at the approach-base and approach-sleeper slab has a great influence on link slab stresses. This issue is highlighted in section 5.4.5.4. This is extremely important in the case of thermal contraction which can develop significantly larger stresses than the concrete modulus of rupture. Hence, providing a 0.025 in. thick polyethylene sheet underneath the entire surface of the approach is recommended. Application examples of such practices can be found from Minnesota and Pennsylvania DOT jurisdictions.

Considering the use of EPS, reducing friction at interfaces, and providing adequate tolerances for girder end movement, bearing details, wingwall and concrete key configurations, and abutment configurations were developed. Proposed detail in standard MDOT Bridge Design Guide format is presented in Appendix H.

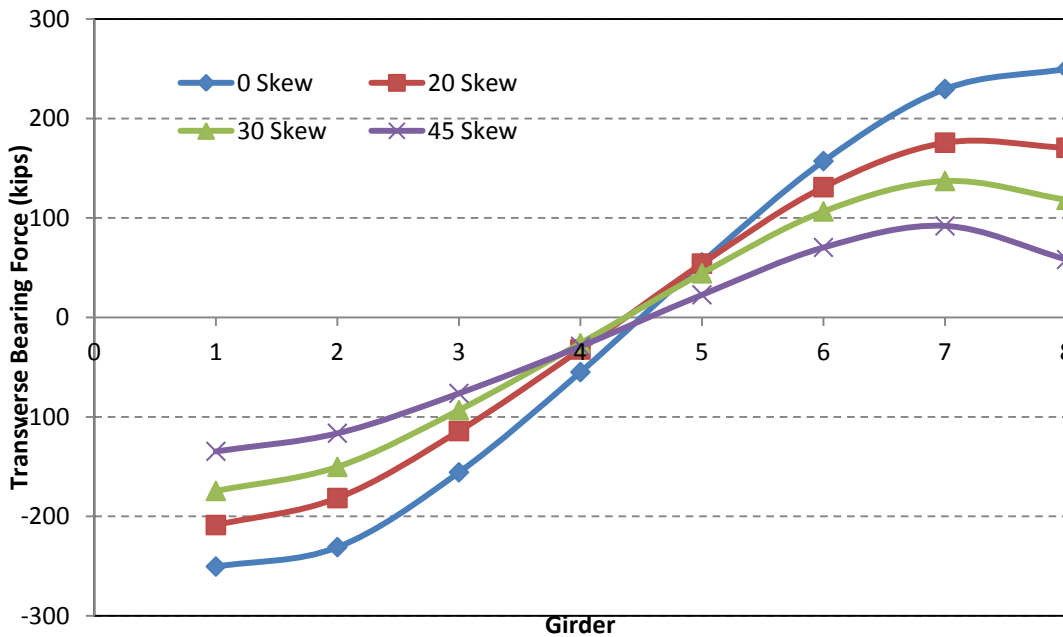


Figure 5-28. Transverse bearing force over abutment under thermal contraction strength load combination

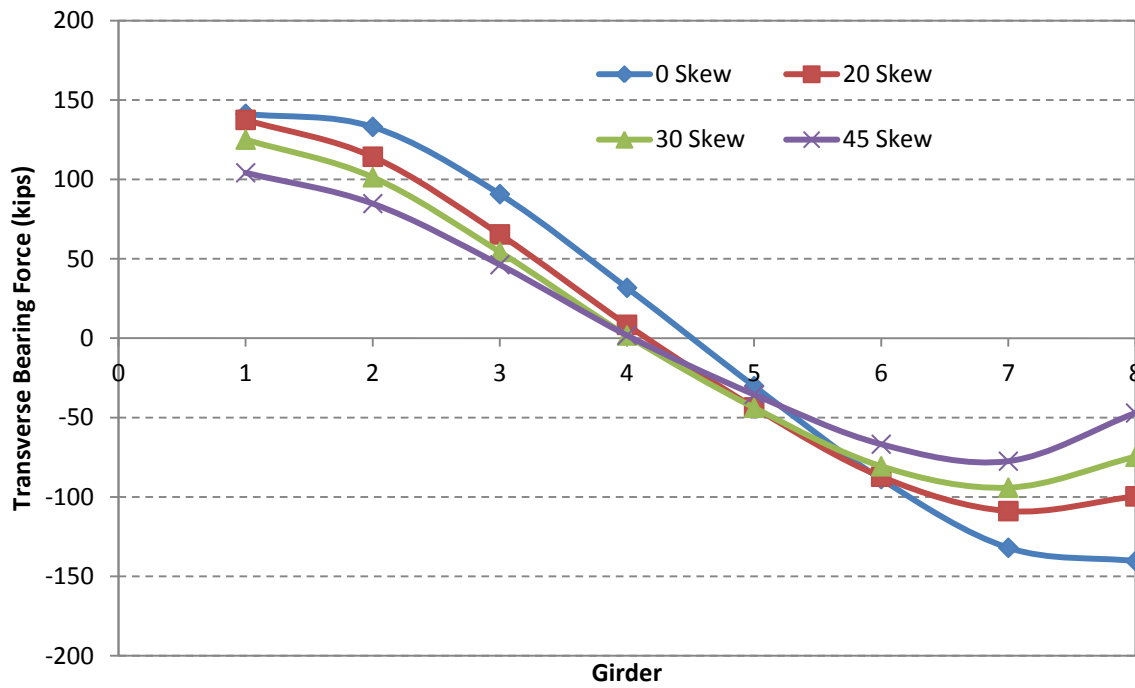


Figure 5-29. Transverse bearing force over abutment under thermal expansion strength load combination

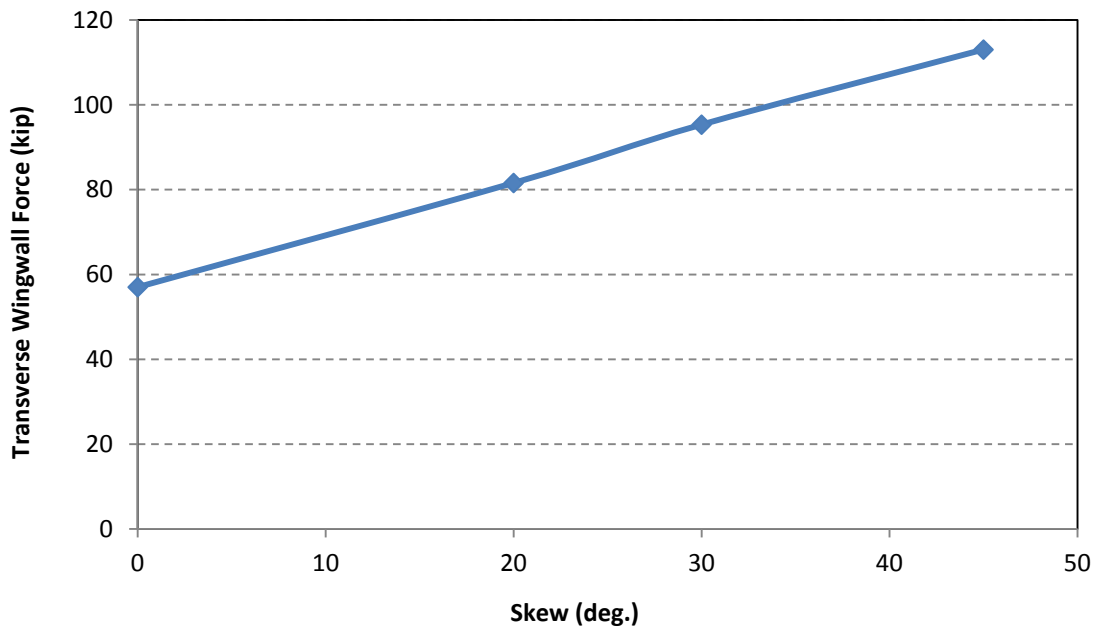


Figure 5-30. Wingwall force due to thermal expansion without transverse restraint over the abutment under strength load combination

5.5 ANALYSIS AND DESIGN PROCEDURES AND DETAILS FOR ABUTMENTS AND BEARINGS

Detailed analysis of two skew abutment configurations namely deck sliding over backwall and semi-integral systems was performed for a range of skew angles from 0^0 to 45^0 and loads and configurations specified in AASHTO (2010) and the Michigan Bridge Design Manual (MDOT 2005). The deck sliding over backwall and semi-integral abutment details presented in Aktan et al. (2008) were used to develop FE models and later modified to accommodate various bearing configurations and wingwalls. The following is a summary of conclusions that are derived from the analysis results and information presented in related literature and design specifications /guidelines.

1. A bridge span with deck sliding over backwall or semi-integral abutments can be analyzed as simply supported spans to calculate girder end rotations and translation (expansion/contraction) demands.
2. Skew bridges expand and contract along the diagonal between acute corners. The movement results in transverse forces at the bearings and other restraint systems. The restraint force magnitudes become considerably larger if adequate tolerances are not provided to accommodate the movements due to thermal loads. The situation requires special consideration when link slabs are implemented over the piers, which in turn increase the effective length of thermal expansion and contraction. Further, the direction of bridge movement under expansion and contraction loads needs to be restricted to the bridge axis. In plane twisting results in large stresses along the edge of link slab (see Chapter 4). Link slab is also flexible under torsion compared to the deck-girder integrated system. Hence, controlling bridge alignment is critical when link slabs are implemented.
3. It is recommended that deck sliding over backwall abutments, is restrain the transverse movement of the center girder end (for odd number of girders) or two centermost girder ends (for even number of girders) using concrete keys with rub plates (shown on Figure 5-8.). Also, larger tolerance is required for the slot in the sole plate and bearings in order to accommodate the transverse movement of unrestrained

- girder ends. Proposed detail in standard MDOT Bridge Design Guide format is presented in Appendix F. The required formulations and variables for movement calculations are presented with the drawings. The rub plate design procedure is based on the VDOT Bridge Design Manual section 20.04 (2010) with modifications and presented in Appendix G.
4. Transverse movement of bearings over the semi-integral abutment is facilitated by increasing the tolerance of the slot at the bearing plate. Transverse restraint for expansion thermal load is provided by a wingwall at the acute corner. Alignment of semi-integral abutment bridge deck with backwall offset from the abutment is managed under contraction thermal loads by placing a concrete key at the center girder. Calculation of the transverse force on the wingwall is adopted from the procedure described in VDOT (2010). Proposed detail in standard MDOT Bridge Design Guide format is presented in Appendix H.
 5. It is recommended that an EPS layer is placed behind the backwall of semi-integral bridges. This will minimize the passive pressure and results in lower transverse forces at the wingwall. Although the passive pressure coefficient of EPS is in reality much lower than four (4), a coefficient of four (4) is recommended for conservative design until additional supporting data is developed (VDOT (2010)). Further, the equation given in VDOT (2010) section 20-06-6 can be used to calculate EPS layer thickness (i.e., Eq. 2-2 in Chapter 2 section 2.4.4).
 6. It is recommended that the maximum bearing tolerance in transverse direction is limited to 0.25 in. Further investigations can be carried out analyzing the impact of the increased fit tolerances of the girder position dowels on the bridge components.
 7. Following link slabs are implemented, controlling friction at the approach slab interfaces is very critical. Increased friction hinders bridge movement restricting expansion bearing movement over the abutment. This results in stresses greater than the concrete modulus of rupture under negative thermal loads. Hence, it is vital to reduce friction at all the contract surfaces at the abutment and approach to facilitate

movement of the bridge under expansion and contraction thermal loads. To reduce friction a 0.025 in. thick polyethylene sheet can be placed during construction over the fill supporting the approach slab.

8. Bridge expansion length, excluding the approach slab, was calculated for width and skew angle ranges of single span steel and prestressed concrete bridges under the MDOT jurisdiction. Strip seal joint width of 3 in. available for thermal movement in the traffic direction and an expansion and contraction thermal load of 115 °F (Figure 5-20 and Figure 5-21) were assumed. Under such limits, expansion length of concrete bridge superstructure without skew should be limited to 300 ft. When steel girder bridges without skew are considered, length should be limited to 275 ft. For skew bridges, length limits are described in the charts shown in Figure 5-20 and Figure 5-21.

Intentionally left blank

6 SUMMARY, CONCLUSIONS, DESIGN RECOMMENDATIONS, AND IMPLEMENTATION PLAN

6.1 SUMMARY AND CONCLUSIONS

Four tasks were performed in this project. The first task was to review and synthesize information related to skew/jointless bridge behavior, modeling and analysis of skew bridge structural system/components, design and detailing of jointless abutments, and performance of jointless bridges. In this task specific design configurations with records of better performance were identified. High skew link slab analysis and design guidelines could not be found in the literature review. Hence, a detailed analysis of a high skew link slab bridge system was performed; design procedures and details were developed. Literature review was very useful in identifying abutment configurations and design details with better performance records. The most functional detail in these configurations were the use of EPS to reduce passive earth pressure and the use of rub plates to guide the bridge expansion and contraction under thermal loads. The Virginia DOT bridge design manual provided calculation details of EPS layer thickness and rub plate design. The manual also provided the passive pressure coefficient of EPS and a detailed procedure for calculating design forces on wingwall.

Task two was field monitoring of a high skew bridge under truck loads and thermal loads. This task was for identifying and documenting the performance of sliding bearings and the behavior of a skew bridge under various loads types. In-depth understanding of skew bridge behavior was essential for the defining the analyses framework carried out in task three and four.

Task three was detailed analysis of skew link slabs and calculation of the associated moment and force envelopes at the link slab section directly over the pier centerline. The analysis was performed for a specific bridge span length, width, and girder type, and at various angles of skew from 0° to 45° . The finite element (FE) models, for these configurations up to 45° skew, were developed and analyzed under loads and load combinations described in AASHTO (2010). Further, the influence of different bearing configurations on the link slab moment and force resultants are also investigated. Finally, the design recommendations were developed for the utilization of link slabs in high skew bridges. The design recommendations

were developed by integrating findings from the literature review, with the FE analysis results, and AASHTO (2010) requirements on strength and service load combinations. A detailed example of skew link slab design procedure is presented in Appendix C.

Task four was the detailed analysis of two skew abutment configurations namely deck sliding over backwall and semi-integral systems. The analysis models were developed for a range of skew angles from 0^0 to 45^0 and analyzed under loads and configurations specified in AASHTO (2010) and the Michigan Bridge Design Manual (MDOT 2005). Deck sliding over backwall and semi-integral abutment details presented in Aktan et al. (2008) was the basis of the FE models. These models were modified to incorporate selected bearing configurations and wingwalls. Based on findings from the FE analysis combined with findings from the literature, design recommendations for bearings, abutments, and restraint systems were developed.

6.2 RECOMMENDATIONS

From the literature review on field assessment of skew bridge behavior under static truck loads and thermal expansion, and simulations by numerous FE models, three design recommendations were developed. One recommendation is for the high skew link slab design, and the other two address the transverse restraint systems, bearing details, and the abutment configuration of deck sliding over backwall and semi-integral abutments in link slab bridges.

6.2.1 Link Slab Design

Current link slab design procedures do not incorporate skew effects. A design procedure was developed following a detailed analysis of skew link slabs and the moment and force envelopes for various boundary and load configurations. Two major findings are (1) moment developed in a link slab under temperature gradient loads remains constant irrespective of span and (2) moment developed in a link slab under live load decreases with increased span. Analysis results verified that the minimum reinforcement amount required in AASHTO LRFD Section 5.7.3.3.2 is adequate for the majority of skew link slabs with HRRR or RRHR support configuration. However, additional reinforcement at the bottom layer is needed to resist large tensile stresses that develop near the boundaries of the debonded region. A

detailed design example is presented in Appendix C. Proposed link-slab detail in standard MDOT Bridge Design Guide format is presented in Appendix E. Three saw cuts are recommended: one at each end of the link slab and one directly over the pier centerline.

6.2.2 Deck Sliding over Backwall

Two changes are proposed to the current MDOT independent backwall detail. The first one is to incorporate 0.025 in. thick polyethylene sheet underneath the approach slab. The second one is a transverse restraint system designed with concrete keys and rub plates. The restraint system is essential to manage the bridge alignment under thermal effects. In conjunction with these change recommendations, design procedures are presented. Proposed detail in standard MDOT Bridge Design Guide format is presented in Appendix F. All the required formulations and variables are presented with the drawings. The rub plate design procedure was adopted from VDOT Bridge Design Manual section 20.04 (2010) with some modifications and presented in Appendix G.

Bridge expansion length, which is the distance along the longitudinal axis measured from abutment to the nearest fixed bearing, is a function of bridge length, width, and skew. Expansion joint effective movement rating and allowable movement at bearings are the limiting factors of bridge expansion length when link slabs are implemented. Based on maximum strip seal joint width of 3 in and expansion and contraction thermal load of 115 °F, the following maximum expansion length are recommended:

Straight concrete bridge ≤ 300 ft.

45° skew concrete bridge of 100 ft wide ≤ 200 ft.

Straight steel bridge ≤ 275 ft.

45° skew steel bridge of 100 ft wide ≤ 175 ft.

6.2.3 Semi-Integral Abutment

Changes are also proposed to semi-integral abutment details. These changes are necessary for managing bridge alignment. Details include the use of wingwalls and girder end restrains such as concrete keys with rub plates. Further, EPS layer is included behind the backwall to reduce passive pressure acting on the backwall. The EPS layer will help with reducing transverse forces on wingwalls and girder end restrains. It is also recommended that a 0.025

in. polyethylene sheet is provided underneath the approach to reduce frictional forces. Reducing frictional forces is necessary for preventing link slab cracking. Transverse force calculation on the wingwall is based on the procedure described in VDOT (2010). Proposed detail in standard MDOT Bridge Design Guide format is presented in Appendix H. The bridge expansion length limitations presented in section 6.2.2 are also valid when link slabs are implemented in semi-integral bridges.

6.3 IMPLEMENTATION PLAN

The focus of this work has been the investigation of the behavior and load demands on high skew link slab and jointless abutment configurations and to develop design modifications to the current link slab, bearing, wingwall, and other girder end restraint configurations. The abutment configurations were limited to those commonly used in Michigan, namely deck sliding over backwall and semi-integral abutments. Also, national and international best practices on controlling abutment distress in skew bridges were reviewed, and promising configurations and details were recommended.

Below, the required future work is outlined. Implementation of the following is required before incorporating the recommendations in MDOT specifications, manuals and guides.

- The proposed link-slab details and support configurations should be incorporated as a pilot implementation project. The implementation project needs to be monitored to document the behavior and performance in order to evaluate and fine-tune the proposed analysis and design procedures.
- An increase to bearing tolerances is recommended for the slot dimensions of the alignment pins. This recommendation is for reducing forces developed at the abutments under thermal expansion and contraction loads. A maximum tolerance limit of 0.25 in. was recommended after reviewing typical bearing details and specification requirements. Additional recommendations were also provided for reducing friction forces on the backwall and approach slab. Again, a pilot implementation project with monitoring that incorporate the recommended details for the abutment region is the next step.

7 REFERENCES

AASHTO (2010). *AASHTO LRFD Bridge Design Specifications*, Fifth Edition, Washington, DC, 20001.

AASHTO (2008). *AASHTO LRFD Bridge Construction Specifications*, Second Edition with 2008 Interims, Washington, DC, 20001.

Aktan, H.M., Attanayake, U., and Ulku, A. E. (2008) *Combining Link-Slab, Deck Sliding over Back-Wall and Revising Bearings*, MDOT RC-1514, Report to the Michigan Department of Transportation, Detroit, MI 48226.

Aktan, H., Koyuncu, Y., Rutyna, J., Ahlborn, T.M., & Kasper, J.M. (2002). *Causes and cures for prestressed concrete I-beam deterioration*, Research report RC-1412, Michigan Department of Transportation, Lansing, Michigan.

Badie, S. S., Tadros, M. K., and Pedersen, K. E. (2001). "Re-examination of I-Girder/Pier Connection Jointless Bridges." *PCI Journal*, Vol. 46, No. 2, pp. 62-74.

Burke, M. P., Jr., (1999). "Cracking of Concrete Decks and Other Problems with Integral-Type Bridges." *Transportation Research Record 1688*, Paper No. 99-0104, Transportation Research Board, Washington, D.C.

Burke, M. P., Jr. (1994a). "Semi Integral Bridges: Movements and forces." *Transportation Research Record 1460*, Transportation Research Board, Washington, D.C.

Burke, M.P., Jr. (1994b). "Semi-Integral Bridges: A Concept Whose Time Has Come?" *Continuous and Integral Bridges*, EAFN Spon, pp. 213-224.

Caner, A. and Zia, P. (1998). "Behavior and Design of Link Slab for Jointless Bridge Decks." *PCI Journal*, May-June 1998, pp. 68-80.

Chandra, V., et al. (1995). *Draft Report on Precast Prestressed Concrete Integral Bridges, State-of-the-Art*. Precast/Prestressed Concrete Institute, 113 pp.

Elragi, A.F. (2011). <http://www.softoria.com/institute/geofoam/material.html#36> (Last accessed May 26, 2011).

FHWA (2011). Rapid embankment construction: Expanded polystyrene (EPS) geofoam. <http://www.fhwa.dot.gov/bridge/abc/eps.cfm> (Last accessed May 27, 2011).

Frydenlund, T. E. and Aabøe, R. (2001). “Long term performance and durability of EPS as a lightweight filling material, EPS Geofoam.” *3rd International Conference*, Salt Lake City.

Gilani, A., and Jansson, D. (2004). *Link Slabs for Simply Supported Bridges: Incorporating Engineered Cementitious Composites*. Draft Report No. MDOT SPR-54181, Michigan Department of Transportation, Lansing, Michigan.

Hambly, E.C. (1991). *Bridge Deck Behavior*, Second Edition, Van Nostrand Reinhold, 115 5th Avenue, New York NY 10003.

Hoppe, E. J. (2005). *Field Study of Integral Backwall with Elastic Inclusion*. Research report VTRC 05-R28, Virginia Department of Transportation, Richmond, VA.

Hoppe, E. J. and Bagnall, T. M. (2008). *Performance of a Skewed Semi-Integral Bridge: Volume I: Field Monitoring*. Research report VTRC 08-R20, Virginia Department of Transportation, Richmond, VA.

Husain, I. and Bagnariol, D. (1999). *Semi-Integral Abutment Bridges*, Report BO-99-03, Ministry of Transportation, Ontario, Canada.

Lutenegger, A. J. and Ciufetti, M. (2009). *Full-Scale Pilot Study to Reduce Lateral Stresses in Retaining Structures Using GeoFoam*, Vermont Agency of Transportation, Materials and Research Section, Montpelier, VT.

Maruri, R., and Petro, S. (2005). “Integral Abutment and Jointless Bridges (IAJB) 2004 Service Summary.” *Proceedings of the IAJB 2005*, March 16-18 2005, Baltimore, Maryland.

MDOT (2006). *Bridge Design Guide*. Michigan Department of Transportation, Lansing, MI.

MDOT (2005). *Bridge Design Manual*. Michigan Department of Transportation, Lansing, MI.

MnDOT (2011). MnDOT Standard Plans, Minnesota Department of Transportation, MN.

Moorty, S., and Roeder, C. (1992). "Temperature-Dependent Bridge Movements." *Journal of Structural Engineering*, Vol. 118, No.4, pp. 1090-1105.

Menassa, C., Mabsout, M., Tarhini, K. and Frederick, G. (2007). "Influence of Skew Angle on Reinforced Concrete Slab Bridges." *Journal of Bridge Engineering*, Vol. 12, No. 2, pp. 205-214.

Nakai, H. and Yoo, C.H. (1988). *Analysis and design of curved steel bridges*, McGraw-Hill, New York, pp. 575.

Najm, H., Patel, R. and Nassif, H. (2007). "Evaluation of Laminated Circular Elastomeric Bearings." *Journal of Bridge Engineering*, Vol. 12, No. 1, pp. 89-97.

NCDOT (2007). <http://www.ncdot.org/doh/PRECONSTRUCT/highway/structur/springfield/2007/site2/default.html> (Accessed: March 2009).

Nicholson, B.A.; Barr, J.M.; Cooke, R.S.; Hickman, R.P.; Jones, C.J.F.P.; and Taylor, H.P.J., (1997). *Integral Bridges: Report of a Study Tour to North America*. Concrete Bridge Development Group, U.K., 93 pp.

Oesterle, R.G., Tabatabai, H., Lawson, T.J., Refai, T.M., Voltz, J.S., and Scanlon, A. (1999). *Jointless and Integral Abutment Bridges*. Summary Report, Final Report to Federal Highway Administration, Washington D.C.

Parke, G. A. R. and Hewson, N. R. (2008). *ICE Manual of Bridge Engineering, 2nd edition*, Thomas Telford, London.

Purvis, R. (2003). *Bridge Deck Joint Performance*. NCHRP Synthesis 319, Transportation Research Board, Washington, D.C.

Roeder, C. W. and Stanton, J. F. (1996). *Steel Bridge Bearing Selection and Design Guide, Highway Structures Design Handbook*, Vol. II, Chapter. 4, American Institute of Steel Construction, Inc., National Steel Bridge Alliance, Chicago, IL.

Romkema, M., Attanayake, U., and Aktan, H. (2010). *Incorporating link slabs in high skew bridges during repair activities - design recommendations*, Technical Report: CCE-10-01, Department of Civil and Construction Engineering, Western Michigan University, Kalamazoo, Michigan.

Sanford, T. C., and Elgaaly, M. (1993). "Skew Effects on Backfill Pressures at Frame Bridge Abutments." *Transportation Research Record*, 1415, Transportation Research Board, Washington, D.C., 1–10.

Stark, T. D., Arellano, D., Horvath, J. S. and Leshchinsky, D. (2004). *Geofoam Applications in the Design and Construction of Highway Embankments*, NCHRP Web Document 65 (Project 24-11), National Cooperative Highway Research Program, Transportation Research Board, Washington, DC 20008.

Steinberg, E. and Sargand, S. (2010). *Forces on Wingwalls from Thermal Expansion of Skewed Semi-Integral Bridges*, FHWA/OH-2010/16, Ohio Department of Transportation, Columbus, Ohio.

Steinberg, E., Sargand, H., and Bettinger, C. (2004). "Forces in Wingwalls of Skewed Semi-Integral Bridges." *Journal of Bridge Engineering*, Vol. 9, No. 6, pp.563-571.

Tabatabai, H., Oesterle, R.G., and Lawson, T.J. (2005). *Jointless Bridges, Experimental Research and Field Studies*. Volume I, Final Report to FHWA, August 2005.

Tindal, T.T. and Yoo, C.H., (2003). "Thermal Effects on Skewed Steel Highway Bridges and Bearing Orientation." *Journal of Bridge Engineering*, Vol. 8, No. 2, pp.57-65.

Ulku, E., Attanayake, U., and Aktan, H. M. (2009). "Jointless Bridge Deck with Link Slabs: Design for Durability," *Transportation Research Record: Journal of the Transportation*

Research Board, No. 2131, Transportation Research Board of the National Academies, Washington, D.C., pp. 68–78.

Van Lund, J., and Brecto, B. (1999). “Jointless Bridges and Bridge Deck Joints in Washington State.” *Transportation Research Record, 1688*, Transportation Research Board, Washington, D.C., 116–123.

VDOT (2010). *Structure and Bridge Manuals*, Virginia Department of Transportation, Richmond, VA.

Weakley, K. (2005). “VDOT Integral Bridge Design Guidelines.” *Proceedings of the IAJB 2005*, March 16-18 2005, Baltimore, Maryland.

Yazdani, N., and Green, T., (2000). *Effects of Boundary Conditions on Bridge Performance*. WPI# 0510843, March 2000, Tallahassee, FL.



MDOT RC-1563



High Skew Link Slab Bridge System with Deck Sliding over Backwall or Backwall Sliding over Abutments

FINAL REPORT – SEPTEMBER 2011
APPENDICES



Western Michigan University
Department of Civil & Construction Engineering
College of Engineering and Applied Sciences

RESEARCH

High Skew Link Slab Bridge System with Deck Sliding over Backwall or Backwall Sliding over Abutments (Appendices)

Project Manager: Mr. Steve Kahl, P.E.

Submitted to:



Submitted by

Dr. Haluk Aktan, P.E.
Professor & Chair
(269) – 276 – 3206
haluk.aktan@wmich.edu

Dr. Upul Attanayake, P.E.
Assistant Professor
(269) – 276 – 3217
upul.attanayake@wmich.edu



Western Michigan University
Department of Civil & Construction Engineering
College of Engineering and Applied Sciences
Kalamazoo, MI 49008
Fax: (269) – 276 – 3211

APPENDIX A - ACRONYMS AND ABBREVIATIONS

AASHTO - American Association of State Highway and Transportation Officials
AASHTO LRFD - American Association of State Highway and Transportation Officials
Load and Resistant Factor Design
CDP – Cotton duck pads
DOT – Department of Transportation
EPS - Expanded polystyrene
EVA - Ethylene vinyl acetate (commonly known as expanded rubber or foam rubber)
FE – Finite element
FHWA – Federal Highway Administration
FRP - Fiberglass-reinforced pad
MDOT – Michigan Department of Transportation
NCDOT – North Carolina Department of Transportation
NTG – Negative Temperature Gradient
OMOT – Ontario Ministry of Transportation
PC – Prestressed Concrete PCI
PEP - Plain elastomeric pad
PTFE – Polytetrafluorethylene
PTG – Positive Temperature Gradient
ROFP – Random oriented fiber pads
SHA – State Highway Agencies
SREB – Steel-reinforced elastomeric bearings
SREP – Steel-reinforced elastomeric pads
VDOT – Virginia Department of Transportation

Intentionally left blank

APPENDIX B

Table B-1. Longitudinal Bearing Translation over South Abutment (in.) – Loading Scenario I

Girder Label	FE Analysis	Tracker
A	-0.044	0.041
B	-0.042	-
C	-0.034	0.027
D	-0.025	-
E	-0.020	0.018
F	-0.018	-
G	-0.016	0.018

Table B-2. Girder Translations – Loading Scenario I

Measurement Point	FE Analysis (in.) ⁺			Tracker Measurement (in.) ⁺⁺		
	Longitudinal	Transverse	Vertical	Longitudinal	Transverse	Vertical
R1	-0.016	0.024	-0.004	0.008	-0.007	0.001
R2	-0.019	0.047	-0.091	0.012	-0.031	0.060
R3	-0.026	0.062	-0.306	0.023	-0.040	0.194
R4	-0.015	0.026	-0.018	0.009	-0.010	0
R5	-0.015	0.034	-0.070	0.009	-0.020	0.036
R6	-0.010	0.058	-0.186	0.003	-0.041	0.115
R7	-0.003	0.067	-0.372	0.001	-0.044	0.242
R8	-0.013	0.016	-0.032	0.007	-0.007	0
R9	-0.010	0.020	-0.066	0.005	-0.012	0.025
R10	-0.003	0.031	-0.141	-0.004	-0.022	0.082
R11	0.012	0.043	-0.277	-0.016	-0.036	0.188
R12	-0.009	0.002	-0.032	0.006	-0.002	-0.003
R13	-0.003	0.003	-0.049	0	-0.003	0.016
R14	0.013	0.006	-0.110	-0.021	-0.009	0.084

+ Refer FE model coordinates (Figure 3-14)

++ Refer Tracker measurement coordinates (Figure 3-32)

Table B-3. Longitudinal Bearing Translation over South Abutment (in.) – Loading Scenario II

Girder Label	FE Analysis	Tracker
A	-0.086	0.088
B	-0.083	-
C	-0.071	0.065
D	-0.056	-
E	-0.047	0.045
F	-0.041	-
G	-0.036	0.040

Table B-4. Girder Translations – Loading Scenario II

Measurement Point	FE Analysis (in.) ⁺			Tracker Measurement (in.) ⁺⁺		
	Longitudinal	Transverse	Vertical	Longitudinal	Transverse	Vertical
R1	-0.037	0.062	-0.007	0.032	-0.029	0.014
R2	-0.046	0.103	-0.199	0.038	-0.071	0.163
R3	-0.062	0.122	-0.571	0.060	-0.080	0.406
R4	-0.035	0.068	-0.037	0.029	-0.033	0.021
R5	-0.035	0.085	-0.161	0.027	-0.053	0.105
R6	-0.029	0.135	-0.414	0.021	-0.096	0.298
R7	-0.023	0.142	-0.762	0.021	-0.090	0.528
R8	-0.030	0.042	-0.070	0.026	-0.023	0.011
R9	-0.025	0.053	-0.154	0.017	-0.035	0.074
R10	-0.010	0.083	-0.336	-0.001	-0.057	0.227
R11	0.015	0.099	-0.637	-0.018	-0.073	0.452
R12	-0.020	0.006	-0.072	0.018	-0.006	-0.002
R13	-0.009	0.012	-0.117	0.004	-0.007	0.046
R14	0.027	0.019	-0.274	-0.040	-0.018	0.204

+ Refer FE model coordinates (Figure 3-14)

++ Refer Tracker measurement coordinates (Figure 3-32)

Table B-5. Longitudinal Bearing Translation over South Abutment (in.) – Loading Scenario III

Girder Label	FE Analysis	Tracker
A	-0.014	0.073
B	-0.018	-
C	-0.024	0.070
D	-0.033	-
E	-0.046	0.068
F	-0.063	-
G	-0.086	0.083

Table B-6. Girder Translations – Loading Scenario III

Measurement Point	FE Analysis (in.) ⁺			Tracker Measurement (in.) ⁺⁺		
	Longitudinal	Transverse	Vertical	Longitudinal	Transverse	Vertical
R1	-0.072	-0.056	-0.344	0.072	0.015	0.171
R2	-0.028	-0.050	-0.125	0.054	0.012	0.084
R3	-0.011	-0.037	-0.015	0.053	0.003	0.051
R4	-0.045	-0.090	-0.528	0.046	0.041	0.239
R5	-0.028	-0.092	-0.286	0.042	0.040	0.129
R6	-0.016	-0.064	-0.104	0.043	0.016	0.054
R7	-0.010	-0.050	-0.015	0.046	0.006	0.035
R8	-0.016	-0.082	-0.482	0.024	0.043	0.192
R9	-0.012	-0.085	-0.260	0.027	0.043	0.081
R10	-0.011	-0.061	-0.101	0.035	0.023	0.011
R11	-0.008	-0.049	-0.012	0.037	0.007	-0.005
R12	-0.001	-0.043	-0.274	0.006	0.035	0.053
R13	-0.004	-0.039	-0.092	0.023	0.027	0
R14	-0.005	-0.027	-0.009	0.021	0.009	-0.035

+ Refer FE model coordinates (Figure 3-14)

++ Refer Tracker measurement coordinates (Figure 3-32)

Table B-7. Longitudinal Bearing Translation over South Abutment (in.) – Loading Scenario IV

Girder Label	FE Analysis	Tracker
A	-0.030	0.103
B	-0.037	-
C	-0.048	0.102
D	-0.064	-
E	-0.085	0.113
F	-0.113	-
G	-0.152	0.149

Table B-8. Girder Translations – Loading Scenario IV

Measurement Point	FE Analysis (in.) ⁺			Tracker Measurement (in.) ⁺⁺		
	Longitudinal	Transverse	Vertical	Longitudinal	Transverse	Vertical
R1	-0.132	-0.088	-0.565	0.139	0.032	0.325
R2	-0.055	-0.077	-0.220	0.099	0.026	0.170
R3	-0.024	-0.063	-0.041	0.090	0.014	0.135
R4	-0.093	-0.148	-0.903	0.098	0.073	0.456
R5	-0.057	-0.145	-0.494	0.089	0.072	0.241
R6	-0.034	-0.102	-0.197	0.081	0.035	0.111
R7	-0.020	-0.081	-0.048	0.079	0.019	0.076
R8	-0.044	-0.143	-0.891	0.049	0.075	0.385
R9	-0.031	-0.147	-0.476	0.056	0.085	0.177
R10	-0.023	-0.100	-0.192	0.059	0.044	0.045
R11	-0.016	-0.079	-0.042	0.060	0.020	0.010
R12	-0.008	-0.080	-0.544	0.014	0.064	0.141
R13	-0.010	-0.074	-0.175	0.043	0.050	-0.033
R14	-0.010	-0.044	-0.028	0.046	0.014	-0.070

+ Refer FE model coordinates (Figure 3-14)

++ Refer Tracker measurement coordinates (Figure 3-32)

APPENDIX C

DESIGN PROCEDURE FOR LINK SLABS

OVERVIEW

AASHTO LRFD (2010) requires combined live and thermal load effects for the service limit state design. The Design Procedure described in the appendix will follow the rationale developed by Ulku et al. (2009). Link slab design moments are calculated using the girder end rotations. HL-93 loading is used to calculate the girder end rotations under live load. Girder end rotations caused by the temperature gradient are calculated using the procedure described by Saadeghvaziri and Hadidi (2002) by ensuring strain and curvature compatibility among sections and reinforcements.

One major improvement in the process presented in this appendix compared to what is given in Ulku et al. (2009) is the inclusion of 3D and skew effects to calculate the resultant link slab design moments and forces.

In order to apply loading, the first step is to establish a composite girder-deck cross-section with an effective width as per AASHTO LRFD (2010) Section 4.6.2.6, the composite moment of inertia, and the modulus of elasticity for concrete.

Girder End Rotations due to Live Load

AASHTO LRFD (2010) procedures can be followed without considering the effects of the link slab.

- Apply HL-93 loading [HS-20 truck with impact and distribution factor (LRFD section 3.6.2.1 and 4.6.2.2.2) + 0.64 kips/ft lane loading (LRFD 3.6.1.2.4)] on the simply supported spans to compute maximum girder end rotations.

Girder End Rotations due to Temperature Gradient

Girder end rotations caused by the temperature gradient are calculated following the procedure described by Saadeghvaziri and Hadidi (2002).

The girder-deck composite cross-section is subjected to the temperature gradient as described in AASHTO LRFD section 3.12.3 (Figure C-1).

Figure C-2 illustrates the compatibility forces and moments developed in the sections and the temperature gradient profile along the cross-section height.

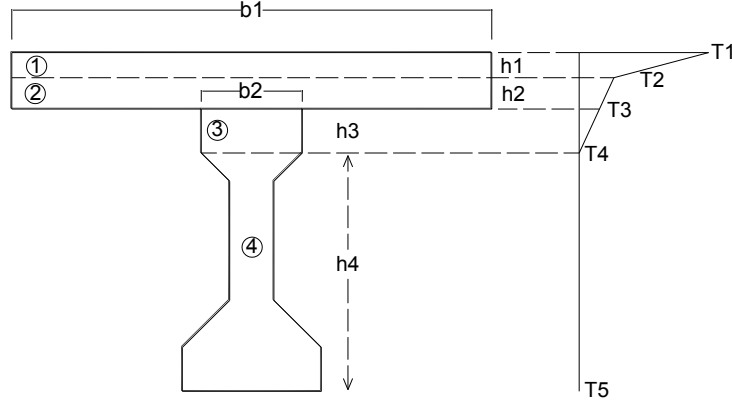


Figure C-1. Temperature profile along cross-section

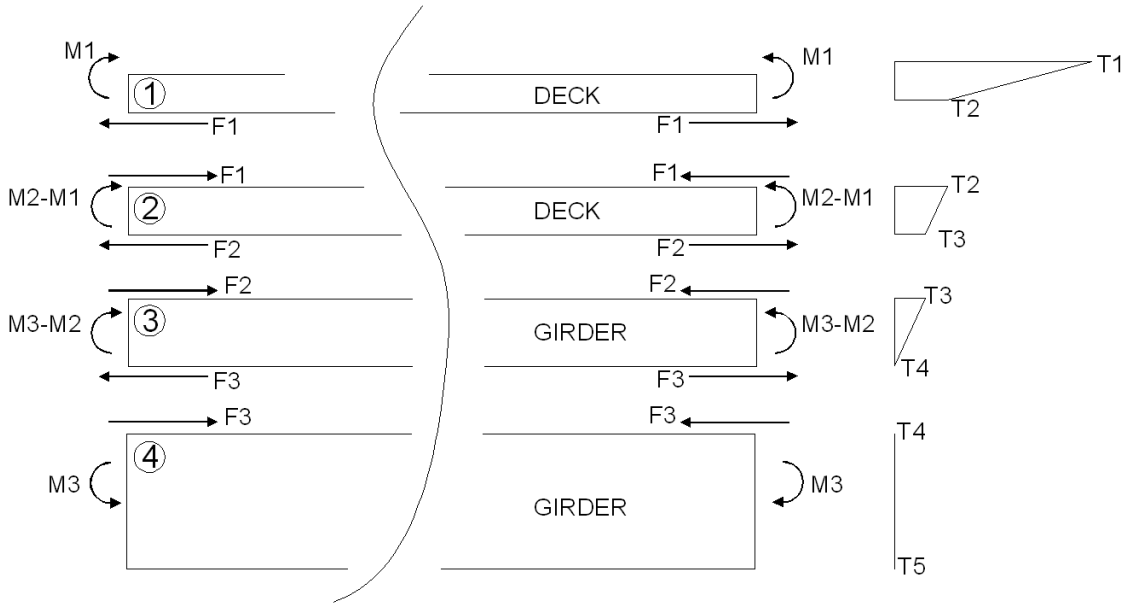


Figure C-2. Compatibility forces and moments and temperature profile along cross-section height

Strain Compatibility

For strain compatibility between sections 1 and 2 (ignoring reinforcement contribution);

$$\begin{aligned}\varepsilon_{Bottom1} &= \alpha_1(T_2) + \frac{M_1}{E_1 S_{b1}} + \frac{F_1}{E_1 A_1} + \frac{F_1 d_{b1}}{E_1 S_{b1}} = \varepsilon_{Top2} \\ \varepsilon_{Top2} &= \alpha_2(T_2) + \frac{M_2 - M_1}{E_2 S_{t2}} + \frac{F_2 - F_1}{E_2 A_2} + \frac{F_2 d_{b2} + F_1 d_{t2}}{E_2 S_{t2}}\end{aligned}\quad (C-1)$$

For strain compatibility between sections 2 and 3;

$$\varepsilon_{Bottom2} = \alpha_2(T_3) + \frac{M_2 - M_1}{E_2 S_{b2}} + \frac{F_2 - F_1}{E_2 A_2} + \frac{F_2 d_{b2} + F_1 d_{t2}}{E_2 S_{b2}} = \varepsilon_{Top3}$$

$$\varepsilon_{Top3} = \alpha_3(T_3) + \frac{M_3 - M_2}{E_3 S_{t3}} + \frac{F_3 - F_2}{E_3 A_3} + \frac{F_3 d_{b3} + F_2 d_{t3}}{E_3 S_{t3}} \quad (C-2)$$

For strain compatibility between sections 3 and 4;

$$\begin{aligned} \varepsilon_{Bottom3} &= \alpha_3(T_4) + \frac{M_3 - M_2}{E_3 S_{b3}} + \frac{F_3 - F_2}{E_3 A_3} + \frac{F_3 d_{b3} + F_2 d_{t3}}{E_3 S_{b3}} = \varepsilon_{Top4} \\ \varepsilon_{Top4} &= \alpha_4(T_4) - \frac{M_3}{E_4 S_{t4}} - \frac{F_3}{E_4 A_4} + \frac{F_3 d_{t4}}{E_4 S_{t4}} \end{aligned} \quad (C-3)$$

Curvature Compatibility

For curvature compatibility between sections 1 and 2;

$$\begin{aligned} \frac{1}{R_1} &= \alpha_1 \left(\frac{T_2 - T_1}{h_1} \right) + \frac{M_1}{E_1 I_1} + \frac{F_1 d_{b1}}{E_1 I_1} = \frac{1}{R_2} \\ \frac{1}{R_2} &= \alpha_2 \left(\frac{T_3 - T_2}{h_2} \right) + \frac{M_2 - M_1}{E_2 I_2} + \frac{F_1 d_{t2} + F_2 d_{b2}}{E_2 I_2} \end{aligned} \quad (C-4)$$

For curvature compatibility between sections 2 and 3;

$$\begin{aligned} \frac{1}{R_2} &= \alpha_2 \left(\frac{T_3 - T_2}{h_2} \right) + \frac{M_2 - M_1}{E_2 I_2} + \frac{F_1 d_{t2} + F_2 d_{b2}}{E_2 I_2} = \frac{1}{R_3} \\ \frac{1}{R_3} &= \alpha_3 \left(\frac{T_4 - T_3}{h_3} \right) + \frac{M_3 - M_2}{E_3 I_3} + \frac{F_2 d_{t3} + F_3 d_{b3}}{E_3 I_3} \end{aligned} \quad (C-5)$$

For curvature compatibility between sections 3 and 4;

$$\begin{aligned} \frac{1}{R_3} &= \alpha_3 \left(\frac{T_4 - T_3}{h_3} \right) + \frac{M_3 - M_2}{E_3 I_3} + \frac{F_2 d_{t3} + F_3 d_{b3}}{E_3 I_3} = \frac{1}{R_4} \\ \frac{1}{R_4} &= \alpha_4 \left(\frac{T_5 - T_4}{h_4} \right) - \frac{M_3}{E_4 I_4} + \frac{F_3 d_{t4}}{E_4 I_4} \end{aligned} \quad (C-6)$$

where

α_i : Coefficient of thermal expansion for Section i

T_i : Girder and deck temperature changes as given in Figure C-1 and Figure C-2

F_i : Force resultant of stresses between section i and i+1

M_i : Moment resultant of stresses between section i and i+1

d_{bi} : Distance from centroid to bottom fiber of Section i

d_{ti} : Distance from centroid to top fiber of Section i

S_{bi} : Bottom section modulus for Section i

S_{ti} : Top section modulus for Section i

E_i : Modulus of elasticity of Section i

A_i : Cross-sectional area of Section i

I_i : Moment of inertia of Section i

Solving the above six simultaneous equations for six unknowns ($F_1, F_2, F_3, M_1, M_2, M_3$), corresponding strain and curvature values can be obtained.

More details including the effect of reinforcement and some other boundary conditions can be found at Saadeghvaziri and Hadidi (2002).

Once the curvature is known, end-slopes can be obtained by integrating curvature along the length;

$$\frac{d\theta}{dx} = \frac{1}{R_1} = \frac{1}{R_2} = \frac{1}{R_3} = \frac{1}{R_4} = \frac{1}{R} \quad \theta(x) = \int \frac{1}{R} dx = \frac{x}{R} + C_1 \quad (\text{C-7})$$

For a simply supported span with length L, since the slope at mid-span will be equal to zero under gradient loading, integration constant C_1 can be calculated as;

$$\theta\left(\frac{L}{2}\right) = \frac{L}{2R} + C_1 = 0 \quad C_1 = -\frac{L}{2R} \quad (\text{C-8})$$

Then, the slope equation and the slope at the end will be equal to;

$$\theta(x) = \frac{x}{R} - \frac{L}{2R} \quad \theta(L) = \frac{L}{R} - \frac{L}{2R} = \frac{L}{2R} \quad (\text{C-9})$$

Link slab moments can be calculated using Eq. C-10 once the girder end rotations are calculated under live and thermal gradient loads.

$$M_a = \frac{2E_c I_d \theta}{L_L} \quad (\text{C-10})$$

where,

I_d : Moment of inertia of the link slab

L_L : Length of the link slab (Debond zone length: sum of 5 % of each adjacent girder span + gap between beam ends)

DESIGN AXIAL FORCE

Axial force for the RHHR support condition can be calculated using a two-span-continuous model and neglecting the effects of debonding.

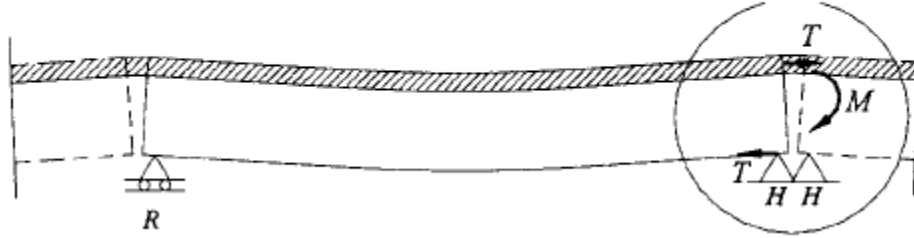


Figure C-3. Effect of RHHR type support condition on continuity (Okeil and El-Safty 2005)

For a two-span system with RHHR boundaries, tensile force developed in the link slab would be equal to the horizontal reactions at the interior supports, and this reaction is equal to the continuity moment divided by the distance between the centroid of deck and bearing location (Figure C-3).

Continuity Moment due to Live Load

Under live load, each span is loaded so as to create maximum negative moment at the interior support (Figure C-4) with composite cross-section properties and neglecting debonding.

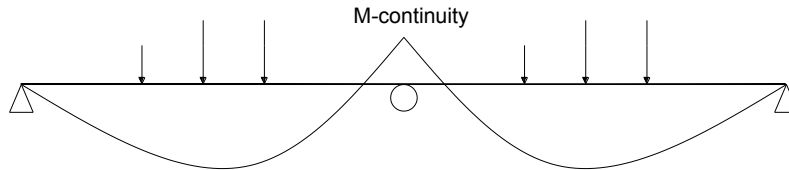


Figure C-4. Continuity moment at the interior support under live load

Continuity Moment due to Temperature Gradient

The continuity moment under temperature gradient loading can be calculated using the superposition concept as given in Saadeghvaziri and Hadidi (2002). For a two-span-continuous system with constant cross-section in both spans, continuity moment $M_{continuity}$ can be calculated as;

$$M_{continuity} = \frac{(F_2 d_{tg} - M_3)(3E_{Composite} I_{Composite})}{2E_{Girder} I_{Girder}} \quad (C-11)$$

where

F_2 : Force resultant of stresses between section 2 and 3 calculated from six simultaneous equations

M_3 : Moment resultant of stresses between section 2 and 3 calculated from six simultaneous equations

d_{tg} : Distance from centroid to top fiber of girder

$E_{Composite}$: Modulus of elasticity of composite section

$I_{Composite}$: Moment of inertia of composite section

E_{Girder} : Modulus of elasticity of girder

I_{Girder} : Moment of inertia of girder

Once the continuity moment is found, tensile force in the link slab is;

$$T = \frac{M_{continuity}}{h} \quad (C-12)$$

where, h is the distance between the centroid of deck and bearing location.

Numerical Example – Skew Link slab Design

STEP 1: Material and Geometric Properties

Cross-section properties of the girder and the composite section are given in Figure C-5.

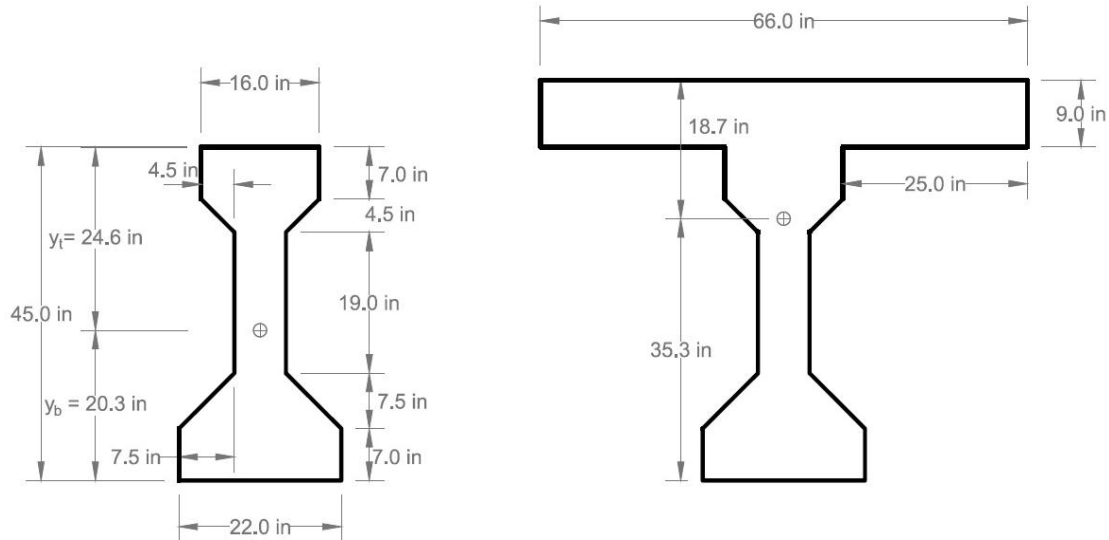


Figure C-5. Girder and composite section geometric properties

Boundary condition	RHHR
Skew (θ)	45^0
Compressive strength of concrete (f'_c)	4,500 psi
Unit weight of concrete (w_c)	0.15 kcf
Concrete modulus of elasticity (E_c) (AASHTO LRFD Section 5.4.2.4)	4,067 ksi
Reinforcement yield strength (f_y)	60 ksi
Steel modulus of elasticity (E_s)	29,000 ksi
Link slab length (L_{LS}) ⁺	84.4 in.
Effective deck width (B) ⁺⁺	66 in.
Link slab thickness	9 in.
Moment of inertia of link slab (I_{LS})	$4,009.5 \text{ in}^4$
Deck overhang (on either side of the beam)	25 in.
Moment of inertia of the composite section ($I_{composite}$)	$375,678 \text{ in}^4$

+ Link slab length = $69.5 \times 12 \times 5\% \times 2 + 1 \text{ in. gap} = 84.4 \text{ inches}$

++ Link slab section perpendicular to bridge longitudinal axis is considered in the example because design moments are calculated perpendicular to bridge longitudinal axis.

STEP 2: Design Moments

Step 2.1: Live Load Moment

HL-93 (AASHTO LRFD 2010) loading is applied at a location to create maximum end rotation on the 69.5 ft span of the bridge. The impact factor is taken as 1.33 from Section 3.6.2.1 of AASHTO LRFD (2010). As per Section 3.6.1.3 AASHTO LRFD (2010), a lane load of 0.64 k/ft is used in addition to the axle loads. Girder end rotation under HL-93 loading is 3.47×10^{-3} radians. The distribution factor is calculated as 0.508 assuming two or more lanes are loaded from the formulation in AASHTO LRFD (2010) Table 4.6.2.2.2b-1.

The maximum girder-end design rotation is calculated as 1.763×10^{-3} radians when the front axle is located 18.4 feet away from the end of the span.

Moment induced by live load =

$$M_a = (2E_c I_d \theta) / L_L = (2 \times 4067 \times 4009.5 \times 0.001763) / (84.4 \times 12) = -56.77 \text{ ft-kips OR}$$

For a 66 in. wide effective section

$$M_a = \frac{2E_c I_d \theta}{L_L} = \frac{2 \times 4067 \times 4009.5 \times 0.001763}{84.4 \times 12 \times (66/12)} = -10.32 \text{ ft-kips/ft}$$

Step 2.2: Moment due to Temperature Gradient Loading

Required information, solutions to simultaneous equations, curvature, girder end rotation, and moments due to temperature gradient loads are presented in chapter 4 and Appendix D.

Moment induced by positive temperature gradient (PTG):

$$M_a = (2E_c I_d \theta) / L_L = (2 \times 4067 \times 4009.5 \times 1.613 \times 10^{-3}) / (84.4 \times 12) = 51.9 \text{ ft-kips OR}$$

For a 66 in. wide effective section

$$M_a = \frac{2E_c I_d \theta}{L_L} = \frac{2 \times 4067 \times 4009.5 \times 1.613 \times 10^{-3}}{84.4 \times 12 \times (66/12)} = 9.44 \text{ ft-kips/ft}$$

Moment caused by negative thermal gradient (NTG) is -0.3 times the positive gradient loading.

$$M_a = 51.9 \times -0.3 = -15.57 \text{ ft-kips OR}$$

For a 66 in. wide effective section

$$M_a = 15.57/(66/12) = -2.83 \text{ ft-kips/ft}$$

The following table summarizes the moments calculated in step 2.1 and 2.2.

Table C-1 Summary of Analytical Girder End Rotations and Analytical Design Moments

Load Case	Analytical Rotation Magnitude (Radians) (a)	Distribution Factor (b)	Analytical Design Rotation Magnitude (Radians) (c) = (a) × (b)	Analytical Design Moment ⁺ (k-ft)/ft (d)
Live	0.003470	0.508	0.001763	-10.32
PTG	0.001613	N/A	0.001613	9.44
NTG	0.000484	N/A	0.000484	-2.83

+ Negative moments cause tension at link slab top fiber. Sign convention is stated in chapter 4

Step 2.3: Moment Reduction due to 3D Effect

AASHTO LRFD (2010) distribution factors are to incorporate 3D effect on load distribution and to find the girder design moments. The following table shows ratios of link slab moments calculated from 3D FE analysis of the specific straight bridge configuration described in chapter 4 of the report to analytical design moments summarized in the above table (i.e., moments calculated in step 2.1 and 2.2). HRRR, RRHR, and RHHH represent different support configurations of a two-span bridge (H-hinge or fixed bearing, R- roller or expansion bearing; HRRR represents expansion bearings underneath the link slab). It is seen that there is a significant reduction in link slab moments based on support configuration and the type of load acting on the bridge. Further, there are no load distribution factors given in AASHTO LRFD (2010) for thermal loads.

Table C-2. Ratios of 3D FE to Analytical Design Moment for a Straight Bridge

Load Case	HRRR	RRHR	RHHH
Live	0.218	0.257	0.887
PTG	0.092	0.111	0.967
NTG	0.080	0.100	0.961

Table C-3. Link Slab Design Moment for a Straight Bridge with RHHH

Load Case	Moment Ratio (a)	Analytical Design Moment (k-ft)/ft (b)	Link Slab Design Moment (k-ft)/ft (c) = a×b
Live	0.887	-10.32	-9.2
PTG	0.967	9.44	9.1
NTG	0.961	-2.83	-2.7

Step 2.4: Moment Reduction due to Skew Effect (Skew Reduction Factors)

Table C-4. Skew Reduction Factors for RHHR

Skew (Degree)	Ratio of Maximum Link-Slab Effective Moment (Skew/Zero Skew) (Skew Reduction Factors)					
	Lane 1 (a)	Lane 2 (b)	Lane Alt 1 (c)	Lane Alt 2 (d)	NTG (e)	PTG (f)
0	1.00	1.00	1.00	1.00	1.00	1.00
20	0.96	0.96	0.97	0.95	≈ 1.00	≈ 1.00
30	0.91	0.90	0.91	0.89	≈ 1.00	≈ 1.00
45	0.77	0.74	0.76	0.72	≈ 1.00	≈ 1.00

Analysis results presented in chapter 4 of the report demonstrated that the *Lane 2* load is the governing live load case. There is no increase or reduction in moments developed in a skew link slab under NTG or PTG for RHHR support configurations; however, there are skew reduction/amplification factors for other support configurations.

The design example is for a 45⁰ skew bridge. Hence, live load moment shall be multiplied by 0.74, and there is no reduction for NTG or PTG moments.

Table C-5. Link Slab Design Moment for Skew Bridge with RHHR

Load Case	Link Slab Design Moment of a Straight Bridge (k-ft)/ft (a)	Skew Reduction Factor (b)	Link Slab Design Moment of a Skew Bridge (k-ft)/ft (c) = a×b
Live	-9.2	0.74	-6.8
PTG	9.1	1.00	9.1
NTG	-2.7	1.00	-2.7

Step 2.5: Resultant Combined Moments

Thermal gradient loading [i.e., NTG and PTG] and live load need to be combined to create critical load combinations. The following load combinations are developed as per AASHTO LRFD (2010) section 3.4. AASHTO LRFD (2010) service 1 load combination requires using load factor of 1.0 for the temperature gradient when the live load is not considered. Exclusion of live load when PTG effect is used in the design yields the critical load combination for positive moment. Hence, it is recommended to use factor of 1.0 for PTG loads.

Service I-Negative Moment: 1.0 Live Load + 0.5 NTG

Service I-Positive Moment: 1.0 PTG

Service I-Negative Moment:

$$M_{SI-N} = -6.8 + 0.5 \times -2.7 = -8.15 \text{ ft-kips/ft}$$

Service I-Positive Moment:

$$M_{SI-P} = 9.1 = 9.1 \text{ ft-kips/ft}$$

Step 2.6: Cracking Moment

Note: Cracking moment calculated using modulus of rupture of $0.24\sqrt{f'_c}$, *ksi* is less than both M_{SI-N} and M_{SI-P} . Hence, the links slab cracks and the amount of top and bottom layer reinforcement should be calculated using M_{SI-N} and M_{SI-P} , respectively. Detailed example of calculating link slab top and bottom layer reinforcement is provided in Ulku et al. (2009). The amount of reinforcement calculated from these two moments is less than the minimum reinforcement required in AASHTO LRFD section 5.4.2.6. Hence, the minimum reinforcement calculation process as per AASHTO LRFD section 5.4.2.6 is presented here.

Modulus of rupture of 4500 psi strength concrete for calculating the minimum reinforcement

$$f_r = 785 \text{ psi } (0.37\sqrt{f'_c}, \text{ ksi}) \text{ and}$$

Cracking moment

$$M_{cr} = S_c(f_r + f_{cpe}) - M_{dnc} \left(\frac{S_c}{S_{nc}} - 1 \right) \geq S_c f_r$$

M_{dnc} - Total unfactored dead load moment acting on the link slab that can be eliminated by considering casting sequence of the link slab (e.g., in retrofit applications expansion joint is removed and link slab is replaced).

f_{cpe} - compressive stress in concrete due to effective prestress forces which is zero in this example because there is no prestress forces in the link slab.

S_c - section modulus of the link slab (I_g / y_t)

I_g - moment of inertia of the gross section

y_t - distance from the neutral axis to the extreme tension fiber

Considering a 9 in. thick, 12 in. wide link slab section;

$$I_g = 12 \times 9^3 / 12 = 729 \text{ in}^4$$

$$y_t = 4.5 \text{ in.}$$

Cracking moment of 9 in. thick, 12 in. wide link slab section;

$$M_{cr} = S_c f_r = 10.6 \text{ ft-kips / ft}$$

Step 2.7: Minimum Flexural Reinforcement

AASHTO LRFD (2010) section 5.7.3.3.2 requires providing adequate steel to develop a factored flexural resistance (M_r) equal to the lesser of $1.2 \times M_{cr}$ or $1.33 \times$ (factored moment required by the applicable strength load combinations).

$$1.2 \times M_{cr} = 1.2 \times 10.6 \text{ ft-kips / ft} = 12.72 \text{ ft-kips / ft}$$

AASHTO LRFD (2010) recommends using a zero (0) load factor for the thermal load gradient when a Strength I combination is used. Hence, “1.33×(the factored moment required by the applicable strength load combinations)” always yields negative moments. For negative moment at the link slab;

$$1.33 \times (1.75 \times -6.8 + 0.0 \times -2.7) = -15.83 \text{ ft-kips / ft}$$

When the specification requirements are considered, calculation of amount of minimum negative moment reinforcement (top reinforcement) is governed by $M_r = 1.2 \times M_{cr} = 12.72$ ft-kips/ft.

AASHTO LRFD section 5.7.3.3.2 requirement of “1.33×(the factored moment required by the applicable strength load combinations)” never yield a positive moment to calculate positive moment reinforcement (i.e., link slab bottom reinforcement). Also, $M_{SI-P} < M_{cr}$.

Hence, using $M_r = 1.2 \times M_{cr} = 12.72$ ft-kips/ft is recommended for calculating positive moment reinforcement.

Step 2.7.1 Negative Moment Reinforcement (i.e., top fiber in tension)

The minimum amount of steel reinforcement is calculated considering 40% of the yield strength, $j \approx 0.9$, and $d = 6.375$ in.

Effective depth (d) is calculated assuming #6 bars are used as the transverse reinforcement in the deck and the clear cover to the top transverse bar is 3 in.

$$d = (\text{link slab thickness}) - (\text{clear cover to transverse rebar}) + (0.5 \times \text{diameter of \#6 bar})$$

$$d = 9 \text{ in.} - 3 \text{ in.} + 0.5 \times 0.75 \text{ in.} = 6.375 \text{ in.}$$

$$A_{\text{steel}} = M_r / (0.4 f_y j d) = (12.72 \text{ ft-kips/ft}) \times 12 / (0.4 \times 60 \text{ ksi} \times 0.9 \times 6.375 \text{ in.})$$

$$= 1.11 \text{ in}^2/\text{ft}$$

$$\text{Use \#6 bars @ 4 in.} = A_{\text{steel}} = 1.32 \text{ in.}^2 > 1.11 \text{ in.}^2$$

Step 2.7.2 Positive Moment Reinforcement (i.e., bottom fiber in tension)

The amount of steel reinforcement is calculated considering 40% of the yield strength, $j \approx 0.9$, and $d = 6.75$ in.

Effective depth (d) is calculated assuming #6 bars are used as the transverse reinforcement in the deck and the distance from bottom surface to the centerline of the bottom transverse bar is 1.5 in.

$d = (\text{link slab thickness}) - (\text{cover to centerline of transverse rebar}) - (\text{diameter of \#6 bar})$
 $d = 9 \text{ in.} - 1.5 \text{ in.} - 0.75 \text{ in.} = 6.75 \text{ in.}$

$$A_{\text{steel}} = M_r / (0.4f_y j d) = (12.72 \text{ ft-kips/ft}) \times 12 / (0.4 \times 60 \text{ ksi} \times 0.9 \times 6.75 \text{ in.})$$

$$= 1.05 \text{ in}^2/\text{ft}$$

$$\text{Use \#6 bars @ 4 in.} = A_{\text{steel}} = 1.32 \text{ in}^2 > 1.05 \text{ in}^2$$

Step 2.7.3 Steel Stress and Crack Width Parameter Limits

Section 5.7.3.4 *Control of Cracking by Distribution of Reinforcement* is not discussed here because the amount of reinforcement provided satisfies crack width limit criterion. Please refer Ulku et al. (2009) for the detailed procedure.

STEP 3: Design Axial Force

Step 3.1: Axial Force due to Live Load

For an RHR boundary condition, the axial force in the link slab needs to be calculated using the maximum negative moment at the interior support of a two-span continuous system. HL-93 (AASHTO LRFD 2010) loading is applied at both spans to create a maximum negative moment of -724 ft-kips at the interior support.

Axial force (F) acting on the link slab due to HL-93 loading:

$$F = \frac{M_{\text{continuity}}}{h} = \frac{-724 \times 12}{(54 - 9/2)} = -176 \text{ kips or } -27.8 \text{ kips/ft} \quad (\text{Tension})$$

Step 3.2: Axial Force due to PTG

Axial force acting on the link slab due to positive temperature gradient:

$$M_{\text{continuity}} = [(F_2 d_{tg} - M_3)(3E_{\text{composite}} I_{\text{composite}})] / (2E_{\text{girder}} I_{\text{girder}})$$

$$= [(25.257 \times 24.73 + 31.742) \cdot (3 \times 4067 \times 375,678)] / (2 \times 4067 \times 125,390)$$

$$= 2,950 \text{ in-kips}$$

$$F = M_{\text{continuity}} / h = 2950 / (54 - 9/2) = 60 \text{ kips or } 11 \text{ kips/ft} \quad (\text{compression})$$

Note that F_2 is the force at layer 2, d_{tg} is the distance from girder top to the girder centroid, and M_3 is the moment at layer 3. F_2 and M_3 calculation is given in MathCAD sheet provided in Appendix D.

Step 3.3: Axial Force due to NTG

Axial force acting on the link slab due to negative temperature gradient:

$$T_{NG} = -0.3T_{PG} = -0.3 \times 60 = 18 \text{ kips} \quad \text{or} \quad -3.2 \text{ kips/ft} \quad (\text{Tension})$$

Step 3.4: 3D and Skew Effects on Axial Force

3D and skew effects discussed in *Step 2.3* and *2.4* can be directly applied to calculate axial load in a skew link slab due to similarities in moment and force ratios. (See chapter 4 of the report for further details.)

Table C-6. Link Slab Design Force for Straight Bridge with RHHR

Load Case	Design Force Ratio (a)	Analytical Design Force (kips)/ft (b)	Link Slab Design Force of a Straight Bridge (kips)/ft (c) = a×b
Live	0.887	-27.8	-24.7
PTG	0.967	11.0	10.6
NTG	0.961	-3.2	-3.1

Table C-7. Link Slab Design Force for Skew Bridge with RHHR

Load Case	Link Slab Design Force of a Straight Bridge k/ft (a)	Skew Reduction Factor (b)	Link Slab Design Force of a Skew Bridge k/ft (c) = a×b
Live	-24.7	0.74	-18.3
PTG	10.6	1.00	10.6
NTG	-3.1	1.00	-3.1

Step 3.4: Resultant Combined Forces

Thermal gradient loading [i.e., NTG and PTG] and live load need to be combined to create critical load combinations.

Service I-Negative Force: 1.0 Live Load + 0.5 NTG

Service I-Positive Force: 1.0 PTG

Service I-Negative force:

$$F_{SI-N} = -18.3 + 0.5 \times -3.1 = -19.85 \text{ kips/ft}$$

Service I-Positive Force:

$$F_{SI-P} = 10.6 = 10.6 \text{ kips/ft}$$

Step 3.5: Check for Axial Load Capacity

$$\text{Steel area provided in the link-slab} = 0.88 \text{ in}^2 + 0.88 \text{ in}^2 = 1.76 \text{ in}^2/\text{ft}$$

Assuming steel carries the total axial load

$$f_{steel} = (19.45 \text{ kips/ft}) / (1.76 \text{ in}^2/\text{ft}) = 11.05 \text{ ksi} < f_{sa} = 0.6 \times 60 \text{ ksi} = 36 \text{ ksi OK.}$$

STEP 4: Moment-Force Interaction

Load Combination	Moment (from Step 2) ft-kips/ft	Axial Force (from Step 3) kips/ft
Service I - Positive	9.1 (i.e., top fiber compression)	10.60 (Compression)
Service I - Negative	8.15 (i.e., top fiber tension)	19.85 (Tension)

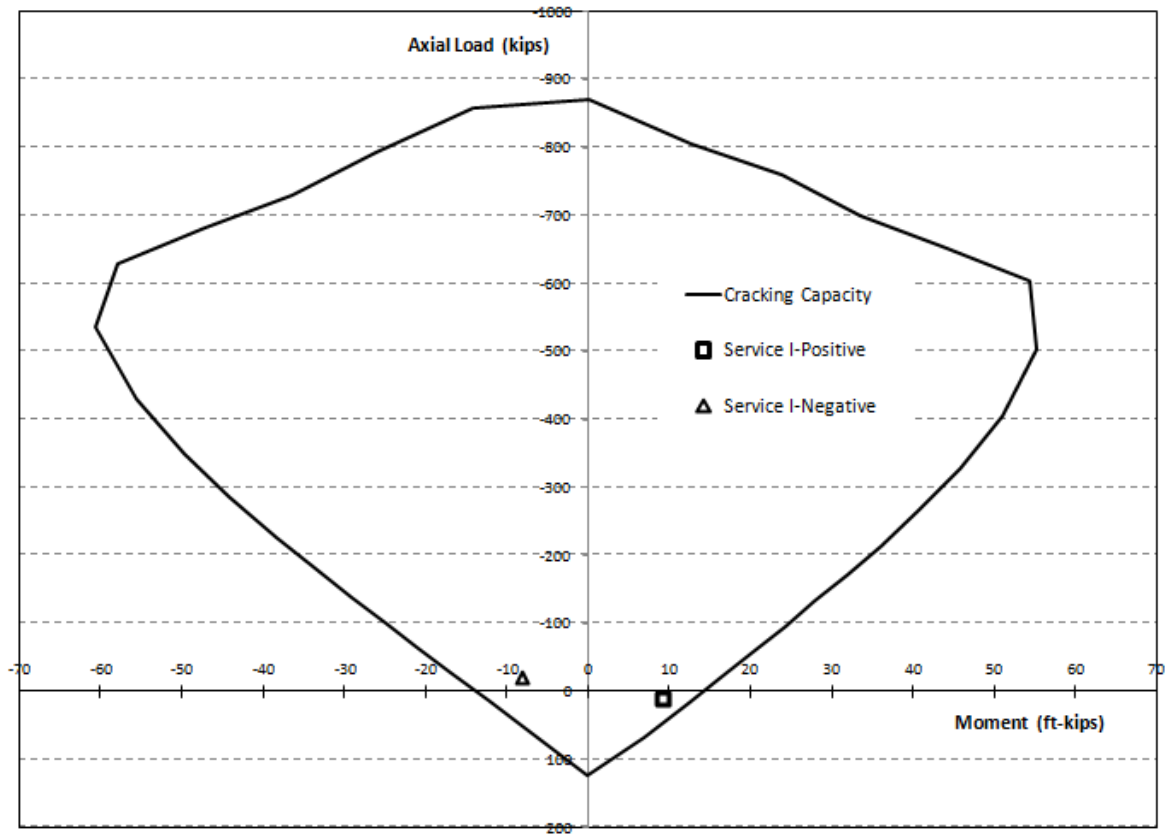


Figure C-1. Moment and Interaction Diagram under Service Loads for unit link slab width

Intentionally left blank

APPENDIX D – LINK SLAB MOMENT DUE TO THERMAL GRADIENT (MathCAD)

Temperature profile through the deck-girder composite section for Postive Temeperature Gradient (PTG)

$$T_1 := 41 \quad T_2 := 11 \quad T_3 := 6.42 \quad T_4 := 0 \quad T_5 := 0$$

Material properties

$$\text{Concrete modulus} \quad E_c := 4067 \text{ ksi}$$

Thermal expansion coefficients, in/in/F

$$\alpha_1 := 6 \cdot 10^{-6} \quad \alpha_2 := 6 \cdot 10^{-6} \quad \alpha_3 := 6 \cdot 10^{-6} \quad \alpha_4 := 6 \cdot 10^{-6}$$

Section properties (length in inches; area in inches²)

$$b_1 := 66 \quad b_2 := 16 \quad h_1 := 4 \quad h_2 := 5 \quad h_3 := 7 \quad h_4 := 38$$

$$d_{b1} := 2 \quad d_{t1} := 2 \quad d_{b2} := 2.5 \quad d_{t2} := 2.5 \quad d_{b3} := 3.5 \quad d_{t3} := 3.5 \quad d_{b4} := 14.91 \quad d_{t4} := 23.09$$

$$A_1 := h_1 \cdot b_1 \quad A_2 := h_2 \cdot b_1 \quad A_3 := h_3 \cdot b_2 \quad A_4 := 447.5$$

$$A_1 = 264 \quad A_2 = 330 \quad A_3 = 112 \quad A_4 = 447.5$$

Length of bridge span (in.)

$$L := 834$$

Length of link slab (in.)

$$L_L := L \cdot 0.05 \cdot 2 + 1 \quad L_L = 84.4$$

Moment of inertia of each layer (in.⁴).

$$I_1 := b_1 \cdot \frac{h_1^3}{12} \quad I_2 := b_1 \cdot \frac{h_2^3}{12} \quad I_3 := b_2 \cdot \frac{h_3^3}{12} \quad I_4 := 61889.67$$

$$I_1 = 352 \quad I_2 = 687.5 \quad I_3 = 457.333 \quad I_4 = 6.189 \times 10^4$$

Section modulus (in.³).

$$\begin{aligned}
 S_{b1} &:= \frac{I_1}{d_{b1}} & S_{b2} &:= \frac{I_2}{d_{b2}} & S_{b3} &:= \frac{I_3}{d_{b3}} & S_{b4} &:= \frac{I_4}{d_{b4}} \\
 S_{t1} &:= \frac{I_1}{d_{t1}} & S_{t2} &:= \frac{I_2}{d_{t2}} & S_{t3} &:= \frac{I_3}{d_{t3}} & S_{t4} &:= \frac{I_4}{d_{t4}} \\
 S_{b1} &= 176 & S_{b2} &= 275 & S_{b3} &= 130.667 & S_{b4} &= 4.151 \times 10^3 \\
 S_{t1} &= 176 & S_{t2} &= 275 & S_{t3} &= 130.667 & S_{t4} &= 2.68 \times 10^3
 \end{aligned}$$

Moment of inertia of the link slab (in⁴)

$$I_d := b_1 \cdot \frac{(h_1 + h_2)^3}{12} \quad I_d = 4.01 \times 10^3$$

Solution process of six simultaneous equations

Initial estimates

$$\begin{aligned}
 M_1 &:= 100 & M_2 &:= 100 & M_3 &:= 100 & M_4 &:= 100 \\
 F_1 &:= 100 & F_2 &:= 100 & F_3 &:= 100 & F_4 &:= 100
 \end{aligned}$$

Given

$$\begin{aligned}
 \alpha_1 \cdot T_2 + \frac{M_1}{E_c \cdot S_{b1}} + \frac{F_1}{E_c \cdot A_1} + F_1 \cdot \frac{d_{b1}}{E_c \cdot S_{b1}} - \alpha_2 \cdot T_2 - \frac{(M_2 - M_1)}{E_c \cdot S_{t2}} - \frac{(F_2 - F_1)}{E_c \cdot A_2} + \frac{(F_2 \cdot d_{b2} + F_1 \cdot d_{t2}) \cdot -1}{E_c \cdot S_{t2}} &= 0 \\
 \alpha_2 \cdot T_3 + \frac{(M_2 - M_1)}{E_c \cdot S_{b2}} + \frac{(F_2 - F_1)}{E_c \cdot A_2} + \frac{(F_2 \cdot d_{b2} + F_1 \cdot d_{t2})}{E_c \cdot S_{b2}} - \alpha_3 \cdot T_3 - \frac{(M_3 - M_2)}{E_c \cdot S_{t3}} - \frac{(F_3 - F_2)}{E_c \cdot A_3} - \frac{(F_3 \cdot d_{b3} + F_2 \cdot d_{t3})}{E_c \cdot S_{t3}} &= 0 \\
 \alpha_3 \cdot T_4 + \frac{(M_3 - M_2)}{E_c \cdot S_{b3}} + \frac{(F_3 - F_2)}{E_c \cdot A_3} + \frac{(F_3 \cdot d_{b3} + F_2 \cdot d_{t3})}{E_c \cdot S_{b3}} - \alpha_4 \cdot T_4 - \frac{(M_3) \cdot -1}{E_c \cdot S_{t4}} - \frac{(F_3) \cdot -1}{E_c \cdot A_4} - \frac{(F_3 \cdot d_{t4})}{E_c \cdot S_{t4}} &= 0 \\
 \alpha_1 \cdot \frac{(T_2 - T_1)}{h_1} + \frac{M_1}{E_c \cdot I_1} + F_1 \cdot \frac{d_{b1}}{E_c \cdot I_1} - \alpha_2 \cdot \frac{(T_3 - T_2)}{h_2} - \frac{(M_2 - M_1)}{E_c \cdot I_2} - \frac{(F_1 \cdot d_{t2} + F_2 \cdot d_{b2})}{E_c \cdot I_2} &= 0 \\
 \alpha_2 \cdot \frac{(T_3 - T_2)}{h_2} + \frac{(M_2 - M_1)}{E_c \cdot I_2} + \frac{(F_1 \cdot d_{t2} + F_2 \cdot d_{b2})}{E_c \cdot I_2} - \alpha_3 \cdot \frac{(T_4 - T_3)}{h_3} - \frac{(M_3 - M_2)}{E_c \cdot I_3} - \frac{(F_2 \cdot d_{t3} + F_3 \cdot d_{b3})}{E_c \cdot I_3} &= 0 \\
 \alpha_3 \cdot \frac{(T_4 - T_3)}{h_3} + \frac{(M_3 - M_2)}{E_c \cdot I_3} + \frac{(F_2 \cdot d_{t3} + F_3 \cdot d_{b3})}{E_c \cdot I_3} - \alpha_4 \cdot \frac{(T_5 - T_4)}{h_4} - \frac{(M_3) \cdot -1}{E_c \cdot I_4} - \frac{(F_3 \cdot d_{t4})}{E_c \cdot I_4} &= 0
 \end{aligned}$$

$$\begin{bmatrix} F_1 \\ F_2 \\ F_3 \\ M_1 \\ M_1 \\ M_1 \end{bmatrix} := \text{Find}(F_1, F_2, F_3, M_1, M_2, M_3)$$

$$F_1 = -33.11 \quad F_2 = 25.257 \quad F_3 = 40.79 \quad \text{kips}$$

$$M_1 = 136.178 \quad M_2 = 181.992 \quad M_3 = -31.742 \quad \text{kip-in}$$

$$\text{Curvature} := \alpha_3 \cdot \frac{(T_4 - T_3)}{h_3} + \frac{(M_3 - M_2)}{E_c \cdot I_3} + \frac{(F_2 \cdot d_{t3} + F_3 \cdot d_{b3})}{E_c \cdot I_3}$$

$$\text{Curvature} = 3.868 \times 10^{-6}$$

$$\theta_{\text{PTG}} := \text{Curvature} \cdot \frac{L}{2} \quad \theta_{\text{PTG}} = 1.613 \times 10^{-3} \quad \text{rad}$$

$$\theta_{\text{NTG}} := \theta_{\text{PTG}}^{-0.3} \quad \theta_{\text{NTG}} = -4.839 \times 10^{-4} \quad \text{rad}$$

Moment calculations

$$\text{Moment}_{\text{PTG}} := 2 \cdot E_c \cdot I_d \cdot \frac{\theta_{\text{PTG}}}{L \cdot 12} \quad \text{Moment}_{\text{NTG}} := \text{Moment}_{\text{PTG}}^{-0.3}$$

$$\text{Moment}_{\text{PTG}} = 51.938 \quad \text{ft} - \text{kips} \quad \text{Moment}_{\text{NTG}} = -15.581 \quad \text{ft} - \text{kips}$$

Design moment for 66 in. wide effective section

$$\text{Des}_{\text{M.PTG}} := \text{Moment}_{\text{PTG}} \cdot \frac{12}{66} \quad \text{Des}_{\text{M.NTG}} := \text{Moment}_{\text{NTG}} \cdot \frac{12}{66}$$

$$\text{Des}_{\text{M.PTG}} = 9.443 \quad \frac{\text{ft} - \text{kips}}{\text{ft}} \quad \text{Des}_{\text{M.NTG}} = -2.833 \quad \frac{\text{ft} - \text{kips}}{\text{ft}}$$

Intentionally left blank

APPENDIX E

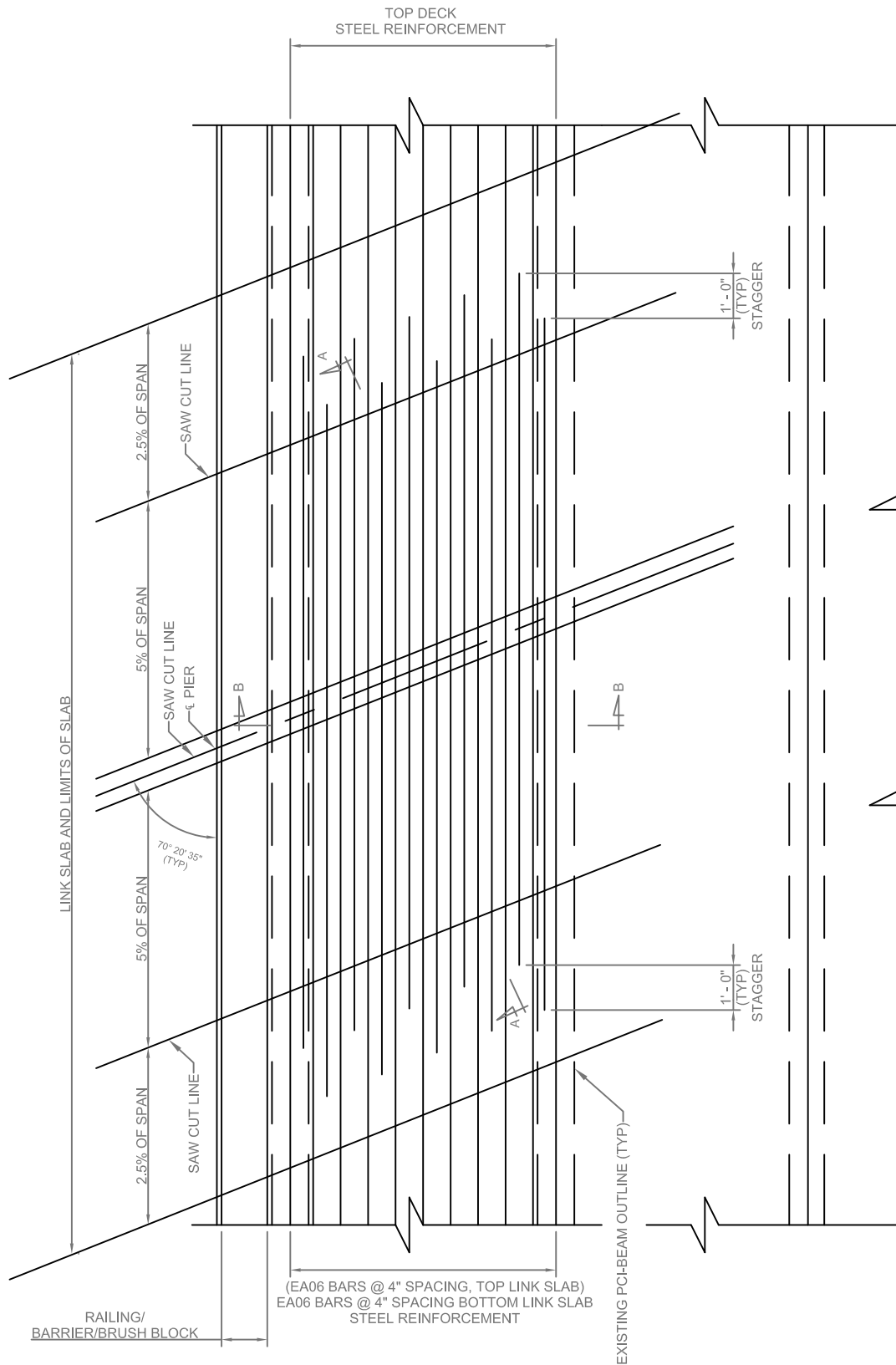
Proposed Design Details in MDOT Design Guide Format
- Skew Link Slab

DRAWN BY:
 APPROVED BY:
 CHECKED BY:

FIGURE E-1: PROPOSED DETAIL

SKEW LINK SLAB DETAIL

ISSUED:
 SUPEREDES:



PARTIAL DECK PLAN @ PIER

TRANSVERSE REINFORCING STEEL IS NOT SHOWN

NOTE:

STEEL REINFORCEMENT FOR THE RAILING AND BRUSH BLOCK SHALL BE REPLACED IN KIND AS DIRECTED BY THE ENGINEER AND AS DETAILED ON PLANS.

ALL SAW CUTS FOR DECK, BRIDGE RAILING AND BRUSH BLOCK REMOVAL SHALL BE INCLUDED IN THE PAY ITEM "Structures, Rehabilitation, Rem Portions (S12-25042 EB)".

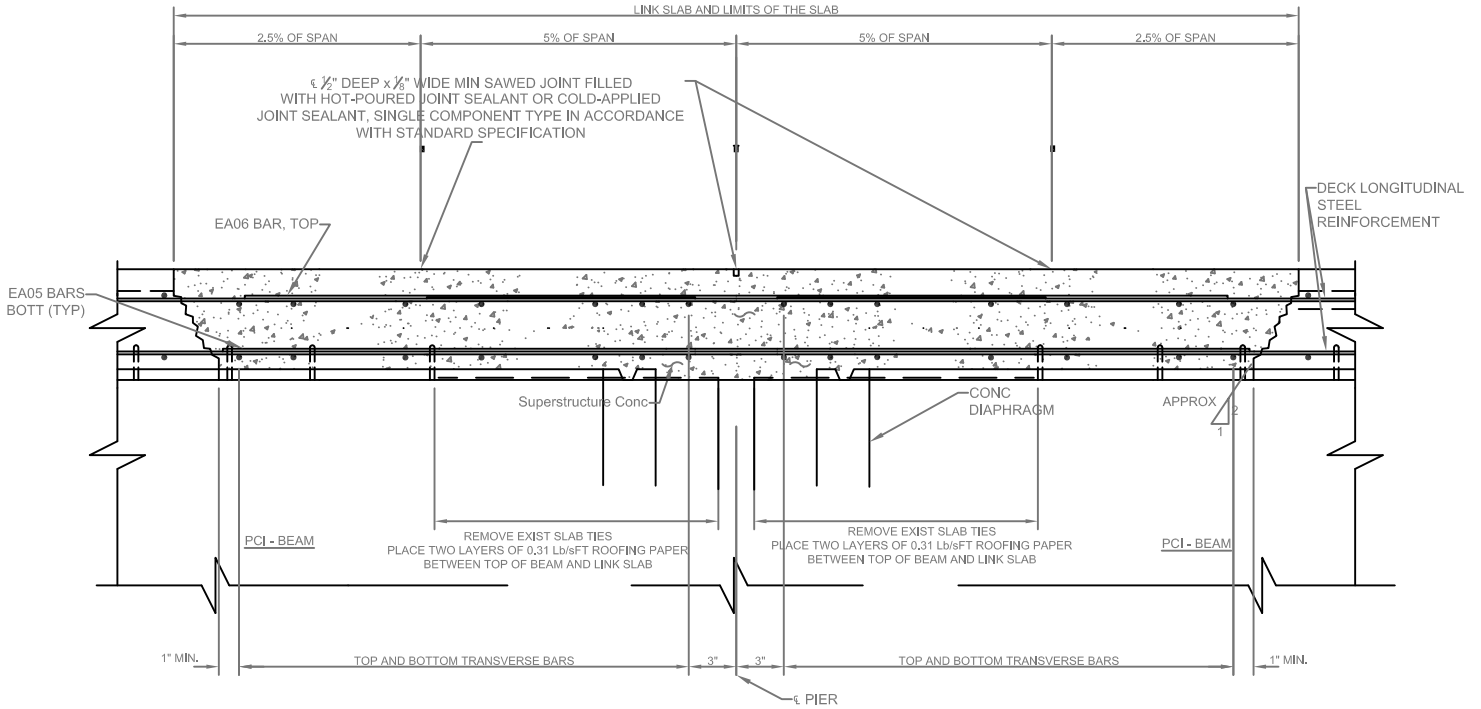
PREPARED BY

DRAWN BY:
 APPROVED BY:
 CHECKED BY:

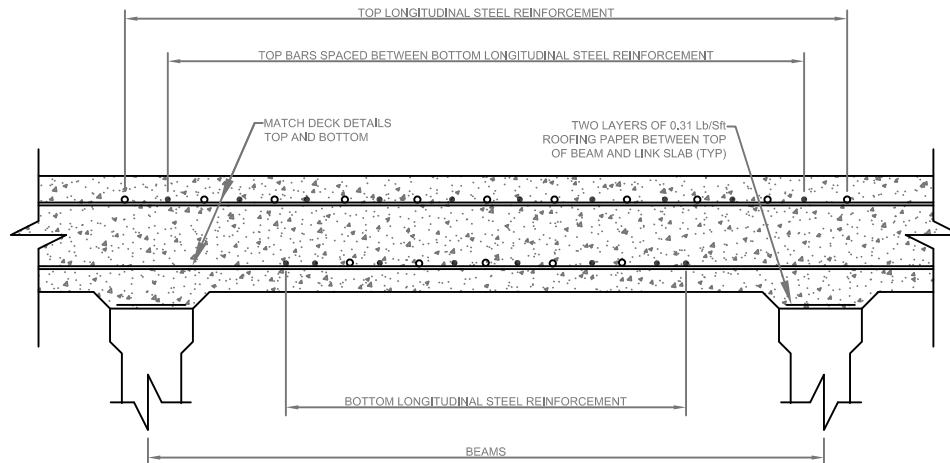
FIGURE E-2: PROPOSED DETAIL

SKEW LINK SLAB DETAIL

ISSUED:
 SUPEREDES:



SECTION A-A (LONGITUDINAL SECTION THRU LINK SLAB)



SECTION B-B (TRANSVERSE SECTION THRU LINK SLAB)

PREPARED BY

Intentionally left blank

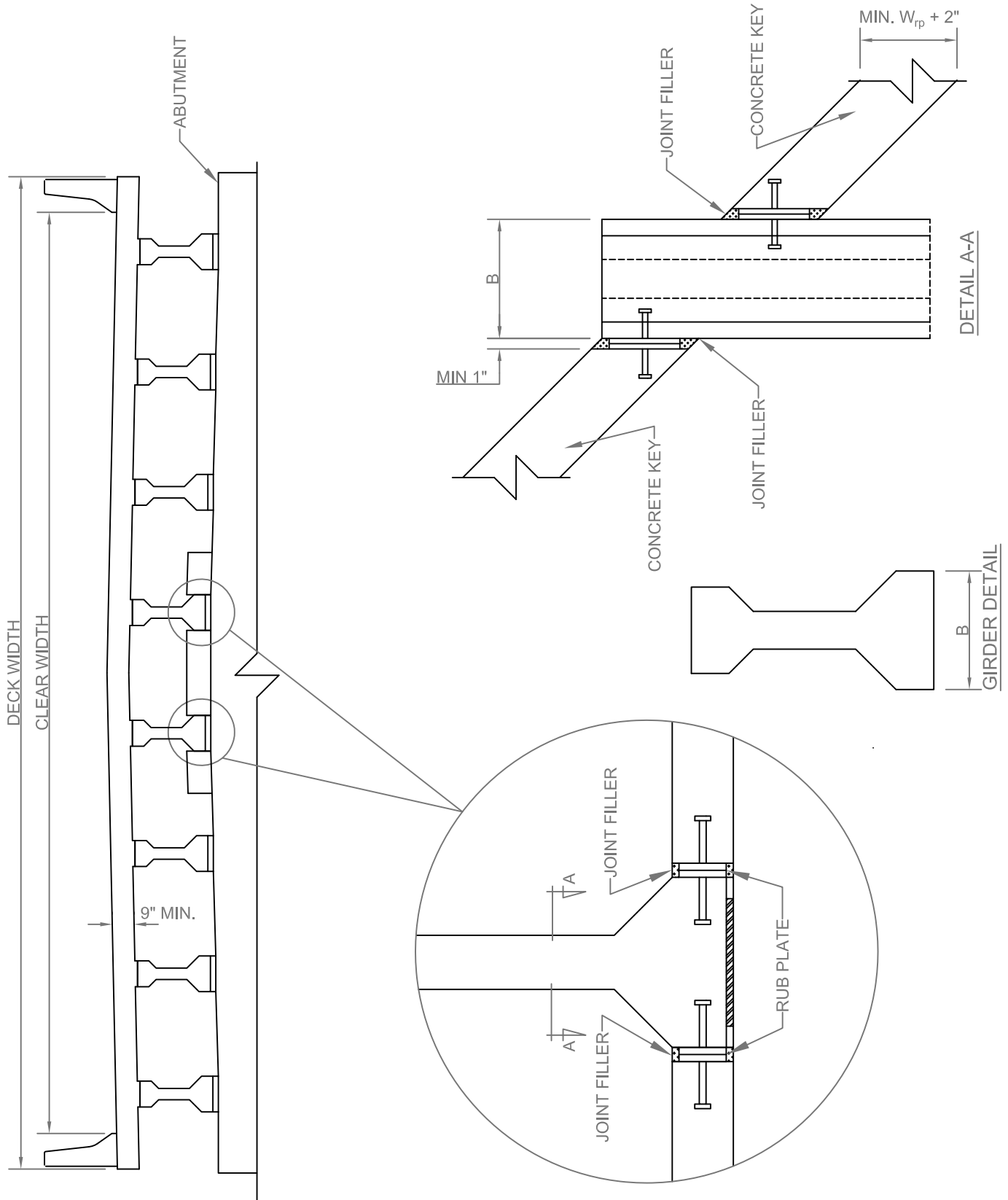
APPENDIX F

Proposed Design Details in MDOT Design Guide Format
- Deck Sliding over Backwall System

DRAWN BY:
APPROVED BY:
CHECKED BY:

FIGURE F-2: PROPOSED DETAILS
DETAILS OF GIRDER END RESTRAIN -
INDEPENDENT BACKWALL

ISSUED BY:
SUPEREDES:



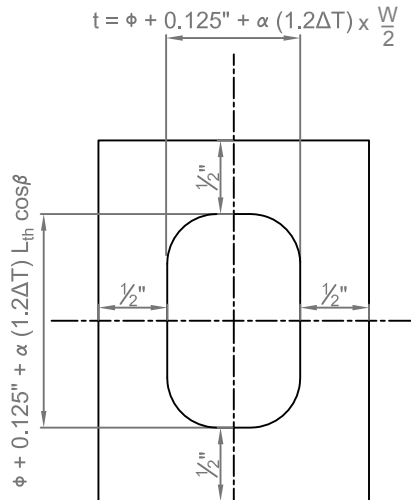
PREPARED BY

DRAWN BY:
 APPROVED BY:
 CHECKED BY:

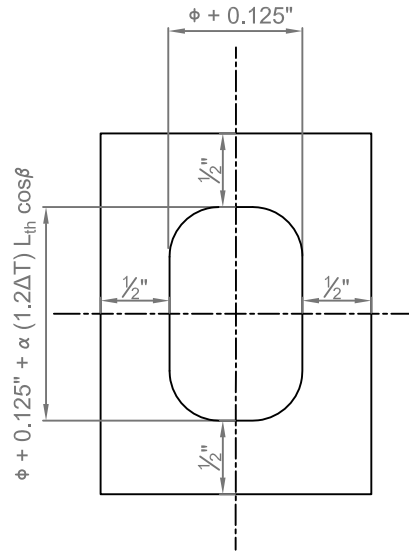
FIGURE F-4: PROPOSED DETAILS

ISSUED BY:
 SUPEREDES:

DETAIL A - DIMENSION OF THE SLOT IN SOLE PLATE
 & BEARING FOR INDEPENDENT BACKWALL SYSTEM

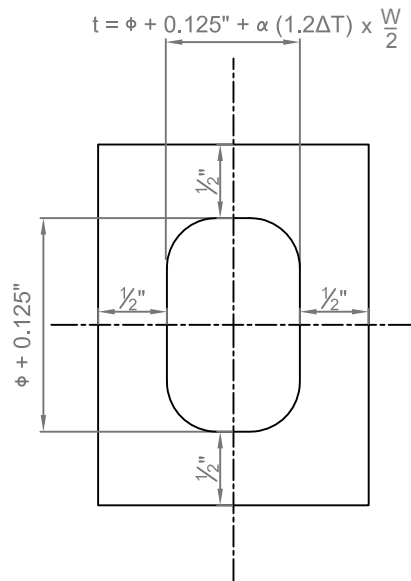


(A) TYPICAL SLOT DETAILS

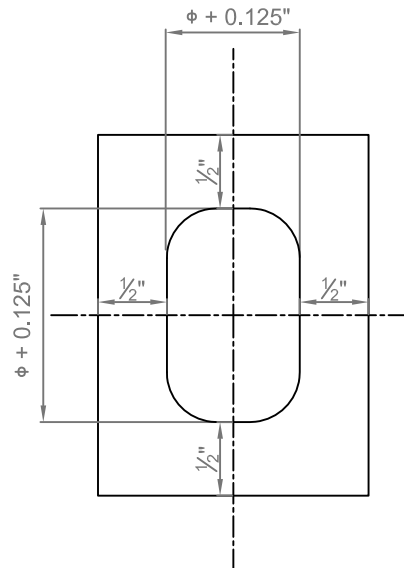


(B) SLOT DETAILS FOR BEARINGS AT GIRDER ENDS RESTRAINT WITH CONCRETE KEYS *

EXPANSION BEARINGS



(C) TYPICAL SLOT DETAILS



(D) FOR BEARING AT BRIDGE CENTERLINE

FIXED BEARINGS

NOTE:

* SEE DETAILS OF GIRDER END RESTRAIN

L: LENGTH OF THE DIAGONAL BETWEEN ACUTE CORNERS (SEE RUB PLATE DESIGN EXAMPLE)

W: DECK WIDTH

beta: ANGLE (SEE RUB PLATE DESIGN EXAMPLE)

phi: DIAMETER OF THE POSITION DOWEL

Delta T: |MAXIMUM TEMPERATURE| + |MINIMUM TEMPERATURE| FROM TABLE 5-2

PREPARED BY

Intentionally left blank

APPENDIX G

Rub Plate Design Procedure

DRAWN BY:
 APPROVED BY:
 CHECKED BY:

FIGURE G-1: PROPOSED RUB PLATE
 DESIGN PROCEDURE

RUB PLATE DESIGN -
 GIRDER END RESTRAIN

ISSUED:
 SUPEREDES:

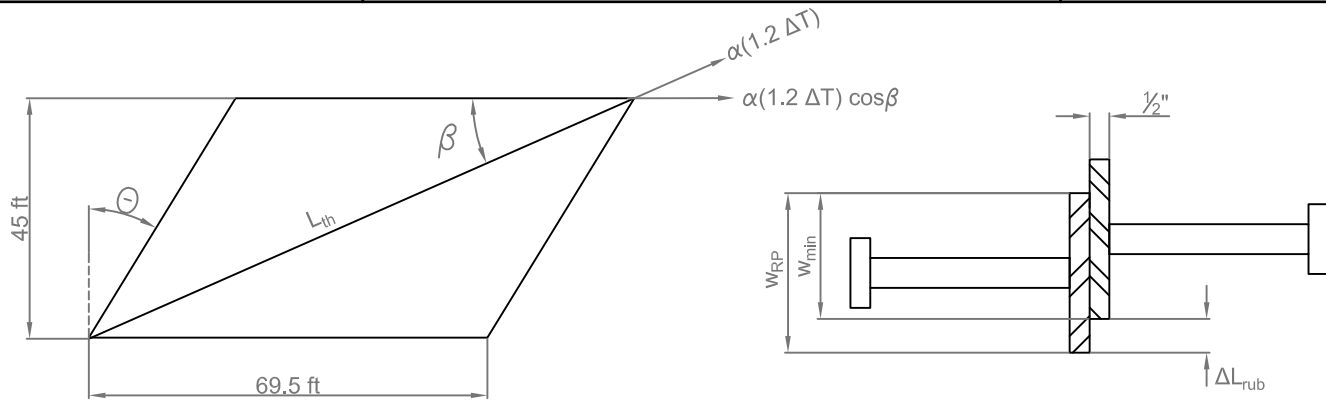


FIGURE A

RUB PLATE DESIGN

TWO GIRDER ENDS ARE RESTRAINED

$$\begin{aligned} \text{FORCES ON THE RUB PLATE } (R_p) &= (10\% \times \text{TOTAL VERTICAL BEARING REACTION})/2 \\ &= (10\% \times 1000 \text{ kips})/2 = 50 \text{ kips} \end{aligned}$$

DETERMINE SIZE OF RUB PLATES:

$$\Delta T = |\text{MAXIMUM TEMPERATURE}| + |\text{MINIMUM TEMPERATURE}| = 115^\circ\text{F} \text{ (TABLE 5-2)}$$

L_{th} = EFFECTIVE LENGTH OF THERMAL MOVEMENT, 123 ft

ESTIMATED MAXIMUM MOVEMENT IN ONE DIRECTION AT THE ABUTMENT.

$$(\Delta L_{rub})_c = L_{th} \times \alpha \times 1.2 \times \Delta T_c = 123\text{ft} \left(12 \frac{\text{in}}{\text{ft}}\right) (6 \times 10^{-6} / ^\circ\text{F}) \times (1.2 \times 72.7^\circ\text{F}) = 0.8 \text{ inch}$$

$$(\Delta L_{rub})_e = L_{th} \times \alpha \times 1.2 \times \Delta T_e = 123\text{ft} \left(12 \frac{\text{in}}{\text{ft}}\right) (6 \times 10^{-6} / ^\circ\text{F}) \times (1.2 \times 42.3^\circ\text{F}) = 0.5 \text{ inch}$$

WHERE ΔT_c = CONTRACTION THERMAL LOAD

ΔT_e = EXPANSION THERMAL LOAD

$(\Delta L_{rub})_c > (\Delta L_{rub})_e$, SO CONSIDER $(\Delta L_{rub})_c$ FOR FURTHER CALCULATIONS

HEIGHT OF RUB PLATE:

$$h_{rp} = T_{\text{bottom flange}} - 2 \text{ inch} = 7 \text{ inch} - 2 \text{ inch} = 5 \text{ inch}$$

THIS EXAMPLE CONSIDERS AASHTO TYPE III GIRDER, OF WHICH BOTTOM FLANGE THICKNESS IS 7 in. CLEARANCE FROM TOP AND BOTTOM IS 1 inch.

MAXIMUM "GALLING STRESS" FOR ASTM A276 TYPE 316 STEEL, OF WHICH THE RUB PLATES ARE CONSTRUCTED:

$$F_g = 2000 \text{ psi}$$

ALLOWABLE GALLING STRESS:

$$f_g = 0.55 F_g = 1100 \text{ psi}$$

MINIMUM RUB PLATE WIDTH:

$$w_{min} = \frac{R_p}{h_{rp} (f_g)} = \frac{50 \text{ kip} (1000 \text{ lbs}/1 \text{ kip})}{[5 \text{ in} (1100 \text{ psi})]} = 9 \text{ inch}$$

ENSURE THE MINIMUM RUB PLATE WIDTH IS MAINTAINED DURING EXTREMES OF THE TEMPERATURE CYCLE

$$w = w_{min} + (\Delta L_{rub})_c = 9 \text{ inch} + 0.8 \text{ inch} = 9.8 \text{ inch} \approx 10 \text{ inch}$$

USE 5 inch x 10 inch x 0.5 inch in rub plate

NOTE: LENGTH OF THE CONCRETE KEY ALONG GIRDER CENTER LINE SHOULD BE MINIMUM OF 10 INCH.

PREPARED BY

APPENDIX H

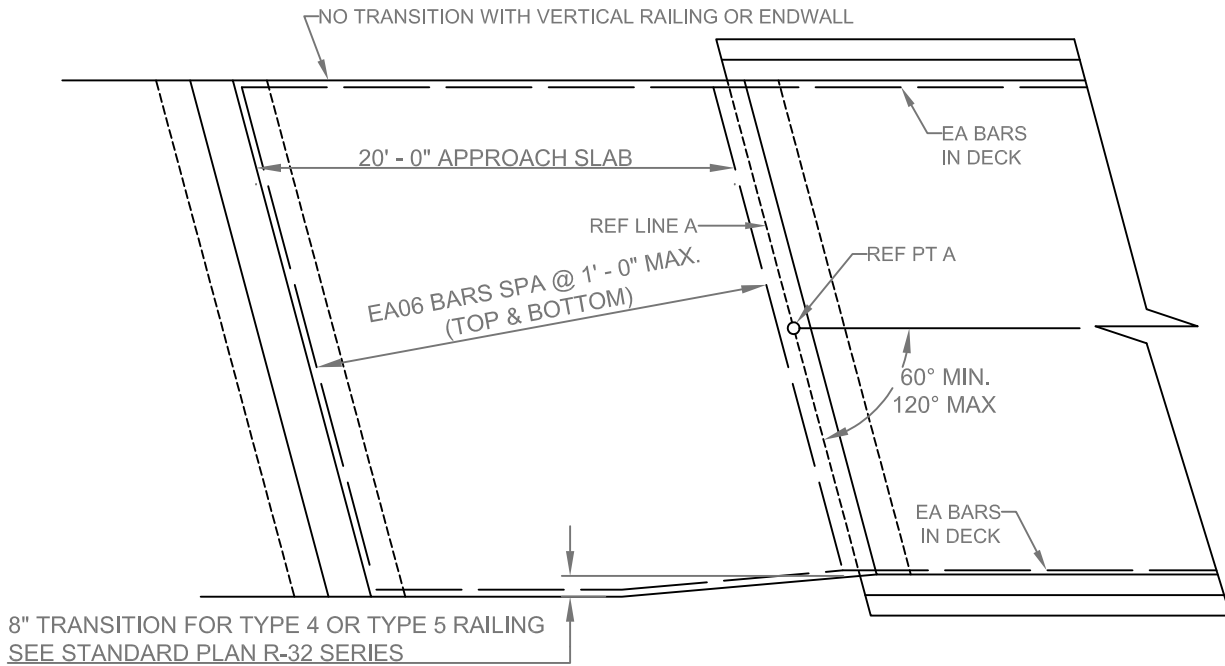
Proposed Design Details in MDOT Design Guide Format
- Semi – Integral Abutments

DRAWN BY:
 APPROVED BY:
 CHECKED BY:

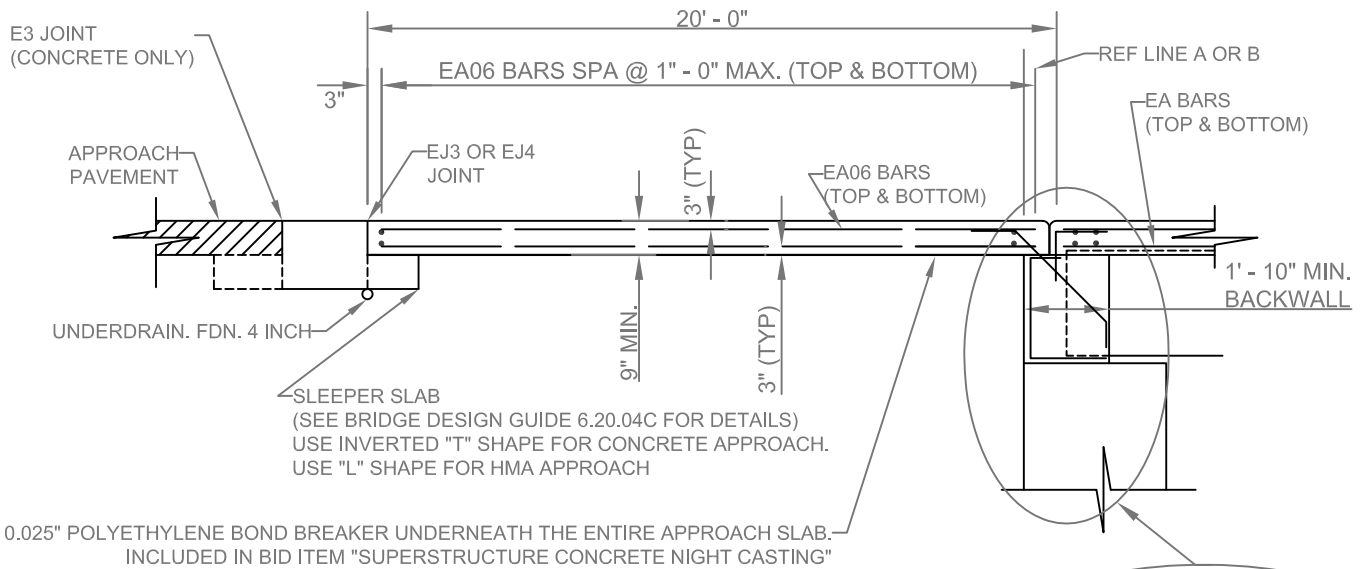
FIGURE H-1: PROPOSED DETAILS

SEMI INTEGRAL ABUTMENT EMPIRICAL APPROACH SLAB
 DETAILS FOR LINK SLAB BRIDGES

ISSUED:
 SUPEREDES:



PLAN OF APPROACH



APPROACH SECTION

SLAB THICKNESS WILL MATCH THE ROAD
 APPROACH PAVEMENT THICKNESS (9" MIN.)

SEE SEMI-INTEGRAL ABUTMENT DETAIL
 - BACKWALL IN-LINE WITH ABUTMENT
 - BACKWALL OFFSET FROM ABUTMENT

NOTES:

ATTACH APPROACH CURB AND GUTTER TO THE APPROACH SLAB WITH BOTTOM MAT TRANSVERSE REINFORCEMENT AND TO THE BRIDGE DECK WITH BOTTOM MAT LONGITUDINAL REINFORCEMENT

POUR APPROACH SLABS FROM EXPANSION LOCATION TOWARD REFERENCE LINE.

APPROACH SLABS SHOULD BE CAST AT NIGHT WITH NIGHT TIME CASTING OF SUPERSTRUCTURE CONCRETE

EJ3 OR EJ4 JOINT WIDTH TO ACCOMMODATE THERMAL MOVEMENT = $L_{th} \times 1.2 (\Delta T_e) \cos \beta$

REFER RUB PLATE DESIGN SHEET FOR L_{th} , ΔT_e AND β DEFINITIONS

USE SLEEPER SLAB WITH ALL APPROACH SLABS INCLUDING HMA ROADWAY

PREPARED BY:

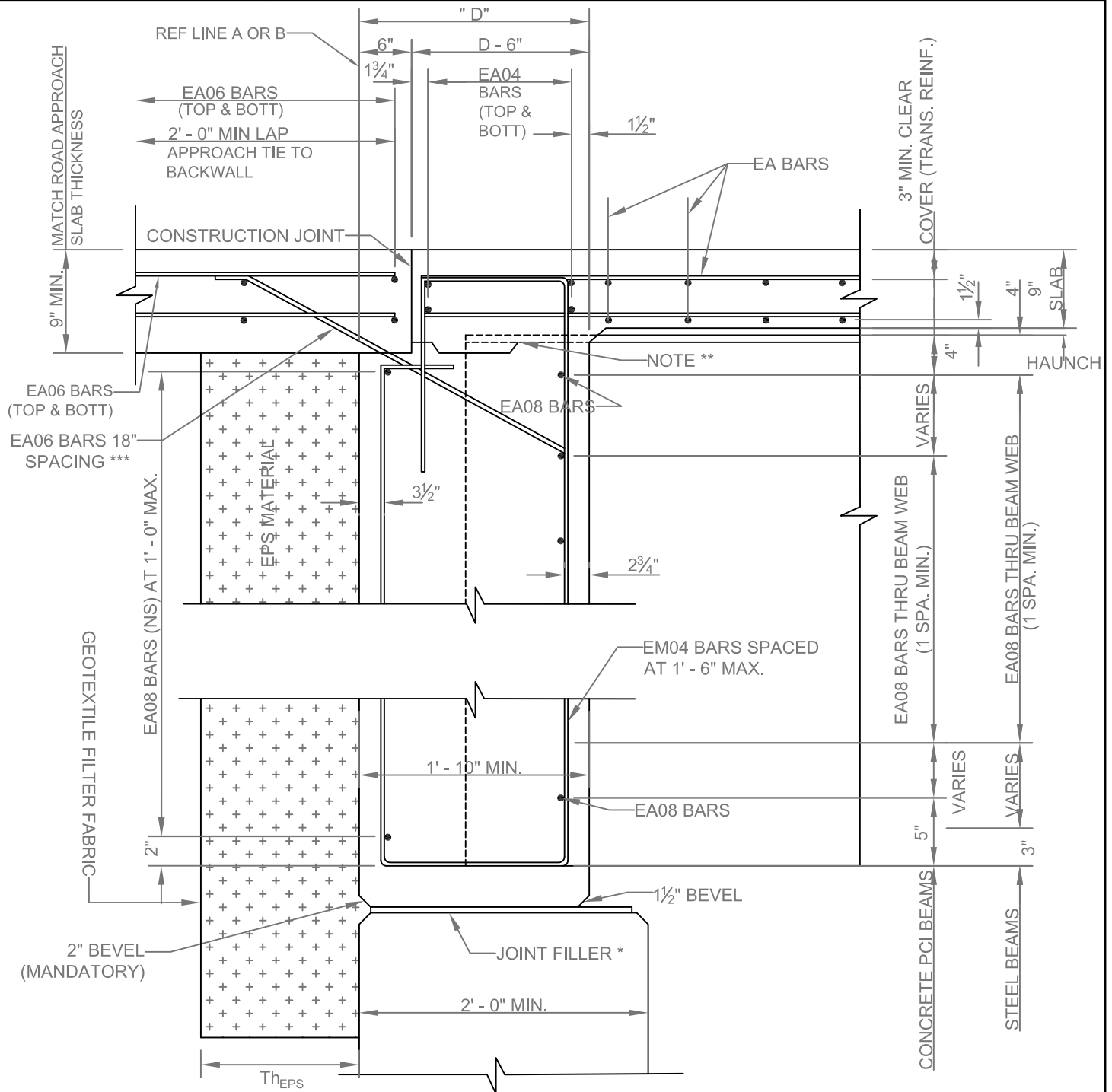
PROPOSAL FOR
 6.20.04B

DRAWN BY:
 APPROVED BY:
 CHECKED BY:

FIGURE H-2 - PROPOSED DETAIL

SEMI - INTEGRAL ABUTMENT DETAILS
 WITH BACKWALL IN-LINE WITH ABUTMENT

ISSUED:
 SUPEREDES:



NOTE:

* THICKNESS = BEARING VERTICAL DEFORMATION PLUS 1"

** OPT. CONSTRUCTION JOINT (IF CONSTRUCTION JOINT IS USED, CAST LOWER PORTION OF BACKWALL PRIOR TO PLACING DECK REINFORCEMENT)

*** EA06 BARS



THE THICKNESS OF THE EPS LAYER (T_{EPS}) SHALL BE DETERMINED USING THE FOLLOWING FORMULA:

h = HEIGHT OF BACKWALL IN INCHES

ΔL = THERMAL MOVEMENT FOR THE ENTIRE TEMPERATURE RANGE IN INCHES (EXPANSION + CONTRACTION)

T_{EPS} = EPS THICKNESS IN INCHES (SHALL NOT BE <10")

$T_{EPS} = 10 [0.01h + 0.67 (\Delta L)]$

PREPARED BY

PROPOSAL FOR

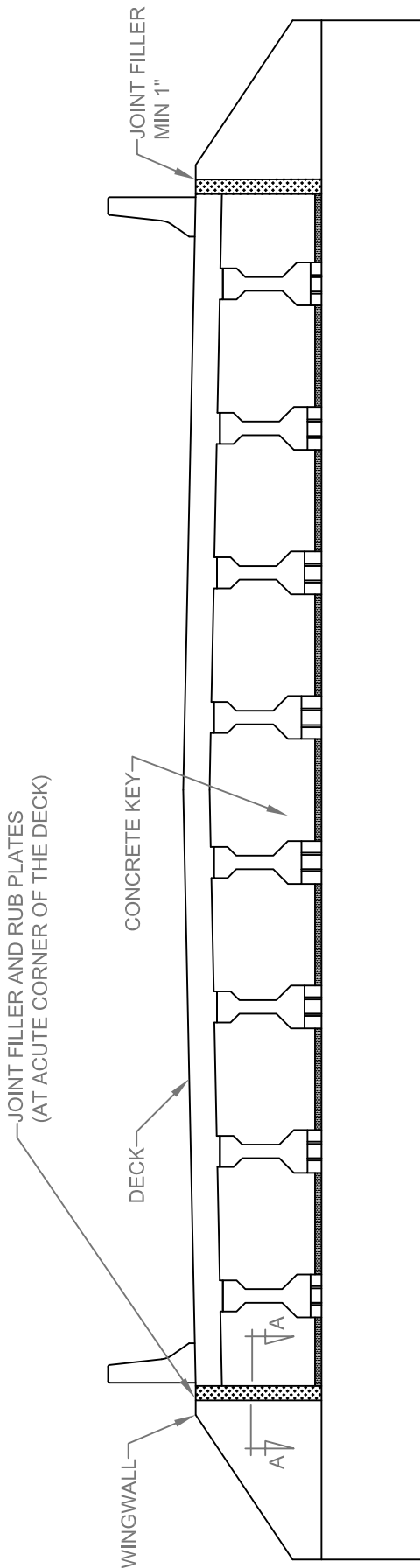
6.20.04

DRAWN BY:
APPROVED BY:
CHECKED BY:

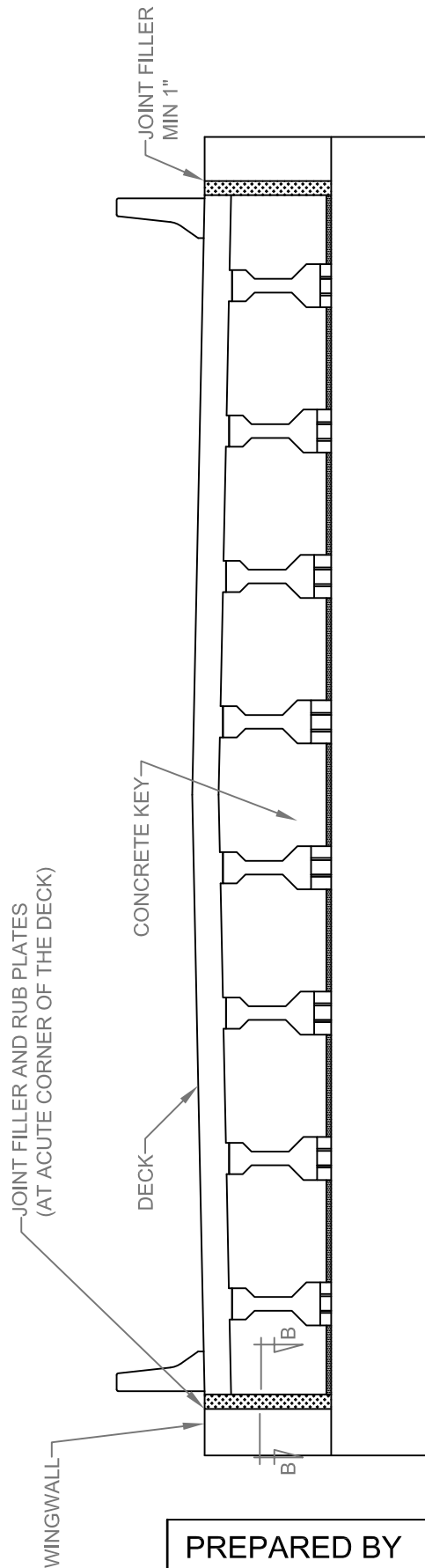
FIGURE H-4: PROPOSED DETAIL

ELEVATION VIEW OF SEMI-INTEGRAL ABUTMENT
WITH BACKWALL IN-LINE WITH ABUTMENT

ISSUED:
SUPEREDES:



ELEVATION VIEW OF WINGWALL CONFIGURATION 1



ELEVATION VIEW OF WINGWALL CONFIGURATION 2

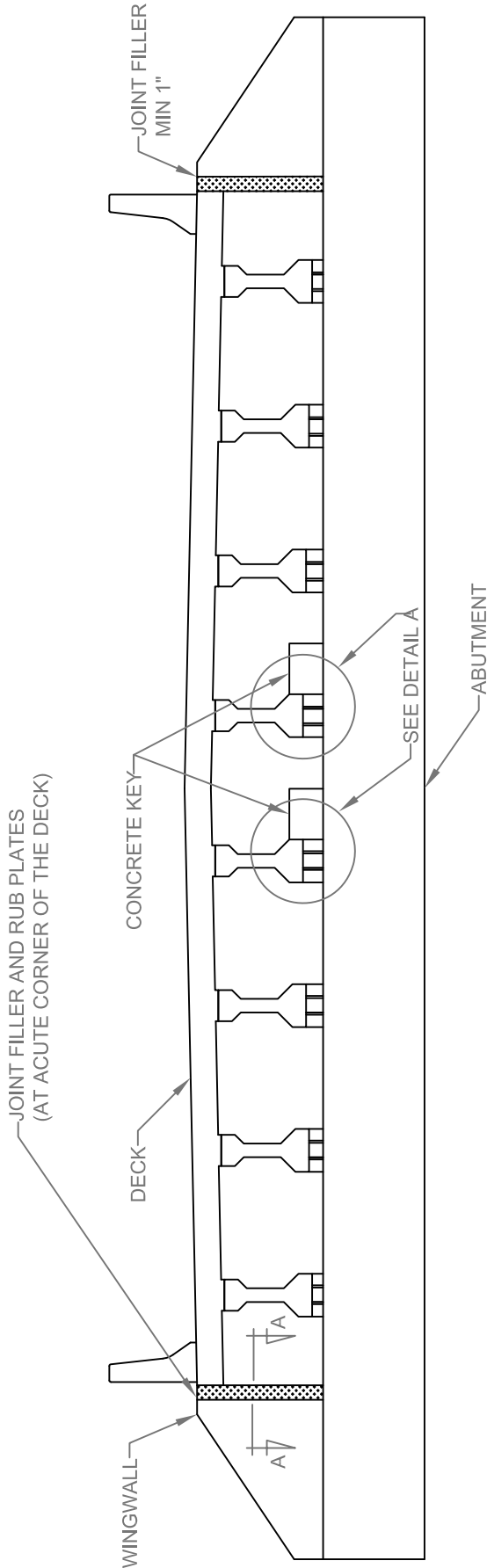
PREPARED BY

DRAWN BY:
APPROVED BY:
CHECKED BY:

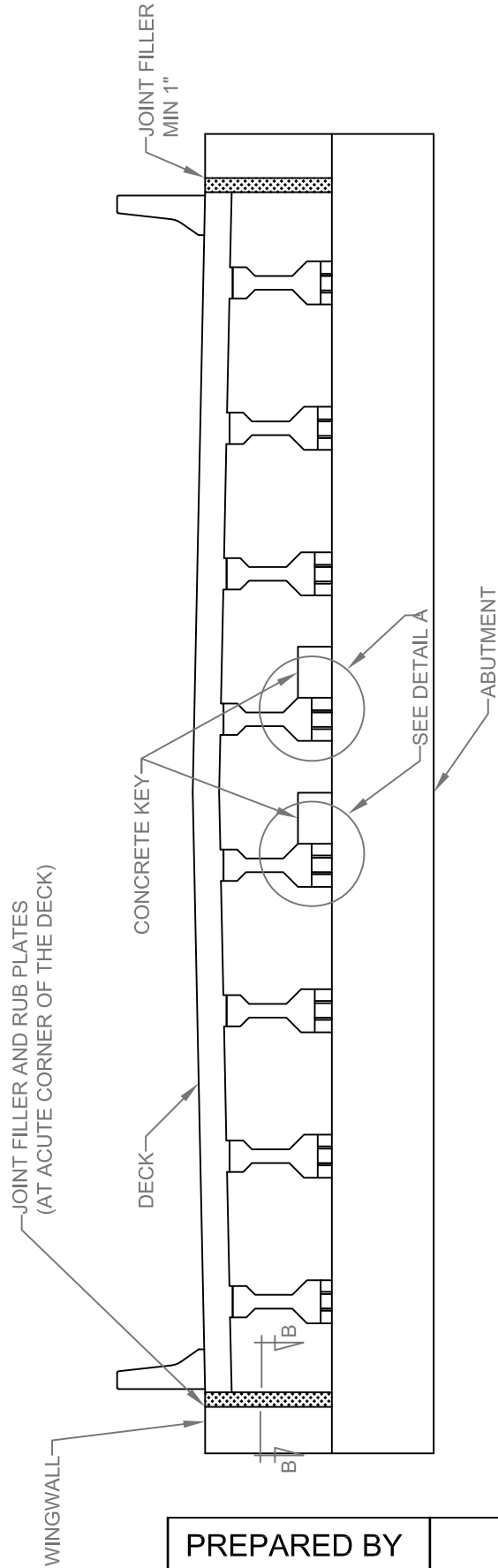
FIGURE H-5: PROPOSED DETAIL

ELEVATION VIEW OF SEMI-INTEGRAL ABUTMENT
WITH BACKWALL OFFSET FROM ABUTMENT

ISSUED:
SUPEREDES:



ELEVATION VIEW OF WINGWALL CONFIGURATION 1



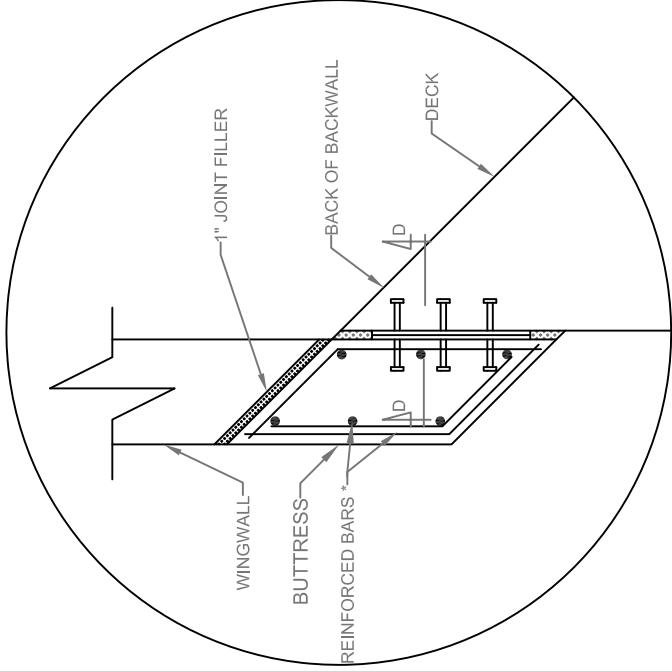
ELEVATION VIEW OF WINGWALL CONFIGURATION 2

PREPARED BY

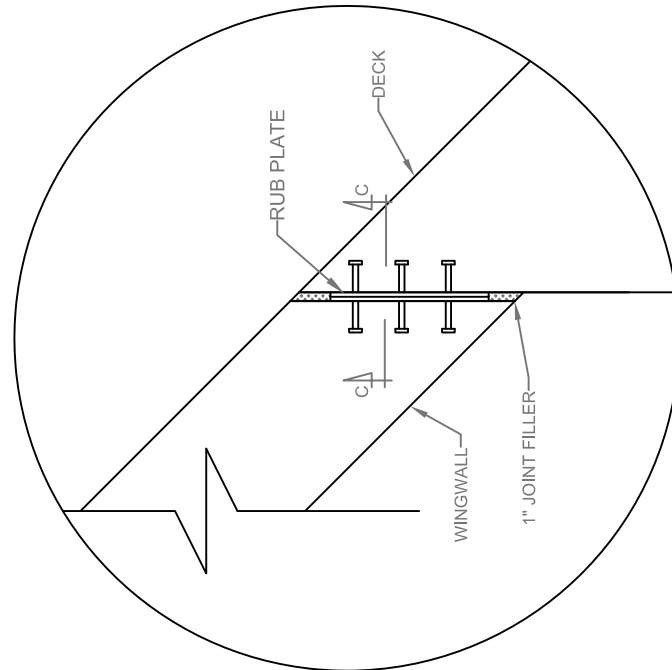
DRAWN BY:
APPROVED BY:
CHECKED BY:

FIGURE H-6: PROPOSED DETAIL
WINGWALL CONFIGURATION DETAIL

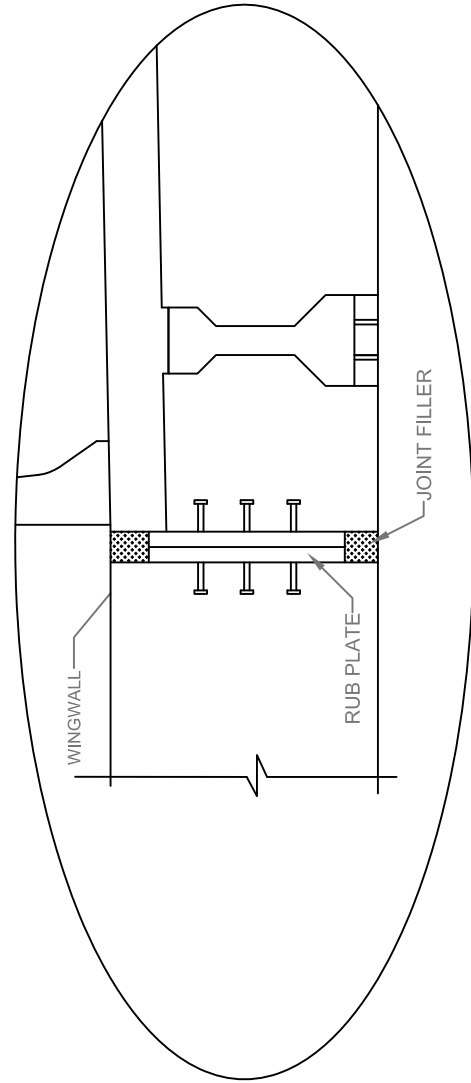
ISSUED:
SUPEREDES:



DETAIL B-B - WINGWALL CONFIGURATION 2



DETAIL A-A - WINGWALL CONFIGURATION 1



SECTION C AND D

NOTE:
* SHOULD BE DESIGNED FOR MOMENT SHEAR

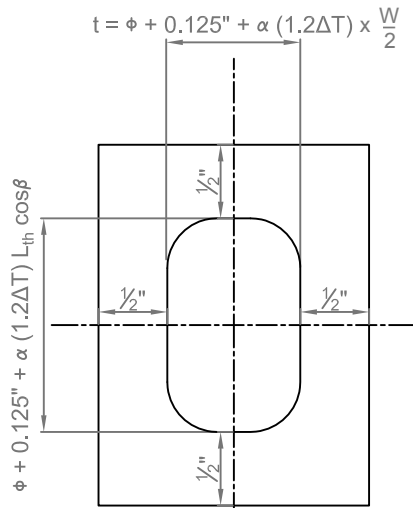
PREPARED BY

DRAWN BY:
 APPROVED BY:
 CHECKED BY:

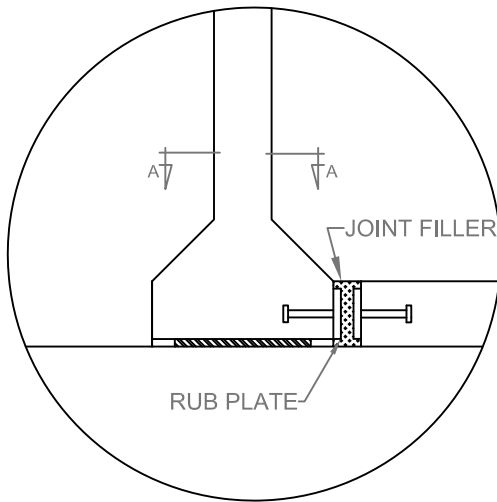
FIGURE H-7: PROPOSED DETAIL

ISSUED BY:
 SUPEREDES:

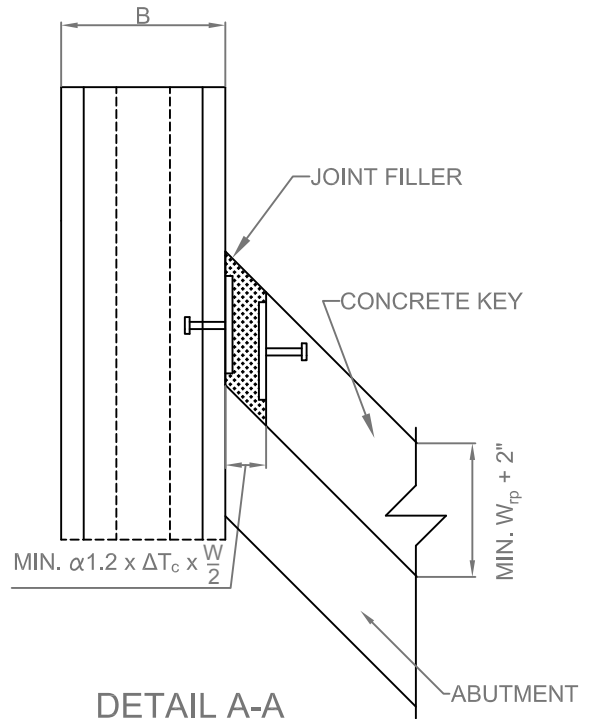
DETAIL A - DIMENSION OF THE SLOT AND CONCRETE KEY
 WITH RUB PLATES FOR SEMI-INTEGRAL ABUTMENT



(A) TYPICAL SLOT DETAILS FOR BEARINGS
 AT THE SEMI-INTEGRAL ABUTMENT



DETAIL A



DETAIL A-A

GIRDER END RESTRAIN DETAILS FOR BACKWALL
 OFFSET FROM ABUTMENT CONFIGURATION

NOTE:

* SEE DETAILS OF GIRDER END RESTRAIN

L_{th} : LENGTH OF THE DIAGNAL BETWEEN ACUTE CORNERS (SEE RUB PLATE DESIGN EXAMPLE)

W: DECK WIDTH

β : ANGLE (SEE RUB PLATE DESIGN EXAMPLE)

ϕ : DIAMETER OF THE POSITION DOWEL

ΔT : |MAXIMUM TEMPERATURE| + |MINIMUM TEMPERATURE| FROM TABLE 5-2

PREPARED BY